The spindle assembly checkpoint in Phallusia mammillata embryos

Marianne Roca

Thèse de doctorat en biologie

Sorbonne Université - Ecole doctorale complexité du vivant – ED515
Laboratoire de biologie du développement de Villefranche sur mer (LBDV) – UMR 7009
Equipe : mitose et contrôle du fuseau

The spindle assembly checkpoint in *Phallusia mammillata* embryos

Par Marianne Roca

Dirigée par Elisabeth Christians and Stefania Castagnetti

Présentée et soutenue publiquement le 29 novembre 2019 à Villefranche sur mer

Devant un jury composé de :

- Dr. Roger Karess, rapporteur
- Pr. Eric Thompson, rapporteur
- Dr. Aude Dupré, examinatrice
- Pr. Elisabeth Chrisitians, directrice de thèse
- Dr. Stefania Castagnetti, encadrante (invité)

Abstract

During mitosis, progression through anaphase must take place only when all chromosomes are correctly attached to spindle microtubules to avoid chromosome mis-segregation and the generation of aneuploid cells (i.e. with an abnormal chromosome number). Embryos containing aneuploid cells can exhibit developmental defects and lethality. Furthermore, cancer cells are often aneuploid. To prevent such deleterious aneuploidy, a control mechanism, the spindle assembly checkpoint (SAC), delays metaphase-anaphase transition until all chromosomes are properly attached to spindle microtubules. However, the SAC is not efficient during early development in some species.

During my thesis, I analyzed the activity of the SAC during the development of the marine chordate *P. mammillata*. I showed that in *P. mammillata* embryos, the SAC becomes efficient at the 8th cell cycle and its efficiency increases progressively in the following cell cycles. Although, I demonstrated that patterning of the embryo along the anteroposterior axis influences SAC efficiency, my experiments suggest that additional parameters modulate SAC efficiency.

I searched the molecular mechanisms, which control SAC efficiency during development. I collected evidence showing that SAC components are present in oocytes and all post-fertilization stages. I found that SAC proteins localize at kinetochores during meiosis and at later stages when there is an efficient SAC while they do not accumulate on unattached kinetochores in early SAC deficient embryos.

My thesis work establishes *P. mammillata* as a valuable experimental organism to study SAC regulation during embryogenesis.

Keyword: Mitosis, Spindle assembly checkpoint, Aneuploidy, Chordates, Nocodazole, Embryo

Résumé

Le point de contrôle du fuseau mitotique (*Spindle Assembly Checkpoint* : SAC) retarde l'anaphase jusqu'à ce que tous les chromosomes soient attachés correctement aux microtubules. Le SAC permet ainsi d'éviter des erreurs de ségrégation des chromosomes aboutissant à des cellules filles aneuploïdes (i.e. avec un nombre anormal de chromosomes). L'aneuploïdie, délétère pour les cellules, peut entrainer des problèmes de développement et est observée dans les cancers. Cependant, chez certaines espèces, le SAC n'est pas efficace au cours de la phase précoce du développement embryonnaire.

J'ai mis en évidence que chez l'ascidie *P. mammillata*, un organisme marin du groupe des chordés, le SAC devient efficace au 8ème cycle cellulaire et son efficacité augmente dans les cycles suivants. J'ai démontré qu'en partie ventrale l'identité des cellules antérieures induisait la présence d'un SAC plus efficace mais que d'autres facteurs modulaient aussi l'efficacité du SAC.

J'ai étudié les mécanismes moléculaires impliqués dans les variations de l'efficacité du SAC au cours du développement. Mes expériences ont révélé la présence des composants du SAC tout au long de l'embryogenèse. Cependant, j'ai pu montrer que les protéines du SAC ne se localisent pas au niveau des kinétochores lorsque le SAC est inefficace au début du développement mais qu'elles s'y localisent bien dans l'ovocyte en méiose et dans l'embryon plus tardif, lequel se caractérise par un SAC actif.

Ma thèse a permis de montrer que *P. mammillata* est un organisme expérimental de grand intérêt pour l'étude du SAC au cours de l'embryogenèse.

Mot-clé : Mitose, Point de contrôle du fuseau mitotique, Aneuploïdie, Chordé, Nocodazole, Embryon

Acknowledgments / Remerciement

First of all, I would like to thank all my jury members for agreeing to look through my work and evaluate it.

Aude Dupré merci pour vos conseils au cours des comités de thèse, c'est un plaisir de vous montrer jusqu'où ma thèse m'a menée.

Roger Karess, I discovered the SAC in your team and it's an honor to have you to judge my work.

Eric Thompson thank you for agreeing to be a reporter bringing a tunicate eye on the project.

After 3 years and more than 5207 mitosis analyzed, I have so many people to thank for helping me pursue my thesis and I hope I won't forget too many.

Stefania and Elisabeth thank you for taking me in your team and for teaching me so much during these 3 years. The time spent in the team was like a fairy tail with thousand and one species.

Stefania you were always available and listening thanks a lot. Thank you for taking so much of your time to improve this manuscript, I learned a lot in scientific English writing thanks to you. Thank you for giving me the possibility to go to so many meetings where I heard and met incredibly smart and nice scientist.

Elisabeth, merci de m'avoir accompagnée, soutenue et d'avoir enduré mon français.

Lydia, je n'aurais pas pu faire cette thèse sans toi. Merci pour toutes les techniques que tu m'as enseignées et merci d'avoir pris la relève quand j'étais sur le point de devenir *Mad* avec mes clonages. Bravo pour ta persévérance avec Bub1. Merci aussi pour les expériences que tu as faites pour moi.

Merci à l'ensemble de l'équipe ABC pour m'avoir tout enseigné, depuis les bases, sur le travail avec ce joli mdm. Sans vous, *P. mammillata* serait resté une illustre inconnue.

Janet, there is so much to say even if you think you did nothing!! Thank you for having been a wonderful tutrice aussi bien en sciences qu'en franglais. Merci pour tes 42 idées nouvelles par semaine (pour ne pas dire jour), il ne me reste plus qu'à trouver la question.

Merci à Gérard et Céline pour la bonne humeur matinale et l'ambiance musicale du matin (je n'oublierai jamais la fois où ce fut *Mélanie*). Céline, merci aussi pour tes conseils, tu m'as montré *le chemin* plus d'une fois. Merci pour tes discussions légères et ton rire quand j'étais prête à *toute envoyer en l'air*.

Remi, j'aurais bien eu du mal à réaliser ce projet si tu n'avais pas eu l'idée d'utiliser le NLS et si tu ne nous avais pas passé la construction, merci beaucoup ! Et merci pour l'image du tadpole (Fig. 12D).

Alex, you tought me a lot about ascidian and cell cycle, you showed me that there was a difference in SAC along the anteroposterior axis in my movies, thanks a lot. Thank you also for showing me how "easy" it is to perform pole ablation of *P. mammillata* eggs. After several months, yoga and diving lessons to help me relax and control my breath, I almost agree!

Genia, where would I be without you? You literally drive me so much thanks a lot!

Anne cela a fait du bien d'avoir quelqu'un à la mezza qui puisse à la fois s'amuser avec les lignes de commandes et s'émerveiller devant la structure d'une cellule !

Isa tu as été un professeur, un mentor, une amie… tu nous as montré à nous autres thésardes qu'il était possible d'arriver au bout and *break free*.

Mon temps passé au LBDV aurait été bien différent sans toi Sophie. Je n'aurais pas risqué de mourir de froid en février mais aurais sûrement écopé d'une piqure de méduse s'y elles ne fuyaient pas par peur que tu les découpes. Je n'aurais pas été fanny 2 ans de suite mais plutôt trois ! Je n'aurai probablement pas une aussi bonne capacité à suivre un protocole/recette. Tout se monnaye…. en chocolat ou gâteau ! Et je n'aurais pas su glisser aussi bien entre les embuches de l'administration. Merci d'avoir galéré juste avant moi.

David, Anna now it is your turn to face the depth of French administration but I have no doubt that you will come back on the surface of this sea of paper.

Julia ton passage fut bref mais intense, merci d'avoir ouvert mon esprit sur de nouveaux sujets.

Maciek, you made me discover how pretty the ctenophors are, thanks for that.

Isabella it was so great to meet you.

Adrien tu as rejoint la mezza au pire moment, merci pour ton aide pour la gène ontologie.

Angelica each time you come it is an event as big as Christmas!

Manon, merci de m'avoir fait découvrir un coin d'Irlande en PACA , désolée, mais sérieusement ce fut un chouette moment !

Merci à tous les membres de la mezza passé, présent et futur. Merci à tous ceux qui ont permis au yogras de prendre une place si important dans ma vie !

En particulier, merci à Coralie pour tes cookies, ils resteront dans mon cœur (et pas que/ qu'eux) à jamais.

Je ne sais pas si je dois dire merci au fantôme pour avoir gardé mon âme d'enfant mais dans la peur d'être hantée je préfère. Merci pour cette parfaite ambiance de travail (sauf à 17h et en cas d'orage).

Lucas, des fois je me demande comment tu fais pour survivre au-dessus de nos têtes, bravo et merci !

Thank you also jean Maetzien for joining us every now and then.

Marta, you are always so nice, How do you do!?

Cat, Laurel, Marion, Geraldine, Manon (bienvenue à la mezza), I don't know you well and I have the feeling that I miss so much.

Mébarek mille mercis pour tes réponses à mes milles question (au moins) de microscopie, j'aurais été bien perdue sans toi. Merci à Sameh d'avoir pris la relève. Avec vous les microscopes sont en bonne compagnie.

Philippe merci de m'avoir aidée à danser au milieu de mes séquences et ligne de code, avec toi, on est en sécurité.

Merci au reste des I^4, en particulier Faisal et ton thé.

Laurent, Loann, Alex merci à vous qui vous occupez si bien de toutes nos bestioles ! Alex merci aussi d'avoir su montrer à quels points les *P. mammillata* sont belles entre vos mains et de me permettre de le montrer à tous (Fig. 12A).

Richard thank you for looking into *P. mammillata* genome for SAC genes.

Cathy merci de m'avoir montrée comment utiliser Imaris.

Thank you to Yas, Clare and Alex Allié for your advice as wise tunicates people.

Guy, le LBDV serait morcelé sans toi pour nous réunir autour des Capricorniens, de la sardinade, nous faire chanter … je compte sur toi pour ressusciter le pétanque cake !

Merci à Frederick et Christelle pour toute la gestion que vous faites.

Merci à tous les membres du LBDV qui font de cette place un lieu idéal pour faire une thèse sur le plan scientifique tout en garantissant notre parfaite santé mentale.

Et merci à tous ceux chez qui j'ai fait du couch surfing, Céline/Joëlle/Gaufrette, Isa, Sophie,… pour sûr je suis devenu très douée dans ce domaine !

I did not know so much the other members of IMEV but the time I crossed you was nice. Especially for the Indie Hop and Yoga, thank you Olivier, Laurent, Ann, Amélie, Manon, encore un Alex et tant d'autres.

Merci à ceux croisés sur le ponton d'avoir ensoleillé mes pauses repas, en particulier à toi Marine.

Merci au corbeau qui avait la clé du savoir.

Merci à toute l'équipe de Rand'eau evasion en particulier Bastien, Gaël et Judicaël avec qui j'ai découvert les fonds marins, ce qui est plutôt chouette quand on fait une thèse à l'institut de la mer de Villefranche sur mer. Grâce à vous je ne me suis pas noyée dans le stress de l'écriture de ce manuscrit !

Merci au genetic furious d'avoir été à mes côtés depuis la L3. Une petite pensée pour vous parce-que faire sa thèse, c'est partout pareil mais il n'y a pas partout la mer. Désolée !

21 décembre 1993, maternité René Dubos, 14 heures moins trois, j'arrive sur cette terre, je n'y vois pas bien clair, Ils viennent de me donner la vie, Merci, A tous les deux. Merci d'avoir su quand venir me voir mais aussi quand ne pas venir . Merci d'avoir toujours été là ! Vous êtes les meilleurs.

Merci aussi à mon grand bout, si écrire sa thèse c'est comme donner naissance, j'avais la meilleure sage-femme pour m'accompagner ! Merci aussi de me rappeler que la vie c'est Peanuts sans toi !

Last but not least, thank you to all the *Phallusia mammillata* that allowed me to pursue my project. With 441 embryos used only to assess mitotic duration, nothing would have been possible without them.

Table of contents

Table of figures

Abbreviation and acronyms

A
APC: Adenomatous polyposis coli
APC/C: Anaphase promoting complex or cyclosome

B
Bub1: Budding uninhibited by benzimidazoles 1
Bub3: Budding uninhibited by benzimidazoles 3
BubR1: Budding uninhibited by benzimidazoles Related 1, also called Bub1B

C
CCAN: constitutive centromere associated network
Cdc20: Cell division cycle protein 20, also called fizzy, Slp1 or $p55^{CDC}$
Cdc25: Cell division cycle protein 25
Cdh1: Cdc20 homolog 1 also called Hct1, Fizzy related 1, Ste9 or Srw1
Cdk1: Cyclin dependent kinase 1, also called cdc2, p34 or cdc28
CSF: cytostatic factor

D
DDR: DNA damage response
DN: dominant negative form of a protein
DNA: deoxyribonucleic acid
Dvl: Dishevelled
dpERK: di-phosphorylated ERK

E
ERK: Extracellular signal regulated kinases

F
Fog: Friend of gata
FoxA-a: Forkhead box A-a
FPKM: fragments per kilobase million

G
GF: glycerol formaldehyde
GSK: Glycogene synthase kinase
GVBD: germinal vesicle breakdown

K
KMN complex: KNL1-MIS12-NDC80 complex
KNL1: Kinetochore null protein, also called CASC5, blinkin, AF15q14, Spc7 or Spc105

M
Mad1: Mitotic arrest deficient 1
Mad2: Mitotic arrest deficient 2
Mad3: Mitotic arrest deficient 3
MAPK: mitogen-activated protein kinase
MAPKK: mitogen-activated protein kinase kinase
MAPKKK: mitogen-activated protein kinase kinase kinase
MBT: Mid Blastula Transition
MEK: MAPK/ERK Kinase

MCC: mitotic checkpoint complex
MFSW: microfiltered sea water
MIS12: Missegregation 12
MPF: maturation promoting factor, correspond to Cyclin B1-Cdk1
Mps1: Monopolar spindle 1, TTK or Mph1
MYT1 or PKMYT1: Protein kinase, membrane associated tyrosine/threonine 1
MZT: maternal to zygotic transition

N
Ndc80: Nuclear division cycle 80, also called Hec1
NEB: nuclear envelope breakdown
NER: nuclear envelope reformation

P
PB: polar body
PBS: Phosphate-buffered saline
PBSTw: PBS with 0.1% Tween 20
PCM: pericentriolar material
PCNA: proliferating cell nuclear antigen
pH3: phosphorilation of histone 3
Plk1: Polo like kinase 1, also called Polo, Cdc5 or Plo1
PP1: phosphoprotein phosphatase 1, also PPP1
PP2A: phosphoprotein phosphatase 2A, also PPP2A

R
RNA: ribonucleic acid
RPKM: reads per kilobase million
RT: Room temperature
RZZ: Rod-ZW10-Zwilch

S
SAC: spindle assembly checkpoint, also called mitotic checkpoint
Sgo: shugoshin
SSC: saline sodium citrate
sFRP1/5: secreted Frizzled Related Protein orthologue to vertebrate gene 1 and 5

T
TBS: Tris-buffered saline
TBSTw: TBS with 0.1% Tween 20
TCF: T-cell factor
TLE: Transducing like enhancer of split
TRIP13: AAA-ATPase Thyroid hormone receptor interacting protein 13

W
WNT: Wingless Int

Z
ZW10: Zeste White 10
ZWINT: ZW10 interacting kinetochore protein

Long résumé français

Introduction :

Le point de contrôle du fuseau mitotique, en anglais : *Spindle Assembly Checkpoint* (SAC), retarde l'anaphase tant que tous les chromosomes ne sont pas attachés correctement aux microtubules du fuseau (Jia et al., 2013; Musacchio and Salmon, 2007). Le SAC empêche ainsi des erreurs de ségrégation conduisant à la transmission d'un nombre anormal de chromosomes aux cellules filles. Ce type d'anomalie chromosomique s'appelle **aneuploïdie**. L'aneuploïdie est délétère pour les cellules et peut conduire à des anomalies au cours du développement allant jusqu'à induire la mort embryonnaire. En cas de mutation des gènes du SAC, la fréquence d'aneuploïdie augmente, un phénomène notamment observé dans des cancers humains (Chunduri and Storchová, 2019; Zhu et al., 2018).

Le **SAC** est composé de six protéines, Mps1, Bub1, BubR1, Bub3, Mad1 et Mad2 (Jia et al., 2013; Musacchio and Salmon, 2007). En prométaphase, ces protéines ont la capacité de se localiser au niveau des kinétochores, un complexe protéique situé aux centromères des chromosomes. Cette localisation des protéines du SAC aboutit à la formation d'un complexe, appelé *mitotic checkpoint complex* (MCC), qui séquestre Cdc20, une protéine requise, en association avec l'APC/C, pour l'entrée en anaphase. En conséquence, dans cette configuration, la transition métaphase-anaphase est empêchée. Lorsque l'attachement des kinétochores aux microtubules est réalisé correctement, la délocalisation des protéines du SAC est induite conduisant à l'inactivation du point de contrôle. Cdc20 est libre et active l'APC/C induisant l'entrée en anaphase suivie de la sortie de mitose (Jia et al., 2013; Musacchio and Salmon, 2007).

Le SAC est un mécanisme conservé chez la majorité des eucaryotes. Il a été largement étudié dans les cellules somatiques de nombreuses espèces. Cependant, des modulations de l'efficacité du SAC sont observées au cours du développement de certains métazoaires et leur cause est encore mal connue. Chez les chordés qui ont été étudiés et à l'exception des mammifères, le **SAC** n'est pas ou peu efficace lors des premiers cycles cellulaires ne devenant efficace que plus tard dans l'**embryogenèse** (Chenevert et al., 2019). Au sein de l'équipe nous cherchons à comprendre les causes de ces variations d'efficacité du SAC au cours de l'embryogenèse.

Parmi les chordés, j'ai utilisé comme organisme d'étude ***Phallusia mammillata*** appelé aussi ascidie blanche (Holland, 2016; Lemaire, 2011). *P. mammillata* est un organisme marin qui appartient au groupe des tuniciers et qui est notamment présent en Méditerranée. Ces embryons sont disponibles en grand nombre et ils sont transparents de la fécondation à la métamorphose. Les données publiées et les résultats de l'équipe disponibles au début de ma thèse montraient que le SAC était inactif en méiose et au stade 2 cellules chez *P. mammillata*. Pour ces raisons, *P. mammillata* nous a paru un modèle intéressant pour l'étude de la régulation du SAC lors du développement embryonnaire des chordés.

L'objectif de ma thèse a été de caractériser le SAC dans l'embryon précoce de *Phallusia mammillata* afin de mieux comprendre les mécanismes moléculaires qui régulent son efficacité.

Résultats :

Mon premier objectif a été de mesurer les variations d'efficacité du SAC au cours du développement de *P. mammillata*.

Afin de **déterminer l'efficacité du SAC,** j'ai induit des défauts au niveau du fuseau en perturbant la dynamique des microtubules par exposition au nocodazole, ce qui est connu pour activer le SAC (Vasquez et al., 1997). En effet dans ces conditions, les chromosomes ne peuvent être attachés correctement aux microtubules générant le signal nécessaire à l'activation du SAC. En conséquence le SAC empêche l'entrée en anaphase induisant un allongement de la durée de la mitose. Plus cet

allongement est important, plus le SAC est considéré comme efficace. J'ai donc mesuré la durée de la mitose en présence, ou non, de nocodazole au cours du développement de *P. mammillata,* de l'œuf au stade neurula.

J'ai ainsi pu montrer que chez *P. mammillata* la durée de la mitose n'augmente en présence de nocodazole qu'à partir du 8ème cycle cellulaire ce qui correspond au stade gastrula. Cet allongement s'accroît au cours des cycles cellulaires suivants (9ème et 10ème). Afin de démontrer l'implication du SAC dans ce prolongement de la mitose, j'ai réalisé la même expérience, en inhibant le SAC, soit via la réversine, un inhibiteur de Mps1 (kinase du SAC activant les autres protéines du SAC) (Santaguida et al., 2010), soit via l'expression d'une forme dominante négative de Mad2 (protéine du SAC séquestrant Cdc20 l'empêchant d'induire l'entrée en anaphase) (Wassmann et al., 2003a). Dans ces deux conditions, aux 8ème et 9ème cycles cellulaires l'exposition au nocodazole entraînait un moindre allongement de la mitose en cas de perte des microtubules alors qu'aucun changement de la durée de la mitose n'était observé au 2ème cycle cellulaire. En conclusion, **le SAC est efficace chez *P. mammillata* à partir du 8ème cycle cellulaire.**

Au stade neurula (9ème cycle cellulaire), j'ai pu déterminer qu'en l'absence de microtubules, l'allongement de la mitose était moins important dans les cellules postérieures que dans les cellules antérieures de l'ectoderme ventral de l'embryon. J'ai fait l'hypothèse que cette différence d'efficacité du SAC le long de l'axe antéropostérieur était associée à une différence d'identité cellulaire. En effet, il a été montré dans l'embryon de *C. elegans* que les cellules de la lignée germinales présentaient un SAC plus efficace comparé aux autres cellules de l'embryon indiquant un lien entre identité cellulaire et efficacité du SAC (Gerhold et al., 2018). Pour tester le rôle de l'identité cellulaire dans l'efficacité du SAC chez *P. mammillata*, j'ai appliqué la même approche expérimentale à un embryon dont l'axe antéropostérieur avait été perturbé au moyen de deux méthodes.

La première méthode était basée sur l'**expression ectopique dans l'ensemble des cellules ventrales de FoxA-a**, un facteur de transcription connu pour induire l'identité antérieure chez une autre ascidie *C. intestinalis* (Lamy et al., 2006). J'ai pu montrer par hybridation *in situ* pour le marqueur spécifique de l'ectoderme antérieur sFRP1/5 que, comme chez *C. intestinalis*, la surexpression de FoxA-a conduit à une antériorisation des cellules postérieures chez *P. mammillata*. Suite à l'ajout de nocodazole au 9ème cycle cellulaire, la durée de la mitose dans les embryons surexprimant FoxA-a est plus grande que dans les embryons sauvages. Ceci indique que l'antériorisation des embryons est associée à un renforcement de l'efficacité du SAC. Ces résultats suggèrent **un lien de cause à effet entre l'identité cellulaire selon l'axe antéropostérieur et l'efficacité du SAC chez *P. mammillata*.**

La seconde méthode utilisée a été **l'ablation du premier pôle de contraction de** l'embryon observé peu après fécondation. Le premier pôle de contraction situé au pôle végétal de l'ovocyte est le résultat d'une série de mouvements qui localisent les facteurs impliqués dans la mise en place de l'axe antéropostérieur. Il a été suggéré que l'altération du développement des embryons due à l'ablation du pôle de contraction correspondait à une perte de la structuration de l'axe antéropostérieur (Dumollard et al., 2017; Nishida, 1996). Les embryons se développant suite à la réalisation de l'ablation du premier pôle de contraction sont appelés **VC-déficients** (VC de l'anglais « *vegetal cytoplasm* »). Des expériences d'hybridation *in situ* pour le marqueur des cellules ectodermiques antérieures sFRP1/5 m'ont permis de montrer que les embryons VC-déficients étaient, comme prédits, antériorisés. J'ai alors analysé la durée de la mitose dans ces embryons exposés au nocodazole à un stade équivalent au stade neurula déterminé par le temps post-fécondation et le nombre de cellules des embryons. Contrairement à mes attentes au vu des résultats obtenus avec la surexpression de FoxA-a, les embryons VC-déficients présentent un SAC de plus faible intensité que les cellules antérieures des embryons control et même que leurs cellules postérieures. J'ai donc supposé **qu'un autre paramètre empêchait le renforcement de l'efficacité du SAC** tel qu'observé dans les embryons sur-exprimant FoxA-a.

Il a été montré, notamment chez *C. elegans* (Galli and Morgan, 2016; Gerhold et al., 2018), qu'un **volume cellulaire** important pouvait diluer le signal du SAC réduisant son efficacité. De plus, j'ai constaté que les cellules des embryons VC-déficients tendent à être plus grandes que les cellules

ectodermiques des embryons d'un même stade. Cette différence étant probablement due au fait que les divisions sont symétriques dans les embryons VC-déficients et asymétriques dans les embryons contrôles. Dans les embryons contrôles, je n'étudie qu'un nombre limité de type cellulaires qui n'inclut pas les cellules à destin musculaire dont le volume cellulaire est le plus important pour les cellules d'un stade embryonnaire donné. Sur la base de ces informations, j'ai donc supposé que chez les embryons VC-déficients le SAC était plus actif du fait de l'identité antérieure mais ne paraissait pas plus efficace que dans les embryons contrôles car le signal était plus dilué. Pour tester cette hypothèse, j'ai utilisé le fait qu'au cours du développement embryonnaire, les cellules cyclent sans croissance et donc que le volume des cellules diminue à chaque mitose. J'ai ainsi pu montrer que les cellules des embryons VC-déficients du 10ème cycle cellulaire présentaient un SAC d'intensité comparable aux cellules antérieures des embryons contrôles du 9ème cycle qui sont de taille similaire. **Le volume apparait donc comme un paramètre pouvant jouer sur l'efficacité du SAC dans ces circonstances expérimentales.** Cependant, d'autres paramètres peuvent avoir été affectés par l'ablation du 1er pôle de contraction entrainant le retard d'un cycle de l'augmentation d'efficacité du SAC attendue du fait de l'antériorisation (voir discussion).

Mon deuxième objectif était d'investiguer les mécanismes moléculaires impliqués dans les variations d'efficacité du SAC au cours de l'embryogenèse de *P. mammillata*.

Dans un premier temps, j'ai recherché **les gènes codant pour les protéines du SAC** (Mps1, Bub1, BubR1, Mad2, Mad1 et Bub3) dans les deux génomes disponibles pour *P. mammillata.* En accord avec les résultats publiés pour une autre ascidie *C. intestinalis*, BubR1 est absent chez *P. mammillata* (van Hooff et al., 2017; Suijkerbuijk et al., 2012). L'absence de BubR1 affectant similairement toutes les cellules de tous les stades du développement de *P. mammillata*, son absence ne peut expliquer les variations dans l'efficacité du SAC. Cependant, Le rôle de BubR1 étant de renforcer la capacité de Mad2 à inhiber Cdc20 prévenant l'entrée en anaphase, il est probable que l'effet maximum du SAC soit plus faible qu'il ne l'aurait été en présence de BubR1. Il est aussi possible que Bub1, le paralogue de BubR1, pallie à son absence. Mise à part l'absence de BubR1, je n'ai pas observé de changement majeur dans la séquence des protéines du SAC que j'ai analysées, en particulier vis-à-vis de leurs différents domaines protéiques et sites de modifications post-traductionnelles.

Dans un second temps, j'ai donc étudié les éléments connus pour être nécessaires à l'activité du SAC pour voir si l'un d'eux était modifié au cours de l'embryogenèse de *P. mammillata* en lien avec les variations d'efficacité du SAC.

L'inefficacité du SAC pourrait être expliquée par l'absence d'une ou plusieurs des protéines appartenant au point de contrôles. J'ai d'abord approché cette question en utilisant les données transcriptomiques disponibles dans la base de données Aniseed (Brozovic et al., 2018) bien que la régulation des protéines puisent avoir lieu au niveau traductionnel. Les **transcrits codant pour les protéines du SAC** (Mps1, Bub1, Mad2, Mad1 et Bub3) sont présents au stade où le SAC est inefficace (64 cellules) ainsi qu'aux stades où le SAC est efficace (gastrula précoces, mi-gastrula, mi-neurula, mi-tailbud et têtard). J'ai complété ces informations avec des expériences d'hybridations *in situ* de l'œuf au têtard et n'ai pu voir aucun signe d'une régulation de l'activité du SAC au niveau de l'ARN. J'ai continué cette étude au niveau protéique par western blot mais l'absence d'anticorps commerciaux reconnaissant les protéines de *P. mammillata* a limité l'analyse à Mad1 et Mad2 pour lesquels nous avons fait générer des anticorps. J'ai ainsi pu voir que **les protéines Mad2 et Mad1** sont présentes à des niveaux comparables au long du développement alors que les stades précoces ont un SAC inefficace et les stades tardifs disposent d'un SAC efficace. Par ailleurs, la **surexpression des protéines** du SAC Mad2, Mad1, Bub3 ou Mps1, ne perturbe pas le développement embryonnaire de *P. mammillata*. De plus, la surexpression de Mad2 n'affecte pas la durée de la mitose et n'augmente pas l'efficacité du SAC au 8ème cycle cellulaire. Ceci suggère que **le manque d'efficacité du SAC n'est pas dû à l'absence d'une des protéines du SAC.** Afin de complétement exclure un contrôle de l'efficacité du SAC par la régulation de l'abondance de ces composants, il serait nécessaire de tester l'effet de la

surexpression de Bub1 et de la co-surexpression des cinq protéines sur le développement et sur la durée de la mitose.

Au-delà de la simple présence des composants du SAC, leur **organisation en complexe** est importante ainsi les interactions entre les protéines Mad2 et Mad1, puis Cdc20 sont nécessaires à la signalisation du SAC. Ces interactions ont été testées par double hybride dans la levure ce qui a permis de montrer qu'elles sont bien fonctionnelles.

Lorsque le SAC est inefficace, il est possible qu'à un niveau de la cascade de signalisation, le signal soit interrompu *in vivo*. Pour déterminer si cela était le cas, j'ai analysé en premier lieu **la localisation des protéines du SAC aux kinétochores lorsque ceux-ci ne sont** pas attachés aux microtubules. Cette localisation est en effet indispensable à leur activation (Jia et al., 2013; Musacchio and Salmon, 2007). Dans l'œuf arrêté en méiose (SAC inefficace) traité avec du nocodazole, les protéines du SAC Mps1, Mad1 et Mad2, mais pas Bub3, fusionnées à un tag fluorescent se localisent, comme attendu en l'absence de microtubules, au niveau des chromosomes. Tandis qu'en mitose, les résultats préliminaires d'immunofluorescence montrent que Mad1 se localise aux kinétochores en présence de nocodazole aux stades tardifs quand le SAC est efficace mais pas aux stades précoces quand le SAC est inefficace. **Le manque d'efficacité du SAC au cours des premiers cycles cellulaires semble donc dû à un défaut d'activation du SAC suggérant une régulation en amont du mécanisme.** Ceci pourrait être confirmé en testant *in vivo* l'interaction de Mad2 avec Cdc20 qui prend place en aval de la localisation des protéines du SAC aux kinétochores.

Puisque la cascade de signalisation du SAC semble interrompue aux stades précoces dès son activation au kinétochores, j'ai cherché quelles protéines pouvaient être impliquées dans la régulation du SAC à ce niveau. D'une part, **ERK**, une MAPK (Mitogen-activated protein kinases), est capable de phosphoryler Mps1. Cette phosphorylation induit la localisation des protéines du SAC aux kinétochores non-attachés par les microtubules conduisant à l'activation du point de contrôle (Borysova et al., 2008; Zhao and Chen, 2006). D'autre part, ERK est hyperactif dans l'œuf non fécondé et est inactivé à la fécondation (Dumollard et al., 2011). A partir de ces informations, j'ai posé l'hypothèse qu'ERK était inactif dans l'embryon précoce empêchant l'activation du SAC et devenait actif au 8ème cycle cellulaire permettant l'acquisition d'un SAC fonctionnel.

Cependant, j'ai pu observer qu'ERK était activé au cours des deux premiers cycles cellulaires lors de l'entrée en mitose. De plus, l'inhibition d'ERK par l'ajout de U0126 un inhibiteur de MEK, la kinase activant ERK, (Dumollard et al., 2011) ne perturbe pas le déroulement de la mitose du 1er au 5ème cycle cellulaire et ne rallonge que légèrement (1,1 fois) la durée de l'interphase. **Mes expériences suggèrent que le manque d'efficacité du SAC au stade précoce n'est pas dû à une absence d'activité d'ERK**. Tester l'effet de la surexpression d'ERK sur la durée de la mitose et sur la fonctionnalité du SAC permettrait de conclure plus fermement sur le rôle d'ERK dans le contrôle de l'efficacité du SAC.

Afin de **rechercher des candidats potentiels pour la régulation du SAC** dans l'embryon de *P. mammillata*, j'ai réalisé une étude non biaisée basée sur la possible interaction entre ces régulateurs et Mad2. Pour cela, j'ai réalisé un extrait protéique d'œufs non fécondés traités au nocodazole et ai passé cet extrait sur une colonne d'affinité pour Mad2. Les protéines retenues de façon spécifique ont été identifiées par spectrométrie de masse et BLAST. Parmi cette liste, des candidats potentiels peuvent être retenus du fait de leur fonction en lien avec le déroulement de la mitose. C'est le cas notamment de la dyneine connue pour être impliquée dans l'inactivation du SAC lors de l'entrée en anaphase (Howell et al., 2001; Silva et al., 2014). De plus la présence de Cdc20 parmi ces protéines confirme que l'expérience permet d'identifier des protéines pouvant interagir avec Mad2.

Discussion :

Au cours de ma thèse, j'ai pu montrer que chez *P. mammillata* le SAC n'était efficace qu'à partir du 8ème cycle cellulaire et que cette acquisition impliquait probablement un changement dans la capacité de localisation des protéines du SAC aux kinétochores non-attachés aux microtubules.

En outre, lorsque le SAC est actif, l'identité cellulaire et le volume cellulaire influencent son efficacité. Ces différences d'efficacité du SAC aux stades tardifs ne semblent par contre pas être dues à une différence de la localisation des protéines du SAC et le mécanisme en cause doit encore être étudié. J'ai posé l'hypothèse que l'efficacité du SAC était contrôlée par les mêmes mécanismes que ceux impliqués dans la formation de l'axe antéropostérieur le long duquel ces différences sont observées. En effet, la surexpression de FoxA-a induisant une augmentation de l'efficacité du SAC, il est possible que ce facteur de transcription soit directement impliqué dans le contrôle du SAC. Par ailleurs, l'identité postérieure est définie par la voie WNT/β-catenin dont l'un de ces composants, GSK3, a été impliqué dans un renforcement de l'efficacité du SAC (Feinberg et al., 2019; Rashid et al., 2018). GSK3 est un inhibiteur de la voie WNT/β-catenin et est donc inhibé quand la voie est active. Il est donc possible que GSK3 soit en cause dans la présence d'un SAC plus efficace en antérieur qu'en postérieur. Finalement, la structuration de l'ectoderme le long de l'axe antéropostérieur nécessite des signaux de la part des cellules du pôle végétale. Ces mêmes signaux pourraient être en cause dans la différence d'efficacité du SAC observée le long de cet axe. En effet, ces cellules sont absentes dans les embryons VC-déficients et pourraient donc expliquer que le SAC soit de faible efficacité dans ces embryons bien que la majorité de leurs cellules aient acquis une identité antérieure (Takatori et al., 2007; Wada et al., 1999).

Les variations d'efficacité du cycle cellulaire au cours du développement et selon l'axe antéropostérieur pourraient aussi être dues aux changements de la durée de l'interphase ayant lieu au cours de l'embryogenèse. En effet, la durée de l'interphase augmente au cours du développement et est plus importante dans les cellules antérieures que dans les cellules postérieures passé le 8ème cycle cellulaire (Dumollard et al., 2013; Ogura and Sasakura, 2016; Ogura et al., 2011). Dans les deux cas, une interphase plus longue corrèle avec la présence d'un SAC plus efficace. Cette hypothèse pourrait aussi expliquer la présence d'un SAC de faible efficacité dans les embryons VC-déficients malgré leur antériorisation. Il est en effet possible que chez ces embryons VC-déficients l'interphase soit de durée égale ou plus petite que dans les cellules postérieures des embryons contrôles et donc nettement plus petites que dans les cellules antérieures des embryons contrôles.

Les résultats obtenus au cours de ma thèse nous ont permis de progresser dans notre connaissance fine des mécanismes moléculaires impliqués dans l'efficacité du SAC, point de contrôle important du cycle cellulaire et montrent que l'embryon de *P. mammillata* est une ressource très intéressante pour étudier cette question.

Summary

The spindle assembly checkpoint (SAC) has a key role to ensure mitotic fidelity by controlling proper chromosome attachment to spindle microtubules and to guarantee correct chromosome segregation. Despite this fundamental role of the SAC, previous work indicates that the SAC is not active in early embryos of several animal species. At the beginning of my PhD work, I participated to a comparative study aimed at analyzing SAC response in early embryos of animal representative of all the main animal groups. This work showed that while most metazoan species have an efficient SAC already from their first embryonic cell cycle, non-mammalian chordates only acquire an efficient SAC later in embryogenesis. These results constitute an article currently under revision (annex 4) and available in bioRxiv (Chenevert et al., 2019). Based on this preliminary work, the overarching question in my PhD work was to understand the underlying mechanisms controlling the switch in SAC activity in chordate embryos. Several hypotheses have been proposed to explain the lack of SAC activity during early development, but no clear answer is yet available. Among chordates *Phallusia mammillata* (*P. mammillata)* is a convenient organism to perform live and fix microscopy and for biochemical studies and we therefore decided to use this species as model organism.

The first aim of this work was to characterize the variation in SAC efficiency during *P. mammillata* embryogenesis by measuring the changes in mitotic duration in the absence of microtubules. I could show that as for *Xenopus laevis* and *Danio rerio* embryos, the SAC is inefficient in early embryos of *P. mammillata* but becomes efficient at gastrulation and its efficiency then increases in the following cell cycles. Moreover, I could show that the SAC response is more efficient in anterior than in posterior ventral ectoderm. I demonstrated that cell fate modulates SAC efficiency but is not enough to explain the difference in SAC efficiency observed along the anteroposterior axis indicating that other parameters are at play, one of which seems to be cell volume.

My second aim was to identify the molecular mechanisms underlying the change in SAC efficiency observed during *P. mammillata* development. I could show that SAC components are available throughout *P. mammillata* embryogenesis, including stages when the SAC is not efficient. SAC localization at kinetochores instead seems to correlate with SAC efficiency, suggesting that the regulation of the SAC takes place at the level of its activation at unattached kinetochores. I could rule out that the ERK pathway is involved in the lack of SAC efficiency in early embryos. Finally, I realized a proteomic analysis of proteins interacting with Mad2 to provide a list of candidates susceptible of influencing SAC activity.

The results of part I represent the main body of work of a manuscript which I will write as first author and whose title currently is "*P. mammillata* embryos acquire an active spindle assembly checkpoint at gastrulation and its efficiency depends on cell identity"

Introduction

I/ Mitosis at the heart of the cell cycle

A/An overview of the eukaryotic cell cycle

Cells are the basic building blocks of all living organisms. In eukaryotes, cells multiply by a process called mitosis, which leads to the division of the mother cell into two daughter cells. The events occurring between two subsequent mitoses constitute a cell cycle (Fig. 1), a sequence of events that allows the cell to duplicate its genome, grow and divide (Cooper, 2000). To ensure cell survival and the generation of a viable progeny, each daughter cell has to receive a full complement of chromosomes to maintain an unaltered set of genetic information. The chromosome number, consisting a set called ploidy, is specific to each species. Cells with a correct chromosome count are known as euploid, whereas cells with an abnormal chromosome number are aneuploid (Chunduri and Storchová, 2019; Zhu et al., 2018).

Aneuploidy is often associated with cellular and organismal defects whose characteristics depend on the affected chromosome and on the species. These defects are thought to arise from the unbalance in expression of the genes present on the extra chromosome, which often results in activation of the stress response pathway and reduction of cellular fitness (Chunduri and Storchová, 2019; Zhu et al., 2018). In budding yeast *Saccharomyces cerevisiae* (*S. cerevisiae)*, presence of extra copies of most of the 16 chromosomes slows down cell cycle progression. In *Mus musculus (M. musculus)* embryos, instead, chromosome gain usually results in faster cell cycle progression (Chunduri and Storchová, 2019; Zhu et al., 2018). Most aneuploidies are deleterious at the organismal level and during embryogenesis aneuploidy often results in embryonic death. In *Homo sapiens (H. sapiens),* for example, trisomies (extra copy of one chromosomes) of only 5 out of 24 chromosomes (22 autosome, X or Y) are viable (Chunduri and Storchová, 2019; Zhu et al., 2018). To reduce the incidence of aneuploidy and prevent cell and organismal lethality, cells have evolved control mechanisms along the cell cycle to protect DNA integrity and allow correct chromosome segregation (Cooper, 2000).

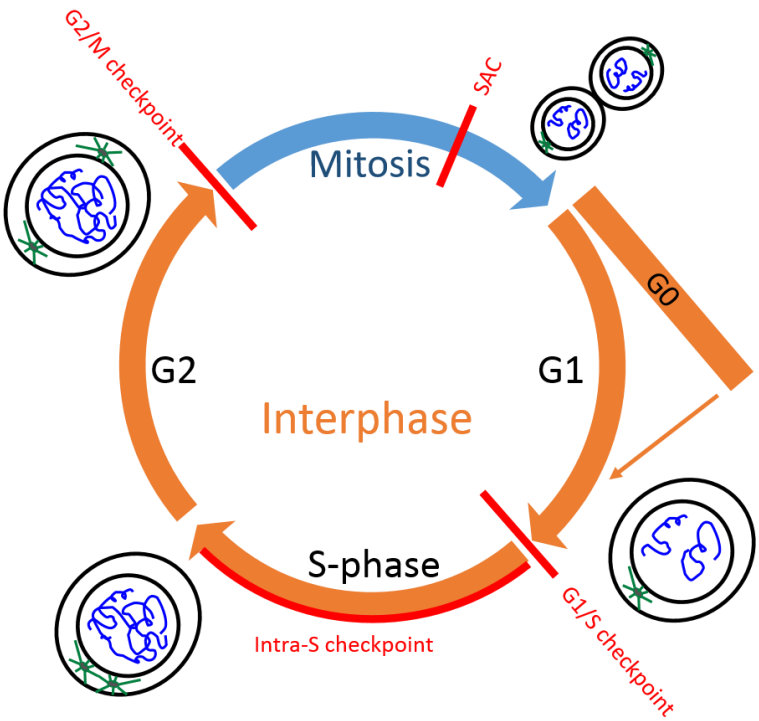

Figure 1 : The eukaryotic cell cycle

Schematic representation of the eukaryotic cell cycle with mitosis in blue, and interphase, including G0, G1, S and G2 phases, in orange. Checkpoints are indicated in red at the step when they can arrest cell cycle progression. Schematics of cells are drawn at the end of each phase with plasma membrane and nuclear membrane in black, chromosomes in blue and centrosomes and microtubules in green.

In eukaryotic cells, the cell cycle is divided into four main steps (Fig. 1): gap 1 (G1), synthetic (S) phase, gap 2 (G2), and mitosis or M phase (Cooper, 2000).

G1, S-phase and G2 together constitute interphase. During G1, the cell grows, produces and imports components and energy, generally acquiring all the elements necessary for cell cycling and especially for the following step, S phase (Cooper, 2000). During S-phase cells undergo DNA replication, resulting in a chromosome with two identical sister chromatids. Sister chromatids are held together until division by a multiprotein complex, called cohesin, composed of four components Smc1, Smc3, Scc1 and Scc2 (Nasmyth and Haering, 2009). The centrosome, the major microtubule organizing center (MTOC) is generally composed of two centrioles embedded in pericentriolar material (PCM). Like DNA, the centrosome duplicates once per cell cycle and its duplication starts during S-phase with the formation of a daughter centriole next to each existing one (Conduit et al., 2015). DNA replication is followed by the G2 phase, another highly metabolically active phase during which the cell continues to grow and produces all proteins required for mitosis. During G2, centrioles elongate to reach their definitive size forming two centrosomes which migrate toward the opposite poles of the nucleus (Cooper, 2000). Finally, during mitosis, sister chromatids segregate towards opposite poles of the cell, defined by the two centrosomes and the cytoplasm is divided during cytokinesis, generating two daughter cells. Daughter cells can then either enter another cell cycle or become quiescent entering an alternative stage called gap 0 (G0), (Cooper, 2000).

The smooth running of the cell cycle requires its different phases to be coordinated. In eukaryotes, the beginning of each cell cycle phase is linked to proper completion of the previous one, which is assessed by control mechanisms called checkpoints (Fig. 1). Checkpoints halt cell cycle progression until earlier processes in the cycle have been completed ensuring cells integrity (Barnum and O'Connell, 2014; Cooper, 2000).

The G1/S and G2/M checkpoints ensure that the cell contains all elements required for progression through S-phase and mitosis respectively and that a cell size sufficient for division has been achieved (Fig. 1). In addition, the two checkpoints are connected to the DNA damage response (DDR) pathway that controls DNA integrity to limit the accumulation of DNA breakages and base damages. The cell is constantly exposed to DNA damaging sources, both endogenous, such as free oxygen radicals produced by normal cell metabolism, and exogenous, such as ultraviolet light from the sun. Depending on the lesion, different branches of the DDR pathway are triggered. For example, in S and G2 phases single strand DNA breaks are detected by Chk1 which activates the G2/M checkpoint delaying mitotic entry (Barnum and O'Connell, 2014).

The intra-S checkpoint, instead, is triggered when replication forks are blocked by DNA damage, and avoids premature dismantling of replication complexes before completion of DNA replication, ensuring proper DNA replication in S phase (Fig. 1) (Barnum and O'Connell, 2014).

In my work I focused on the spindle assembly checkpoint (SAC), a control mechanism active during mitosis which ensures proper segregation of sister chromatids to the daughter cells (Fig. 1), (Barnum and O'Connell, 2014). In the next sections, I will provide a summary of the literature relevant to the spindle checkpoint and its modulation during embryonic development.

B/Mitosis

Mitosis which was described by Flemming in 1880 (Flemming, 1965) represents the final step of the cell cycle (Fig. 1). It is an accurate process that culminates in chromosome segregation and cell division. The heart of mitosis is the segregation of duplicated chromosomes, which relies on a complex and dynamic microtubule based structure known as the mitotic spindle (Fig. 2).

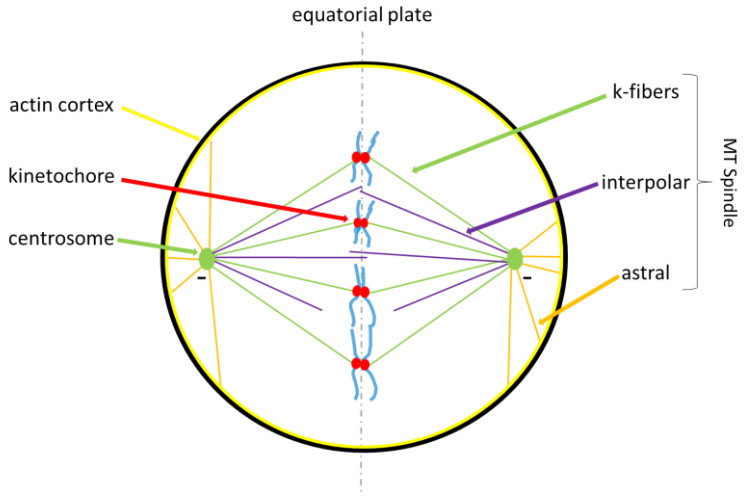

Figure 2 : Mitotic spindle.

The mitotic spindle allows chromosome segregation during mitosis. Microtubules (MT) of the spindle are organized in 3 groups: interpolar (purple), astral (orange) and k-fibers (green), that connect centrosomes (green disks) respectively to each other, to the actin cortex (yellow) and to kinetochores (red). Kinetochores are protein complexes localized at the centromere of chromosomes (blue). Kinetochore-microtubule attachment allows chromosome alignment on the equatorial plate (grey) prior to segregation. Minus end of microtubules (-), plasma membrane (black). Adapted from Meunier and Vernos, 2012.

During mitosis, microtubules, polarized polymers of α- and β-tubulin, are nucleated and organized into a bipolar structure by centrosomes located at opposite poles of the cell. The minus ends of microtubules are focused on the two spindle poles. Three classes of microtubules emanate from centrosomes forming the spindle: astral microtubules, interpolar microtubules and kinetochores fibers (k-fibers), (Fig. 2). Astral microtubules connect each centrosome to the cortex, an actin network present near the plasma membrane. Astral microtubules are involved in centrosome migration prior to mitotic entry and in spindle positioning. Interpolar microtubules connect the two centrosomes with each other and their plus ends overlap in the spindle midzone forming an antiparallel array. These microtubules contribute to spindle bipolarity and participate in chromosome movements. Kinetochore microtubules, or k-fibers connect the spindle poles to chromosomes and allow segregation of sister chromatids (Meunier and Vernos, 2012). K-fibers interact with chromosomes through a multiprotein complex, called the kinetochore which assembles on a specific region of the chromosome, known as the centromere (Fig. 2), (Cleveland et al., 2003).

Mitosis is divided in 5 main steps: prophase, pro-metaphase, metaphase, anaphase and telophase, each characterized by a specific set of events (Fig. 3).

During prophase chromosomes condense and centrosomes migrate to opposite poles of the cell. Microtubules start to be organized from the two centrosomes to form the mitotic spindle (Malmanche et al., 2006). The cohesin complex which keeps sister chromatids together, is removed from chromosome arms, leaving the chromatids attached exclusively in the centromeric area (Nasmyth and Haering, 2009). Prophase ends with nuclear envelope breakdown (NEB), marking entry into prometaphase (Fig. 3).

During prometaphase, microtubule k-fibers attach to kinetochores. Each kinetochore is attached to microtubules emanating from only one centrosome and sister chromatids are attached to microtubules coming from opposite poles. This results in bipolar attachment (bi-orientation), a condition mandatory for proper segregation of sister chromatids to the two daughter cells. Following attachment of kinetochores to spindle microtubules, chromosomes move to the spindle equator, a process known as chromosome congression and align on the equatorial plate, forming the metaphase plate (Jia et al., 2013; Malmanche et al., 2006; Meunier and Vernos, 2012; Musacchio and Salmon, 2007). This marks completion of the metaphase stage (Fig. 3).

Once all chromosomes are correctly aligned on the metaphase plate, the cell enters anaphase. Cohesin complexes still present in the centromeric region are cleaved by a protein called separase (ESPL1 in human), (Nasmyth and Haering, 2009), releasing sister chromatids which are segregated away from each other towards the spindle poles (Fig. 3). At this stage spindle elongation also contributes to chromosome segregation.

During the last phase of mitosis, telophase, the nuclear envelope reforms (nuclear envelope reformation, NER) around the segregated chromosomes which decondense, while spindle microtubules disassemble allowing the reformation of the interphase microtubule network (Fig. 3), (Malmanche et al., 2006).

Cytokinesis takes place in parallel with anaphase and telophase and results in the division of the cytoplasm to the two daughter cells. In animal cells, cytokinesis is driven by the constriction of an actomyosin ring. This process requires microtubules of the midzone, the region between segregating sister chromatids, which help positioning the actomyosin ring and participate in the ingression of the cleavage furrow. In addition, microtubules are required for the transport of vesicles toward the cleavage furrow. Sealing of the membrane, a process called abscission, completes mitosis, generating two daughter cells (Fig. 3), (Malmanche et al., 2006; Straight and Field, 2000).

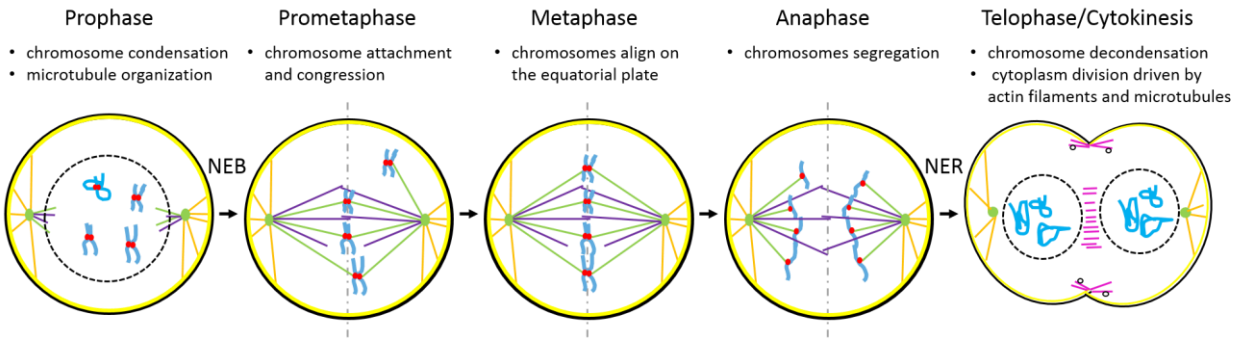

Figure 3 : Mitosis.

Schematic representation of the five steps of mitosis: prophase, prometaphase, metaphase, anaphase and telophase. Cytokinesis, which separates the two daughter cells, occurs in parallel with anaphase/telophase. NEB takes place at the end of prophase and NER in telophase. Membranes (black); chromosomes (blue); kinetochores (red); centrosomes (green disk); microtubules: interpolar (purple), astral (orange), k-fibers (green), microtubules required for the cytokinesis (pink); actin cortex (yellow); equatorial plate (grey). Cytokinesis adapted from Straight and Field, 2000.

C/ Molecular control of mitosis

Proper progression through the cell cycle and mitosis relies on a complex set of regulatory pathways. These mechanisms are mostly conserved between eukaryotes and therefore results obtained from different organisms can be merged to provide a general model which I introduce here focusing on mitosis in metazoan species, i.e. animals (Fig. 4).

The major regulators of the cell cycle are members of the Cyclin dependent kinase (Cdk) family, serine/threonine protein kinases whose activity requires their association with specific partners known as Cyclins. Binding to Cyclins increases Cdk activity by 40 000 folds and determines substrate specificity (Arellano and Moreno, 1997). Cyclins were first identified in the sea urchin *Arbacia punctulata (A. punctulata),* as proteins whose level changes during development in a cell cycle dependent manner (Evans et al., 1983). Cyclins were then identified in many other organisms as proteins regulated at the level of transcription, translation and degradation throughout the cell cycle. Changes in the availability of cyclins modulate the activity of Cdks allowing a precise control of the different cell cycle phases.

Mitotic entry and mitotic progression require only one Cdk: Cdk1, in association with two Cyclins: Cyclin A2 and Cyclin B1. Cyclin A2 can also interact with Cdk2, while Cyclin B1 interacts exclusively with Cdk1. The first evidence of the role of Cdk1 and Cyclin B1 in control of mitotic entry came from experiments carried out in *Xenopus laevis (X. laevis)*. Injection of cytoplasm from mitotic cells, but not from interphase cells, was able to induce NEB in immature *X. laevis* oocytes arrested in prophase of meiosis I. At the time it was hypothesized that a specific factor capable of inducing meiotic maturation, which was called maturation promoting factor (MPF), was present in mitotic cells (Wasserman and Smith, 1978). MPF was later identified as the Cyclin B1-Cdk1 complex, even though

Cyclin A2-Cdk1/2 was later shown to be also able to induce mitotic entry (Arellano and Moreno, 1997; Hégarat et al., 2016). Active Cdk1 is sufficient to induce all cellular changes taking place during mitosis: cytoskeleton rearrangements, chromosome condensation and NEB (Gavet and Pines, 2010).

The correct timing of mitotic transitions relies on tight control of Cdk1 activity whose activation depends on the accumulation of Cyclin A2 and Cyclin B1, and whose inactivation depends on their degradation (Fig. 4) (Hégarat et al., 2016; Wieser and Pines, 2015). Cyclin A2 accumulates starting from S-phase, while Cyclin B1 accumulates in G2. This temporal control of Cyclins accumulation is the result of regulation at the transcriptional and translational levels (Fig. 4B). *Cis*-regulatory elements present in the Cyclin promotor regions inhibit their transcription in G1. Cyclin A2 transcription is upregulated in S-phase and Cyclin B1 transcription in G2, allowing their accumulation. Cyclin A2-Cdk2 activity is required to promote transcription of Cyclin B1, explaining their sequential accumulation. In addition, Cyclin B1 transcription is inhibited by the DDR pathway, preventing mitotic entry in the presence of DNA damage (Fung and Poon, 2005).

The accumulation of Cyclin A2 and Cyclin B1 drives mitotic entry, whereas their degradation triggers the metaphase to anaphase transition. Cyclin degradation is mediated by the proteasome and is regulated by ubiquitination, a post-translational modification, which requires three enzymes E1, E2 and E3. Ubiquitin moieties carried by E1 are transferred to the E2 ubiquitin-conjugating enzyme, which with E3 forms a complex known as ubiquitin ligase. E3 interacts with the target and allows the transfer of the ubiquitin moiety from E2 to the target protein. E3 provides substrate specificity by recognition of specific degradation signals in the target protein. Proteins which are degraded during mitosis, like Cyclin A2 and Cyclin B1, are recognized by the multisubunit E3 ligase known as Anaphase-promoting complex or Cyclosome (APC/C) (Arellano and Moreno, 1997).

APC/C activity and specificity are regulated by two coactivators: cell division cycle protein 20 (Cdc20) and Cdc20 homolog 1 (Cdh1) (Musacchio and Salmon, 2007; Watson et al., 2019; Wieser and Pines, 2015). Cdc20 associates with APC/C in anaphase to induce chromosome segregation, while Cdh1 interacts with the APC/C from late anaphase to G1 and induces the cell changes required to reset the cell to an interphase state (Hégarat et al., 2016; Musacchio and Salmon, 2007; Wieser and Pines, 2015). Low APC/C-Cdc20 activity in prometaphase is sufficient to target Cyclin A2 for degradation which results in the inhibition of Cdk2. On the other hand, full activation of APC/C-Cdc20 in metaphase is required to induce the degradation of Cyclin B1 and Securin (Fig. 4C). Securin is an inhibitor of Separase which blocks its activation prior to metaphase, preventing precocious sister chromatid separation. Upon Securin degradation, active Separase cleaves the Scc1 subunit of Cohesin allowing sister chromatids to segregate away from each other (Arellano and Moreno, 1997; Wieser and Pines, 2015). In parallel, Cyclin B1 degradation leads to the inactivation of Cdk1. This reduction in Cdk1 activity relieves Cdh1 inhibition that in turn can interact with APC/C, targeting Cyclin B1 and Plk1 for degradation. APC/C-Cdc20 and APC/C-Cdh1 are also involved in the degradation of Geminin (Fig. 4). Geminin prevents untimely DNA replication before completion of mitosis by inhibiting the activity of the licensing factor Cdt1, which primes origins of replication (Clijsters et al., 2013; Qiao et al., 2010).

Mitotic entry and progression require then the coordinated control of Cyclin B1-Cdk1 and APC/C. Accumulation of mitotic cyclins in G2 requires the inhibition of APC/C. Therefore in G2 the interaction of APC/C with Cdc20 and Cdh1 is prevented respectively by Cyclin A2-Cdk2 and by Cyclin B1-Cdk1 (Fig. 4B), (Hein and Nilsson, 2016; Kramer et al., 2000; Yam et al., 2002). APC/C inhibition combined with up-regulation of protein synthesis in G2, ensures the accumulation of Cyclin B1 necessary to drive mitotic entry (Fig. 4B), (Hégarat et al., 2016; Wieser and Pines, 2015).

As Cyclin B1 accumulates, during interphase the level of Cyclin B1-Cdk1 complex increases. However, this complex is maintained in an inactive state until a threshold concentration required for mitotic entry is reached, preventing untimely mitotic commitment. The concentration of Cyclin B1 required for activation of the Cyclin B1-Cdk1 complex and mitotic commitment is higher than the amount required for mitotic progression, ensuring that the transition from interphase into mitosis is irreversible and once cells enter mitosis the division can be completed without early return to

interphase (Hégarat et al., 2016; Wieser and Pines, 2015). Precocious activation of Cyclin B1-Cdk1 in G2 is prevented by two kinases, Wee1 and Myt1 that phosphorylate Cdk1 on Threonine 14 (T14) and tyrosine 15 (Y15). At the end of G2, removal of these inhibitory phosphates by the phosphatases Cdc25 activates Cdk1 allowing mitotic entry (Fig. 4A and B) (Hégarat et al., 2016; Wieser and Pines, 2015).

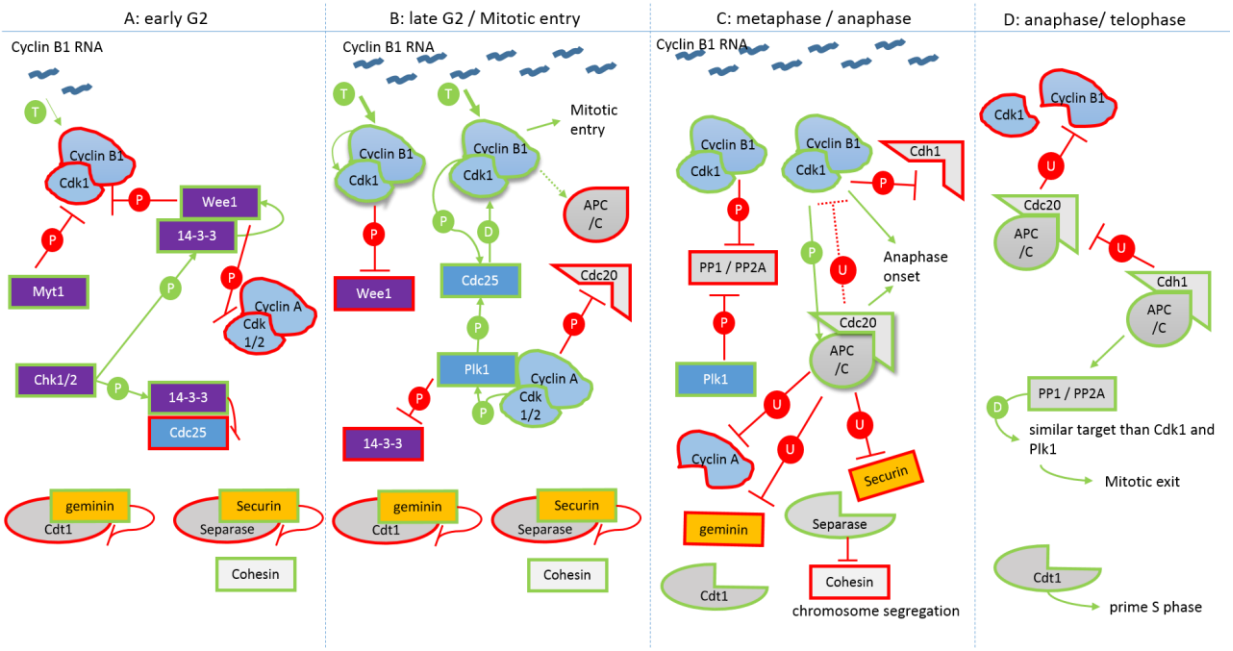

Figure 4 : Molecular control of mitotic progression

Mitotic entry and mitotic progression rely on the activity of the serine/threonine kinase Cdk1, whose activity depends on binding to its partner Cyclin B1. Cyclin B1 concentration is regulated by controlled transcription and translation (T) and APC/C-dependent proteolysis. Cyclin B1-Cdk1 activity is then regulated by phosphorylation (P). Four groups of proteins regulate mitotic progression and can be classified as: inhibitors of mitotic entry (purple), inducers of mitotic entry (blue), inhibitors of mitotic exit (orange) and inducers of mitotic exit (grey). These proteins can activate (green arrow) or inhibit (red bar) each other by phosphorylation (P), dephosphorylation (D), ubiquitination followed by degradation (U) or by direct interaction. These regulations can either inactivate (red border) or activate (green border) the target.

The switch mediated by Wee1, Myt1 and Cdc25 is subject to feedback regulatory loops that amplify Cyclin B1-Cdk1 activation to ensure commitment to mitosis (Fig. 4A and B). Cyclin B1-Cdk1 phosphorylates Wee1, promoting its own degradation, while Cyclin B1-Cdk1 mediated phosphorylation of Myt1, causes its inhibition. In human cells, Wee1 inhibition leads to Cyclin A2-Cdk1/2 activation, which in turn activates polo like kinase 1 (Plk1). Active Plk1 phosphorylates Cdc25, releasing it from its inhibitor 14-3-3. Cdc25 is also directly activated by Cyclin B1-Cdk1 (Fig. 4B). (Gheghiani et al., 2017; Hégarat et al., 2016). These critical feedback loops ensure a rapid and irreversible commitment to mitotic entry preventing Cyclin B1-Cdk1 inactivation before mitotic completion (Hégarat et al., 2016; Wieser and Pines, 2015).

The regulation of Wee1, Myt1 and Cdc25 integrates several signals coming from pathways assessing DNA integrity or cell size ensuring that cells enter mitosis only when they are ready to do so. For example, the G2/M checkpoint delays mitotic commitment until damaged or incompletely replicated DNA is repaired. The G2/M checkpoint controls Cdc25 via the kinases Chk1 and Chk2. Chk1/2 phosphorylation promotes binding of 14-3-3 to Wee1 and Cdc25. 14-3-3 binding inhibits Cdc25 but activates Wee1 preventing mitotic entry (Fig. 4A and B), (Hégarat et al., 2016).

Cyclin B1-Cdk1 also inhibits proteins that would otherwise counteract its own action (Fig. 4C). Among these proteins are the phosphatases PP1 and PP2A/B55 that dephosphorylate Cdk1 and Plk1 substrates, including Cdc25 (Gheghiani et al., 2017; Hégarat et al., 2016; Wieser and Pines, 2015). Inhibition of phosphatases PP1 and PP2A is relieved at mitotic exit following the fall in Cyclin B1-Cdk1 activity allowing dephosphorylation of Cdk1 and Plk1 substrates and mitotic exit (Hégarat et al., 2016; Wieser and Pines, 2015)

D/ Meiosis

1/ A specialized division

At the base of sexual reproduction are meiosis and fertilization. Meiosis enables a reduction in ploidy generating from one diploid cell, containing two copies of each chromosome, four haploid cells, each containing a copy of each chromosome. Conversely fertilization gives rise from the fusion of two haploid cells to a new diploid cell. These processes allow the mixing of genetic information increasing diversity between individuals (Gilbert, 2000a).

To obtain four haploid gametes, in meiosis, cells divide twice consecutively without intervening DNA replication. At meiotic entry, the mother cell contains two copies of each chromosome, known as homologous chromosomes or homologs, each composed of two sister chromatids. During the 1st meiotic division, called reductional, homologs are segregated to the two daughter cells, each receiving one copy of each chromosome. These cells enter directly the 2nd meiotic division, called equational, and separate sister chromatids as in mitosis, giving rise to four haploid cells (Alberts et al., 2002).

The 1st meiotic division starts with prophase I when meiotic recombination takes place. Meiotic recombination is triggered by DNA double strand breaks which generate single strand DNA extremities that allow DNA base pairing interactions mediated by sequence homology. These crossing over between homologs form chiasmata and can result in exchange of genetic information between homologous chromosomes. In addition, chiasmata hold the homologous chromosome together. These associated homologous chromosomes are called bivalents (Alberts et al., 2002). At NEB, microtubules attach to kinetochores but, differently from mitosis, kinetochores of one chromosome are attached to the same pole, giving rise to mono-oriented chromosomes. Kinetochores of homologs are attached to opposite spindle poles and the presence of at least one chiasma per pair guarantees alignment of bivalent on the equatorial plate (Alberts et al., 2002). At the onset of anaphase I, remaining chiasmata are resolved and the cohesin localized between homologous chromosomes is removed. This allows the segregation of homologous chromosomes to opposite poles, giving rise, in association with cytokinesis, to two haploid cells. These two cells directly enter prometaphase II, and undergo a division analogous to mitosis: kinetochores of sister chromatids attach to microtubules emanating from opposite spindle poles, cohesin is removed and sister chromatids segregate in anaphase II. With telophase II and a second cytokinesis, four haploid cells are obtained (Alberts et al., 2002).

2/ The oocyte

In animals, gametes are specialized into a large immotile female gamete, the oocyte, and a small motile male gamete, the spermatozoid. Oocytes carry all the elements required for early embryogenesis, including components required for energy production (glycogen, protein, lipid) which constitute the yolk and mRNAs required for early embryonic development, as transcription is silenced during the first cell cycles (Gilbert, 2000a).

During oogenesis, meiosis is slightly modified to produce only one gamete instead of four (Fig. 5). Both in meiosis I and meiosis II, cell division is highly asymmetric and one cell inherits most of the cytoplasm while the 2nd cell, called the polar body, receives only a set of chromosomes (Gilbert, 2000a; MacLennan et al., 2015).

This ultra-asymmetric division is not the only specificity of oogenesis. In most species, oocytes arrest twice while undergoing meiosis (Fig. 5). The 1st arrest happens in prophase I prior to NEB with assembled bivalents and a nucleus, called the germinal vesicle. This arrest is kept until a hormonal signal induces germinal vesicle break down (GVBD) (Extavour, 2009). The oocyte then progresses

through meiosis until a 2nd arrest. For vertebrates, this second arrest is in metaphase II (MacLennan et al., 2015) whereas in invertebrates, the oocyte does not always arrest at the same phase of the cell cycle prior to fertilization. In tunicates, eggs arrest in metaphase I, while cephalochordate eggs arrest in metaphase II and sea urchin and cnidarians eggs arrest in interphase following completion of meiosis (Fig. 5), (Costache et al., 2014; Dupré et al., 2011). Oocytes in their last arrest are called mature oocytes and are ready to be fertilized.

Meiotic progression relies mostly on the same control mechanisms as mitosis based on Cyclin B1-Cdk1 and APC/C, but additional mechanisms are present. Physiological signals induce the release from the primary arrest by causing a rise in MPF activity, active Cyclin B1-Cdk1 complex (Dupré et al., 2011). The secondary arrest relies on the stabilization of MPF activity by the cytostatic factor (CSF), a cytoplasmic activity first identified in frogs, capable of inducing a cell cycle arrest. The molecular components of CSF were later identified as the Mos/MAPK pathway (Dupré et al., 2011; Extavour, 2009; Gilbert, 2000a; Maller et al., 2002).

Mos was the first component of the CSF pathway to be identified in *X. laevis*. It fulfills all the criteria defining CSF activity: it accumulates during oocyte maturation, it is present in arrested oocytes, it disappears upon fertilization and it causes a cell cycle arrest when injected in mitotically dividing blastomeres. Further work then showed that in vertebrates the Mos-induced CSF arrest relied on the mitogen-activated protein kinase (MAPK) pathway, including MEK and Erk1/2. As for the other MAPK pathway, the ERK pathway comprises three kinases. A MAPKK-kinase (MAPKKK), Mos in oocytes, activates the MAPK-kinase (MAPKK) MAPK-ERK kinase (MEK) that activates extracellular signal regulated kinases (ERK), (Dupré et al., 2011; Extavour, 2009; Gilbert, 2000a; Maller et al., 2002). The Mos/ERK pathway phosphorylates $p90^{Rsk}$ which indirectly inhibits the APC/C, blocking oocyte meiosis in metaphase II for vertebrates and in metaphases I for tunicates (Costache et al., 2014; Maller et al., 2002). In other invertebrates, the Mos/ERK pathway was shown to have a similar CSF activity independently of the cell cycle stage at which the arrest takes place (Costache et al., 2014; Dupré et al., 2011).

In most species studied, sperm entry induces a Ca^{2+} wave at fertilization. This Ca^{2+} influx inactivates CSF allowing cells to restart the cell cycle and begin embryogenesis (Gilbert, 2000a; Maller et al., 2002).

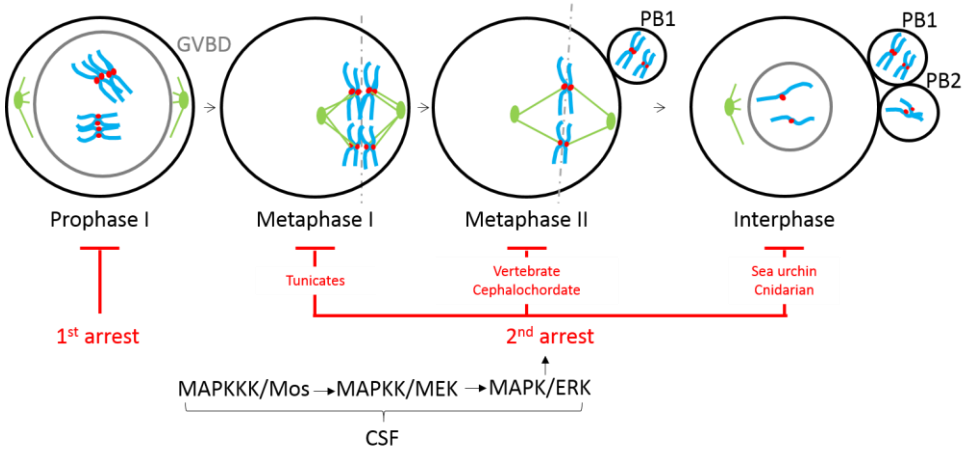

Figure 5 : Meiosis in oocytes

In oocytes, meiosis is asymmetric giving rise to only one gamete, the oocyte, and two polar bodies (PB). During oogenesis, meiosis is arrested first in prophase I prior to GVBD. A 2nd arrest induced by CSF is observed in most animals and occurs at a different stage depending on species. Some examples are indicated below each meiotic stage. Plasma membranes (black); nuclear membranes (grey), kinetochores (red), microtubules (green), equatorial plates (grey line), chromosomes (blue). Adapted from Costache et al., 2014 and Dupré et al., 2011.

II/ The Spindle assembly checkpoint (SAC)

A/ General information about the SAC

1/ A checkpoint is required in mitosis

Mitotic progression is controlled by modulation of Cyclin B1-Cdk1 and APC/C activities as introduced in the previous section. However, feedbacks from cellular events are also necessary to guarantee the completion of a step before the beginning of the following one. Based on the model provided in the previous section, APC/C-Cdc20 mediates proteasome degradation of its substrates at mitotic entry. In the absence of other regulatory mechanisms, therefore, the time available for chromosome alignment before anaphase onset corresponds to the time required to degrade Cyclin B1 and Securin (Wieser and Pines, 2015). In some species, like *Drosophila melanogaster (D. melanogaster*), it has been shown that this time is sufficient for cells to properly segregate their chromosomes, giving rise to a viable progeny (Buffin et al., 2007). However, in most cells, mitosis based only on Cyclins and Securin turnover leads to defects in chromosomes segregation and the generation of aneuploid cells (Fig. 6A), (Meraldi et al., 2004).

An additional layer of control is then necessary to delay APC/C activation from prometaphase to metaphase ensuring a sufficient amount of time for microtubules to attach to chromosomes. This additional layer is the SAC, also known as the mitotic checkpoint (Wieser and Pines, 2015). The SAC is also a quality control mechanism (Fig. 6B and C) and inhibits APC/C activation until all chromosomes are correctly attached to spindle microtubules, delaying the metaphase to anaphase transition (Fang et al., 1998). Consequently, the SAC increases the probability of correct chromosome segregation and the generation of euploid cells (Jia et al., 2013; Musacchio and Salmon, 2007; Wieser and Pines, 2015). The SAC is well conserved among eukaryotes and most SAC core genes are present in all subgroups of eukaryotes (Vleugel et al., 2012). A general model for SAC function can be drawn from data obtained from yeast to human (Jia et al., 2013; Musacchio and Salmon, 2007).

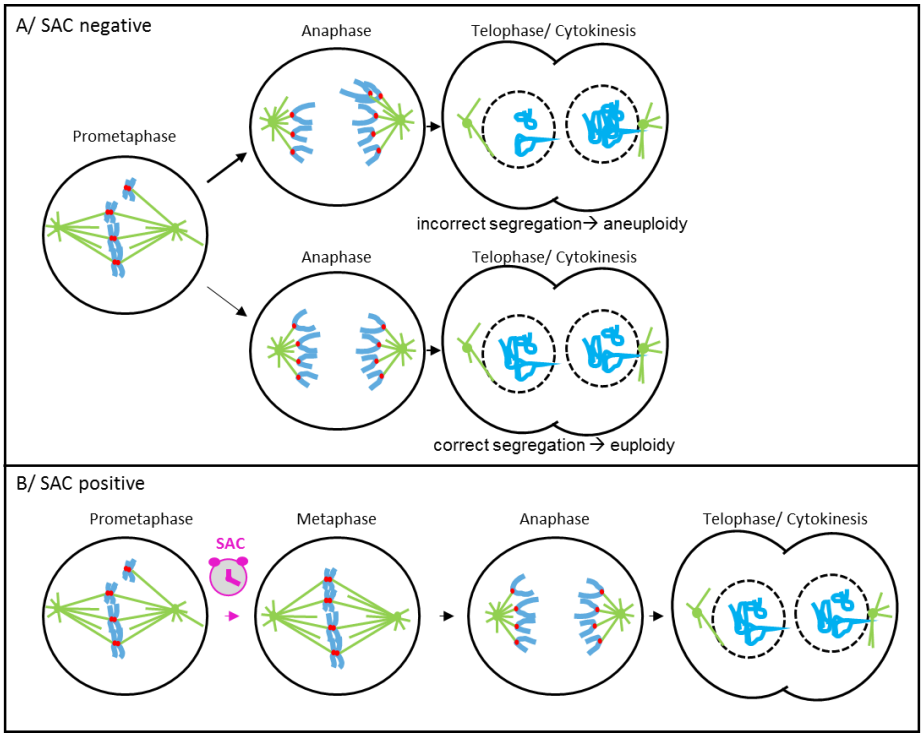

Figure 6 : The SAC prevents chromosome mis-segregation.

Possible mitotic outcomes in the absence (A) or in the presence (B) of an active SAC. In the absence of SAC, cells enter anaphase irrespectively of the presence of unattached kinetochores, giving rise to both euploid and aneuploid cells. When the SAC is active, it delays anaphase until all chromosomes are properly attached to spindle microtubules, ensuring correct chromosome segregation and reducing the incidence of aneuploidy. Membranes (black), chromosomes (blue), kinetochores (red), centrosomes (green disk), microtubules (green), SAC active (pink)

2/ How to study the SAC?

Work aimed at better understanding SAC activity often relies on drug treatments or mutants affecting microtubule dynamics. Alterations in microtubule dynamics interfere with correct chromosome attachments producing the signal to activate the SAC. The SAC induces a mitotic delay until all chromosomes are correctly attached (Fig. 6B). In the absence of an efficient SAC, cells exit mitosis without delay but the incidence of chromosomes segregation errors increases (Fig. 6A), (Hoyt et al., 1991; Jia et al., 2013; Li and Murray, 1991; Musacchio and Salmon, 2007).

Microtubule dynamics can be affected in two ways: either inducing microtubule depolymerization with drugs like nocodazole, colchicine, colcemide and vimblastine or stabilizing microtubules with drugs like taxol. As microtubules are highly dynamic during mitosis and are required for chromosome congression, metaphase is the first phase affected by those treatments (Bates and Eastman, 2017). However, high concentration of microtubule depolymerizing drugs also prevents completion of cytokinesis, due to the requirement for microtubules in this process (Straight and Field, 2000).

The use of different drugs at different concentrations and of different mutants affects more or less spindle dynamics, causing different types of defects, like unattached or mis-attached chromosomes. This was shown to provoke a more or less strong delay of mitotic exit in metaphase showing that the SAC despite being often seen as an all or nothing mechanism, is a gradual mechanism (Subramanian and Kapoor, 2013). In this regard, the lower the number of unattached kinetochores required to activate the SAC, the more sensitive the SAC is and the longer the SAC induced mitotic arrest, the more efficient the SAC is.

3/ SAC components

The SAC was first identified by means of two screens performed in budding yeast *S. cerevisiae* which allowed the identification of mutants that exit mitosis in the absence of microtubules. Those mutants affected the *Mitotic arrest deficient* genes, *Mad1, Mad2, Mad3*, and the *Budding uninhibited by benzimidazoles* genes: *Bub1, Bub*3 (Hoyt et al., 1991; Li and Murray, 1991). Another SAC component, the kinase Monopolar spindle 1 (Mps1), was identified, in a screen for mutants with defects in spindle pole body duplication (Winey et al., 1991). It was later shown that *Mps1* mutant cells are also unable to arrest following treatment with the microtubule depolymerizing drug nocodazole and that this phenotype is independent of the role of Mps1 in spindle pole body duplication (Weiss and Winey, 1996). These screens allowed the identification of the six SAC core components (Hoyt et al., 1991; Li and Murray, 1991; Weiss and Winey, 1996; Winey et al., 1991). Among these proteins two have a kinase activity: Mps1 and Bub1 (Musacchio and Salmon, 2007).

Mad3 and *Bub1* are paralogue genes meaning that they arose by gene duplication (Fig. 8). In some species like the tunicate *Ciona intestinalis (C. intestinalis)*, only one copy of this gene remains (van Hooff et al., 2017; Suijkerbuijk et al., 2012). This duplication happened at least nine independent times in eukaryotic evolution from an ancestral gene usually referred to as *Madbub*. Each duplication was then followed by subfunctionalization. In most cases, *Bub1* but not *Mad3*, retained the kinase domain. However, in vertebrates and insects, the ancestral kinase domain was kept both in *Bub1* and *Mad3*. In this case, *Mad3* is called *Bub-Related 1 (BubR1)* (van Hooff et al., 2017; Suijkerbuijk et al., 2012). BubR1 kinase is functional in *D. melanogaster* but appears to be a pseudo-kinase in vertebrates (van Hooff et al., 2017; Rahmani et al., 2009; Suijkerbuijk et al., 2012).

B/ SAC signaling

1/ The kinetochore, at the origin of SAC signal

The SAC monitors microtubules-kinetochores attachments and prevents anaphase onset in the presence of unattached kinetochores.

The role of kinetochores in SAC signaling was first shown by laser ablation experiments in Ptk1 cells. When kinetochores were ablated cells underwent anaphase even if the corresponding sister chromatids were not attached to spindle microtubules. This showed that the SAC is not able to detect unattached chromosomes if they lack kinetochores and that unattached kinetochores are the trigger for SAC activation (Rieder et al., 1995). SAC proteins localize to unattached kinetochores to trigger the production of a signal to arrest mitotic progression. Mad2 was the first SAC component to be observed at kinetochores in *X. laevis* cells and *H. sapiens* cells (Chen et al., 1996). Since then, all SAC components have been shown to localize to unattached kinetochores in many cell types explaining how kinetochores are connected to the SAC signaling pathway (Cheeseman and Desai, 2008; Jia et al., 2013; Musacchio and Salmon, 2007).

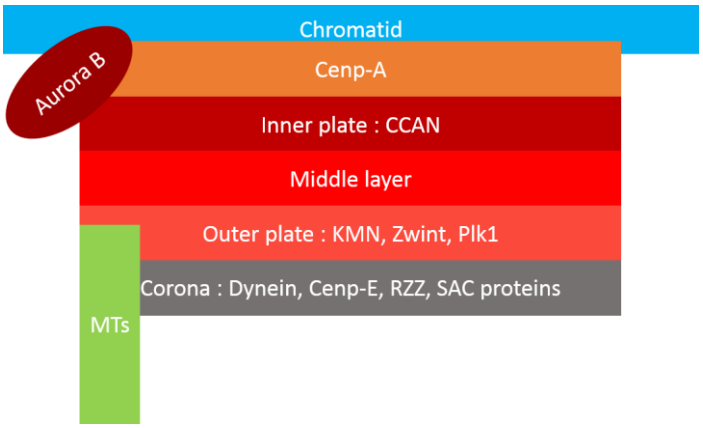

Figure 7 : Kinetochore structure

In mitosis, a kinetochore is composed of four layers: inner plate, middle layer, outer plate and corona. Example of proteins localized in each layer are given inside boxes representing each layer. Kinetochores assemble on centromeric DNA marked by the histone H3 variant, Cenp-A. Microtubules (MTs) attach to chromosomes through interaction with proteins of the outer plate and corona. Aurora B localizes to the centromeric region. Adapted from Musacchio and Salmon, 2007.

Kinetochores are multi-protein complexes, composed of more than 80 components organized in four layers identifiable by electron microscopy: the inner plate, the middle layer also called central kinetochore, the outer plate and the corona (Fig. 7), (Cheeseman and Desai, 2008; Jia et al., 2013; Musacchio and Salmon, 2007). The kinetochore can cover the full length of the chromatid in so called holocentric chromosomes, as in *C. elegans*, or can be localized to a specific site, in monocentric chromosomes, like in *H. sapiens* (Cheeseman and Desai, 2008).

The kinetochore site is defined epigenetically by binding of the histone H3 variant, Cenp-A to specific DNA loci called centromeres which consist of small repeated DNA sequences called microsatellites. Cenp-A localizes at centromeric regions throughout the cell cycle. In early G1, new Cenp-A is incorporated in the newly separated centromeres, allowing preservation of the epigenetic mark in the following cell cycle (De Rop et al., 2012). Cenp-A is required for the recruitment of proteins of the inner kinetochore that also remain associated with centromeres for the whole cell cycle and form the constitutive centromere associated network (CCAN) (Fig. 7), (Cheeseman and Desai, 2008).

At roughly the time of NEB, Cenp-A and CCAN proteins allow the assembly of the outer kinetochore starting with the recruitment of the KMN network. The KMN network is composed of Knl1 (also called Spc105), Mis12 (also called Mtw1) and Ndc80 (also called Hec1). The KMN network then recruits Zwint allowing the localization of the Rod-ZW10-Zwilch (RZZ) complex. This complex which is absent in yeast but present in animal cells, is required to recruit the minus end motor dynein to kinetochores. Dynein, the kinesin Cenp-E (plus end motor) and the KMN network are involved in the interaction with spindle microtubules. These outer kinetochore proteins remain associated with the kinetochores from prophase to anaphase (Cheeseman and Desai, 2008; Musacchio and Salmon, 2007). Similarly, the corona is composed of proteins transiently required at kinetochores for mitotic progression, such as SAC proteins (Fig. 7), (Musacchio and Salmon, 2007).

Proteins of the outer kinetochore and of the corona, as well as microtubule plus end-associated proteins ensure that correct microtubule-kinetochore attachments are achieved. For accurate chromosome segregation, the kinetochore of each sister chromatid must be attached to microtubules coming exclusively from one spindle pole (amphitelic attachment) and sister kinetochores must be attached to opposite poles (biorientation). Incorrect kinetochore-microtubule

attachments need to be corrected prior to anaphase onset to avoid segregation errors. Error correction relies on the activity of the Aurora B kinase (Cheeseman and Desai, 2008; Musacchio and Salmon, 2007), which phosphorylates Ndc80 decreasing its affinity for microtubules and destabilizing incorrectly attached microtubules (Iimori et al., 2016). This generates new unattached kinetochores capable of activating the SAC until a correct attachment is established (Cheeseman and Desai, 2008; Musacchio and Salmon, 2007). Once kinetochores are correctly attached, PP1 counteracts Aurora B activity, while Plk1 phosphorylates Ndc80 and BubR1, stabilizing the attachments (Karess et al., 2013; Liu et al., 2012). BubR1 stabilization of kinetochore-microtubule attachments is independent of its SAC role (Karess et al., 2013).

2/ SAC activity

Unattached kinetochores are the trigger for the activation of the SAC to prevent entry into anaphase (Fig. 8). In the absence of spindle microtubules, SAC proteins are recruited to unattached kinetochores. The first SAC protein to be recruited is the kinase Mps1 (Fig. 8A). Kinetochore localization of Mps1 requires only Ndc80 a component of the KMN complex. Indeed, ectopic localization of Ndc80 away from centromeres is sufficient for the ectopic recruitment of Mps1 to the same Ndc80 enriched loci. The affinity of Mps1 for Ndc80 is increased by Mps1 auto-phosphorylation (Hiruma et al., 2015) and by Aurora B phosphorylation of Ndc80 (Manic et al., 2017).

Once on kinetochores, Mps1 phosphorylates Knl1, another KMN member, allowing the recruitment of other SAC components to unattached kinetochores. In *Schizosaccharomyces pombe (S. pombe)* and HeLa cells, expression of phosphodead forms of Knl1 impairs kinetochore localization of Bub1, Bub3, Mad3/BubR1 and Mad1 and prevents SAC-mediated arrest in the presence of spindle defects. On the other hand, the phophomimetic form of Knl1 induces kinetochore localization of Bub1 and Bub3 independently of Mps1, although Bub1 and Bub3 still require each other. Moreover expression of phosphomimic Knl1 constitutively activates the SAC leading to a mitotic block (Yamagishi et al., 2012). This study showed that Mps1-mediated phosphorylation of Knl1 is necessary for SAC activation by favoring the localization of Bub1 and Bub3 to unattached kinetochores (Fig. 8B). Bub1 and Bub3 then promote BubR1 localization, while Mps1 and Bub1 are required for Mad1 localization. Mad2 which is bound to Mad1 in a tetramer already in interphase, is localized at kinetochores at this step (Fig. 8B), (Jia et al., 2013).

Knl-1 is not the only complex that allows SAC localization to kinetochores. Knl-1 depleted human cells (RPE-1 and HeLa) are able to arrest in mitosis following nocodazole treatment, suggesting that the SAC is activated. In these cells, Mad2 but not Bub1 is localized at kinetochores albeit at lower levels than in control cells. The level of Mad2 at kinetochores is reduced further by co-depletion of Rod. This co-depletion prevents SAC activity entirely (Silió et al., 2015). Similarly, depletion of Rod alone only reduces SAC activity. In cells depleted for Rod, Mad1, but not Bub1 or BubR1, localization at unattached kinetochores is reduced but not suppressed and the co-depletion of Bub1 is required to totally impair Mad1 localization (Zhang et al., 2019). Thus, both the RZZ complex and the KMN network, in association with Bub1, are required for recruitment of Mad1-Mad2 to kinetochores (Fig. 8B).

Once localized to unattached kinetochores the SAC needs to inhibit the APC/C to prevent anaphase onset by sequestrering the APC/C coactivator Cdc20.

Cdc20 was first shown to be the target of the SAC in *S. cerevisiae* (Hwang et al., 1998). Overexpression of Cdc20 was able to overcome the SAC arrest induced by nocodazole treatment or by Mps1 overexpression. In addition, co-immunoprecipitation experiments showed that Cdc20 directly interacts with Mad2 and Mad3 in cells arrested in mitosis by nocodazole treatment. In the absence of Mad2, Mad3 is not able to bind Cdc20 while Mad2 is still able to bind Cdc20 in Mad3 knockout cells. This indicates that Cdc20 is bound to Mad2 prior to its interaction with Mad3 (Hwang et al., 1998). To interact with Cdc20, Mad2 needs to switch configuration from an open (O-Mad2) to a close configuration (C-Mad2). This conformational change requires a protein sequence in the C-terminal part of Mad2 called the safety-belt. O-Mad2 is present in the cytoplasm while C-Mad2 is bound to Mad1.

Interaction between free O-Mad2 and C-Mad2 bound to Mad1 at kinetochores allows the switch of O-Mad2 to C-Mad2. In the template model, C-Mad2 bound to Mad1 catalyzes the transition of O- to C-Mad2 (Fig. 8C). Differently from C-Mad2 bound to Mad1, the new C-Mad2 is available to bind Cdc20 (De Antoni et al., 2005). C-Mad2 sequesters Cdc20 hiding the Cdc20 protein domain required for its interaction with APC/C. Mad2-Cdc20 is then able to interact with BubR1-Bub3 to form the mitotic checkpoint complex (MCC), (Fig. 8C), (Jia et al., 2013; Sudakin et al., 2001). In *S. cerevisiae*, tethering Mad2 to either Mad3 or Cdc20 removes the requirement for its interaction with Mad1 and with the other SAC components. This shows that Mps1, Mad1 and Bub1 are required to prime Mad2 but are not directly inhibiting Cdc20. Mad3/BubR1 and Bub3 instead are required to amplify the capacity of Mad2 to inhibit Cdc20 in the MCC (Lau and Murray, 2012). Finally, the APC/C is also integrated in the MCC further strengthening SAC mediated inhibition of anaphase onset (Fig. 8C), (Jia et al., 2013; Sudakin et al., 2001)

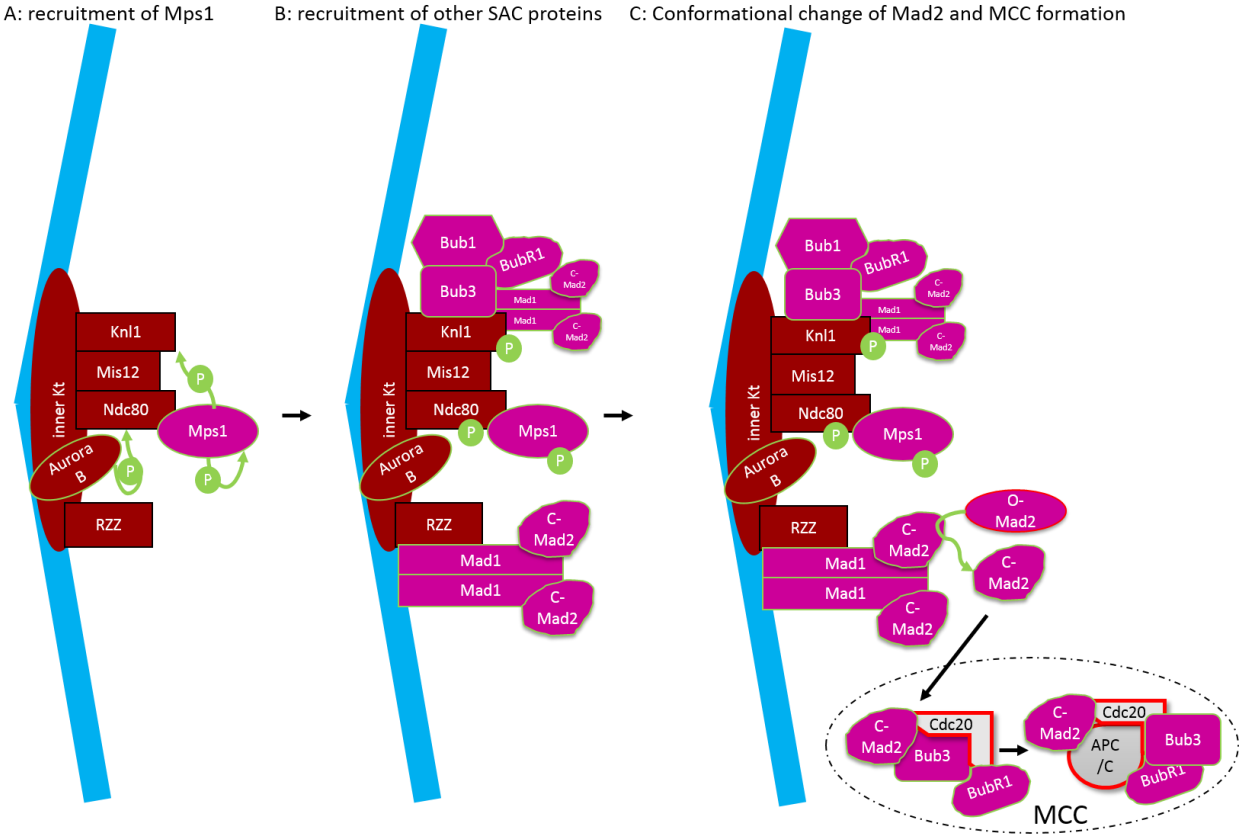

Figure 8 : SAC activation in prometaphase.

A-B/ Mps1 is recruited to unattached kinetochores (red). Aurora B and Mps1-mediated phosphorylation (P) of kinetochore proteins promotes the recruitment of other SAC components. **C/** Mad1-Mad2 tetramers recruited to kinetochores induce a conformational change of cytoplasmic O-Mad2 to C-Mad2. C-Mad2 binds Cdc20 and interacts with BubR1 and Bub3 to inhibit the activity of the APC/C in the mitotic checkpoint complex (MCC).

SAC activation also occurs independently of kinetochores in interphase. Indeed, following knockout of Mad1, Cyclin B1 levels do not rise as much as in control cells during G2, probably because APC/C becomes active, inducing Cyclin B1 degradation. In interphase, Mad1 and Mad2 are already in a complex but localize to nuclear pores allowing the formation of C-Mad2 and the inhibition of Cdc20. Mutations that interfere with Mad1 localization at nuclear pores do not affect SAC activation in mitosis, as shown by its capacity to prevent anaphase in the presence of nocodazole. However, those cells make more chromosome segregation errors than wild type cells probably due to inefficient SAC activation at mitotic entry (Rodriguez-Bravo et al., 2014). In mitosis, following dismantling of nuclear pores at NEB, the SAC signal depends entirely on unattached kinetochores.

3/ SAC inactivation

In metaphase when all kinetochores are aligned on the metaphase plate and attached to spindle microtubules, the SAC is satisfied and inactivated allowing anaphase onset (Jia et al., 2013).

SAC components and microtubules both interact with the KMN complex in a mutually exclusive way (Fig. 9A), (Jia et al., 2013). *In vitro,* Mps1 interaction with Ndc80 is inhibited by an increase in microtubule polymers induced by addition of taxol. Moreover, when Ndc80 is ectopically localized, Mps1 is also lost in the presence of microtubule attachments indicating that the localization of Mps1 to kinetochores is mutually exclusive with microtubules, without requirement any for additional components (Hiruma et al., 2015).

When Mps1 is removed from kinetochores, PP1 and PP2A become active and dephosphorylate the KMN preventing localization of other SAC components (Fig. 9A), (Jia et al., 2013; Manic et al., 2017). Depletion by RNAi of PP1-87B, the orthologue of PP1α, in S2 cells of *D. melanogaster* prevents SAC inhibition and results in a mitotic block in the presence of correctly attached kinetochores. In those cells, Mad1 and Mps1 localize to attached kinetochores. In PP1-depleted cells, Mps1 autophosphorylation increases, over-activating the SAC. A similar mitotic block is also observed when Mps1 is mutated in the site required for its interaction with PP1-87B. The mitotic block can be overcome by depletion of SAC components or by expression of a kinase dead form of Mps1. Similarly, following colchicine treatment, inhibition of Aurora B decreases Mps1 phosphorylation reducing SAC efficiency, except if Mps1 can not interact with PP1-87B. PP1 is important to inhibit the SAC also in the absence of kinetochores. Following mutations of the inner kinetochore protein Cenp-C, a cytoplasmic pool of Mps1 remains phosphorylated at mitotic entry and requires PP1 to be inactivated (Moura et al., 2017).

Removal of SAC proteins from kinetochores also relies on dynein transport along microtubules (Fig. 9A), (Jia et al., 2013). Following a reduction in ATP, Mad2, BubR1, Mad1, Bub1 and Bub3 move away from kinetochores towards spindle poles. However, this can be prevented by treatment with microtubule depolymerizing drugs or by inhibition of dynein. Dynein inhibition alone prevents mitotic exit with Mad2 localized at attached kinetochores despite correct kinetochore-microtubule attachments. The mitotic arrest is prevented by Mad2 inhibition. Thus, dynein allows SAC inhibition by moving SAC components away from kinetochores (Howell et al., 2001; Silva et al., 2014). Dynein

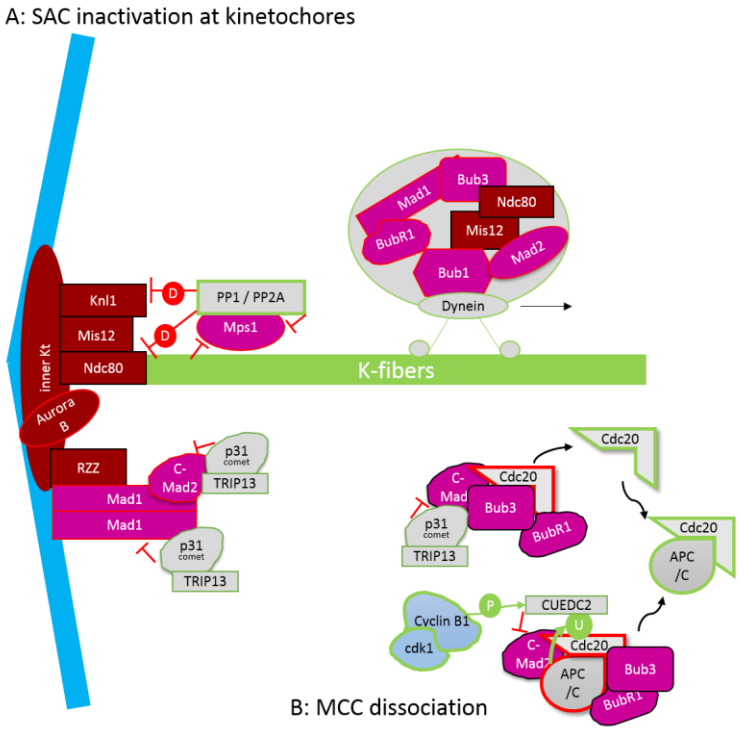

Figure 9 : SAC inactivation in metaphase.

SAC inactivation requires its delocalization from kinetochores (A) and disassembly of the MCC (B). Delocalization of SAC components from kinetochores is a result of direct competition between microtubules (green) and Mps1 for interaction with Ndc80, PP1 and PP2A-mediated dephosphorylation (D) and dynein-mediated removal of SAC proteins from kinetochores toward spindle poles. In addition, $p31^{comet}$-TRIP13 prevents the generation of new C-Mad2 and induces MCC disassembly. Cdc20 ubiquitination by the APC/C itself and Cdc20 interaction with CUEDC2 also contribute to MCC dissociation. SAC protein (pink), kinetochores (red), protein active (green border) protein inactive (red border).

removes also the KMN components Ndc80 and Mis12 that are required for SAC localization (Fig. 9A), (Silva et al., 2014).

When the SAC is satisfied, formation of the MCC must also be prevented and the existing MCC must be dismantled to free Cdc20 and allow APC/C activation. MCC inactivation requires p31^{comet} (Fig. 9A and B). In human cell lines, p31^{comet} knockout cells spend more time in mitosis than wild type cells and exit mitosis more slowly following nocodazole removal. To test if this delay was due to a defect in SAC inhibition, p31^{comet} knockout cells were released in MG132, an inhibitor of the proteasome. Proteasome inhibition prevents mitotic exit downstream of APC/C activation and independently of the SAC. MG132 treatment therefore prevents anaphase onset although all chromosomes are properly attached and the SAC is satisfied. When the drug is removed cells can enter anaphase directly. Following release from MG132 arrest, p31^{comet} knockout cells degrade Cyclin B1 as fast as control cells. This indicates that the delay in mitotic exit is upstream of APC/C activation and is probably due to a delay in SAC inactivation (Ma and Poon, 2016). Indeed, preventing the interaction between p31^{comet} and Mad2 is sufficient to lengthen mitosis despite the presence of correct microtubule-kinetochore attachments (Westhorpe et al., 2011). Consistent with a role in SAC inactivation via disassembly of the MCC complex, p31^{comet} knockout cells have higher levels of MCC and of C-Mad2 (Ma and Poon, 2016). p31^{comet} interacts with Mad2 bound to Mad1 and in the MCC. *In vitro* and *in vivo*, p31^{comet} is able to remove Mad2 from the MCC except if the APC/C is part of the complex (Fig. 9B), (Westhorpe et al., 2011).

p31^{comet} acts in association with the AAA-ATPase Thyroid hormone receptor interacting protein 13 (TRIP13). Following p31^{comet} overexpression, early Cyclin B1 degradation is prevented by depletion of TRIP13. After release from a nocodazole arrest, Cyclin B1 degradation is delayed by depletion of TRIP13 increasing the time cells spend in metaphase. This occurs in parallel with a delay in MCC dissociation (Wang et al., 2014). By interfering with the association between Mad1 and Mad2, but also with the MCC, TRIP13 allows SAC inactivation (Fig. 9A and B), (Wang et al., 2014). However, TRIP13 knockout cells do not arrest in mitosis following nocodazole treatment, despite the presence of high levels of C-Mad2. This result suggests that C-Mad2 alone is not sufficient for SAC activation. The switch from O-Mad2 to C-Mad2 instead is required for SAC activity and the loss of TRIP13 prevents the dynamic change between these two forms (Ma and Poon, 2016). By increasing the turnover of Mad2, TRIP13 allows a dynamic control of the SAC.

To summarize, p31^{comet} and TRIP13 act both by preventing the generation of new C-Mad2 that would generate new MCC and by dissociating existing MCC (Fig. 9A and B), (Jia et al., 2013).

MCC dissociation is also induced by its target, APC/C through direct Cdc20 ubiquitination (Fig. 9B), (Jia et al., 2013). Overexpression of UbcH10, an E2 protein involved in APC/C activity, accelerates mitotic exit both in untreated and nocodazole treated cells. UbcH10 allows multi-ubiquitination of Cdc20 impairing its interaction with Mad2. This leads to SAC inactivation, increasing the ability of the APC/C to ubiquitinate its targets inducing an acceleration of securin degradation. Early ubiquitination of Cdc20 is prevented by the kinetochore protein, Usp44 (Reddy et al., 2007). The action of UbcH10 and p31^{comet} are additive. Indeed, addition of both proteins to HeLa cell extract treated with nocodazole increases APC/C substrate degradation more than the addition of only one of them. Similarly, in cell lines knocking down both UbcH10 and p31^{comet} by RNAi, impairs substrate degradation more that depletion of each of them individually (Reddy et al., 2007).

MCC inactivation relies also on CUE domain containing protein 2 (CUEDC2). The domain CUE allows the interaction with ubiquitin. CUEDC2 interacts with Cdc20 and Cdc27, an APC/C subunit. In cells depleted for CUEDC2, Mad2 interaction with Cdc20 is prolonged suggesting that the protein is required for MCC dissociation. In agreement with this hypothesis, CUEDC2 depletion prevents Cyclin B1 degradation following the release from a nocodazole block. Even in untreated cells, CUEDC2 depletion leads to metaphase lengthening despite correct chromosome attachments. This phenotype is prevented by Mad2 depletion supporting a defect in SAC inactivation. Yet, Mad2 and BubR1 are not localized at kinetochores. This is in agreement with the unique requirement of CUEDC2 in MCC

disassembly (Fig. 9B). CUEDC2 activity requires its phosphorylation by Cdk1. CUECD2 phosphorylation is lost following Cdk1 inhibition, while Cdk1 overexpression increases it. Kinase assays indicate that Cdk1 directly phosphorylates CUEDC2 (Fig. 9B), (Gao et al., 2011). This highlights another negative feedback controlling Cdk1 activity, since CUEDC2 activates APC/C which in turn degrades Cyclin B1 leading to Cdk1 inactivation.

Most of the mechanisms involved in SAC inactivation are already in place when kinetochores are still unattached. In addition, mechanism of SAC activation, SAC inactivation, mitotic entry and anaphase onset are tightly entwined. It is the balance between activator and inhibitor that dictates mitotic outcomes enabling, in a very efficient and dynamic way, control of the process (Jia et al., 2013; Wieser and Pines, 2015).

4/ Mitotic slippage: mitotic exit without SAC inactivation

Incorrect attachment of kinetochores to microtubules induces a mitotic arrest in prometaphase due to SAC activation which delays mitotic progression until the problem is resolved. However, in long-term treatments, some cells undergo anaphase and exit mitosis despite the presence of an active SAC. This phenomenon is called mitotic slippage or adaptation. During mitotic slippage misegregation of chromosomes can often be observed leading to aneuploidy in daughter cells. When microtubules are absent, cells undergoing mitotic slippage cannot complete cytokinesis and keep all chromosomes in one cell forming either one nucleus or several micronuclei. These cells can then follow different pathways, die by necrosis or apoptosis, remain in G1 or undergo a new cell cycle, giving rise to more aneuploid cells. This last phenomenon is a problem well known in cancer treatments that rely on microtubule targeting drugs (Rieder and Maiato, 2004).

In *S. cerevisiae,* mitotic slippage was shown to be associated with precocious activation of APC/C-Cdh1. Deletion of Bub2 or Cdc14, two proteins that inhibit Cdh1, leads to mitotic exit in the presence of nocodazole. In these cells, Mad2 is properly localized at unattached kinetochores indicating that anaphase onset takes place in the presence of an active SAC. Under these conditions, the SAC appears to be bypassed by the ectopic activation of APC/C-Cdh1, which is able to degrade APC/C-Cdc20 targets leading to mitotic slippage (Toda et al., 2012).

However, in slippage from nocodazole arrest of wild type cells (Ptk1 or RPE1), APC/C-Cdh1 targets are not degraded indicating that another mechanism exists. In this case, SAC components like BubR1, Mad1 and Mad2 are localized at kinetochores but Cyclin B1 is degraded by the proteasome. This suggests a residual APC/C-Cdc20 activity, indicating that the SAC does not fully inhibit APC/C (Brito and Rieder, 2006). Proteasome dependent Cyclin B1 and Securin degradation was also found in HEK293 cells during nocodazole arrest. In those cells ihibition of transcription or translation led to mitotic slippage while control cells remain arrested in mitosis for over 18 hours, suggesting that these processes compensate the residual APC/C cdc20 activity. As the RNA and protein levels of Cdc20 and SAC components were not affected by inhibition of either transcription or translation, these processes are then not required for maintaining levels of SAC components but are rather required to compensate the residual activity of APC/C-Cdc20 and maintain a high level of Cyclin B1 to arrest cells in prometaphase (Mena et al., 2010).

III/The spindle assembly checkpoint during embryogenesis

During early embryogenesis, the cell cycle differs compared to somatic cells. In most species, eggs are very large compared to somatic cells: human oocyte are $4*10^6\ \mu m^3$ while most somatic human cell type are around $3*10^3\ \mu m^3$ (Philips, website). This removes the requirement for cell growth during the early embryonic cell cycles that constitute the cleavage stage. Indeed, no gap phases are observed and in most embryos S-phase and mitosis alternate rapidly allowing a fast increase in cell number. As

embryos develop, G2 and G1 phases are acquired and cells transition towards a more somatic-like cell cycle (Cooper, 2000; Siefert et al., 2015).

Another major difference which was observed between somatic and embryonic cell cycles relates to checkpoint control of cell cycle progression. Strikingly, despite the importance of checkpoints for ensuring the generation of viable cells, these controls are often silenced or weak in cleaving embryos (Siefert et al., 2015). In the case of the SAC, some embryos have been shown to have an active SAC from the first mitosis while others have an inefficient SAC during early cleavage cycles. Several hypotheses have been suggested to explain how SAC activity is controlled in these embryos but without reaching a conclusion.

In the first part of this section, I will introduce the differences in SAC efficiency in early metazoan embryos and I will then discuss mechanisms underlying the change in SAC efficiency during embryogenesis in the second part of this section.

A/Activity of the SAC in embryos

The SAC was long considered to be inactive in metazoan embryos (Clute and Masui, 1992; Ikegami et al., 1997; Zhang et al., 2015). However, SAC activity can be detected in non-chordate metazoan species already in 2-cell stage embryos (Fig. 10):

In cnidarians, embryos of the jellyfish *Clytia hemispherica* (*C. hemispherica*) have an active SAC from the beginning of development. In 2-cell embryos treated with nocodazole, NER is delayed and phosphorylation of PP1A and of histone 3 (pH3), both normally occurring during mitosis, are maintained for the duration of a whole cell cycle. These phenotypes depend on an active SAC and can be suppressed by impairment of SAC signaling due to the exposure to the Mps1 inhibitor, reversine (Chenevert et al., 2019).

In the two mollusk species *Spisula solidissima* (*S. solidissima*) and *Mytillus galloprovincialis* (*M. galloprovincialis)* the SAC was also found to be efficient. Impairing microtubule dynamics during the first mitosis of embryos of the clam *S. solidissima* extends the time cells spend with condensed mitotic chromosomes and high levels of Cyclin B1 (Hunt et al., 1992). In the 2-cell embryos of the mussel *M. galloprovincialis,* an active SAC was shown to be involved in the delay in NER and in maintaining pH3 phosphorylation following nocodazole treatment (Chenevert et al., 2019).

For arthropods, analysis of early embryonic mitoses is more difficult as spindles are deep into the cytoplasm. However, experiments suggest that the SAC is active at the earliest cell cycles studied. In the midge *Heteropeza pygmaea (H. pygmaea),* treatments with drugs that affect microtubule dynamics prevented yolk oscillation in early cleaving embryos and the mitotic index, measured by orcein staining of chromosomes, increased, indicating that cell cycle progression was impaired (Kaiser and Went, 1987). In *D. melanogaster*, interference with microtubule dynamics delays mitotic progression in a BubR1-dependent manner at the 3rd cell cycle, indicating a functional SAC (Pérez-Mongiovi et al., 2005).

In sea urchin 1- or 2-cell stage embryos, mitotic duration is lengthened following treatments with microtubule depolymerizing drugs. NER was delayed in *Lytechinus variegatus (L. variegatus)* (Sluder, 1979) and *Paracentrotus lividus (P. lividus)* (Chenevert et al., 2019). In *A. punctulata* degradation of mitotic Cyclins was prevented when embryos were treated with either colchicine or taxol, suggesting APC/C inhibition by the SAC, (Evans et al., 1983). In addition, pH3 staining was maintained for at least the equivalent of a whole cell cycle in *P. lividus, Arbacia lixula (A. lixula), Sphaerechinus granularis (S. granularis)* and *Strongylocentrotus purpuratus (S. purpuratus)* (Chenevert et al., 2019). In *P. lividus*, the arrest was lost following Mps1 inhibition by reversine (Chenevert et al., 2019). Altogether these observations indicate that the SAC is efficient from first mitosis in sea urchin embryos. The SAC is also efficient in another class of echinoderms: the Asteroidea. In 2-cell embryos of the starfish *Hacelia attenuata* (*H. attenuata)*, following nocodazole treatment, pH3 was maintained for twice as long as in control embryos (Chenevert et al., 2019).

In the nematode *Caenorhabditis elegans* (*C. elegans)*, nocodazole treatment doubles the duration of the first mitosis. This lengthening requires the SAC components Mad1 and Mad2, called respectively Mdf1 and Mdf2 in *C. elegans* (Encalada et al., 2005; Gerhold et al., 2018). Furthermore, SAC activity which is weak in the 1st cell cycle, increases in the following cell cycles inducing a more pronounced lengthening of mitosis as the embryo develops (Galli and Morgan, 2016; Gerhold et al., 2018).

In all the phyla presented above, the SAC is efficient from the first cell cycle following fertilization. In chordates both SAC proficient and SAC deficient early embryos exist (Fig. 10):

In *H. sapiens*, the SAC was shown to be efficient at day 5 post-fertilization, when the embryo is a blastocyst of around 58 cells (Hardy et al., 1989). SAC efficiency is less clear in the previous cell cycles. In morula, nocodazole treatment leads to a slight increase in pH3 staining, indicating that cells spend more time in mitosis in the presence of microtubule defects. However, accumulation of multinucleated and tetraploid cells is observed in preimplantation embryos indicating that cells exit mitosis (Jacobs et al., 2017) with high rates of aneuploidy (Nagaoka et al., 2012; Vera-Rodriguez et al., 2015). This suggests that the SAC is active but has a low efficiency in human embryos.

In the mouse *M. musculus,* early work indicated that the SAC was efficient in embryos. Indeed, when mouse embryos are treated with nocodazole before the first mitosis, Cdk1 remains phosphorylated whereas it is dephosphorylated in control embryos, indicating a mitotic arrest (McConnell and Lee, 1989). This mitotic block depends on the SAC components Bub3, BubR1 and Mad2 (Wei et al., 2011). In addition, in 2-cell stage embryos and at the blastocyst stage (E3.5), few unattached kinetochores, induced by treatment with low concentration of nocodazole, are sufficient to lengthen mitotic duration, indicating that the SAC is active and also sensitive in those stages. On the other hand, analysis of the intervening cell cycles (4-cell and morula stages) showed that only high concentrations of nocodazole were able to induce a mitotic arrest, suggesting that SAC is less sensitive (Vázquez-Diez et al., 2019).

SAC efficiency was also assessed in *M. musculus* oocytes, during meiosis. Overexpressing Mad2 induces a meiotic block without any spindle defects (Wassmann et al., 2003a), whereas disturbing microtubule dynamics during the first meiotic division prevents Cyclin B1-Cdk1 inactivation, chromosome decondensation and segregation of homologues, indicating an arrest in meiosis. Expression of a dominant negative form of Mad2 or knockdown of Bub1 result in loss of Cyclin B1-Cdk1

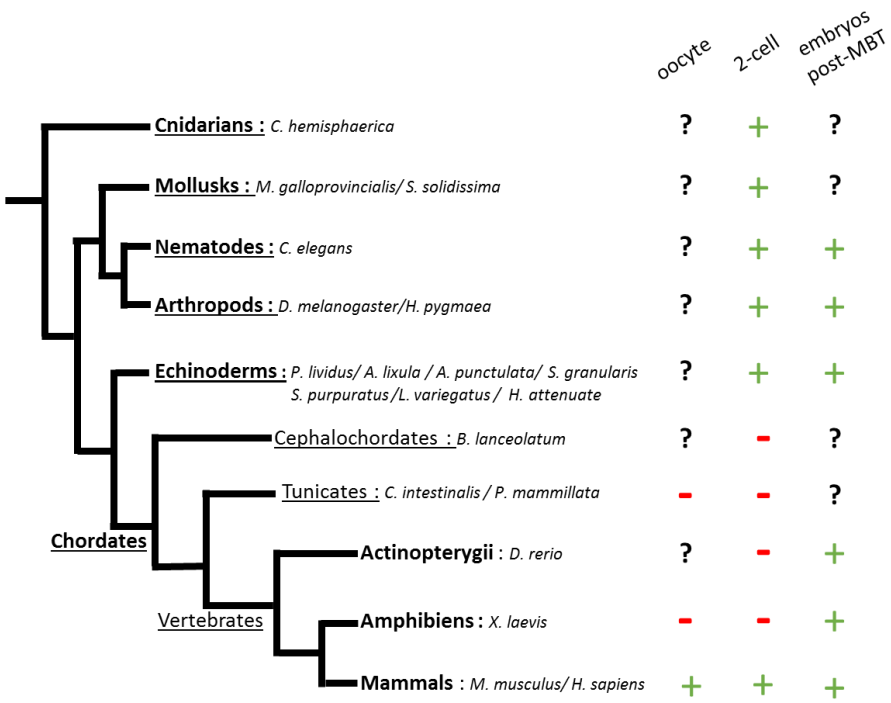

Figure 10 : SAC efficiency in metazoan embryos.

Phylogenetic tree of metazoans with phyla (underlined and bold), subphyla (underlined) and classes (bold). Species for which data about SAC efficiency is available are indicated next to the corresponding branch (italics). Whether the SAC is active (+) or inactive (-) in oocytes, 2-cell stage embryos and embryos after MBT is reported for each group (right). Data are not always available (?). Adapted from Chenevert et al, 2019.

activity and polar body extrusion, confirming SAC requirement for the meiotic arrest (McGuinness et al., 2009; Wassmann et al., 2003a). However, SAC sensitivity is not as good as in somatic cells. Aged oocytes can arrest meiotic progression following nocodazole treatments, but untreated oocytes complete meiosis even in the presence of unattached chromosomes not aligned on the metaphase plate (Sebestova et al., 2012). Similarly, mouse oocytes carrying mutations in NuMA (nuclear mitotic apparatus protein) or Mlh1 (MutL homolog 1), which interfere with the formation of the metaphase plate without affecting SAC activity, undergo meiosis in the presence of incorrect attachments (Kolano et al., 2012; Nagaoka et al., 2011). No meiotic delay was observed in XO mouse oocytes which have only one X chromosome that can not be paired with its homologue in metaphase I (LeMaire-Adkins et al., 1997). Similarly, following mutations in a complex required for the formation of chiasmata, chromosomes can not pair, but each chromosome is bioriented as it normally happens in metaphase II or mitosis. In all these situations, the lack of SAC efficiency was ascribed to formation of incorrect attachments not detected by the SAC (Kouznetsova et al., 2007).

In non-mammalian chordates instead, the SAC is not efficient in early embryos (Fig. 10):

In the cephalochordate *Branchiostoma lanceolatum* (*B. lanceolatum),* nocodazole treated 2-cell embryos undergo NER at the same time as control embryos, indicating that these cells are cycling with unaltered timing. This also suggests that the SAC is not active in early embryos of this species (Chenevert et al., 2019).

In *X. laevis,* during metaphase I, the SAC fails to prevent bivalent separation in the presence of spindle perturbations (Shao et al., 2013). Similarly, in early embryos, blocking microtubule polymerization does not alter cycling of Cyclin B1-Cdk1 activity (Gerhart et al., 1984), and does not prevent timely chromosome decondensation (Clute and Masui, 1992). This indicates that the SAC is not efficient in early *X. laevis* embryos. In those embryos, the SAC is activated at the 12^{th} cell cycle when it delays mitotic exit following nocodazole treatment (Clute and Masui, 1992). This cell cycle corresponds to the transition of the embryo toward a more somatic-like status marked by the activation of zygotic transcription, a phenomenon called maternal to zygotic transition (MZT), cell cycle lengthening with the addition of G2 phase and the appearance of cell cycle asynchrony between blastomeres. These changes define a developmental phase known as the mid-blastula transition (MBT).

In *Danio rerio (D. rerio)* embryos, nocodazole treatment of embryos at the 4- or 8-cell stage, respectively the 3^{rd} or 4^{th} cell cycle, leads to the accumulation of multinucleated cells, indicating precocious mitotic exit and SAC inefficiency. Following MBT, 10^{th} to 12^{th} cell cycle, instead, cells arrest in mitosis in the presence of microtubule defects (Ikegami et al., 1997). Later work confirmed that mitotic duration is unaffected by nocodazole treatment before MBT while the mitotic index (pH3 staining) increases after MBT (Zhang et al., 2015).

Therefore, the SAC is acquired at the time of MBT in both *D.rerio* and *X. laevis*.

Finally, in tunicates, SAC efficiency was assessed in two ascidians. In *P. mammillata*, the species I studied during my thesis, nocodazole treatment does not induce a delay in pronuclear formation in oocytes following fertilization suggesting lack of SAC activity during meiosis (Dumollard et al., 2011). In nocodazole treated 2-cell stage embryos, pH3 staining is lost at the same time than in untreated embryos. In both *P. mammillata* and *C. intestinalis,* NEB and NER continue to occur at the same rhythm than in control, indicating that the SAC is also not efficient in ascidian early embryos (Chenevert et al., 2019).

In summary, a panel of studies tested SAC efficiency during embryogenesis in metazoan embryos. These studies allowed the identification of two groups of embryos with different mitotic behaviors in the presence of spindle defects (Fig. 10): SAC deficient embryos, which include non-mammalian chordates, and SAC proficient embryos which can induce a SAC dependent mitotic delay already during cleavage cycles although their SAC is not as sensitive as in somatic cells.

B/Parameters that impact SAC efficiency in embryos:

The variability in SAC efficiency described in the last section raises the questions of what parameters influence the difference between developmental stages and across species and which mechanisms control the shift in SAC efficiency during development within an embryo. Although the molecular basis of this control remains largely unknown, several possibilities can be envisaged and I will discuss in the following sections some of the factors known to influence SAC activity and their potential implication in controlling SAC differences during development (Fig. 11A).

1/ Molecular mechanisms that control SAC activity

The change in SAC efficiency observed among metazoans during embryogenesis may rely on variable abundance in SAC core components and regulators in the cells. Protein presence in embryos is a result of maternal contribution, transcription, translation and degradation. In *H. sapiens*, the level of aneuploidy in embryos during development can be predicted using transcriptomic data by variations in the abundance of a set of RNAs including Bub1 RNA (Vera-Rodriguez et al., 2015). In *D. rerio* and *X. laevis*, inhibition of transcription, by treatment with α-amantinin, does not prevent SAC acquisition (Clute and Masui, 1995; Zhang et al., 2015), whereas in *X. laevis* treatment with the translation inhibitor, cycloheximide, delays SAC acquisition (Clute and Masui, 1995). This indicates that protein content is important in SAC acquisition. However, in *C. elegans,* for which SAC efficiency increases at each cell cycle, the level of Mad1 and Mad2 protein is constant during embryogenesis (Galli and Morgan, 2016). This suggests that even if changes in the presence of embryonic proteins can impact SAC activity, SAC efficiency is not strictly regulated by the abundance of its core proteins, at least in embryos from some species.

SAC efficiency may also be modulated at the level of its activation by affecting the localization of SAC proteins to unattached kinetochores. In *X. laevis* egg extract to which a high concentration of sperm was added to restore SAC activity, localization of SAC proteins at kinetochores and mitotic arrest in the presence of nocodazole required the phosphorylation of Mps1 by ERK. In these extracts, a phosphodead form of Mps1 or inhibition of MEK by U0126 prevents SAC activation (Zhao and Chen, 2006). Similarly, ERK inhibition by the MAPK phosphatase MHP-1 (mice orthologous of the *X. laevis* XL100) or by immunodepletion of ERK results in loss of mitotic arrest. In addition, in *X. laevis* embryos that are normally SAC deficient, addition of the MAPKKK Ste11 activates ERK and induces a mitotic block (Minshull et al., 1994; Takenaka et al., 1997). ERK is involved in cell cycle control through its role in CSF-mediated arrest in oocyte (see introduction part I.D) and is inactivated at fertilization. Hence, it can be hypothesized that the existence of SAC deficient and SAC proficient species could be due to a progressive ERK reactivation which would take a different number of cell cycles depending on the species.

Kinetochore localization of SAC proteins was tested in relation with the variation in SAC efficiency in *C. elegans* and *M. musculus.* In *C. elegans,* SAC efficiency increases at each cell cycle but the amount of Mad1 (Mdf1 in *C .elegans*) at kinetochores remains unchanged. This suggests that SAC proteins are recruited as efficiently in all cell cycles despite the difference in SAC efficiency (Galli and Morgan, 2016). Similarly, in *M. musculus* early embryos, Mad1 and Mad2 could localize to single unattached kinetochores but a high number of unattached kinetochores was required to detect SAC activity (Vázquez-Diez et al., 2019). These results suggest that either SAC efficiency is regulated downstream of SAC activation at kinetochores or that SAC deficient cells undergo very efficient mitotic slippage.

2/ Cellular parameters influencing SAC efficiency

SAC efficiency could be influenced by specific cellular characteristics of embryonic cells. For example, cell volume decreases during embryogenesis due to cell division in the absence of cell growth e.g. mouse blastocyst cells are 40 times smaller than the zygote (Vázquez-Diez et al., 2019). Work carried out in *C. elegans* suggested that the SAC signal can be diluted in a large cytoplasmic volume preventing mitotic arrest despite SAC activation. In *C. elegans,* SAC efficiency increases at each cell cycle and it was observed that mutations leading to the formation of triploid cells give rise to a stronger SAC while addition of exogenous DNA devoid of kinetochores did not impact SAC activity (Galli and Morgan, 2016; Gerhold et al., 2018). As the SAC signal is produced at unattached kinetochores, it was speculated that the effect of cell volume was affected by the number of kinetochores present in the cell and SAC efficiency would be influenced by the kinetochore to cell volume ratio, rather than by cell volume directly (Fig. 11B). However, in *M. musculus* embryos, the SAC is less efficient at 4-cell stage than at 2-cell stage despite the reduction in cell size. Moreover, cytoplasmic ablation at 2-cell has no effect on SAC efficiency following nocodazole treatment. Altogether, this data indicates that SAC efficiency is not influenced by cell volume during mitosis in mice (Vázquez-Diez et al., 2019). The effect of cell volume on SAC efficiency however may be different during meiosis. In *M. musculus* cytoplasmic ablation in the oocyte delayed anaphase onset in a SAC dependent manner and resulted in a more sensitive SAC. However, the effect was observed only if the cytoplasm was removed before NEB indicating that in this case the nuclear to cytoplasmic ratio rather than kinetochore to cytoplasm ratio influenced SAC efficiency (Kyogoku and Kitajima, 2017; Lane and Jones, 2017).

The effect of cell volume on SAC activity in mitosis can also be evaluated in species that are SAC deficient. The low kinetochore to cytoplasmic ratio does not appear to explain the lack of SAC activity in *P. mammillata* and *X. laevis* early embryos. Indeed, in *P. mammillata* nocodazole treated 2-cell embryos, the increase in kinetochore to cytoplasmic ratio caused by several rounds of DNA synthesis without intervening cytokinesis does not result in an increase in mitotic duration (Chenevert et al., 2019). Reducing the size of *X. laevis* zygotes by removing a part of the cytoplasm does not alter the time when the SAC is acquired (Clute and Masui, 1995). Aphidicoline treatment of *X. laevis* blastomeres at the 5th cleavage inhibits DNA replication lengthening their cell cycle, without arresting it. Therefore, when control embryos reach the 11th/13th cell cycles, blastomeres treated with aphidicoline are in the 9th/10th cell cycles. Both treated and untreated embryos acquired the SAC, irrespective of their cell cycle stages and of the kinetochore to cytoplasmic ratio (Clute and Masui, 1997). Similar results were obtained in *D. rerio.* Expression of a phosphomimic form of Chk1 (see part I, Fig. 4) allows early acquisition of G2, lengthening the cell cycle. In those embryos, the SAC becomes efficient at an earlier cell cycle, with a lower kinetochore to cell volume ratio than in control embryos, indicating again that cell volume does not control the time of SAC acquisition. In addition, in this experiment G2 and cell cycle lengthening are observed prior to SAC activation suggesting that SAC acquisition is also not due to interphase elongation (Zhang et al., 2015).

Finally, when SAC efficiency is compared between 2-cell embryos from several species that are SAC deficient or SAC proficient, no correlation could be found between SAC efficiency and cell volume, chromosome number or kinetochore to cell volume ratio (Chenevert et al., 2019).

Thus, differences in cell volume are unlikely to explain the difference in SAC activity observed across different embryos and to be sufficient to drive the switch in SAC activity observed in certain species during development. However, it is possible that cell volume modulates SAC activity in SAC proficient embryos.

In the experiments described above, cell cycle lengthening in *X. laevis* and *D. rerio* embryos did not delay SAC acquisition, despite the reduction in number of elapsed cell cycles (Clute and Masui, 1997; Zhang et al., 2015). These experiments suggested that a developmental timer controls SAC acquisition but the molecular nature of this timer still remains unknown.

Another parameter to consider is that cells progressively differentiate during embryogenesis and acquire different identities. In *C. elegans* embryos, germline cells have a more efficient SAC than other cells, at the same embryonic stage. At the analyzed stages (2-16 cell stage), germline precursors are always smaller than the somatic cells, but the difference in SAC activity between these two cell lines cannot be accounted exclusively by the difference in cell size. Instead, both cell size and cell fate appear to contribute to SAC efficiency. In those embryos, loss of either cell identity, like in Par1 or Mex5/6 depleted cells, or cell size asymmetry, as in Gpr1/2 depleted embryos, only partially reduces the difference in SAC efficiency between germline precursors and somatic cells. Instead, depletion of Par6, which results in loss of both cell identity and cell size asymmetry, eliminates the difference in SAC efficiency between blastomeres (Gerhold et al., 2018). The mechanism linking cell fate and SAC efficiency is still unknown.

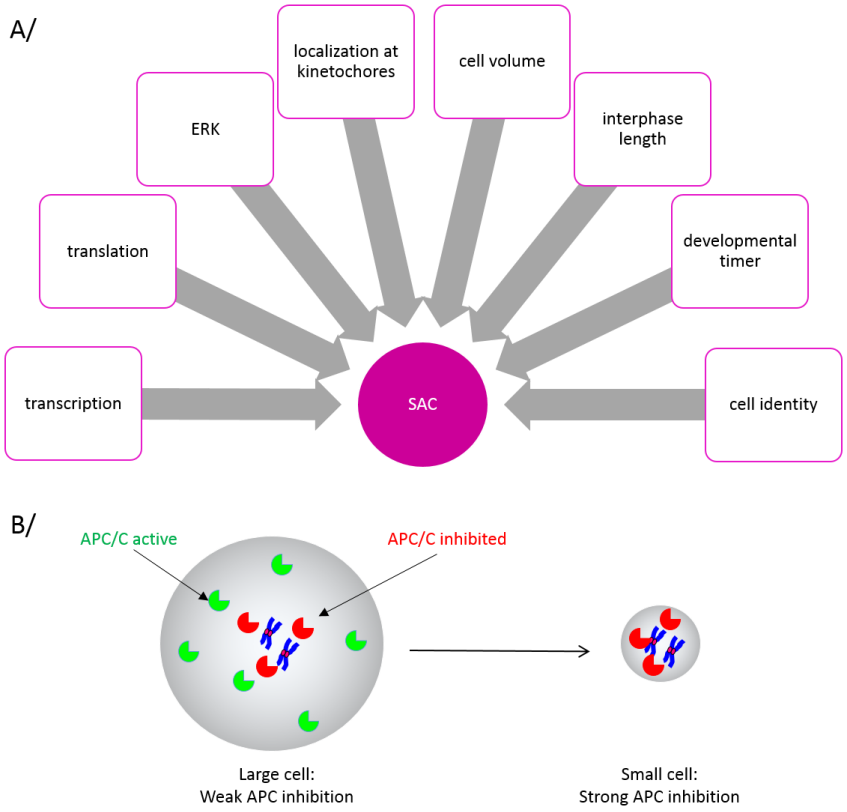

Figure 11: Parameters influencing SAC efficiency in metazoan embryos.

A/ SAC activity during embryogenesis can be modulated by several parameters indicated in the boxes. **B/** Model for the effect of cell volume on SAC activity: a large cell volume dilutes SAC signal preventing full inactivation of the APC/C. Adapted from Galli and Morgan, 2016.

IV/ *Phallusia mammillata,* as a model for embryogenesis

A/Overview of *P. mammillata*

The work described in this thesis has been carried out using embryos of *P. mammillata*, the white sea squirt, an animal which belongs to the group of tunicates (previously known as urochordata). Tunicates are marine organisms present worldwide. Their body or zooid is surrounded by a cellulose shell, called the tunic (Fig. 12A and B). As adults, tunicates filter sea water to obtain nutrients (Fig. 12A). From the evolutionary point of views, tunicates are the closest group to vertebrates and together with cephalochordates constitute the phylum chordata (Fig. 12E). Chordates are characterized by a notochord, a rod-shaped structure of mesodermal origin, which runs along the anteroposterior axis of

the embryo parallel to the ventral neural tube. In tunicates, this structure can be observed only in the larvae, which is called a tadpole (Fig. 12D). Unfertilized ascidian oocytes are encapsulated in an inner layer of test cells and an acellular chorion with adhering follicle cells. Embryogenesis (Fig. 12C) takes place inside the chorion until hatching of the tadpole (Sardet et al., 1989). At the end of development, tunicates belonging to the ascidian group, like *Phallusia*, settle on a substrate and undergo metamorphosis (Delsuc et al., 2018; Holland, 2016; Kocot et al., 2018; Lemaire, 2011).

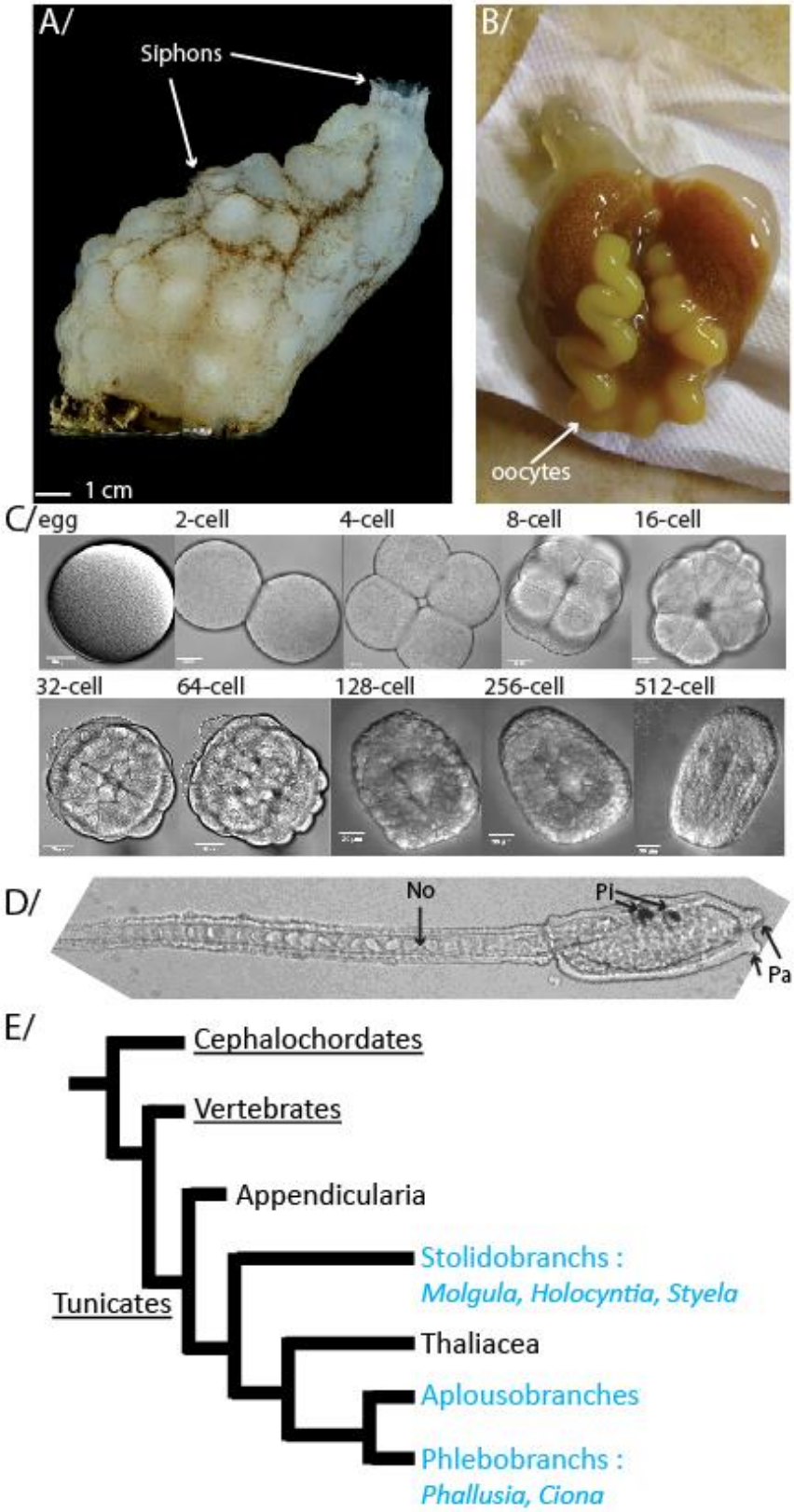

Figure 12 : *P. mammillata*, a model organism to study SAC acquisition in chordates

A/ *P. mammillata* adult with an open and a closed siphon. **B/** *P. mammillata* body retrieved after dissection of tunic. Oocytes can be recognized by their yellow color and arrow indicates oviduct full of oocytes. The sperm duct is localized under the oviduct and is not visible. **C/** Representative pictures of *P. mammillata* egg and embryos from 2- to 512-cell stage. Scale bar 30 µm **D/** A *P. mammillata* tadpole with notochord (No), adhesive papillae (Pa), pigmented cells (Pi) indicated by arrows. **E/** Phylogenetic tree of chordates with subphyla (underlined). The tunicates are more detailed with ascidians marked in blue. Representative genus are indicated in italics. Adapted from Delsuc et al., 2018 and Kocot et al., 2018.

Ascidians are subdivided into three groups based on morphology: phlebobranchs, aplousobranchs and stolidobranchs (Fig. 12E). *P. mammillata* belongs to the phlebobranch characterized by a vascular branchial sac. Similarly to aplousobranchs, their gonads are surrounded by the gut (Fig. 12B). Recent work using genomic data has revised tunicate phylogeny still grouping together phlebobranch and aplousobranchs but evolutionary closer of the thaliacea rather than the stolidobranchs. Thaliacea are free swimming species and are for this reason not part of the ascidians. Despite this revision making the ascidians a paraphyletic group, ascidians share several characteristics allowing to compare results across different species (Delsuc et al., 2018; Kocot et al., 2018).

P. mammillata is a solitary ascidian whose adults measure around 15 cm (Fig. 12A). It is found from 2 to 200 m under the sea level in the Mediterranean Sea, along the Atlantic coast, in the North Sea and in the Channel (Reguieg et al., 2018). This species is hermaphrodite and is self-fertile, although fertilization is more efficient between different individuals. Fertilization is external: both female and male gametes, spermatozoid and oocytes, are released in the sea, where fertilization occurs (Holland, 2016; Lemaire, 2011).

P. mammillata has been shown to be a convenient organism to study developmental mechanisms. Indeed, large number of gametes can be obtained thoughout the year, and *in vitro* fertilization can be easily performed to obtain large number of embryos. At 18°C, those embryos develop into a tadpole within 22 h, hence all embryonic stages can be obtained in a short time window (Holland, 2016; Lemaire, 2011). As large amounts of biological material can be easily obtained this species is amenable to biochemical approaches. Furthermore, transparency of *P. mammillata* eggs and embryos makes them excellent specimens for brightfield microscopy. In addition, injection of RNA or DNA allows expression of proteins of interest from the unfertilized eggs to the end of embryogenesis. This allows to realize functional analysis and to express fluorescent proteins to perform live microscopy. Finally, *P. mammillata* genome has been sequenced and annotated (Brozovic et al., 2018), as well as genomes of other ascidians such as *C. intestinalis* and *Ciona robusta (C. robusta),* (Delsuc et al., 2018; Kocot et al., 2018). *Ciona* genome is 160 Mb and encodes around 16 400 genes (Brozovic et al., 2018; Oda-Ishii and Satou, 2018). *P. mammillata* genome is composed of 19 400 genes subdivided into 8 chromosomes. As the species is diploid 16 chromosomes are present per cell (Brozovic et al., 2018; Colombera, 1971).

B/Embryogenesis

In this section, I will introduce ascidian development which is mostly conserved among different species. When possible, I will focus on data obtained from *P. mammillata*, the species I used for my work. However, most of the studies available have been carried out in *C. intestinalis*, *C. robusta* and *Halocynthia roretzi (H. roretzi)*. *Ciona* species are closely related *to P. mammillata* while *Halocynthia* is a more distant genus (Fig. 12E), (Delsuc et al., 2018; Kocot et al., 2018). I will try to extend the information available to *P. mammillata* while taking into account that differences could have arisen during ascidian evolution even if many processes have been shown to be conserved.

1/ From egg to embryo

During prophase I of meiosis, the oocyte increases in volume mostly by accumulating large amounts of yolk, which constitutes the nutritional stockpile for the early developing embryo. At the end of the growth phase, *P. mammillata* oocyte reaches a diameter of 130 µm and enters meiosis as indicated by breakdown of the nuclear envelope or germinal vesicle breakdown (GVBD). At this stage the meiotic spindle, which forms in the oocyte center, migrates towards the animal pole in an actin-dependent manner. Meiotic progression is then arrested at metaphase I until fertilization. As described in part I.D, this arrest is due to CSF activity dependent on the kinase Mos that activates ERK, inhibiting the APC/C to prevent Cyclin B1 degradation. Release from the CSF arrest and meiotic resumption are

induced by fertilization. In ascidians, fertilization takes place in the animal area of the egg (Costache et al., 2014; Dumollard et al., 2011; McDougall et al., 2011). The proteins required for meiotic resumption are the phosphatases PP2A and Calcineurin, whose activation leads to an increase in APC/C activity and the subsequent degradation of Cyclin B1. Pharmacological inhibition of either Calcineurin or PP2A activity results in a decrease in the efficiency of Cyclin B1 degradation, whereas inhibition of both phosphatases totally prevents Cyclin B1 degradation. Inactivation of ERK also induces meiotic resumption in unfertilized eggs (egg activation) and requires PP2A activity to release the CSF arrest (Levasseur et al., 2013). Following meiotic completion, the fertilized egg, or zygote, enters the first mitotic cycle.

In *P. mammillata*, fertilization is also the trigger of several egg shape changes associated with cytoplasmic movements (Fig. 13). This process is known as ooplasmic segregation (Sardet et al., 1989). It results in the segregation of morphogens and determinants to specific regions of the zygote. To describe these segregation process, I will focus on the movements of the most abundant maternal RNA, called Pem1 (posterior end markers), (Yoshida et al., 1996) and of the mitochondria rich cytoplasm, called myoplasm. Prior to fertilization, both Pem1 and the myoplasm tend to accumulate close to the plasma membrane (Sardet et al., 1989).

Following fertilization, a contraction is observed at the animal pole quickly followed by the formation of a lobe at the opposite vegetal side (Fig. 13A, B and C). This vegetal lobe is known as first contraction pole. Movements underlying the formation of this first contraction pole require the actin cytoskeleton (Sardet et al., 1989) and result in the localization of the myoplasm and of Pem1 RNA to the vegetal side of the egg. Few minutes after the formation of the first contraction pole, the first polar body is emitted on the opposite animal side (Sardet et al., 1989). The vegetal lobe is then reabsorbed and microtubules allow a second ooplasmic segregation starting with a second animal contraction (Goto et al., 2019; Sardet et al., 1989). At this stage, the sperm aster begins to assemble and mitochondria become less localized. A second contraction pole forms again on the vegetal side of the embryo, just before second polar body emission (Fig. 13D). Finally, the sperm aster and the male pronucleus migrate towards the female pronucleus (Fig. 13E and F). This movement is associated with movement of the myoplasm in the same direction, while Pem1 RNAs becomes localized in a subequatorial region of the ventral half of the eggs. The female pronucleus migrates also towards the egg center where male and female pronuclei meet 40 minutes after fertilization (Fig. 13F). A few minutes later, NEB occurs and the embryos enters the first mitotic cell cycle (Sardet et al., 1989).

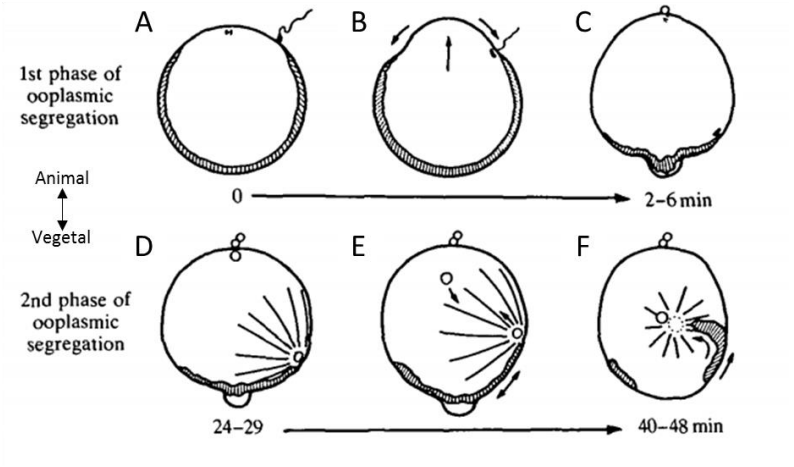

Figure 13: Morphogenetic movements in *P. mammillata* eggs.

Following fertilization, two phases of ooplasmic segregation (1st: A-C and 2nd: D-F) are observed in *P. mammillata*. The drawing indicates the shape changes undertaken by the zygotes post-fertilization. Successive movements of the myoplasm to the vegetal pole and then to equatorial position are represented in gray. Polar bodies are emitted on the animal side 6 and 29 minutes post-fertilization. Pronuclei migrate toward each other and meet at the center prior to mitotic entry around 40/48 minutes post-fertilization. Zygotes are oriented with the animal pole towards the top. From Sardet et al., 1989.

2/ From a cell to a tadpole

a/ The invariant cleavage pattern

After fertilization, cell division and morphogenesis lead to the formation of a tadpole of about 2 600 cells in 22 h (McDougall et al., 2011). In ascidians, the pattern of division is invariant which means that the time and orientation of each cell division is the same in all embryos, and as a consequence, embryos of a given stage look always alike. The ascidian cleavage pattern was first described by Conklin in 1905, using embryos of *Styela partita,* also known as *Cynthia*. This cleavage pattern is conserved among ascidians including *P. mammillata* (Dumollard et al., 2017).

The first cleavage divides the zygote following the left-right axis, partitioning the factors localized in the eggs equally within the two daughter cells. In the following cell cycles asymmetrical divisions progressively segregate maternal factors into specific blastomeres. The differential distribution of maternal factors participates in the specification of both the anteroposterior axis and the animal-vegetal axis. In addition, asymmetric cell divisions give rise to cells of different sizes starting from the 4th mitosis, 8- to 16-cell stage. In particular, this 4th cleavage gives rise to a small posterior dorsal cell easily identifiable towards which the yolk is preferentially localized and which will continue to divide asymmetrically (Fig. 12C and Fig. 14, cell B6.3) and will give rise to the germ cell lineage (Conklin EG, 1905).

Thanks to this invariant cleavage, each blastomere can be precisely identified based on its positions with respect to the three main axes: left-right, animal-vegetal and anterior-posterior and can be named based on the rules explained below (Fig. 14), (Conklin EG, 1905) :

Each blastomere is identified firstly by a letter which depends on the position along the anteroposterior axis: anterior blastomeres are identified by the letter “A” and posterior blastomeres by the “B”. A capital letter is used if the cell belongs to the vegetal pole whereas a lower case indicates that the cell belongs to the animal pole, which is defined as the side of polar body emission. The number of cell cycles that a cell has undergone since fertilization, with 1 corresponding to the zygote, is then indicated. Finally, each blastomere is identified by a specific number reported after the full stop. As left-right symmetry is maintained throughout embryogenesis, blastomeres on each half are indicated with the same name. When there is a need to distinguish between them, the cell name of one side is underlined.

Based on these rules, it can be easily established that cell A6.1 (Fig. 14) is an anterior (A) vegetal (capital) cell of the 32-cell embryo (6th cell cycle), (Conklin EG, 1905).

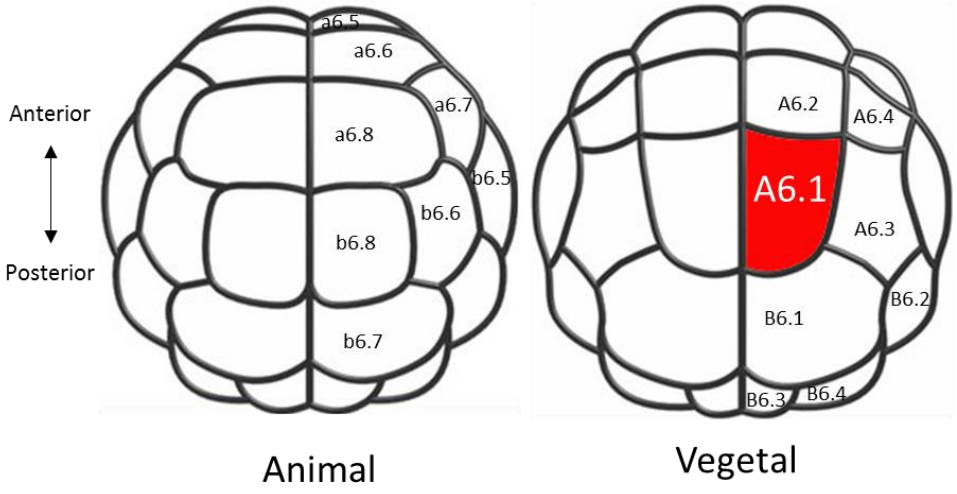

Figure 14 : Cell identification in ascidian embryos:

Animal and vegetal views of a schematic *C. robusta* embryo at 32-cell stage. Blastomere names are indicated according to ascidian nomenclature. The blastomere A6.1 used as an example in the text is shown in red. Drawing was retrieved from Aniseed database, Brozovic et al., 2018.

b/ Cell cycle variations during embryogenesis

In *P. mammillata* embryos, mitosis was shown to have a constant duration and to last 13 minutes at 19°C from the 2-cell stage to at least the 110-cell stage, 2nd to 8th cell cycles (Fig. 15), (Dumollard et al., 2013). Interphase duration instead increases during embryogenesis, starting from the 2-cell stage. In the first four cycles, to the 16-cell stage, lengthening of interphase occurs equally in all blastomeres and all cell cycles are therefore synchronous. Asynchrony in cell cycle duration among blastomeres begins to appear at the 16-cell stage (Fig. 15). In these embryos, vegetal blastomeres, forming the "A" and "B" lines, divide first, with the germline precursor, B5.2, dividing few minutes after the others. Animal-vegetal asynchrony is due to a delay in mitotic entry in animal blastomeres compared to vegetal blastomeres, caused by an increase in interphase duration. In somatic cells, treatment with aphidicolin, a drug that impairs DNA replication, arrests cells in S-phase or G2 due to the activation of the DNA replication checkpoint. Instead, in early embryos of *P. mammillata,* the DNA replication checkpoint is not efficient and does not block progression through the cell cycle. Therefore, in the presence of aphidicolin, blastomeres continue to progress through the cell cycle without undergoing proper DNA replication and DNA bridges form between daughter cells when mitosis occurs in the presence of unreplicated DNA regions. Those defects, however, only occur if aphidicolin treatment is performed prior to completion of S-phase. Aphidicolin treatments showed that animal blastomeres spend more time in S phase than vegetal cells and therefore reach mitotic entry asynchronously. Aphidicolin treatment also indicates that animal cells enter mitosis several minutes after exiting S phase. This suggests that a G2 phase is already present in 16-cell stage embryos (Fig. 15), (Dumollard et al., 2013).

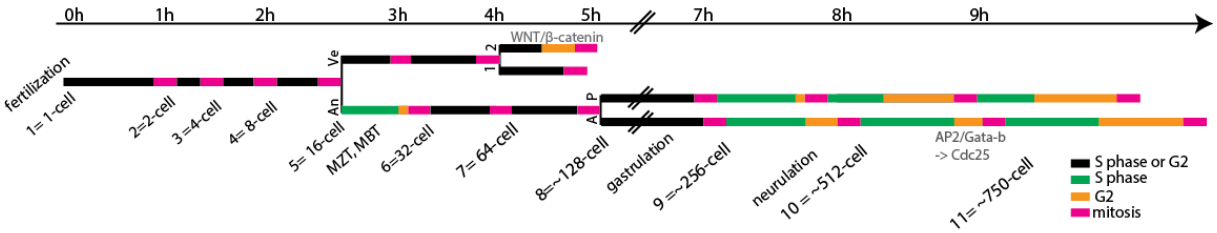

Figure 15 : Cell cycles during embryogenesis in ascidians

Schematic representation of embryonic cell cycles during *P. mammillata* development from fertilization to neurula. Mitosis is indicated in pink. Mitotic duration is constant throughout embryogenesis. Interphase is marked in black in the early stages when no distinction between different phases is possible. For later stages, when the information is available, S phase (green) and G2 (orange) are indicated. The figure combines data from *P. mammillata* for 1st to 7th cell cycle (Dumollard et al., 2013) and from *C. intestinalis* for 8th to 11th cell cycle (Ogura and Sasakura, 2016; Ogura et al., 2011). The duration of the different cell cycle stages is not absolute but indicative of the ratio between different stages within each cycle. Branches indicate separation of different embryonic domains: animal (An) later divided into anterior (A) and posterior (P), and vegetal (Ve) later divided into vegetal 1 (1) and vegetal 2 (2). Cell divisions continue beyond indicated times in each domain, but no data is available in the literature for these later cycles. Pathways involved in cell cycle changes (grey) are indicated at the time when they are activated. A timeline for *P. mammillata* development at 18°C is given above. Embryonic cell cycle and corresponding cell number are provided on the bottom.

The asynchrony between vegetal and animal blastomeres in early embryos is due to specific activation of the WNT/β-catenin pathway in vegetal cells (Dumollard et al., 2013). The WNT/β-catenin pathway is involved in many developmental processes. Here I will briefly introduce the canonical WNT/β-catenin pathway (Fig. 16).

When the WNT pathway is inactive, β-catenin is in a complex with axin, dishevelled (Dvl), APC, CK1, and Glycogene synthase kinase 3 (Gsk3). APC and Axin are scaffold proteins that allow the complex to be formed, while GSK and CK1 are kinases that phosphorylate β-catenin. Once phosphorylated, β-catenin is ubiquitinated and degraded by the proteasome. In these cells, TCF a chromatin regulator is bound to the transducing-like enhancer of split (TLE/groucho) preventing gene expression.

When the WNT pathway is activated, the extracellular ligand wingless (WNT) activates the transmembrane receptor Frizzled, inducing its association with the Lipoprotein receptor related protein (LRP), another transmembrane protein. Frizzled and LRP then recruit Axin and Dvl from the cytoplasm to the plasma membrane, leading to the disassembly of the complex targeting β-catenin to the proteasome. Free β-catenin migrates into the nucleus where it associates with TCF, enabling transcriptional activation (Tortelote et al., 2017).

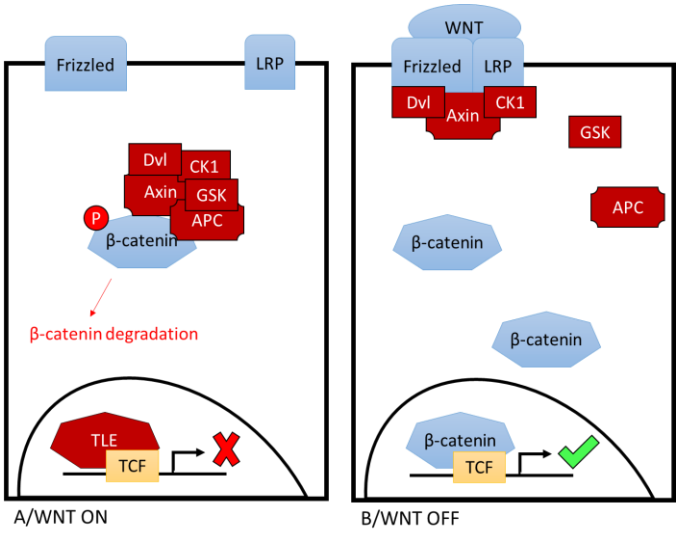

Figure 16 : WNT/ β-catenin canonical pathway.

A/In the absence of WNT ligand, the WNT pathway is inactive and GSK and CK1, in a complex with Dvl, Axin and APC, phosphorylate β-catenin marking it for degradation by the proteasome. Under this condition, TCF bound to TLE inhibits gene expression. **B/** When the WNT pathway is active, WNT binding to its receptors Frizzled and LRP recruits Dvl, Axin and Ck1 to the plasma membrane. β-catenin is no longer phosphorylated and can accumulate in the nucleus where it interacts with TCF inducing expression of target genes. Adapted from Tortelote et al., 2017.

In *P. mammillata* 16-cell embryos, β-catenin is nuclear in vegetal blastomeres, indicating an active WNT/β-catenin pathway, but is cytoplasmic and inactive in animal blastomeres. Both activation of the WNT/β-catenin pathway in animal blastomere by GSK inhibition or β-catenin overexpression, or inactivation of the WNT pathway in vegetal cells by morpholino against β-catenin or a dominant negative form of TCF (DN-TCF), result in synchronized division of animal and vegetal cells. These experiments show that the difference in WNT/β-catenin activity controls cell cycle asynchrony. WNT/β-catenin is itself controlled by Pem1. Indeed, ablation of the 1st contraction pole, where Pem1 RNA is localized, induces loss of WNT/β-catenin activity and leads to a slower cell cycle in vegetal cells, similar to the cell cycle in animal blastomeres. On the contrary, Pem1 overexpression activates the WNT/β-catenin pathway in all blastomeres leading to a faster cell cycle in animal cells, which become similar to vegetal blastomeres (Dumollard et al., 2013).

It is also at the 16-cell stage, 5th cell cycle, that zygotic transcription is mostly activated in ascidians, although a few genes are already expressed at low level a cell cycle earlier (Fig. 15). Even though in ascidians, maternal transcripts are not actively degraded and continue to influence embryonic development, the acquisition of zygotic transcription allows embryos to depend less on maternal factors, marking the maternal to zygotic transition (MZT), (Matsuoka et al., 2013; McDougall et al., 2011; Oda-Ishii and Satou, 2018). As cell cycle asynchrony, G2 and MZT are all acquired at the 16-cell stage (Fig. 15), this stage is often considered as the the mid-blastula transition (MBT) (Matsuoka et al., 2013; McDougall et al., 2011; Oda-Ishii and Satou, 2018).

At the 7th cell cycle (64-cells), in addition to the asynchrony between vegetal and animal blastomeres, a new asynchrony starts at the vegetal pole with the vegetal 1 domain entering mitosis before the vegetal 2 domain (Fig. 15). Aphidicolin treatment at this stage, shows that this difference is due to the presence of a longer G2 phase in the 2nd vegetal group (Dumollard et al., 2013). The following cycles have not been analyzed for these blastomeres, although cells continue cycling. At the end of the 7th cell cycle some blastomeres delay in interphase while the others undergo mitosis. This

leads to the formation of an embryo with 110 cells. During this 8th cell cycle, ascidian embryos start to gastrulate (Fig. 15), (Conklin EG, 1905).

For cell cycles 9th to 11th, I will only focus on cells that continue to divide at a similar rhythm, especially animal blastomeres which give rise to the epidermis (Fig. 15). To study these late cell cycles, authors have relied on a combination of methods based on cell cycle events. During S-phase, DNA replication results in the integration of new nucleotides in the DNA. Incorporation of specific nucleotides like 5–ethynyl–2'–deoxyuridine (EdU) in the DNA allows the identification of cells that have undergone S-phase. Another technique that permits to follow transitions through the cell cycle is based on fluorescent sensors fused to cell cycle regulators, present only at specific phases of the cell cycle. Typically, Cdt1, which accumulates in G1, and Geminin, which accumulates in S-phase, G2 and mitosis are used. Given their dynamic pattern of accumulation and degradation, the co-expression of these two proteins fused to RFP and GFP respectively allows the progression through the cell cycle to be followed and the different cell cycle stages to be identified based on the relative concentration of the two proteins. This technique is called fluorescent ubiquitination-based cell cycle (FUCCI). Finally, a classical marker of proliferating cells is the proliferating cell nuclear antigen (PCNA) which localizes in the nucleus during interphase and forms foci during S phase (Ogura and Sasakura, 2016; Ogura et al., 2011).

Using a combination of these techniques, it was shown that during the 9th to 11th cell cycles, G1 is still not acquired in *C. intestinalis* epidermis. In addition, posterior blastomeres divide before anterior ones creating a mitotic wave along the epidermis. More precisely, four mitotic domains, defined by separate waves of mitosis, could be observed in the embryo: ventral, dorsal, trunk lateral side and tail lateral side. These mitotic waves are due to variations in the duration of S- and G2-phase, which in turn impacts the time of mitotic entry. Using the three tools described above, the following variations in cell cycle progression in the ventral epidermis could be described (Fig. 15), (Ogura and Sasakura, 2016; Ogura et al., 2011):

- During the 9th cell cycle, anterior cells become delayed compared to posterior cells due to a longer G2.
- During the 10th cell cycle, G2 is elongated in posterior cells, which have instead a shorter S phase than anterior cells, giving rise to interphase of similar duration along the whole anteroposterior axis and therefore maintaining the same asynchrony present during the previous cell cycle. The extension of G2 is due to a stronger expression of Cdc25 induced by GATA-b and AP2-like2 in anterior cells compared to posterior cells.
- During the 11th cell cycle, G2 is extended equally both in anterior and posterior cells increasing the time spent in interphase for all cells along the anteroposterior axis. However, interphase is shorter in posterior cells due to a shorter S-phase. This results in an increase in the asynchrony between anterior and posterior cells.

Following the 11th cycle, cell cycle continues to slow down while cell movements cause the displacement of the animal vegetal axis and the formation of a trunk and a tail, giving rise to a tailbud. At the same time intercalation of notochord cells allows them to be organized in a single line along the anteroposterior axis. Notochord cells form vacuoles, which provide rigidity to the tail. In the tailbud, pigmentation of two cells, otolith and ocellus, can progressively be observed in the trunk. The pigmented cells become able to detect gravity and light intensity. Protrusions, called palps, form at the anterior of the larva giving rise to a structure that will allow the larva to attach to the substrate. This fully formed tadpole (Fig. 12D) hatches from the chorion (Hotta et al., 2007). Ascidian tadpoles swim by tail beating and orient themselves by using the pigmented cells. When the tadpole reaches an adequate substrate, its palps allow adhesion to the substrate which triggers metamorphosis (Karaiskou et al., 2015).

During embryogenesis, cell cycle dynamics and morphogenesis are closely connected. Indeed, relative changes in cell cycle length between blastomeres can affect the invariant cleavage pattern

leading to malformed embryos. It was shown that both animal-vegetal and anterior-posterior asynchrony are required for proper development (Dumollard et al., 2017; Ogura and Sasakura, 2016; Ogura et al., 2011).

From the 5th to 7th cell cycle (16- to 64-cell stage), loss of cell cycle asynchrony in *P. mammillata* caused by changes in the WNT/β-catenin pathway or by Wee1 expression in vegetal cells, gives rise to malformed embryos (Dumollard et al., 2017). In the absence of cell migration, the relative position of cells within the embryo is determined by the plane of cell division during cytokinesis. Cytokinesis takes place perpendicularly to the mitotic spindle, which is oriented along the longest apical cell axis. Cell shape depends on the shape of neighboring cells, which changes during their cell cycles. In mitosis, cells become rounder. Consequently, to perform cytokinesis always at the same place, blastomeres have to divide when their neighboring cells are at a specific step of the cell cycle. When animal-vegetal asynchrony is lost, blastomeres define their axis while being in contact with mitotic cells rather than with interphase cells. The difference in the shape of neighboring cells influences the positioning of the plane of cytokinesis ultimately modifying the position of the daughter cells and altering the cleavage pattern (Dumollard et al., 2017).

In the 11th cell cycle, interphase lengthening is required for neurulation. Overexpression of Cdc25, which accelerates mitotic entry, impairs neural tube closure. Aphidicolin treatment, which increases S-phase duration at this stage, rescues the neurulation defect observed in Cdc25 overexpressing embryos, showing that lengthening of interphase duration, and not specifically of G2, is required for proper neurulation (Ogura and Sasakura, 2016; Ogura et al., 2011).

3/Anteroposterior patterning

During my thesis work, I observed a difference in control of mitosis along the anteroposterior axis. Therefore, I will present here in more detail how the anteroposterior axis is patterned during ascidian embryogenesis.

a/ Maternal contribution in anteroposterior patterning

Following fertilization, ooplasmic segregation localizes maternal factors in specific areas of the zygote (Fig. 17A). Their role in embryonic patterning was analyzed mostly by microsurgery in *H. roretzi.* Except for absolute timing, ooplasmic segregation occurs in a similar way in *H. roretzi* and in *P. mammillata* (Nishida, 1994, 1996; Sardet et al., 1989).

Ablation of the vegetal cytoplasm localized in the 1st contraction pole, generates eggs deficient in vegetal cytoplasm (VC-deficient). VC-deficient embryos do not undergo gastrulation and instead give rise to nearly spherical permanent blastulas, formed by a monolayer of cells surrounding one or more cavities. These embryos are composed almost exclusively by epidermal cells indicating loss of cell fates specific to the vegetal pole. This loss of embryo shape and cell fates is associated with the complete loss of the invariant cleavage pattern. All divisions become symmetric and the yolk, which in wild type embryos accumulates preferentially in vegetal cells, is distributed equally between animal and vegetal cells. Orientation of cell division is also disturbed, leading to the formation of embryos (16-/32-cell), which are radially symmetric, both along the left-right and the anteroposterior axis. These embryos are often referred to as radialized embryos (Fig. 17B and C), (Nishida, 1996). Radialized embryos were also obtained when similar polar ablations were performed in *P. mammillata* (Dumollard et al., 2017). These experiments suggest that in ascidian embryos, factors required for gastrulation and determinants of vegetal and posterior identities are localized in the most vegetal area of the egg between the 1st and 2nd ooplasmic segregation (Fig. 17A), (Nishida, 1996). Factors that are known to be present in the 1st contraction pole in *H. roretzi* and *P. mammillata* are the RNA of Pem1 and the centrosome attracting body (CAB). The CAB is required for asymmetric division of germline progenitor

cells and its loss in VC-deficient embryos can explain at least in part the loss of proper cleavage pattern (Dumollard et al., 2017; Nishikata et al., 1999).

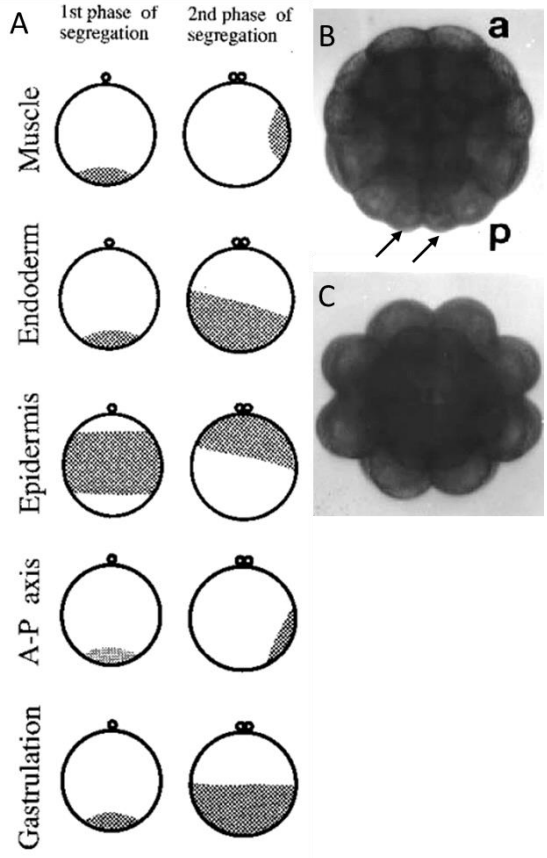

Figure 17 : Maternal factors required for embryonic patterning are specifically localized in the egg.

A/ Following fertilization, ooplasmic segregation localizes maternal factors to specific areas of the zygote. The localization pattern for factors required for specification of muscle, endoderm, epidermis, for patterning of the anteroposterior (A-P) axis and for gastrulation are indicated both during the 1st and the 2nd phase of segregation (shaded area). Zygotes are oriented with the animal pole upward. **B/** Representative photo of a 32-cell *H. roretzi* embryos. Cells located at the anterior (a) and posterior (p) poles have different shapes and the embryo can be oriented. Arrow indicates the smallest cells of the embryo present at the posterior pole. **C/** Picture of a 32-cell *H. roretzi* VC-deficient embryos resulting from the ablation of the 1st contraction pole. These embryos are radially symmetrical with identical anterior and posterior poles. Adapted from Nishida, 1996.

Following the 2nd ooplasmic segregation in *H. roretzi*, almost half of the egg cytoplasm has to be removed to impair gastrulation, showing that factors previously tightly localized near the vegetal cortex, are relocalized and distributed in a wider vegetal area (Fig. 17A). However, factors required for anteroposterior patterning remain tightly localized to a restricted area which is displaced to a subequatorial ventral region (Fig. 17A). Indeed, ablation of this part of the fertilized egg leads to the development of embryos containing epidermis, endoderm and an increased number of notochord cells but no muscle cells. In control embryos, this cell fate repartition is characteristic of the anterior fate. Moreover, in ablated embryos, the position of cells with respect to their fates is also similar to the anterior part of control embryos. This indicates that embryos are anteriorized. Conversely, graft of cytoplasm from the ventral subequatorial region to the opposite side of the egg leads to posteriorization of the embryo (Nishida, 1994).

Thus, maternal factors required for patterning of the anteroposterior axis are already present in the egg and their ablation prevents correct patterning of the embryo.

b/ Patterning of the epidermis along the anteroposterior axis

In ascidians, all epidermal cells derive from animal cells of the “a” and “b” lines. Using *in situ* hybridization with specific probes, the epidermis can be divided into five domains along the anteroposterior axis. These domains are progressively specified during embryogenesis and are best identified at the tailbud stage. Using data from both *H. roretzi* and *C. intestinalis*, and keeping in mind that some details may differ among different ascidian species, gene expression in those five domains can be described as follows from anterior to posterior (Fig. 18).

The most anterior domain, corresponding to the anterior part of the trunk, expresses Dll-1 and Ror-a. Oth, sFRP1/5 and Otx are also expressed in this anterior domain but their expression is broader and extends into the 2nd domain, which does not express Dll-1 and Ror-a. Fox-F and Hox1 are expressed in the 2nd and 3rd domain. sFRP1/5 and Otx are also expressed in the 3rd domain, which instead does not express Oth. The 3rd domain covers the tailbud trunk. The 4th domain constitutes most of the tail and is specified by the expression of Cad and Cdx. The 5th domain is localized in the tail tip and is defined by the expression of TT1 or Hox12. In addition, Zf115 was shown to be expressed both in the 4th and 5th domains (Fig. 18).

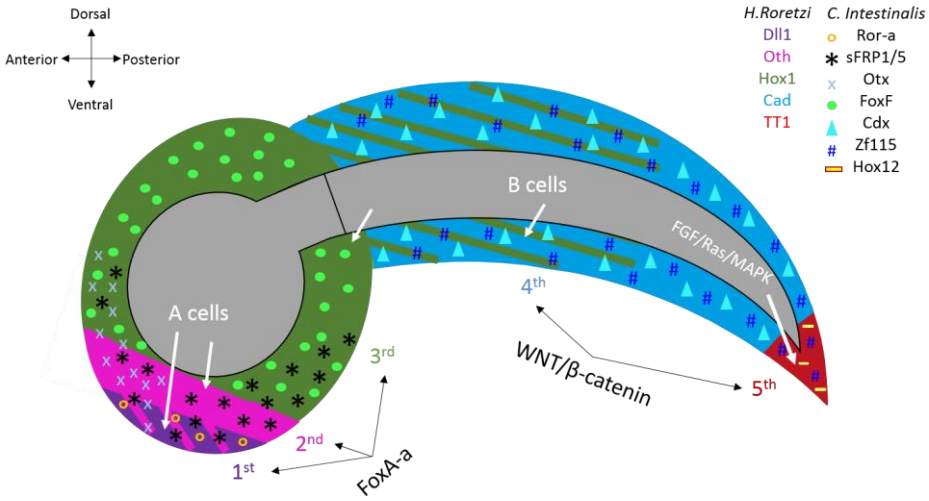

Figure 18 : Patterning of the epidermis along the anteroposterior axis.

In ascidians, the epidermis is divided in five domains along the anteroposterior axis. These domains are defined by patterns of gene expression that were visualized by *in situ* hybridization with specific probes listed on the right-hand corner of the figure. Data summarized in the schematic representations come from experiments performed in *H. roretzi* and *C. intestinalis.* Transcripts whose expression was analyzed in *H. roretzi* are represented by background colors, whereas data from *C. intestinalis* by symbols. Pathways (black arrows) involved in the patterning of the epidermis, and inductive signals (white arrow) coming from vegetal cells localized inside the embryo (grey, A and B cells) are indicated. Adapted from Feinberg et al., 2019; Lamy et al., 2006; Takatori et al., 2007; Wada et al., 1999.

Patterning of the epidermis is achieved through induction by the vegetal cells. More precisely, anterior vegetal cells of the "A line" allow the specification of the 1st and 2nd domains, whereas posterior vegetal cells of the "B line" allow the specification of the 3rd, 4th and 5th domains. Epidermis specification by vegetal cells was tested in *H. roretzi*. Following the isolation of animal cells, expression of all epidermal markers was lost. However, when only half of the vegetal cells was removed, either the "A line" or the "B line", only some domains were lost, respectively 1st and 2nd or 3rd, 4th and 5th. Loss of certain epidermal domains did not lead to an expansion of the remaining domains. Microsurgery experiments aimed at removing specific vegetal cells at different embryonic stages, showed that the 1st to 4th domains require vegetal signals until the 32-cell stage, while the 5th domain requires inductive signal until neurula stage (Takatori et al., 2007; Wada et al., 1999).

The FGF-Ras-MAPK pathway participates in the induction of the 5th domain in *H. roretzi*. Treatment with inhibitors of either FGF or MEK at 1-cell, 64-cell or gastrula stages prevents the expression of TT1 in favor of Cad in the 4th domain. This indicates that the FGF-Ras-MAPK pathway is required to induce the identity of the 5th domain and to repress the identity of the 4th domain in the most posterior cells. However, if treatments with those inhibitors are performed after the activation of TT1 expression, no changes in the expression pattern can be observed. This indicates that once cell fate is specified, the FGF-Ras-MAPK pathway is no longer required for maintenance of the 5th domain (Takatori et al., 2007).

Experiments performed in *C. intestinalis,* however*,* indicate that vegetal signals and the FGF-MAPK pathway are not sufficient to explain patterning of the epidermis along the anteroposterior axis. Indeed, treatment with MEK inhibitors or removal of vegetal cells at the 8-cell stage did not affect expression of sFRP1/5 in the 1st, 2nd and 3rd anterior domains. sFRP1/5 starts to be expressed at 64-cell stage in anterior animal cells of the "a" line. This expression relies on a *cis*-regulatory region in its promoter which is recognized by the transcription factor FoxA-a. Morpholinos against FoxA-a induce loss of sFRP1/5 expression, while ectopic expression of FoxA-a in all epidermal cells, leads to sFRP1/5 expression throughout the epidermis. FoxA-a was shown to affect in a similar fashion the expression of Otx, starting from neurula. This indicates that FoxA-a induces gene expression in the 2nd and 3rd anterior domains. Moreover, FoxA-a inhibits expression of two markers of the posterior peripheral nervous system (Delta2 and Msxb). This suggests that not only FoxA-a allows the expression of genes specific for the identity of the anterior domains but also prevents the expression of those genes specific to posterior domains (Lamy et al., 2006).

In situ hybridization experiments revealed that FoxA-a is expressed similarly in embryos of *P. mammillata* and *C. robusta.* FoxA-a is among the first genes to be expressed in 8-cell stage embryos and is highly expressed at the 16-cell stage. FoxA-a is expressed in both animal and vegetal cells but its expression is limited to anterior cells (Madgwick et al., 2019). The restriction of FoxA-a to the anterior part of the embryo depends on Pem1 and injection of morpholinos against Pem1 leads to the expression of FoxA-a in posterior cells (Oda-Ishii et al., 2018). Conversely, injection of Pem1 RNA results in the loss of anterior tissues, such as palps and pigmented cells (Yoshida et al., 1996).

Finally, the Wnt/β-catenin pathway was also shown to be involved in anteroposterior patterning and to be required for the specification of the posterior domain. In gastrula of *C. intestinalis*, inhibition of Wnt signaling by either DN-TCF or sFRP1/5 overexpression reduces expression of markers of the 5th domain. Ectopic activation of the pathway, either by injection of a constitutively active form of β-catenin or by GSK inhibition (Fig. 16), instead leads to loss of trunk domains. This is associated with the expansion of the 4th and 5th posterior epidermal domains. When the treatment was performed at the neurula stage only the formation of epidermal sensory neurons was affected and no effect was observed when the treatment was performed at tailbud stage, further supporting that the epidermal domains are fully specified by the neurula stage (Feinberg et al., 2019).

Results

During my thesis, I aimed at studying SAC efficiency in *P. mammillata* during embryogenesis in order to determine if the SAC that is not efficient at the 2-cell stage, is acquired at a later stage (part I). I then aimed at beginning to decipher the mechanisms that underlie the lack of SAC efficiency in early embryos (part II).

All experiments reported in this work have been carried out by myself, except:

- Lydia Besnardeau prepared all probes for *in situ* hybridization and performed the experiments for Cdc20 and SAC RNAs. She performed yeast two hybrid experiments and participated in cloning required for this study. She made *P. mammillata* Mad1 and Mad2 recombinant proteins that were used for antibody production.
- Stefania Castagnetti carried out the western blot for Mad1
- Janet Chenevert recorded 2-cell embryos treated with DMSO or nocodazole that are the same movies used for the paper Chenevert et al., 2019 submited at Development (annex 4). She also performed the immunofluorescence for Mad1.

I/ SAC efficiency during *P. mammillata* embryogenesis

A/Nocodazole efficiently disrupts mitotic spindles

To assess SAC efficiency during the development of *P. mammillata*, I used the microtubule depolymerizing drug, nocodazole which leads to the formation of unattached kinetochores (Vasquez et al., 1997). I used a high concentration of nocodazole (10 µM) to depolymerize all visible microtubules generating a full set of unattached kinetochores and to produce maximal possible signal for SAC activation (Subramanian and Kapoor, 2013).

To confirm that in this condition, nocodazole efficiently prevents microtubule polymerization, I co-injected eggs with RNAs encoding histone 2B bearing a red fluorescent tag, H2B-RFP, and the microtubule associated protein EB3, bearing a green fluorescent tag, EB3-3GFP. I then let embryos develop until the gastrula stage before adding either DMSO or nocodazole to the sea water. In DMSO treated embryos, both EB3-labelled centrosomes and mitotic spindles were easily visible (Fig. 19). Following nocodazole treatment no spindle structures could be detected in mitotic cells, which were identified by the presence of condensed chromosomes (Fig. 19).

Microtubules were harder to detect at early stages of development due to the low level of expression of EB3-3GFP and the large cell size. However, immunofluorescence with anti-tubulin antibodies showed that nocodazole treated 2-cell embryos had no visible spindle microtubules (Chenevert et al., 2019).

In most experiments, the effect of nocodazole on microtubules was not assessed directly but as microtubules are also required for cytokinesis, the absence of cytokinesis confirmed lack of microtubules.

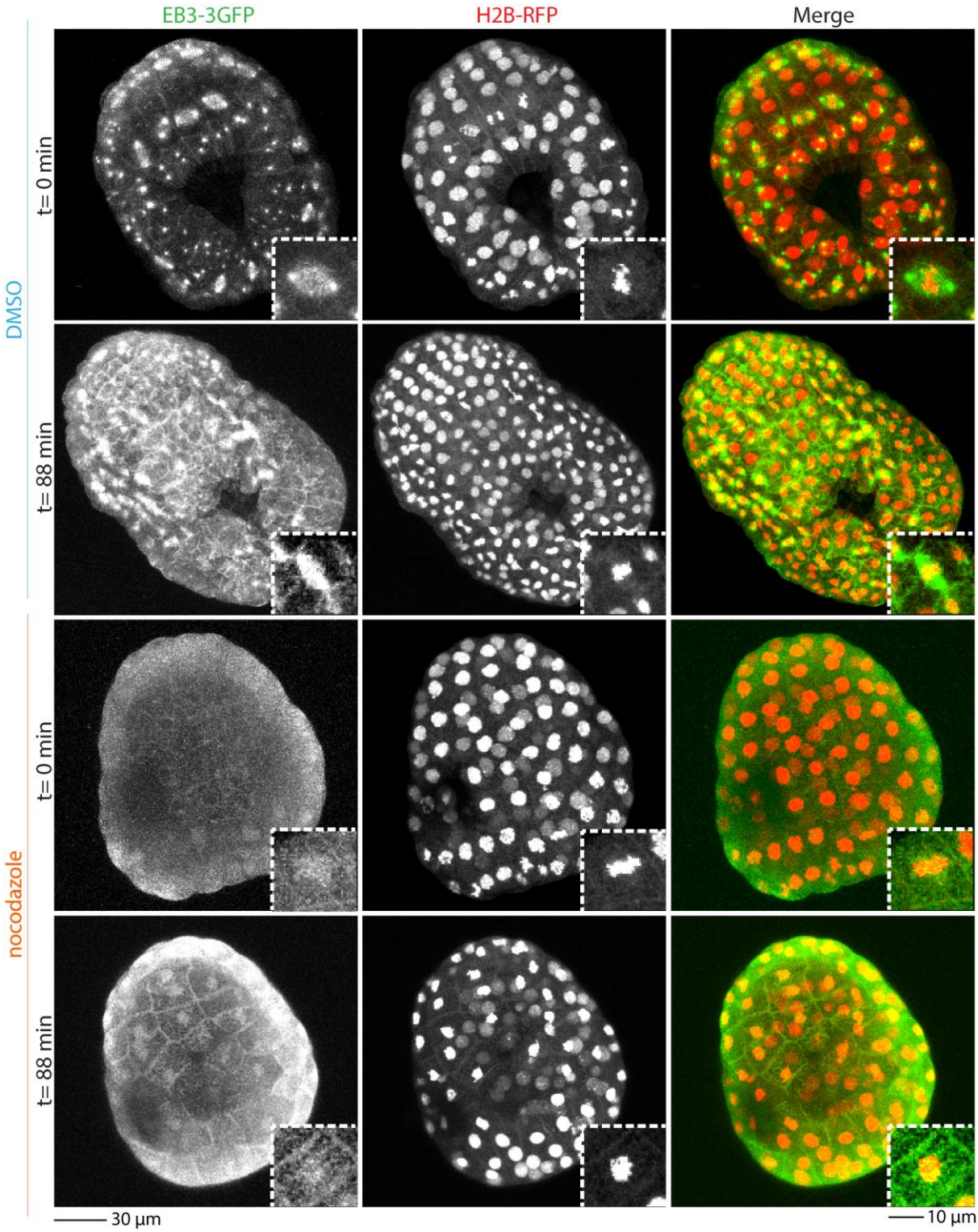

Figure 19: Nocodazole induces microtubule depolymerization

Z-projections of confocal stacks from beginning and end of time lapse video recordings of embryos expressing EB3-3GFP and H2B-RFP, to visualize microtubules and DNA respectively. 128-cell embryos were treated with either DMSO (top) or with 10 µM nocodazole (bottom), before the beginning of acquisition. Embryos were imaged for 88 minutes. Scale bar for full embryos is 30 µm (left) and for insets is 10 µm (right).

B/The SAC is not efficient in meiosis

In *P. mammillata* oocytes, following fertilization, meiosis resumes and the pronucleus forms with similar timing both in the presence and in the absence of nocodazole, indicating that those cells exit meiosis without delay in the absence of microtubules and are therefore SAC deficient (Dumollard et al., 2011). However, meiosis consists of two divisions and the observation of pronuclear formation does not imply that both divisions were performed but only that the cell went back in interphase. I therefore decided to confirm lack of SAC activity in meiosis by analysing progression through meiosis in the presence, or not, of nocodazole. I used the phosphorylation status of PP1A, a direct target of Cyclin B1-Cdk1, as a marker of Cdk1 activity (Lewis et al., 2013). PP1A is phosphorylated by Cyclin B1-Cdk1 from late G2 to metaphase. However, when the cells enter anaphase, following APC/C mediated Cyclin B1 degradation, Cdk1 is inactivated resulting in a decrease in PP1A phosphorylation (Fig. 20A). In cells with an efficient SAC, spindle defects cause APC/C inhibition and subsequent maintenance of high Cyclin B1-Cdk1 activity, which results in prolonged PP1A phosphorylation (Wu et al., 2009).

P. mammillata unfertilized eggs are arrested in metaphase I of meiosis (see introduction part I.D and IV.B). Meiosis resumption can be induced by treatment with ionomycine, an ionophore that causes an increase in intracellular Ca^{2+} levels, mimicking fertilization (Dumollard et al., 2011). Therefore, to test SAC activity during meiosis in *P. mammillata*, I treated unfertilized eggs with either nocodazole or DMSO for 15 minutes, before activating them with ionomycine (Fig. 20B). I then sampled eggs every minute until completion of the 1st meiotic division (12/15 min) and analyzed changes in PP1A phosphorylation. While performing this analysis, I observed that PP1A protein levels varied extensively between different egg batches (batch = ensemble of eggs retrieved from the same adult)

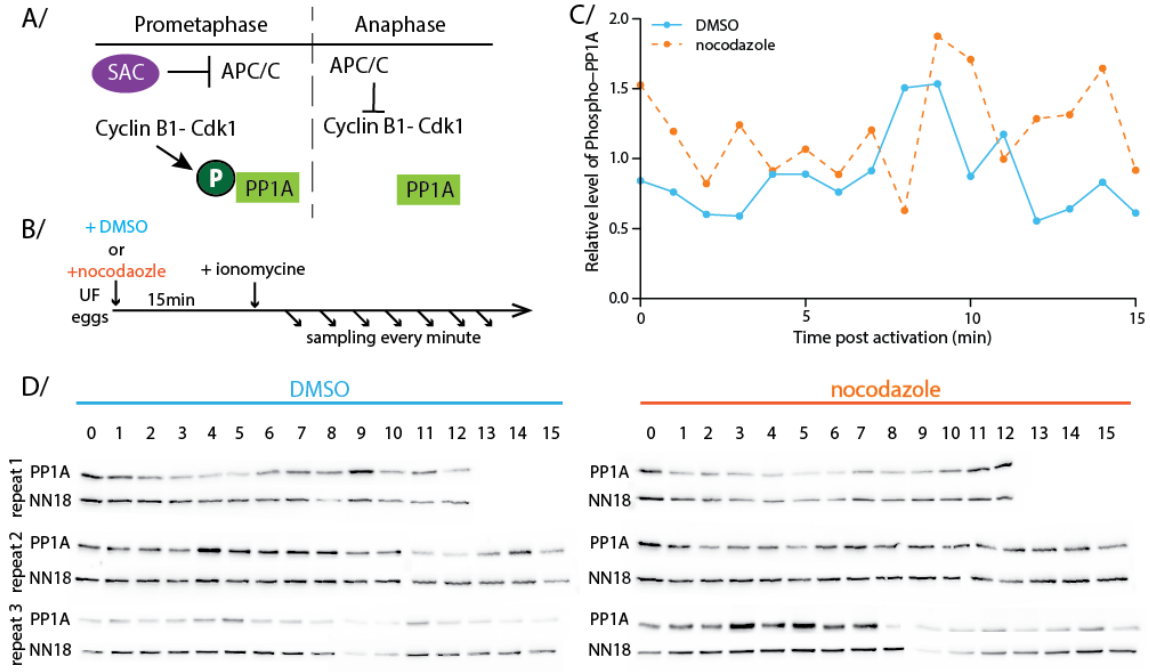

Figure 20 : The SAC is inefficient in meiosis.

A/ Schematic representation of the control of PP1A phosphorylation during mitosis. In prometaphase, SAC activation results in inhibition of APC/C and stabilization of the Cyclin B1-Cdk1 complex that can phosphorylate PP1A. At the onset of anaphase, inactivation of the SAC releases APC/C resulting in inhibition of Cyclin B1-Cdk1 and PP1A dephosphorylation. **B/** Schematic of experimental design: unfertilized (UF) eggs were incubated for 15 minutes with either nocodazole or DMSO, prior to activation with ionomycine. Following activation, 20 eggs were retrieved every minute to assess PP1A phosphorylation by western blot. **C/** PP1A phosphorylation levels were quantified with ImageJ and normalized using NN18 levels. The average of the three repeats was plotted for each time point. **D/** Western blots used for quantification reported in B. Time of sampling (in minutes) is indicated above. In the first experiment (top) sampling was carried out only for 12 minutes.

and even within the same batch. This is in agreement with data from the ascidian *C. intestinalis* showing that only 25% of genes are expressed at comparable levels between batches in unfertilized eggs (Matsuoka et al., 2013).

Despite this great variability, I could observe that PP1A phosphorylation decreased in the presence of nocodazole with similar dynamics to control DMSO treated eggs (Fig. 20C and D), indicating that Cyclin B1-Cdk1 inactivation occurs without delay. Moreover, PP1A levels rose again in both control and nocodazole treated eggs, indicating progression into the second meiotic division. This data confirms that the SAC is inefficient during *P. mammillata* meiosis. In addition, because these experiments were performed without fertilization, it excludes the possibility that spermatozoa bring specific components that inactivate the SAC upon fertilization.

C/In the absence of microtubules, mitotic duration is extended beginning at the 8th cell cycle

P. mammillata 2-cell embryos are SAC deficient (Chenevert et al., 2019), however it is not known if the SAC becomes active during embryogenesis. To address this question, I analyzed mitotic duration at all developmental stages from 2-cell to neurula. When the SAC is activated, mitotic exit is delayed and this increases the time a cell spends in mitosis. I measured mitotic duration in control DMSO-treated embryos and nocodazole treated embryos at all stages to determine whether the SAC was active or not. I expected that mitotic duration would be comparable in DMSO and nocodazole treated embryos when the SAC is inefficient. In contrast, when the SAC becomes efficient, mitotic duration would be extended in nocodazole treated embryos compared to control embryos (Fig. 21B). Mitotic duration was measured as the time spent between NEB and NER (Fig. 21A). In early stages (2- to 16-cell embryos) nuclei could be followed directly by brightfield microscopy. However, for later stages, this was not possible any more as the different layers of cells make it difficult to see nuclei. I therefore labelled nuclei using microinjected constructs to express a fluorescent protein, either Venus or Tomato, fused to a nuclear localization signal (NLS-3Venus or NLS-Tomato) (Fig. 21C). During interphase, prior to NEB, the NLS protein localizes to the nucleus, but following NEB the signal disperses in the cytoplasm and nuclei are no longer identifiable until NER at mitotic exit when the protein localizes again to the re-assembled nucleus (Fig. 21C). Mitotic duration was measured as the time when cells have no nuclear NLS signal. In the experiments performed with late stage embryos (more than 64-cells), the embryonic stage and corresponding cell cycle was determined by counting the number of nuclei using the Imaris software. *P. mammillata* embryos undergo gastrulation during the 8th cell cycle. At this stage they contain around 128-cells. Embryos with about 256-cells are in the 9th cell cycle and embryos with about 512-cells are at the neurula stage and in the 10th cell cycle. Finally, when analyzing mitotic duration I compared medians of the population as the mean can be affected by extreme values and is highly impacted by outliers (Gaddis and Gaddis, 1990). However, for completion, means and standard deviations are also provided in the text.

In accordance with previously published data (Dumollard et al., 2017), the duration of mitosis in control DMSO treated embryos was similar in cells from all stages I analyzed. At 20°C, mitotic duration in control embryos lasted on average 10 minutes (stage: mean±SD, 2-cell: 11.6±2.4, 4-cell: 9.0±1.2, 8-cell: 11.2±2.2, 16-cell: 11.8±2.5, 32-cell: 7.8±1.4, 64-cell: 7.7±2.2, 128-cell: 9.1±1.8; 256-cell: 9.1±2.4, 512-cell: 10.8 ±2.5 minutes). As mitotic duration is very sensitive to temperature, the small differences observed between different stages may be due to temperature fluctuations. To minimize the impact of temperature in my analysis, DMSO and nocodazole treated embryos were always recorded in parallel on the same microscope (Fig. 21C and D).

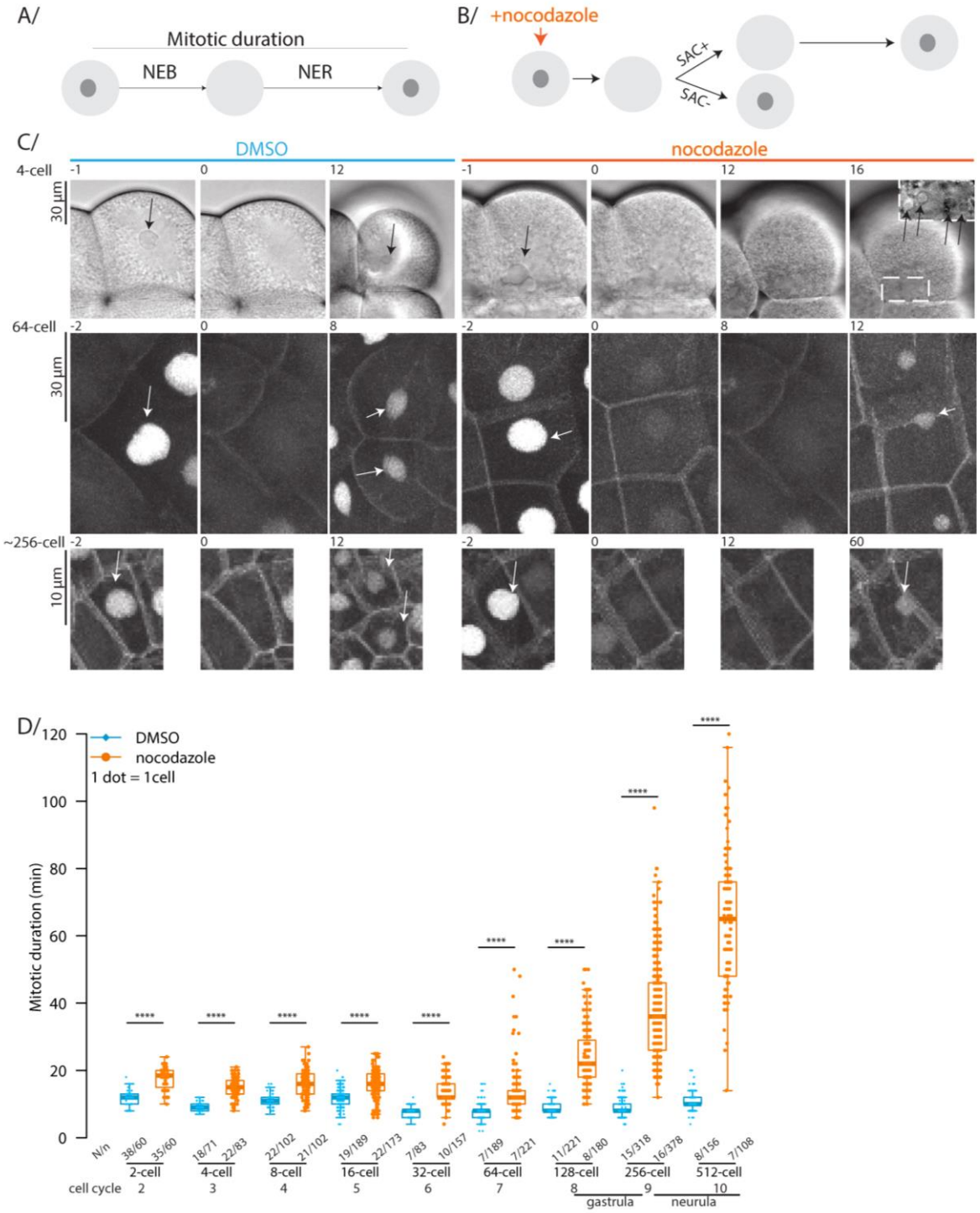

Figure 21 : Nocodazole treatment causes lengthening of mitotic duration from the 8th cell cycle.

A/ Mitotic duration was measured as the time between NEB and NER visualized either by the absence of nuclei in brightfield or by the absence of concentrated nuclear NLS protein bearing a fluorescent protein tag. **B/**Following nocodazole treatment mitotic duration is lengthened in SAC efficient (+), but not in SAC inefficient (-) cells. **C/** Pictures of cells from representative 4-cell (top), 64-cell (middle) and 256-cell (bottom) embryos treated with DMSO (left) or with 10µM nocodazole (right). Nuclei were visualized by brightfield imaging (4-cell) or by NLS-3Venus (64- and 256-cell). Plasma membrane is labeled with PH domain-GFP. Fluorescence images are Z projections of the stack covering the cell. Arrows indicate nuclei in the cell of interest. Time in minutes to NEB is indicated above each picture. **D/** Quantification of mitotic duration in DMSO (blue) or nocodazole (orange) treated embryos from 2-cell to 512-cell stage, corresponding to 2nd to 10th cell cycle. The drug was added prior to mitotic entry of the analyzed cell cycle. Each dot represents one cell. Boxes represent 25-75th percentiles and the median is shown. Number of embryos (N) and cells (n) analyzed for each stage is given under each plot.t-test: non significatif (ns), p-value ≤ 0.05 (*), p-value ≤ 0.01 (**), p-value ≤ 0.001 (***), p-value ≤ 0.0001 (****).

From the 2- to 64-cell stage, when embryos were treated with 10 µM nocodazole, I observed that mitosis was extended 1.5 fold (ratio of medians), (stage: mean±SD, 2-cell: 17.8±3.4, 4-cell: 15.0±3, 8-cell: 15.9±4.1, 16-cell: 16.1±3.8, 32-cell: 13.5±3.5, 64-cell: 12.8±6 minutes), (Fig. 21 C and D). This delay is rather short compared to that observed in somatic cells. Indeed, treatment with nocodazole at similar concentrations prolongs mitotic duration 9 times over the 30 minutes long control mitosis in PtK1 cells and by 50 fold in RPE1 cells, whose mitosis lasts 17 minutes (Brito and Rieder, 2006).

At the 64-cell stage, 9 of the 221 analyzed cells spent more than 25 minutes in mitosis following nocodazole treatment, which is noticeably longer than all other cells at this stage (Fig. 21D). As these cells belonged to 5 different embryos, this suggests that this extended delay is not due to a technical artifact. Moreover, when analyzing the identity of those cells, I observed that they were always different (B7.1; B7.2; B7.3; A7.5; A7.6; a7.11; a7.12; b7.14; b7.15). This indicates that this extended delay was not a lineage effect.

At the 128-cell stage the mitotic delay is extended throughout the embryo (Fig. 21 D). In those embryos, following nocodazole treatment, mitotic duration is 2.5 times longer than in control embryos, lasting 24.5±8.5 minutes. The mitotic delay then extends progressively in the following cell cycles (Fig. 21C and D) and mitotic duration is 3 times longer in nocodazole treated 256-cell embryos (32.1±13.2 minutes). At the 10th cell cycle, when embryos have reached 512-cell, nocodazole treated cells spend 6.5 times longer in mitosis than control embryos (Fig. 21 D), with mitosis lasting 64.3 ±20 minutes. These results suggest that the SAC becomes efficient at the 8th cell cycle and that its efficiency then increases progressively in the following cell cycles.

D/SAC efficiency is acquired at the 8th cell cycle

To confirm that the mitotic delay observed from the 8th cell cycle is due to SAC acquisition, I impaired SAC activity by inhibiting either Mad2 or Mps1 and then analyzed mitotic duration in nocodazole treated embryos at different developmental stages.

Mad2 is a key component of SAC signaling, involved in sequestering the APC/C activator Cdc20 (Fig. 22A, see introduction part II.B, Fig. 8). Mutation of 3 serines towards aspartic acid in human Mad2 produces a dominant negative form of Mad2 (Mad2-DN) that prevents its interaction with Cdc20, impairing SAC activity (Fig. 22A and sequences in annex 2E), (Wassmann et al., 2003a). I injected *P. mammillata* eggs with an RNA encoding Mad2-DN (gift from K. Wassmann) and assessed SAC efficiency in those embryos.

Expression of Mad2-DN in untreated (DMSO) *P. mammillata* embryos, did not interfere with mitotic progression and mitotic duration was comparable in Mad2-DN expressing embryos and uninjected embryos (Fig. 22B). As mentioned above, following treatment with 10 µM nocodazole at the 2-cell stage, mitosis was extended by 1.5 fold lasting 17.8±3.4 minutes compared to control DMSO-treated embryos, which spend 11.6±2.4 minutes in mitosis. This delay was maintained in Mad2-DN-expressing embryos which spent 16.6±4 minutes in mitosis when treated with nocodazole, compared to 12.1±1.8 minutes in the presence of DMSO (Fig. 22B). Hence, Mad2-DN expression does not affect mitotic duration in nocodazole treated embryos at 2-cell stage. On the other hand, at 128- and 256-cell stage the delay observed in nocodazole treated embryos was significantly reduced when the SAC was impaired by Mad2-DN expression. Indeed, in Mad2-DN expressing embryos, mitosis was extended by 1.5 fold in nocodazole compared to DMSO treated embryos (128-cell: 9.8±1.6 to 15.6±3.5 minutes; 256-cell: 9.9±1.8 to 13.6±2.4 minutes), instead of 2 fold in 128-cell embryos (9.1±1.8 to 24.5±8.5 minutes) and 3 fold in 256-cell embryos (8.7±2.3 to 32.1±13.2 minutes), (Fig. 22B). Taken together these observations confirm that at 2-cell stage embryos are not SAC efficient whereas the mitotic delay observed from the 128-cell stage depends on SAC activity.

I further confirmed that the mitotic lengthening observed in nocodazole treated embryos is due to SAC activation, by inhibiting the SAC kinase Mps1, using the specific inhibitor reversine (Fig. 22A and B), (Santaguida et al., 2010). As previously observed with Mad2-DN, co-treatment of 256-cell stage embryo with both reversine (0.5 µM) and nocodazole resulted in shortening of mitotic duration

compared to nocodazole treatment only, from 32.1±13.2 minutes to 12.9±5.2 minutes. Mitotic duration in embryos simultaneously treated with nocodazole and reversine (12.9±5.2 minutes) was comparable to mitotic duration in DMSO treated embryos (10.2±2.3 minutes). Taken together, these results show that the SAC is silenced during cleavage divisions in *P. mammillata* embryos and becomes efficient around the time of gastrulation in the 8th cell cycle.

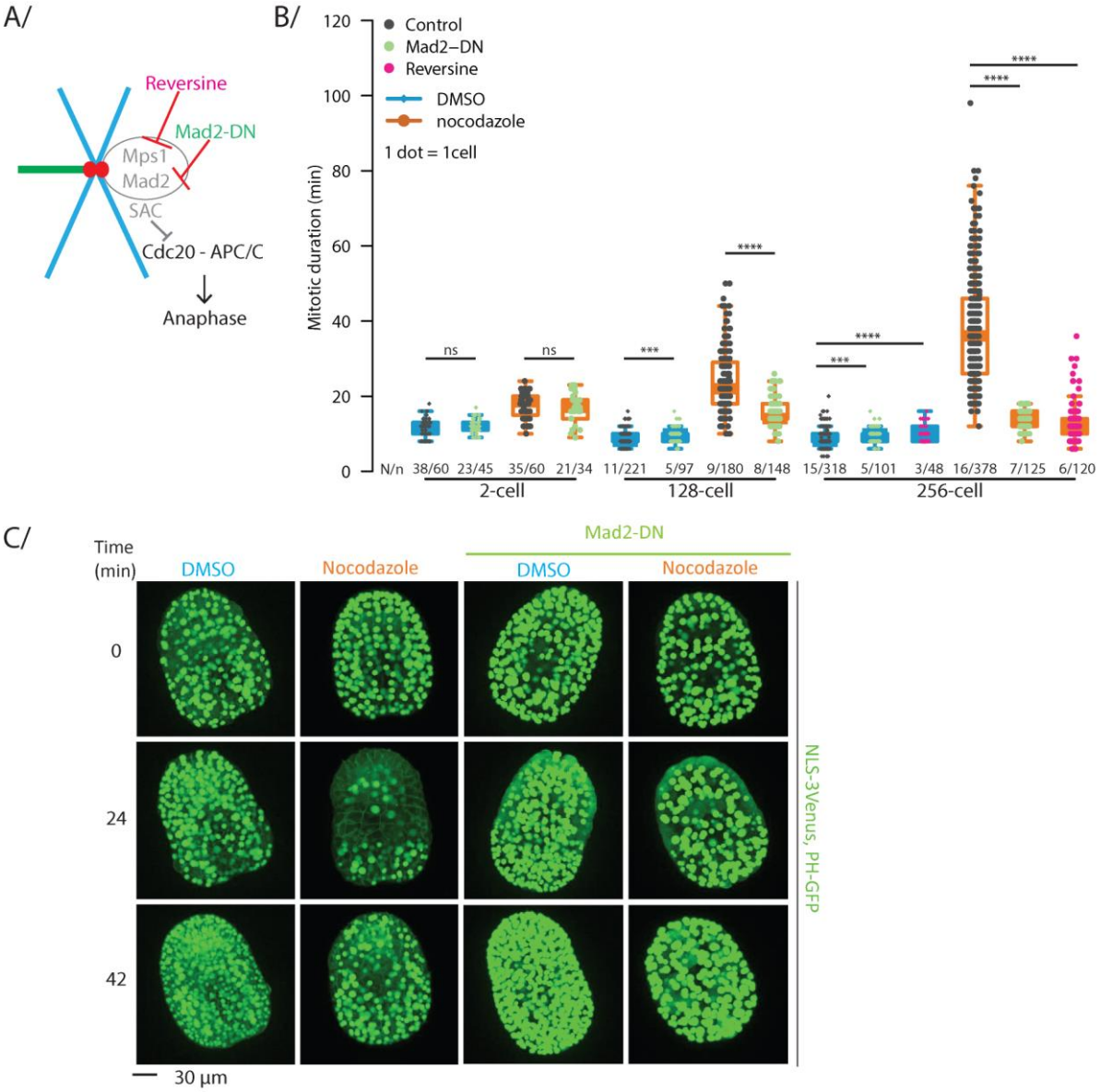

Figure 22 : SAC activity is acquired at the 8th cell cycle

A/ Schematic representation of a chromosome (blue) with one kinetochore (red) attached to microtubules (green) and one unattached leading to activation of the SAC (grey). SAC activity can be impaired by treatment with reversine, an inhibitor of Mps1, or by overexpression of Mad2-DN. **B/** Quantification of mitotic duration in DMSO (blue) or nocodazole (orange) treated embryos at 2-cell, 128-cell and 256-cell stage in control embryo (grey) or following SAC impairment by expression of Mad2-DN (green) or treatment with reversine (pink). Mitosis was measured as time from NEB to NER. Each dot represents one cell. Boxes represent 25-75th percentiles and the median is shown. Number of embryos (N) and cells (n) analyzed for each treatment and stage is given below each plot. Values for mitotic duration in control DMSO or nocodazole treated embryos are the same as reported in figure 21. **C/** Z-projection of stacks of confocal images of 256-cell stage embryos expressing NLS-3Venus to mark nuclei and PH-GFP to label the plasma membrane. Control embryos (left) and embryos expressing Mad2-DN (right) were treated either with DMSO or with 10 µM nocodazole and filmed for 90-120 minutes. Selected frames corresponding to 0, 24 and 42 minutes after beginning of time lapse acquisition are shown. t-test: non significatif (ns), p-value ≤ 0.05 (*), p-value ≤ 0.01 (**) ,p-value ≤ 0.001 (***), p-value ≤ 0.0001 (****).

The effect of SAC activation following nocodazole treatment can also be visualized by directly looking at the fluorescent NLS signal in embryos at the 256-cell stage. In control DMSO treated embryos, few cells are in mitosis at each time point and therefore most of the embryo has well defined nuclei (Fig. 22C). In embryos treated with nocodazole, instead, SAC activation delays mitotic progression resulting in an important reduction of interphase cells corresponding to an accumulation of mitotic cells and therefore an easily visible decrease in the number of distinct NLS-stained nuclei (Fig. 22C). In Mad2-DN expressing embryos treated with nocodazole, instead, as mitotic duration is short, only few cells are in mitosis at any given time, as in DMSO treated embryos, giving rise to embryos with mostly discrete NLS stained nuclei (Fig. 22C).

E/ The SAC is more efficient in the anterior ventral ectoderm

While analyzing SAC efficiency at different embryonic stages (Fig. 21), I noticed that, although starting from the 8th cell cycle, all analyzed cells had an efficient SAC and delayed mitosis, the lengthening of mitotic duration is highly variable even within a given embryo (annex 1A). Such variability has been already investigated in other species and various parameters that could influence SAC efficiency have been identified (see introduction part III.B.2). In *C. elegans* and in *M. musculus,* two parameters which influence SAC efficiency resulting in differences in mitotic delay during embryonic development, are cell volume and cell identity (Galli and Morgan, 2016; Gerhold et al., 2018; Kyogoku and Kitajima, 2017; Lane and Jones, 2017; Vázquez-Diez et al., 2019).

To test whether either of these factors could explain the variability I observed in *P. mammillata* embryos, I analyzed mitotic duration in relation to either cell volume or cell identity. At 128-cell stage SAC efficiency is still low and at 512-cell the mitotic delay is extremely prolonged, therefore, I decided to perform this analysis at the 256-cell stage when the SAC induces a delay that allows significant differences between cells within an embryo to be detected when the delay is still easily recordable.

In order to measure cell volume, I coinjected a mRNA encoding a fluorescent plasma membrane marker (PH domain bearing either GFP or Tomato), (Stauffer et al., 1998), with the NLS RNA in eggs, and performed 3D reconstruction of the cell surface using Imaris software (Fig. 23A). In control DMSO treated embryos, mitotic duration was the same in all cells irrespective of their volume (Fig. 23C). In nocodazole treated embryos, mitotic duration was variable, but this variability did not correlate with cell volumes with cells of similar volume extending mitosis by different lengths of time (Fig. 23D). This suggests that cell volume is not the main parameter influencing SAC efficiency in *P. mammillata* embryos.

To test whether the difference in SAC response correlates with different cell identities, I divided cells into four subgroups based on their position in the embryo: anterior ventral ectoderm, posterior ventral ectoderm (Fig. 23B), notochord and dorsal cells. Again, mitotic duration in DMSO treated embryos was the same for the four groups (Fig. 23E). However, I observed that in nocodazole treated embryos, duration of mitosis was extended differently in the 4 subgroups of cells. Mitosis was lengthened by 4.8 fold in anterior ventral ectodermal cells (9.9±2.4 to 49.3±11.9 minutes, DMSO and nocodazole respectively), 3.5 fold in both posterior ventral ectodermal cells (9.5±2.2 to 34.9±11 minutes) and dorsal cells (10.2±2.1 to 34.6±14 minutes) and 2.2 fold in notochord cells (9.8±2.2 to 22.3±3.7 minutes) compared to control DMSO treated cells (Fig. 23F and annex 1A). For this experiment, I analyzed mitotic duration for cells from 14 different 256-cell embryos. However, because of their position inside the embryo, mitotic duration in notochord cells was analyzed only in 3 embryos. Given the small available sample size, results regarding SAC behavior in notochord cells are inconclusive and those cells were not further analyzed. Instead, I focused on the difference in SAC efficiency along the ventral ectoderm with anterior cells showing a more efficient SAC than posterior cells. Consistent with the analysis on whole embryos, at 256-cell no significant difference in cell volume

was observed between posterior and anterior ventral ectoderm cells (Fig. 23D). This further supports that the difference in SAC efficiency is not dictated by differences in cell size and suggests that SAC efficiency may be impacted by cell identity itself.

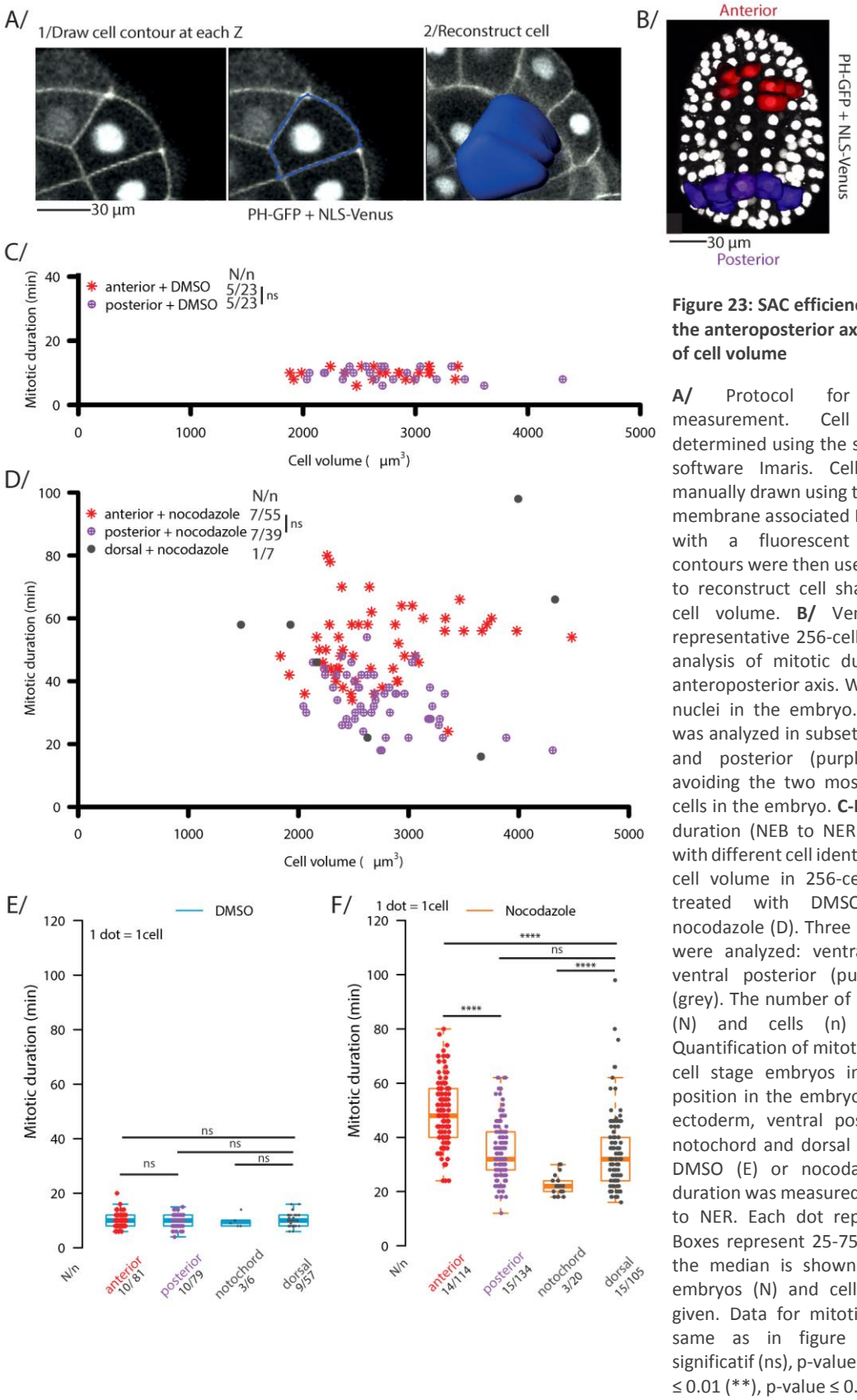

Figure 23: SAC efficiency varies along the anteroposterior axis independently of cell volume

A/ Protocol for cell volume measurement. Cell volume was determined using the surface tool of the software Imaris. Cell contours were manually drawn using the signal from the membrane associated PH domain tagged with a fluorescent protein. These contours were then used by the software to reconstruct cell shape and calculate cell volume. **B/** Ventral view of a representative 256-cell embryo used for analysis of mitotic duration along the anteroposterior axis. White dots mark all nuclei in the embryo. Mitotic duration was analyzed in subsets of anterior (red) and posterior (purple) cells, always avoiding the two most central rows of cells in the embryo. **C-D/** Plots of mitotic duration (NEB to NER) for sets of cells with different cell identity as a function of cell volume in 256-cell stage embryos treated with DMSO (C) or with nocodazole (D). Three subgroups of cells were analyzed: ventral anterior (red), ventral posterior (purple) and dorsal (grey). The number of analyzed embryos (N) and cells (n) is given. **E-F/** Quantification of mitotic duration in 256-cell stage embryos in relation to cell position in the embryo: ventral anterior ectoderm, ventral posterior ectoderm, notochord and dorsal cells treated with DMSO (E) or nocodazole (F). Mitotic duration was measured as time from NEB to NER. Each dot represents one cell. Boxes represent 25-75th percentiles and the median is shown. The number of embryos (N) and cells (n) analyzed is given. Data for mitotic duration is the same as in figure 21. t-test: non significatif (ns), p-value ≤ 0.05 (*), p-value ≤ 0.01 (**), p-value ≤ 0.001 (***), p-value ≤ 0.0001 (****).t

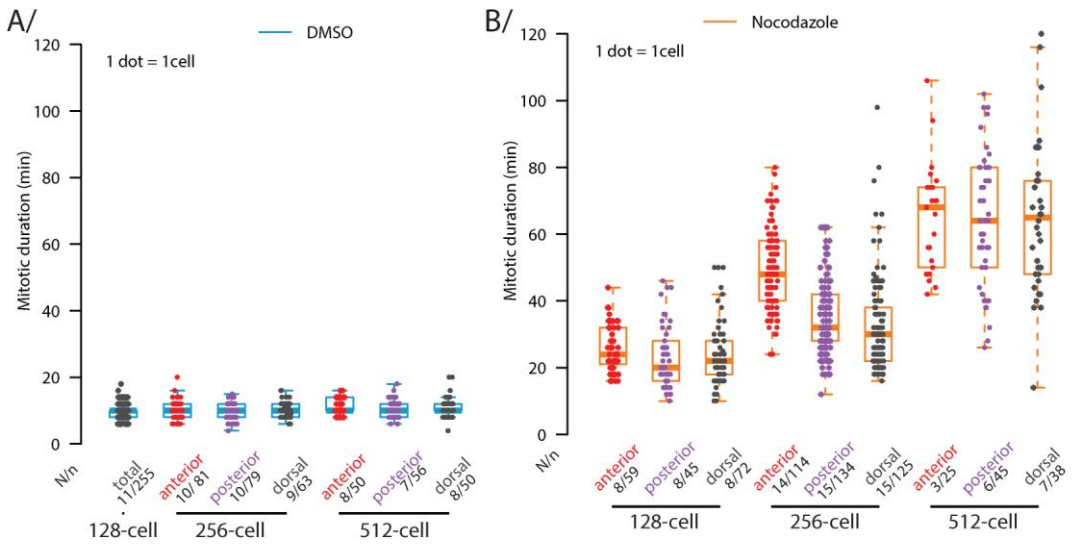

Figure 24: SAC efficiency varies along the anteroposterior axis from the 8th to 10th cell cycle

A-B/ Quantification of mitotic duration at 8th (128-cell embryos), 9th (256-cell embryos) and 10th (512-cell embryos) cell cycle in relation to cell position within the embryo: ventral anterior ectoderm (red), ventral posterior ectoderm (purple), and dorsal (grey) cells treated with DMSO (A) or nocodazole (B). Mitotic duration was measured as time from NEB to NER. Each dot represents one cell. Boxes represent 25-75th percentiles and the median is shown. The number of embryos (N) and cells (n) analyzed is given. Data used for this analysis are the same as those presented in figure 21.

I then analyzed whether this difference along the anteroposterior axis was already present when SAC is activated in 128-cell embryos and conserved when the SAC becomes more efficient in the 512-cell stage. Indeed, the same trend could be observed (Fig. 24 A and B and annex 1A), however, the difference is not as marked as in 256-cell embryos.

F/ SAC efficiency depends on cell identity

To test whether SAC efficiency depends on cell identity, I set up experiments to interfere with patterning of the ventral ectoderm along the anteroposterior axis and then analyze the effect on mitotic progression and SAC activation. In *C. intestinalis* embryos, the fate of the anterior ectoderm is controlled by the transcription factor FoxA-a. FoxA-a induces the expression of genes specific for the anterior domains of the embryos while inhibiting genes specific for posterior domains (see introduction part IV.B), (Lamy et al., 2006). In *C. intestinalis,* overexpression of FoxA-a using the promotor of Fog to drive its expression in all animal blastomeres from 16-cell stage was shown to induce ventral posterior cells to acquire an anterior fate. As most of the processes underlying embryonic development are conserved between *C. intestinali*s and *P. mammillata* (see introduction part IV)(Madgwick et al., 2019), I used a similar approach to alter anteroposterior patterning and injected a plasmid coding for pFog>Venus-FoxA-a in *P. mammillata* eggs. To confirm that in *P. mammillata*, overexpression of FoxA-a in ventral posterior cells induces them to acquire an anterior ectodermal fate, I analyzed the pattern of expression of the anterior marker sFRP1/5 by *in situ* hybridization. In *C. intestinalis,* sFRP1/5 expressions was detected in posterior cells following FoxA-a overexpression (Lamy et al., 2006).

In *P. mammillata*, I found that, like in *C. intestinalis*, sFRP1/5 RNA expression was restricted to the anterior part of the neurula in control embryos both uninjected or injected with NLS-tomato and PH-domain-GFP (Fig. 25A). In embryos injected with pFog>Venus-FoxA-a (35ng/µl), sFRP1/5 expression was still present in the anterior region, but its expression was extended towards the posterior pole. Indeed, posterior ectodermal cells were stained for the presence of sFRP1/5 RNA in embryos overexpressing FoxA-a but never in controls embryos (Fig. 25A). The effect was dependent on plasmid

concentration as indicated by the progressive loss of the normal neurula shape. At intermediate plasmid concentration, (35 ng/µl), most embryos overexpressing FoxA-a lost their shape and become round suggesting a full lost of anteroposterior patterning (Fig. 25A). At higher concentration of plasmid (45 ng/µl to 130 ng/µl), I obtained only round embryos associated with a high incidence of embryonic death, whereas at low plasmid concentration (20 ng/µl) the effect was too weak to warrant analysis (data not shown). Altogether, these results indicate that in *P. mammillata*, similarly to what was previously shown for *C. intestinalis*, FoxA-a overexpression is sufficient to induce an anterior ectodermal fate in posterior cells. For the following analysis, I used an intermediate plasmid concentration (35 ng/µl), which induced an almost complete loss of posterior ectodermal cells, without significant reduction in embryo viability.

I then asked whether loss of anteroposterior patterning following FoxA-a overexpression had an impact on the difference in mitotic duration observed in wild type embryos along the anteroposterior axis following nocodazole treatment. If SAC efficiency is a characteristic associated with different cell identities, I expected that, in the presence of nocodazole, posterior cells overexpressing FoxA-a would delay mitotic exit more efficiently, like anterior cells, and the difference

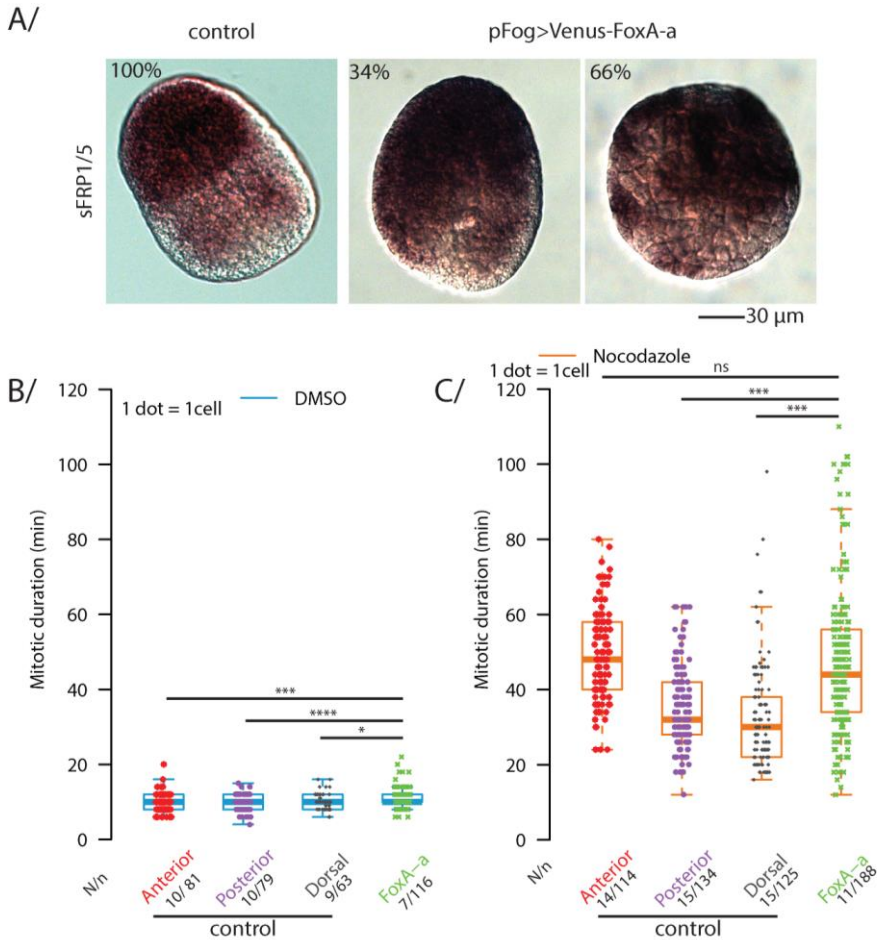

Figure 25 : Ectopic expression of the anterior determinant FoxA-a results in a more efficient SAC in embryos

A/ Representative images of control uninjected embryos and of embryos injected with 35ng/µl pFog>Venus-FoxA-a, NLS-tomato and PH-tomato, showing expression of the anterior marker sFRP1/5 asses by *in situ* hybridization. For pFog>Venus-FoxA-a injected embryos percentage of the two classes of phenotypes observed is reported. The experiment was performed 4 times with a total of 64 (22 neurula-like and 42 rounds) FoxA-a overexpressing embryos. **B-C/** Quantification of mitotic duration in control embryo and in embryos injected with pFog>Venus-FoxA-a (green) treated with DMSO (B) or nocodazole (C) at the 256-cell stage. For control embryos, cells were subdivided depending on position (anterior, posterior and dorsal). Mitotic duration was measured as time from NEB to NER. Each dot represents one cell. Boxes represent 25-75th percentiles and the median is shown. The number of embryos (N) and cells (n) analyzed is given. Data for control embryos used for this analysis are the same as those presented in figure 21. t-test: non significatif (ns), p-value ≤ 0.05 (*), p-value ≤ 0.01 (**) ,p-value ≤ 0.001 (***), p-value ≤ 0.0001 (****).

in mitotic duration between anterior and posterior cells would be lost or greatly reduced in FoxA-a overexpressing embryos.

Expression of a microinjected construct in *P. mammillata* is known to display a mosaic pattern (not all cells inherit or express the plasmid). In order to analyze only cells that overexpressed FoxA-a, I generated a plasmid bearing FoxA-a fused to Venus, under the control of the Fog promoter. Using this tool, I could select embryos that expressed FoxA-a in most cells. However, since non-autonomous induction of the anterior identity may exist, by example due to the secreted protein sFRP1/5, not only those cells expressing Venus could be affected by FoxA-a overexpression, but also their neighboring cells. I therefore decided to analyze all cells, positive and negative for Venus, together. In addition, as embryos became round and could not be oriented, I could no longer distinguish anterior and posterior cells and therefore analyzed them together.

FoxA-a overexpression had no effect on mitotic duration under control conditions (Fig. 25B). However, following nocodazole treatment, mitotic duration was increased 4.4 fold over DMSO treated embryos (11.1±2.6 to 48±21.7 minutes), (Fig. 25C and annex 1B) which is longer than the overall mitotic delay observed in control embryos (3 fold), and close to the lengthening observed in anterior cells (4.8 fold). These observations support the hypothesis that cells of the anterior ectoderm have a more efficient SAC than those with a posterior fate because of their FoxA-a dependent cell identity. This suggests that as in *C. elegans*, cell fate influences SAC efficiency in *P. mammillata* embryos.

G/Cell fate is not the only parameter modulating SAC efficiency in early embryo

To further test the link between cell identity and SAC efficiency, I decided to use another approach to interfere with patterning along the anteroposterior axis. As previously described in the introduction (part IV.B), in ascidian re-localization of specific maternal factors following fertilization is essential for the establishment of the embryonic axes. In *H. roretzi*, it was shown that the first contraction pole contains factors required for posterior identity (see introduction part IV.B.2, Fig. 17 and Fig. 26A), (Nishida, 1996). This localization appears to be conserved in *P. mammillata* (Dumollard 2017).

Using a microneedle, I therefore ablated the 1st contraction pole, as shown in figure 26B, to remove the posterior-inducing factors, generating vegetal cytoplasm deficient (VC-deficient) embryos. As previously observed, VC-deficient embryos developed into a monolayer of epidermal cells surrounding cavities looking like permanent blastula (Nishida, 1996). Cell number in VC-deficient embryos increased with a similar timing to that of control. Cell number and time from fertilization were therefore used as parameters to stage these micromanipulated embryos. I then analyzed the pattern of expression of the anterior marker sFRP1/5 by *in situ* hybridization, to determine the effect of this ablation on anteroposterior patterning. VC-deficient embryos expressed sFRP1/5 in most to all cells (Fig. 26C), indicating that these embryos are completely anteriorized. The variability in the number of cells expressing sFRP1/5 could be a consequence of the different amount of cytoplasm aspirated for the ablation.

I then assessed mitotic duration in DMSO and nocodazole treated 256-cell VC-deficient embryos to determine whether loss of anteroposterior patterning resulted in a change in SAC efficiency. I expected that, as for FoxA-a embryos, if anterior cell identity is associated with a more efficient SAC, VC-deficient embryos should have a prolonged mitotic duration like that in anterior wild type cells (4.8 fold). Mitotic duration was comparable between control and VC-deficient embryos, in the presence of DMSO, indicating that the ablation did not affect mitosis itself (Fig. 26D). Treatment with nocodazole of VC-deficient embryos resulted in a delay in mitotic exit, indicating that SAC acquisition was also unaffected in these embryos. However, in VC-deficient embryos mitosis was

extended from 11.5±2.3 minutes to 34±19.6 minutes, which corresponds to only a 2.2 fold extension of mitotic duration (Fig. 26E and annex 1C). Opposite to the predicted outcome, mitotic duration in VC-embryos was not prolonged as in anterior cells, but instead mitosis was even shorter than in posterior cells from non-manipulated embryos (3.5 fold).

However, I noticed that as VC-deficient embryos are only composed of epidermal cells and all cytokinesis become symmetric, all cells had the same volume. In wild type embryos muscle cells have large cytoplasm, about twice that of ectodermal cells, and constitute a large part of the total embryonic volume, whereas epidermal cells have small volumes. Because in VC-deficient embryos the total embryonic volume is divided equally between cells, I reasoned that the volume of those cells would be larger than that of wild type ectodermal cells. As mentioned earlier, cell volume can impact SAC efficiency, and larger cells have been shown to have a weaker SAC response due to the dilution of SAC signal in the cytoplasm (Galli and Morgan, 2016; Gerhold et al., 2018). I therefore wondered whether the weaker SAC response observed in VC-deficient embryos, was a consequence of a general increase in cell volume. I first confirmed that average cell volume was not affected by nocodazole treatment and was increased in VC-deficient embryos. Indeed, cell volume in VC-deficient embryos (4000 μm^3) was 1.5 times bigger than in wild type ectodermal cells (2750 μm^3), (Fig. 28F and G).

I reasoned that if the weak SAC response observed in VC-deficient embryos was due to dilution of the SAC signal in these large epidermal cells, a reduction in cell volume should be sufficient to restore the SAC response and extend mitotic duration to that observed in wild type anterior ectoderm. As embryonic cells divide without cell growth reducing cell volume at each division, SAC efficiency should increase at each division. I therefore measured cell volume in 512-cell embryos and confirmed that cells were smaller both in control (1800 μm^3) and VC-deficient embryos (2200 μm^3) (Fig. 26F and G). The VC-deficient cells in 512-cell stage embryos, were larger that control cells of the same cell cycle (1.25 fold) but were about the same size as control cells in 256-cell stage embryos (0.9 fold). Strikingly, in VC-deficient embryos at the 512-cell stage, mitotic duration was 4.8 times longer in nocodazole than in DMSO (11.7±3 to 55.6±24.1 minutes), (Fig. 26E), which is the delay observed in similarly sized wild type anterior cells at the 256-cell stage. Taken together these data suggest that in cells with the same identity SAC efficiency can be modulated by changes in cell volume. Further experiments are required to rule out that other parameters affected by the ablation of the 1st contraction pole, or differences between the 9th and 10th cell cycles are responsible for the observed differences in SAC efficiency (see discussion). However, my experiments suggest that, as previously shown for *C. elegans*, both cell volume and cell identity influence SAC efficiency in *P. mammillata* embryos.

Figure 26 : Depletion of posterior determinants from the zygote anteriorizes embryos but does not increase SAC efficiency

A/ Following fertilization, ooplasmic segregation localizes factors required to induce posterior fate to the first contraction pole (purple) on the vegetal side of the zygote. **B/**The first contraction pole was ablated by aspiration using a glass needle. **C/** Representative images of *in situ* hybridization using a probe for the anterior marker sFRP1/5. Percentage of embryos in each category is reported in the corresponding photo. The experiment was repeated 3 times with a total of 20 (10 in each category) VC-deficient embryos. **D-E/** Quantification of mitotic duration in control (anterior, posterior and dorsal) and VC-deficient (yellow) embryos treated with DMSO (D) or nocodazole (E) at 256-cell and 512-cell stages. Mitosis was measured as time from NEB to NER. Each dot represents one cell. Boxes represent 25-75th percentiles and the median is shown. The number of embryos (N) and cells (n) analyzed is given. **F-G/** Cell volume measurement in control (anterior, posterior and dorsal) and VC-deficient embryos treated with DMSO (F) or nocodazole (G) at 256-cell and 512-cell stages. Each dot represents one cell. Boxes represent 25-75th percentiles and the median is shown. The number of embryos (N) and cells (n) analyzed is given. Mitotic duration and cell volume of control embryos (DMSO or nocodazole) are the same as in figure 21 and 23. t-test: non significatif (ns), p-value ≤ 0.05 (*), p-value ≤ 0.01 (**), p-value ≤ 0.001 (***), p-value ≤ 0.0001 (****).

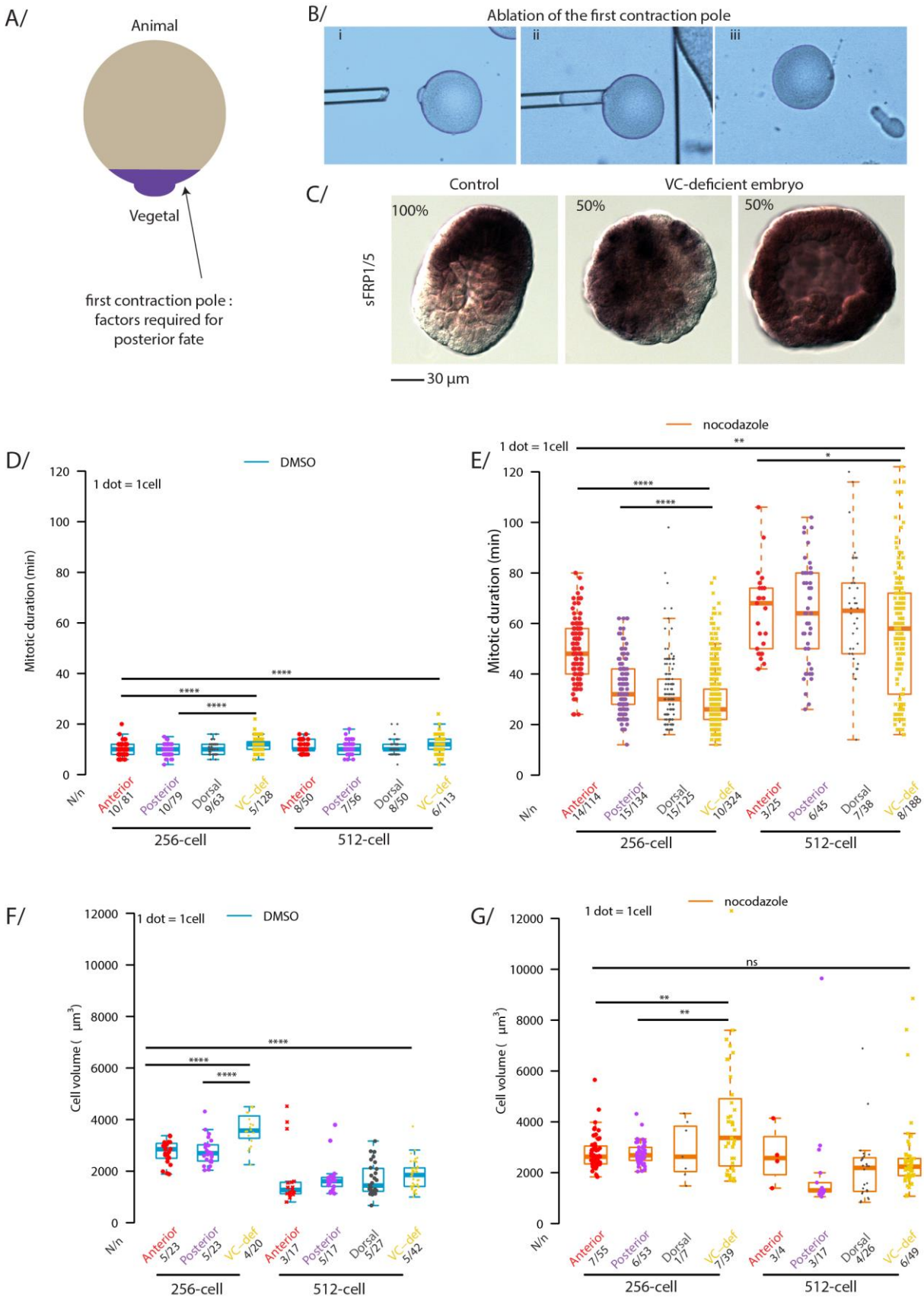
A/
Animal
Vegetal
first contraction pole : factors required for posterior fate
B/
Ablation of the first contraction pole
i
ii
iii
C/
Control
VC-deficient embryo
100%
50%
50%
sFRP1/5
30 µm
D/
DMSO
1 dot = 1cell
Mitotic duration (min)
N/n
Anterior 10/81
Posterior 10/79
Dorsal 9/63
VC-def 5/128
Anterior 8/50
Posterior 7/56
Dorsal 8/50
VC-def 6/113
256-cell
512-cell
E/
nocodazole
1 dot = 1cell
Mitotic duration (min)
N/n
Anterior 14/114
Posterior 15/134
Dorsal 15/125
VC-def 10/324
Anterior 3/25
Posterior 6/45
Dorsal 7/38
VC-def 8/188
256-cell
512-cell
F/
DMSO
1 dot = 1cell
Cell volume (µm3)
N/n
Anterior 5/23
Posterior 5/23
VC-def 4/20
Anterior 3/17
Posterior 5/17
Dorsal 5/27
VC-def 5/42
256-cell
512-cell
G/
nocodazole
1 dot = 1cell
Cell volume (µm3)
ns
N/n
Anterior 7/55
Posterior 6/53
Dorsal 1/7
VC-def 7/39
Anterior 3/4
Posterior 3/17
Dorsal 4/26
VC-def 6/49
256-cell
512-cell

II/ SAC regulation during *P. mammillata* embryogenesis

In the previous part, I presented the experiments I performed to study SAC efficiency in *P. mammillata* embryos. I could show that the SAC is inefficient from meiosis to the 7th cell cycle and that its efficiency increases in the following cell cycles (8th to 10th). In addition, once acquired SAC efficiency is stronger in anterior than in posterior cells of the ventral ectoderm. Finally, I could show that both cell volume and cell identity contribute to SAC efficiency during embryogenesis.

In this part, I will present the experiments that I performed to begin to understand the mechanisms underlying the switch in SAC efficiency during embryogenesis and its variation along the anteroposterior axis.

A/SAC components are mostly conserved in *P. mammillata*

I first looked if SAC proteins were conserved in *P. mammillata* using available genomic databases. I searched for homologs of the six core SAC components (Mps1, Mad1, Mad2, Bub1, Bub3 and BubR1) and could identify five of them: Mps1, Mad1, Mad2, Bub1 and Bub3 (Brozovic et al., 2018). Consistent with previous data indicating the absence of *BubR1* gene in the genome of the ascidian *C. intestinalis* (van Hooff et al., 2017; Suijkerbuijk et al., 2012), I could not identify a *P. mammillata* homologue of *BubR1* in genomes available in the database Aniseed (Brozovic et al., 2018) or in the LBDV database Octopus. BubR1 is known to be a paralog of Bub1, it is therefore possible that, in ascidians, Bub1 carries the function of both proteins (van Hooff et al., 2017; Suijkerbuijk et al., 2012). BubR1 role is to amplify the inhibitory SAC signal (see introduction part II.B, Fig.10), (Jia et al., 2013; Musacchio and Salmon, 2007). Therefore it is possible that in ascidians the MCC still forms but that its strength is not reinforced due to the lack of BubR1. This would reduce the maximum efficiency that the SAC can reach. However, lack of the *BubR1* gene impacts all cells and cannot therefore explain the variability in SAC efficiency within the embryo.

For the five core SAC proteins present in *P. mammillata*, I analyzed the protein sequences using the software clustal omega (Sievers et al., 2011) and aligned and compared them to protein sequences from *S. cerevisiae, S. pombe, D. melanogaster, P. lividus, C. intestinalis, P. mammillata, M. musculus* and *H. sapiens* (annex 2).

Mps1 is the first SAC protein to localize to unattached kinetochores where its kinase activity promotes localization of the other SAC proteins (see introduction part II, Fig. 8), (Jia et al., 2013; Musacchio and Salmon, 2007). *P. mammillata* Mps1 is an 80 kDa protein that has a well conserved kinase domain (annex 2A). In addition, sites of post-translational modifications, which were identified in *H. sapiens*, are either conserved in *P. mammillata* or generally not conserved among all species used in the alignment. This suggests that Mps1 has not undergone major evolutionary changes that would affect its functionality in *P. mammillata*.

Bub1 interacts with Knl1 and promotes the localization of Bub3 and Mad1 to unattached kinetochores (see introduction part II, Fig. 8), (Jia et al., 2013; Musacchio and Salmon, 2007). Bub1 is a large protein of 130 kDa. For my analysis I used both the protein predicted in the database Aniseed as well as the one that I obtained using the database Octopus (annex 2B). Both proteins contained the domain involved in loading Mad1 at kinetochores as well as the kinase domain, whereas the domain required for kinetochore localization and the Bub3 interacting domain were present only in the sequence obtained from Octopus (van Hooff et al., 2017; Suijkerbuijk et al., 2012). Despite the conservation of its functional domain, the percentage of identity with the other analyzed Bub1 proteins is of around 25%.

Bub3 interacts with Mad2 and Cdc20 thanks to WD40 repeats (see introduction part II, Fig. 8),(Fraschini et al., 2001). *P. mammillata* Bub3 is a 31kDa protein which is highly conserved and includes the same number of WD40 domains than in *H. sapiens* Bub3 (annex 2C).

Mad1 is a 67kDa protein constitutively associated with Mad2, facilitating its recruitment to kinetochores (see introduction part II, Fig. 8), (Jia et al., 2013; Musacchio and Salmon, 2007). Differently from the other components, Mad1 is not a well conserved protein (19% to 44% of identity, annex 2). However, the phosphorylation sites required for modulation of Mad1 activity in *H. sapiens* as well as the domains required for Mad1 interaction with NEK2 and IK (annex 2D), whose depletion impairs SAC activity (Lou et al., 2004; Yeh et al., 2012) are conserved in *P. mammillata* Mad1. Moreover, the domain required for Mad1 interaction with Mad2 is also conserved (Sironi et al., 2002).

Mad2 links the activation of the SAC at kinetochores with the generation of the inhibitory signal. At kinetochores Mad2 undergoes a configurational change from an inactive O-Mad2 form to an active C-Mad2 form that can interact with Cdc20 (see introduction part II, Fig. 8), (Jia et al., 2013; Musacchio and Salmon, 2007). Mad2 is a small 23 kDa protein highly conserved among eukaryotes (annex 2E). *P. mammillata* Mad2 shares 42% identity with Mad2 from *S. pombe* and *S. cerevisiae,* 45% with *D. melanogaster,* 54% with *P. lividus,* 56% with mammals *(H. sapiens* and *M. musculus*) and 79% with the ascidian *C. robusta*. Mad2 is regulated by phosphorylation and mutation, in human Mad2, of three serines (170, 178 and 195) into aspartic acid leads to the dominant negative form of Mad2 that I used in part I to impair SAC activity (Wassmann et al., 2003a). Serine 170 and 178 are conserved in *P. mammillata* while serine 195 aligns to a glycine. Serine 195 is presents only in mammalian Mad2 suggesting that this site is not as important as the other two. The safety belt that allows the configurational switch from O-Mad2 to C-Mad2 is especially well conserved. Similarly, the domain required for Mad2 interaction with Cdc20 is conserved. Consistently, *P. mammillata* Mad2 interacts with Cdc20 and Mad1 in yeast two hybrid assays.

Therefore, SAC proteins are mostly conserved in *P. mammillata* compared to other eukaryotes especially when considering functional domains.

B/SAC components are present in *P. mammillata* early embryos

Variations in SAC efficiency could be a straightforward consequence of changes in the availability of one or more SAC components. I therefore checked as a first approach, whether transcripts of the five genes encoding the main SAC proteins are present during embryonic development. Transcriptomic data for *P. mammillata* egg, 64-cell, early gastrula, mid gastrula, mid neurula, mid tailbud and hatching larva are available on the database Aniseed (Brozovic et al., 2018). By plotting the average of the two data sets available for SAC genes as well as their target Cdc20, I found that the RNA levels of Mps1, Mad1, Bub1 and Bub3 are low throughout embryogenesis (Fig. 27A). This includes stages, after gastrulation, when the SAC becomes efficient at inducing a mitotic delay, suggesting that this low expression level does not underlie the variation in SAC efficiency. Mad2 and Cdc20 RNA levels are high in the egg then decrease during embryogenesis probably highlighting a maternal contribution of these RNAs.

However, available transcriptomic data do not cover the period between the egg and the 64-cell stage, which are most of the SAC deficient stages. Moreover, RNAseq data does not provide spatial information about the distribution of SAC transcripts in eggs and embryos. I therefore analyzed the spatial distribution of SAC transcripts during embryogenesis by *in situ* hybridization. This analysis confirmed the presence of RNAs encoding the five SAC proteins and their target Cdc20 in all stages from eggs to tadpoles (Fig. 27B, preliminary results). In addition, signal intensity was similar at all stages despite the difference in SAC efficiency. I did not observe a decrease in signal intensity for Mad2 or Cdc20, which would be expected based on the transcriptomic analysis, but *in situ* hybridizations are not quantitative. All SAC transcripts were evenly distributed in the embryo at all stages and no specific pattern of localization could be detected. The only exceptions were Bub1 and Cdc20, which seem to be more abundant in the dorsal part of the tadpole head. However, as I did not test SAC efficiency in these cells, I do not know whether this difference is related to SAC activity.

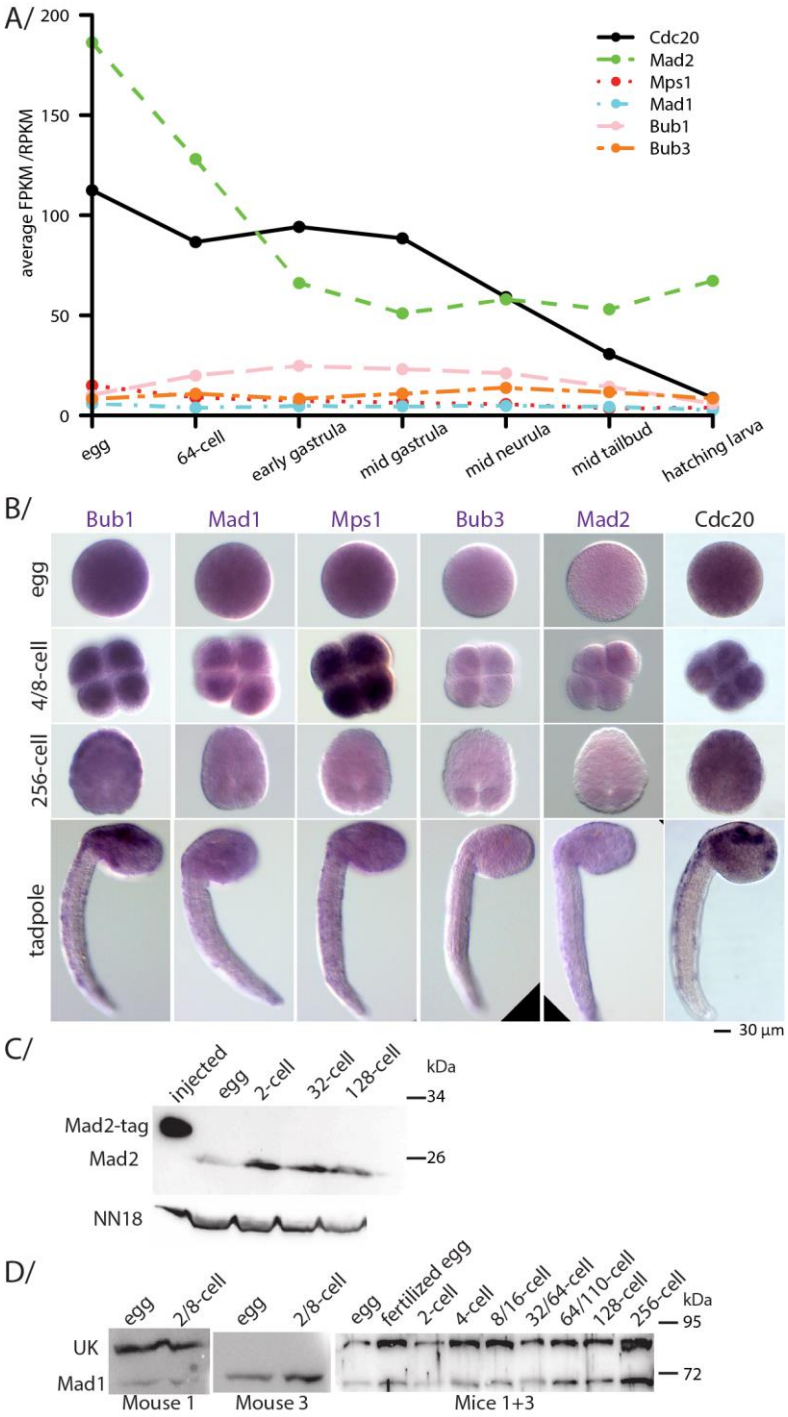

Figure 27: SAC components are present throughout embryogenesis

A/ Level of transcripts encoding SAC proteins and their target Cdc20 at different embryonic stages. FPKM or RPKM from two RNAseq datasets retrieved from the database Aniseed were averaged in this graph (Brozovic et al., 2018). **B/** Representatives images of *in situ* hybridization using specific probes for SAC components (Bub1, Mad1, Mps1, Bub3 and Mad2, in pink) or the SAC target Cdc20, in unfertilized eggs, 4-cell, 256-cell and tadpole stages. **C/** Western blot analysis of Mad2. Mad2 protein (23kDa) levels are the same in SAC deficient (egg, 2-cell, 32-cell) and SAC efficient (128-cell) embryos. 12 µl of packed embryos were loaded in each lane, alongside 5 neurula stage embryos overexpressing Mad2-tag (1st lane). **D/** Western blot analysis of Mad1. Four antibodies were tested. Both mouse 1 and 3 antibodies recognize a 67 kDa band corresponding to the size of Mad1; mouse 1 antibody also recognizes a second larger unknown protein (UK). Mad1 protein level is constant throughout development both in SAC deficient (egg to 64-cell) and SAC efficient stages (128-cell and 256-cell). Ponceau staining was used to control that each sample contains similar levels of proteins.

Based on this analysis no specific localization pattern could be identified which would explain either the lack of SAC efficiency in early embryos or the variation in SAC efficiency along the anteroposterior axis.

Although the presence of RNA is often used as a proxy for protein availability, many factors are regulated at protein level. As mentioned before this is the case for many cell cycle proteins, like Cyclin B1 whose accumulation during interphase dictates mitotic commitment (Hégarat et al., 2016; Kronja and Orr-Weaver, 2011; Wieser and Pines, 2015) or like Cdc20 whose RNA is sequestered in the nuclei in prophase delaying its translation to prometaphase in *Arabidopsis thaliana* (Yang et al., 2017). I therefore set out to analyze SAC protein levels. As commercially available antibodies did not cross-

react with *P. mammillata* proteins and no specific antibodies against *P. mammillata* SAC proteins existed, new antibodies were generated by our team. The first antibody to be generated was a mouse antibody against *P. mammillata* Mad2. To test antibody specificity, I injected into *P. mammillata* eggs RNA encoding Mad2 without its stop codon to generate an elongated version of Mad2 with few extra amino acids, called herein Mad2-tag. Five embryos expressing this construct were sufficient to easily detect by western blot a band of the predicted size that was absent in uninjected embryos (Fig. 27C), suggesting that this antibody specifically recognizes Mad2. I then tested Mad2 protein levels in eggs, 2-cell, 32-cell and 128-cell stage embryos. A band of comparable intensity at the correct molecular weight was detected at all stages, except in eggs where the signal was barely visible. This means that Mad2 protein is equally abundant in stages were the SAC is inefficient (2-cell, 32-cell) as in the gastrula where the SAC is efficient. However, for all stages I had to collect 12 µl of packed embryos (around 1300 embryos) and ECL signal detection required around 15 minutes exposures suggesting that Mad2 protein is not abundant in these cells.

An antibody against Mad1 was also generated and a similar analysis showed that like Mad2, Mad1 seems to be present at comparable levels throughout embryogenesis from eggs to tadpoles (preliminary results), indicating that Mad1 level does not correlate with variation in SAC efficiency (Fig. 27D). Differently from Mad2, however, Mad1 appears to be very abundant, as only 30 embryos were required to detect Mad1 in Western blot analysis. The presence and abundance of the other SAC proteins could not be assessed as antibodies against *P. mammillata* proteins are not yet available.

C/Overexpression of SAC proteins does not activate the SAC

My results indicate that Mad2 protein is likely to be present at a very low level in *P. mammillata* embryos. Hence, I wondered whether it was a limiting factor for SAC activation and whether its overexpression could increase SAC efficiency, resulting in earlier SAC activation during development. Indeed, in other species, such as in *D. melanogaster* (Oliveira et al., 2010), in *X. laevis* egg extracts (Chen et al., 1998) and in *S. pombe* (He et al., 1997), Mad2 overexpression can activate the SAC even in the absence of incorrect microtubule-kinetochore attachments. Consequently, I injected eggs with RNA encoding either Mad2-tag or wild type Mad2. The injected embryos developed properly and with normal timing, reaching the late neurula stage at the same time as control embryos indicating that cell cycle is not arrested or delayed in those embryos (Fig. 28A). At late neurula stage, embryos were retrieved and the high level of Mad2 was confirmed by western blot (Fig. 27C). This means that in *P. mammillata* embryos Mad2 overexpression alone is not sufficient to activate the SAC neither in early SAC deficient embryos, nor in late SAC efficient embryos.

However, as it was shown that the level of Mad2 protein influences SAC efficiency, I asked whether, once the SAC is active, Mad2 low protein level can influence mitotic length. Indeed, human and mouse cells with only one wildtype allele of Mad2 have an increased occurrence of aneuploidy (Michel et al., 2001). On the other hand, in mouse oocytes, a 4 fold overexpression of Mad2 allows meiotic exit while a 15 fold Mad2 overexpression prevents meiotic exit (Homer et al., 2005). I therefore checked whether Mad2 overexpression rather than arresting the cell cycle, resulted in mitotic lengthening. To test this possibility, I performed live imaging of NLS-3Venus expressing embryos and measured mitotic duration in control embryos and in embryos overexpressing Mad2. This analysis was performed at the 128-cell stage when the SAC is active but induces only a short increase in mitotic duration (2.2 fold) that would allow even a small increase in SAC efficiency to be detected. In the presence of DMSO, mitosis lasted 9.1±1.8 minutes in embryos overexpressing Mad2 and 10.22±2.1 minutes in uninjected embryos (Fig. 28B). Following nocodazole addition, mitotic duration was extended equally, (2.5 fold over DMSO) both in control (24.5±8.5 minutes) and Mad2 overexpressing embryos (26.7±15.8 minutes), (Fig. 28B). Thus, Mad2 is not the limiting factor for SAC activity in *P. mammillata* and its overexpression is not sufficient to induce checkpoint activation during development.

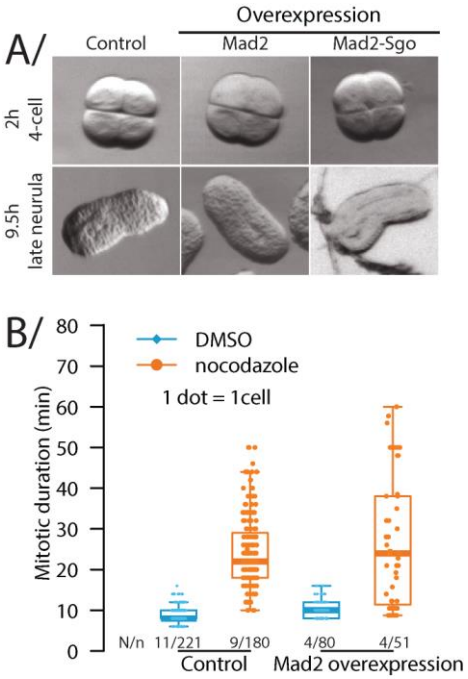

Figure 28: Mad2 overexpression does not activate the SAC

A/ Pictures of embryos injected with RNAs coding for Mad2 or Mad2-Sgo, 2 hours and 9,5 hours post-fertilization. Injected eggs were left overnight to allow protein expression prior to fertilization. This experiment was repeated three times with around five embryos per condition. **B/** Quantification of mitotic duration in control embryos and in embryos overexpressing Mad2 treated with DMSO or nocodazole the 128-cell stage. Mitosis was measured as time between NEB and NER. Each dot represents one cell. Boxes represent 25-75th percentiles and the median is shown. The number of embryo (N) and cells (n) analyzed is given. Data for mitotic duration in controls embryos (DMSO or nocodazole) is the same as in figure 21.

This results is not entirely surprising as in some human cell lines that have an efficient SAC, Mad2 overexpression does not induce a phenotype without the co-expression of Mad1 that is required to induce a sustained SAC dependent arrest (Sironi et al., 2001). As Mad1 is required for Mad2 localization at kinetochores, I asked whether Mad2 overexpression was ineffective because the protein could not be recruited to kinetochores. Unfortunately, I could not directly test this hypothesis, as the antibody we made against *P. mammillata* Mad2 did not work in immunofluorescence. However, I reasoned that if Mad1 was required for Mad2 localization at kinetochores, forcing Mad2 on kinetochores should activate the SAC. I therefore generated a chimeric Mad2 protein fused to Shugoshin (Mad2-Sgo), a protein which localizes at kinetochores in mitosis (Cheeseman and Desai, 2008; Dumollard et al., 2013; Musacchio and Salmon, 2007). Embryos expressing Mad2-Sgo, however, developed normally and were indistinguishable from control embryos (Fig. 28A). Although I could not yet verify Mad2-Sgo localization at kinetochores, these results suggest that recruitment of Mad2 to kinetochores is not the limiting step in SAC activation during early development. Consistently, co-injection of Mad1 and Mad2 RNAs does not activate the SAC (preliminary results, data not shown).

As for Mad2, eggs injected with RNA encoding Mad1, Mps1 or Bub3 fused with fluorescent protein were able to develop until at least the late neurula stage without delay compared to control embryos (data not show). This indicates that overexpressing these proteins does not activate the SAC. In conclusion, the lack of any individual SAC protein does not explain the lack of SAC activity in the early embryos of *P. mammillata.*

D/SAC localization at unattached kinetochores depends on embryonic stage

Localization of SAC proteins to unattached kinetochores is required for checkpoint signaling and mitotic arrest. Hence, mutations that prevent kinetochore localization of SAC proteins impair SAC signaling (Yamagishi et al., 2012), (see introduction part II.B, Fig. 8). Therefore, I analyzed whether SAC proteins were able to localize to unattached kinetochores in *P. mammillata* early embryos.

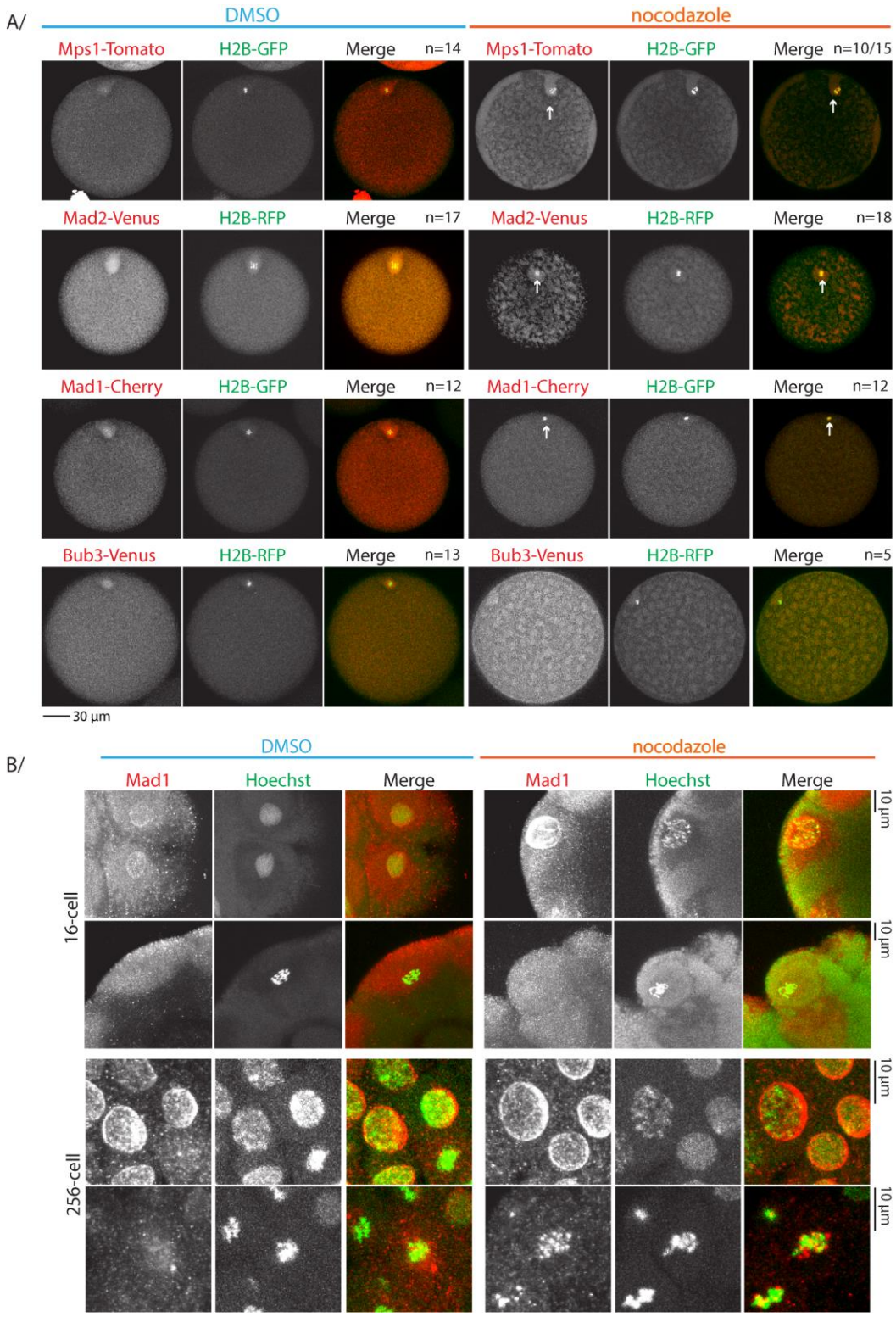

Figure 29: Variation in SAC efficiency during embryogenesis seems to be due to a change in SAC protein localization at kinetochores.

A/Representative confocal images (Z-projections) of unfertilized eggs expressing fluorescently tagged SAC proteins (red) and H2B (green) in the presence of DMSO (left) or nocodazole (right). Arrows indicate the localization of SAC protein on the DNA. The number of eggs observed for each condition is indicated on the right. In nocodazole, Mps1-tomato localized on DNA only in 10 out of 15 eggs. Scale bar is indicated at the bottom of the panel. **B/** Localization of Mad1 was tested by immunofluorescence in 16-cell (above) and 256-cell (bottom) stage embryos treated with DMSO (left) or with nocodazole (right). For each stage and condition a Z- projection of an interphasic cell (upper line) and of mitotic cell (bottom line) is shown. Scale bars are indicated at the right of each line.

As a first step I examined the behavior of exogenous SAC proteins (Mad1, Mad2, Mps1 and Bub3) fused to fluorescent proteins by injecting RNA coding for them into unfertilized eggs. *P. mammillata* unfertilized eggs are arrested in metaphase I of meiosis with all kinetochores attached to the meiotic spindle and chromosomes aligned on the metaphase plate. I could not detect any of the analyzed SAC proteins on DNA, which was marked with fluorescent histone H2B, in *P. mammillata* eggs (Fig. 29A). This is expected since in the meiotic metaphase arrest of unfertilized eggs, kinetochores are attached to spindle microtubules.

However, when eggs were treated with 10 µM nocodazole to depolymerize spindle microtubules and generate unattached kinetochores, Mad1, Mad2 and Mps1, but not Bub3, localized to the DNA (Fig. 29A). This means that in unfertilized eggs, kinetochores are competent for SAC localization. Nevertheless, in meiosis SAC is not efficient but SAC protein localization was assessed in unfertilized eggs before release from the CSF arrest. This suggests that either the loss of SAC activity happens downstream of its localization at kinetochores or that SAC localization at kinetochores is lost at fertilization.

Consequently, I decided to test the localization of SAC proteins in early embryos. Since the SAC is inefficient in the early embryos, even in the presence of nocodazole the time cells spend in mitosis is short. For this reason, the use of fluorescent proteins in live embryos did not allow me to conclude whether there was a transient prometaphase localization of SAC proteins. Immunofluorescences overcomes this problem as it relies on fixed embryos but requires specific antibodies. Therefore, preliminary results could be obtained only for Mad1. In fixed *P. mammillata* embryos of all stages, Mad1 is found at the nuclear envelope during interphase (Fig. 29B). In neurula, Mad1 localizes to the DNA but only in presence of nocodazole, suggesting that Mad1 localizes to unattached kinetochores, as seen in somatic cells (Musacchio and Salmon, 2007) and in agreement with the presence of an efficient SAC at this stage. In 8- and 16-cell SAC deficient embryos, colocalization of Mad1 signal and DNA staining was never observed even in presence of nocodazole (Fig. 29B). These preliminary results suggest that the lack of SAC efficiency is due to the absence of recruitment of one or more SAC proteins to unattached kinetochores.

E/ ERK is active in early embryos but is not required for mitosis

SAC efficiency varies during *P. mammillata* embryogenesis and this variation is associated with a change in kinetochore recruitment of specific SAC components. As SAC components are always present in *P. mammillata* embryos I asked what modulates this recruitment to unattached kinetochores. The kinase Mps1 is first recruited on kinetochores and its activity is required to phosphorylate the kinetochore complex KMN allowing the localization of the other SAC proteins (Jia et al., 2013). In *X. laevis* egg extracts and in HeLa cells, ERK phosphorylates Mps1 promoting the recruitment of SAC proteins to kinetochores and leading to SAC activation (Borysova et al., 2008; Zhao and Chen, 2006). ERK is also highly activated in *P. mammillata* oocytes and inactivated at fertilization (Dumollard et al., 2011), at the same time as the apparent loss of SAC protein localization at unattached kinetochores. Therefore, I wondered whether lack of ERK activity in early embryos is sufficient to prevent recruitment of SAC proteins to unattached kinetochores.

I first asked whether ERK is inactive during the early cells cycles of *P. mammillata* development by assessing ERK phosphorylation, an indicator of ERK activity (Minshull et al., 1994; Takenaka et al., 1997). I collected 40/50 embryos over the two first mitosis (every 4 minutes from 44 to 98 minutes post fertilization), and samples were analyzed by western blot. ERK phosphorylation was determined using an antibody specific for di-phosphorylated ERK (dpERK). Five unfertilized eggs were loaded on the same gel as positive control for active ERK (Fig. 30A).

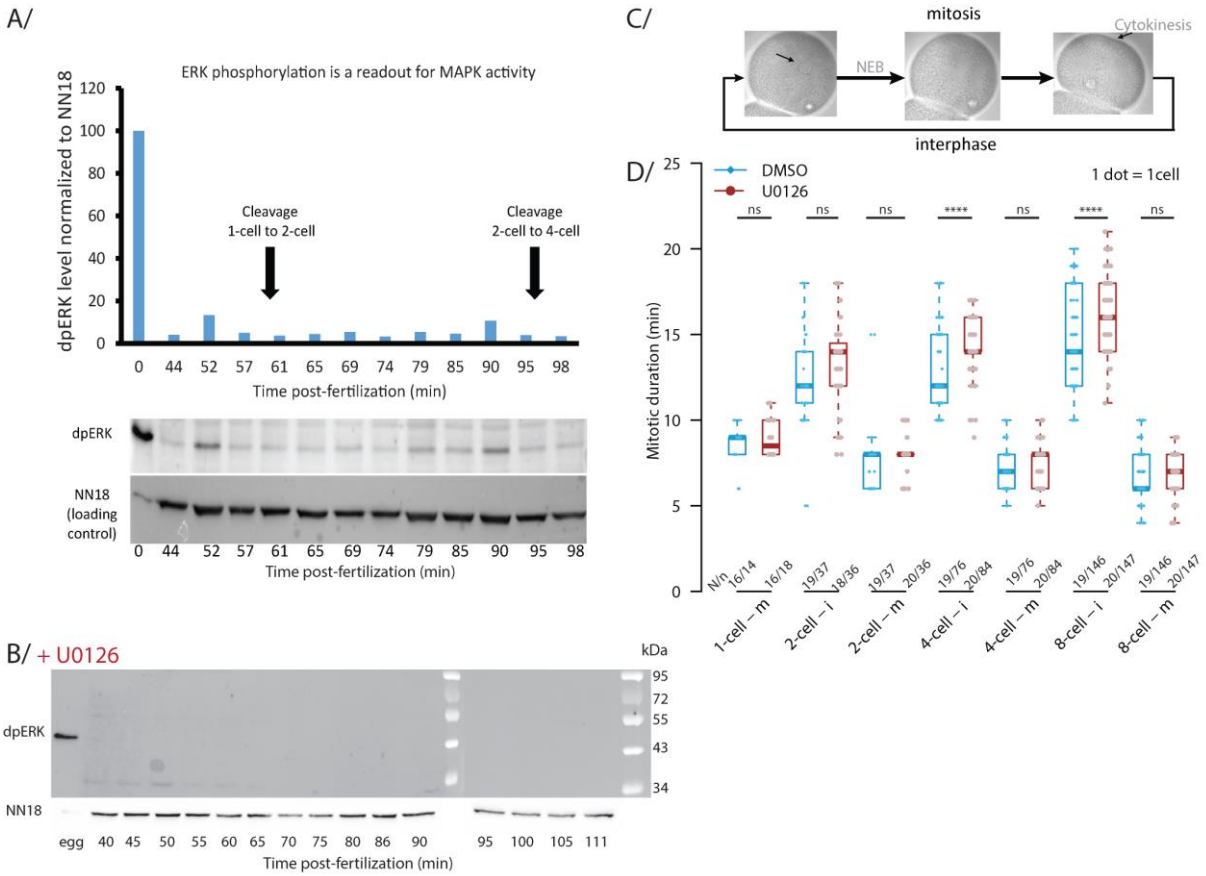

Figure 30 : ERK is active at mitotic entry but is not required for mitotic progression

A/ Quantification of signal intensity in western blots for dpERK, normalized to the loading control NN18 during the first two cell cycles following fertilization. Signal intensity is plotted as a percentage of the signal present in unfertilized eggs (t=0). dpERK phosphorylation was used as a marker of MAPK activity. Arrows indicate time of cleavage. 30 embryos were loaded in each lane apart from t0 for which 5 eggs were loaded. The western blot used for quantification is presented under the graph. This experiment is representative of three repeats. **B/** Western blot analysis of the ERK phosphorylation status (dpERK) following inhibition of MAPK activity with the MEK inhibitor, U0126. No signal corresponding to dpERK was detected following U0126 treatment. Unfertilized eggs were used as positive control. NN18 was used as loading control. **C/** Cell cycle progression was followed by live video microscopy. Mitotic duration was measured as the time between NEB and cytokinesis (mitotic exit). **D/** Quantification of mitotic (m, NEB to cytokinesis) and interphase (i, cytokinesis to NEB) duration in embryos cycling in the presence of either DMSO or 5 µM U0126. Each dot represents one cell. Boxes represent 25-75th percentiles and the median is shown. The number of embryos (N) and cells (n) analyzed is given. t-test: non significatif (ns), p-value ≤ 0.05 (*), p-value ≤ 0.01 (**), p-value ≤ 0.001 (***), p-value ≤ 0.0001 (****).

As expected ERK was highly phosphorylated in unfertilized eggs arrested by CSF activity (Fig. 30A), (Dumollard et al., 2011). Following fertilization, ERK phosphorylation was barely detectable throughout the first two cell cycles (Fig. 30A). However, I observed a low intensity signal at 50 and 90 minutes post fertilization. Intensity of the bands was measured with the software Fiji/ImageJ and results were normalized using the loading marker NN18. This showed that the level of ERK phosphorylation was markedly reduced in early embryos reaches at most 10% of the level observed in comparison with unfertilized eggs (ratio early embryo/ unfertilized eggs). ERK phosphorylation occurred 5/10 minutes before cytokinesis which takes place concomitantly with telophase (Fig. 30A). Taking into consideration that in *P. mammillata* mitosis lasts 8/12 minutes, ERK is phosphorylated at mitotic entry. These results are similar to the data available for *X. laevis* early embryos which show that ERK is phosphorylated at mitotic entry, but to a degree 10 times less than in arrested oocytes (Minshull et al., 1994; Takenaka et al., 1997).

I then tested if ERK activity was required in mitosis by inhibiting the MAPK pathway. I used U0126, an inhibitor of MEK, the MAPKK which phosphorylates ERK (Dumollard et al., 2011). U0126 efficiency was confirmed by western blot analysis for dpERK following drug treatment. Indeed, no phosphorylated ERK could be detected in embryos treated with U0126, indicating that the MAPK pathway was efficiently inhibited (Fig. 30B).

To test the role of ERK in mitosis, embryos were treated with U0126 30 minutes post-fertilization to allow completion of meiosis but to be able to observe mitotic entry (NEB) in most embryos. In these experiments, cell cycle progression from 1- to 16-cell stage was followed using NEB as marker of mitotic entry and the beginning of cytokinesis furrow ingression as the beginning of interphase (Fig. 30C). Cytokinesis is easier to assess than NER but could not be used in previous experiments because nocodazole treatment prevents it. Interphase was slightly lengthened in embryos treated with U0126 at 4-cell (control: 12.9±2.3, U0126: 14.3±1.6) and 8-cell (control: 14.6±2.8, U0126: 16±2.2), suggesting a role of ERK in interphase (Fig. 30D). Mitosis duration was however unaffected by inhibition of the MAPK pathway (Fig. 30D), indicating that ERK activity is not required in mitosis.

In conclusion, the lack of SAC activity is not due to the lack of ERK activation in *P. mammillata* early embryos. To conclude on the role of ERK on SAC activity, it would be interesting to test whether ectopic activation of the MAPK pathway in early embryos leads to Mad1 localization at kinetochores and the effect of ERK inactivation on the SAC efficiency in late embryos.

F/ Search for molecular control of SAC activity: identification of Mad2 interacting proteins

I decided to use an unbiased approach to search for proteins that could regulate the SAC and influence its activity during ascidian development. Mad2 is a central player connecting SAC localization at unattached kinetochores to the formation of the MCC generating the inhibitory signal (see introduction part II, Fig. 8), (Jia et al., 2013; Musacchio and Salmon, 2007). Therefore, I looked for proteins that directly interact with Mad2 and could possibly modulate its activity.

To do so, I produced a recombinant Mad2 protein bearing a 6 histidines tag in C-terminal. Histidine interacts with Nickel allowing Mad2 to be loaded on Nickel columns (Fig. 31). Protein extracts from *P. mammillata* unfertilized eggs treated with nocodazole were then passed through the column. Elution fractions were run on a SDS-PAGE gel and the bands specific to the Mad2 eluate, and absent from the mock column (no Mad2), were analyzed by mass spectrometry. This allowed the identification of 228 proteins. I used BLAST (States and Gish, 1994) to identify them and obtained a list of 194 different proteins (annex 3). One of them was Mad2, which could be either the recombinant protein eluted from the column or Mad2 from the extract. Indeed, Mad2 is known to dimerize (Sironi et al., 2001). I also retrieved Cdc20 which both consistent with that Mad2 interacts with Cdc20 in *P. mammillata* and that my purification protocol allowed the identification of true Mad2 interacting proteins.

Several of the proteins retrieved were involved in transcription, translation, stress response and mitochondrial metabolism. As these proteins are known to usually be the most abundant in the cell, their interaction with Mad2 is probably non-specific or not involved in SAC regulation. Among these abundant proteins detected, tubulin and actin monomers could interact specifically with Mad2 given the known connection between the SAC function and the cytoskeleton, (Jia et al., 2013; Musacchio and Salmon, 2007).

By excluding all these proteins, I reduced my candidates to 36 proteins which I then searched using gene ontology to identify interesting candidates. After this secondary analysis I retrieved dynein, some proteasome subunits and the protein phosphatase 1 regulatory subunit 37 (an inhibitory subunit). At anaphase onset SAC inactivation requires Dynein and PP1 (see introduction part II, Fig. 9),

whereas the proteasome is involved in the degradation of APC/C targets (Jia et al., 2013; Musacchio and Salmon, 2007). A second class included proteins involved in mitotic control, such as 14-3-3 which is required to prevent mitotic entry (see introduction part I, Fig. 4), (Hégarat et al., 2016) and Phb2 which protects cohesion between sister chromatids (Takata et al., 2007), both indirectly preventing anaphase onset. A final group included proteins known to be involved in embryogenesis, which could be good candidates to control SAC efficiency during development. Among them, I retrieved Vasa DEAD-box, which controls Cyclin B1 level in echinoderms and whose depletion induces a mitotic block (Yajima and Wessel, 2011).

I selected a few candidates based on their known function: protein phosphatase 1 regulatory subunit 37, 14-3-3, Phb2 and Vasa DEAD-box for further analysis and decided to use yeast two hybrid assay to confirm their interaction with Mad2. Unfortunately, none of them was able to interact with Mad2 in this condition and I therefore did not pursue their analysis further.

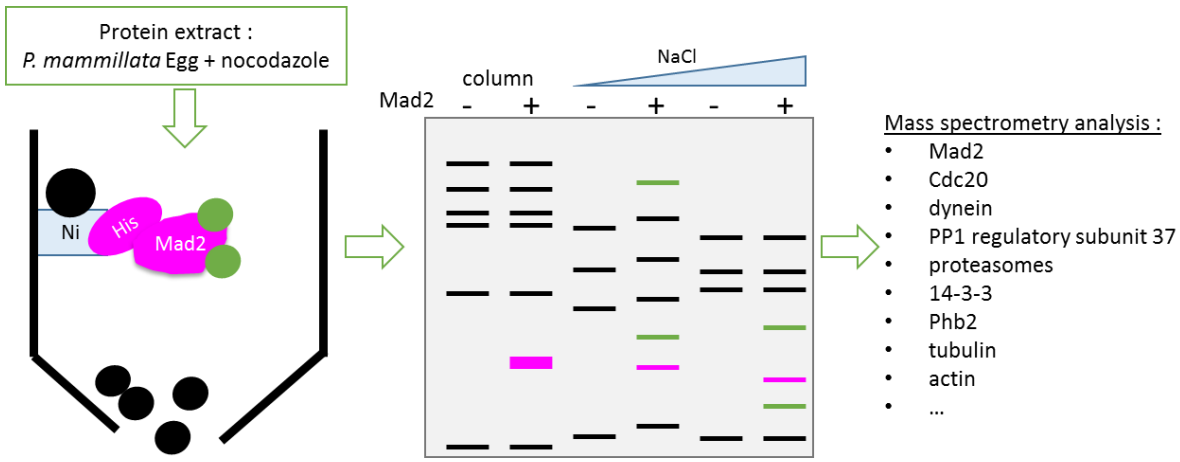

Figure 31 : A screen for Mad2 interacting proteins

Protein extracts from unfertilized eggs treated with nocodazole (Green and black) were passed through a Nickel column load with Mad2-6His (pink). After elution, proteins were run on a 10% polyacrylamide gel and colored with Silver ruby. Proteins present only in the elution of the Mad2 column (green) were analyzed by mass spectrometry. Some of the retrieved proteins are indicated on the right. The full list is available in annex 3.

Discussion

During my thesis, I studied SAC efficiency during *P. mammillata* embryogenesis. I confirmed that the SAC is not efficient in meiosis (Dumollard et al., 2011) and showed that following fertilization the SAC is inefficient in mitosis from 2-cell to 64-cell stage (Fig. 32A). SAC activity is acquired at gastrulation, during the 8th cell cycle, corresponding to 128-cell embryos and its efficiency increases along the three subsequent cell cycles (Fig. 32A). In addition, I showed that once acquired SAC activity is not equal across the embryo, instead its efficiency varies in different cell populations. By focusing on the ventral ectoderm, I could show that the SAC is more efficient in anterior than in posterior cells (Fig. 32B) and that anterior cell identity is associated with greater SAC efficiency. However, my results indicate that other parameters, such as cell volume, modulate SAC efficiency in embryonic cells. Finally, I have analyzed some aspects of SAC signaling during development to try and identify the key steps that control the variability in SAC activity. Possible mechanisms, which could either control SAC acquisition at the 8th cell cycle, modulate the SAC along the anteroposterior axis or both, are discussed here.

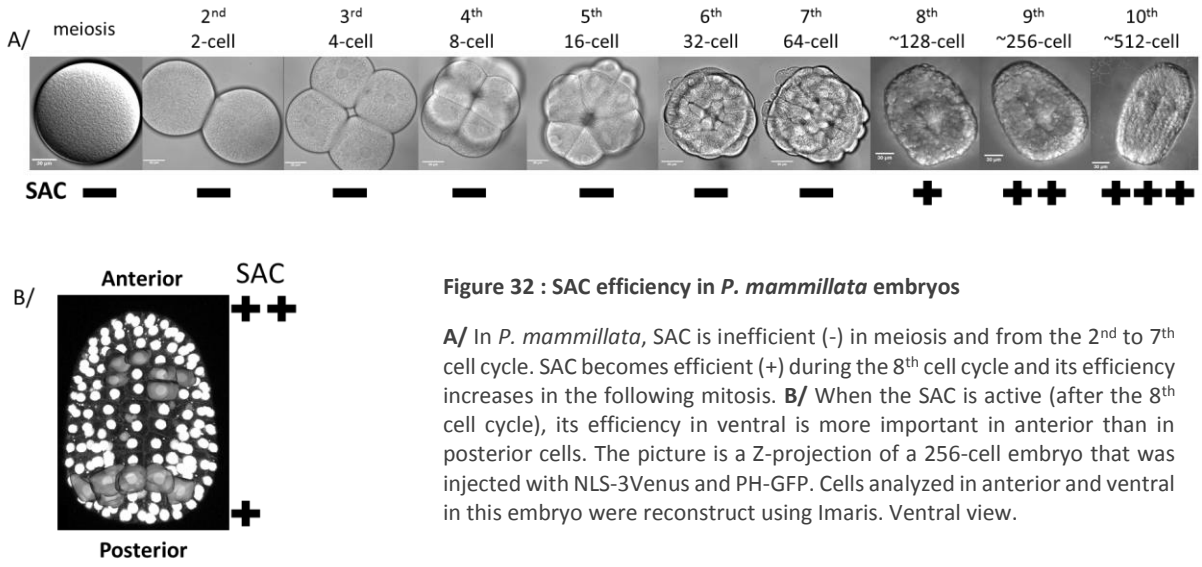

Figure 32 : SAC efficiency in *P. mammillata* embryos

A/ In *P. mammillata*, SAC is inefficient (-) in meiosis and from the 2nd to 7th cell cycle. SAC becomes efficient (+) during the 8th cell cycle and its efficiency increases in the following mitosis. **B/** When the SAC is active (after the 8th cell cycle), its efficiency in ventral is more important in anterior than in posterior cells. The picture is a Z-projection of a 256-cell embryo that was injected with NLS-3Venus and PH-GFP. Cells analyzed in anterior and ventral in this embryo were reconstruct using Imaris. Ventral view.

A/ Molecular control of SAC efficiency during embryogenesis

Modulation of SAC efficiency in embryos may be a straightforward consequence of changes in the availability of SAC components during embryogenesis. However, this hypothesis is not supported by the data currently available. Analysis of available transcriptomic data does not show any difference in the cytoplasmic level of RNAs encoding SAC proteins or the SAC target, Cdc20 (Brozovic et al., 2018). Similarly, protein levels, at least for SAC components I have been able to test (Mad1 and Mad2), are comparable during embryogenesis in both SAC deficient and SAC efficient stages. Consistently, Mad2, Mad1, Bub3 or Mps1 overexpression did not affect normal embryonic development and Mad2 overexpression did not result in an increase in SAC efficiency even following nocodazole treatment. This is in contrast with data available for mouse zygotes where overexpression of either Mad2 or Bub3 prevents anaphase onset for several hours with SAC components localized on attached kinetochores, indicating activation of the SAC (Wei et al., 2011). Although for completion, the effect of Bub1 overexpression should be determined as well as of the co-overexpression of all SAC components in both control and nocodazole treated embryos, this analysis suggests that in *P. mammillata* early embryos SAC efficiency is not modulated by the cytoplasmic availability of its components. As the SAC inhibits anaphase onset by sequestering Cdc20, a change in the level of Cdc20 could also affect the

capacity of the SAC to prevent mitotic exit. Indeed, overexpression of Cdc20 in cancer and human cell lines is associated with a reduction in SAC efficiency and an increase in the rate of aneuploidy (Mondal et al., 2007). Similarly, in *S. cerevisiae* Cdc20 overexpression allows APC/C activation even in the presence of nocodazole (Hwang et al., 1998). Our preliminary results (data not shown), however, suggest that Cdc20 level is constant during embryogenesis indicating that the variation in SAC efficiency is also not due to a change in the abundance of the SAC target Cdc20.

Instead my results suggest that the lack of SAC activity during cleavage stages is due to the inability of unattached kinetochores to recruit SAC components. SAC activation relies on the localization of SAC proteins to unattached kinetochores (see introduction part II.B, Fig. 8). I observed that in early SAC deficient *P. mammillata* embryos, Mad1 does not localize to unattached kinetochores, but does in late SAC efficient embryos. Although the localization of other SAC components has not yet been tested, this preliminary data suggests that in early embryos the SAC pathway is inhibited at its most upstream step and therefore lack of SAC activity in those embryos is not due to fast mitotic slippage. Instead proteins required for the localization of SAC proteins at kinetochores may be missing or inactive in the early embryo. For example, Aurora B may not phosphorylate Ndc80 in early embryos limiting recruitment of Mps1 and consequently all other SAC components to unattached kinetochores (see introduction part II.B) (Manic et al., 2017). An alternative possibility could be that SAC components localize normally to unattached kinetochores but in early embryos their association with kinetochores is short lived and they are quickly removed by dynein, $p31^{comet}$ and TRIP13 (see introduction part II.B) (Jia et al., 2013).

Interestingly, in oocytes, which are arrested in metaphase I of meiosis, Mad1, Mps1 and Mad2, localize to unattached kinetochores, suggesting that kinetochores are competent for SAC activation prior to fertilization. However, I could not detect Bub3 at kinetochores and did not test the localization of Bub1. It is possible that in the oocyte only Mad1, Mad2 and Mps1 can localize to unattached kinetochores, leading only to a partial activation of the SAC that is not sufficient to sustain APC/C inhibition during meiosis. Alternatively, as Mad1 localization was observed in unfertilized oocytes but is lost in mitosis following fertilization, an event occurring at fertilization could interfere with SAC recruitment to unattached kinetochores already in meiosis.

Lack of SAC protein localization at unattached kinetochores could explain the lack of SAC activity during early cleavage stages but does not explain the difference in SAC efficiency observed along the anteroposterior axis. As I could show that interfering with patterning along the anteroposterior axis results in a change in SAC response, I hypothesized that the mechanisms modulating SAC efficiency are linked with the mechanisms controlling anteroposterior patterning. Indeed, ectopic expression of the anterior determinant FoxA-a (Lamy et al., 2006) leads to an increase in SAC efficiency. Induction of the posterior identity requires activation of the WNT/β-catenin pathway (Feinberg et al., 2019). In cell lines, the WNT/β-catenin pathway modulates SAC efficiency through the activity of its inhibitor GSK3 (Rashid et al., 2018). GSK3 overexpression increases mitotic index, whereas, following taxol treatment, GSK3 inhibition decreases mitotic index and reduces Mad2, BubR1 and Bub1 localization at kinetochores. GSK3 inhibition does not totally prevent the localization of SAC proteins at kinetochores, instead it induces a progressive release from SAC arrest. These experiments suggested that GSK3 contributes to SAC efficiency but is not required for SAC activation (Rashid et al., 2018). In *P. mammillata,* the WNT/β-catenin pathway is active in the posterior ectoderm cells, while GSK3, the WNT/β-catenin inhibitor, should be active in anterior cells. Therefore, it is possible that in *P. mammillata* embryos, inhibition of WNT/β-catenin pathway by FoxA-a in anterior ventral ectoderm activates GSK3 which stimulates the efficiency of the SAC. In posterior, WNT activation inhibits GSK3 preventing it from reinforcing SAC efficiency. Although I have not tested this hypothesis directly yet, I noticed in my experiments that not only cells overexpressing FoxA-a but also the neighboring cells have a more efficient SAC. This suggests a non-autonomous effect of FoxA-a on SAC efficiency that might be

dependent on the induction of sFRP1/5 expression. Indeed, sFRP1/5 encodes a secreted protein able to inhibit the WNT/β-catenin pathway (Kawano and Kypta, 2003; Lamy et al., 2006).

B/ Cellular parameters that can influence SAC efficiency during embryogenesis

Lack of SAC efficiency in early embryos was already observed in other chordate embryos (Chenevert et al., 2019; Gerhart et al., 1984; Ikegami et al., 1997). In *X. laevis* and *D. rerio* the SAC is inactive during cleavage and is acquired respectively at the 12th and 10th cell cycles (Clute and Masui, 1992; Zhang et al., 2005). As shown by my work, in *P. mammillata* the SAC is acquired during the 8th cell cycle. Although the number of cell cycles prior to SAC activation is different in embryos from different species, the SAC becomes efficient at gastrulation both in *P. mammillata* and in *X. laevis*. However, *P. mammillata* VC-deficient embryos do not gastrulate (Nishida, 1996) and still acquire the SAC showing that as for *X. laevis* (Clute and Masui, 1995), gastrulation itself is not required for SAC acquisition. In both *X. laevis* and *D. rerio*, the SAC is acquired at MBT (Clute and Masui, 1995; Zhang et al., 2015) whereas in *P. mammillata,* the SAC is acquired four cell cycles after MBT (Matsuoka et al., 2013; McDougall et al., 2011; Oda-Ishii and Satou, 2018). Several changes that allow early embryonic cells to evolve toward a more somatic cell life take place at MBT: activation of zygotic transcription, acquisition of G2 phase and appearance of cell cycle asynchrony between blastomeres. One or more of these events may be a prerequisite for SAC activation in embryos.

Testing the role of transcription in SAC activation is challenging, as inhibition of transcription would affect not only the SAC but also a plethora of cellular mechanisms. However, currently available evidence does not support a role for transcription in SAC activation during embryogenesis. Firstly, levels of transcripts coding for SAC proteins do not increase during *P. mammillata* embryogenesis. Moreover, inhibition of transcription in *D. rerio* and *X. laevis* does not prevent SAC acquisition showing that in those animals SAC acquisition at MBT does not depend on transcription (Clute and Masui, 1995; Zhang et al., 2015).

MBT is also marked by cell cycle lengthening with the addition of G2 phase. In G2, SAC proteins are already activated at nuclear pores and can inactivate the APC/C (see introduction part II.B.2). In somatic cells, interference with interphase activation of the SAC results in an increase in chromosome segregation defects suggesting that SAC activation in mitosis is not sufficient to prevent them (Rodriguez-Bravo et al., 2014). It is therefore possible that SAC is more efficient when interphase is lengthened. Interestingly, in *P. mammillata,* although G2 is acquired at MBT (5th cell cycle) (Dumollard et al., 2013), the duration of interphase does not lengthen significantly until the 8th cell cycle when it increases from 20 minutes to more than 50 minutes (see introduction part IV.B.2, Fig. 15). Consequently, the SAC is acquired when interphase, and probably G2, starts to properly lengthen. Interphase duration then increases in the following cell cycles (9th and 10th), as does SAC efficiency. The duration of interphase might also be part of the explanation of the differences in SAC efficiency along the anteroposterior axis. Indeed, interphase is longer in anterior cells where the SAC is most efficient (Ogura and Sasakura, 2016; Ogura et al., 2011). This possible link between SAC activity and interphase length could also explain why cells of VC-deficient embryos have an inefficient SAC despite having acquired an anterior identity. I observed that in VC-deficient embryos, cells enter mitosis slightly earlier than corresponding control cells, suggesting a shorter interphase duration than control cells. Careful recording of the full cell cycle in those embryos to measure interphase duration would be necessary to support this hypothesis. Taken together, these observations suggest that longer interphase correlates with a more efficient SAC. Mechanisms involved in control of G2 may therefore regulate SAC efficiency. From the proteomic analysis, I retrieved 14-3-3, an inhibitor of mitotic entry, as a Mad2 interacting protein (see introduction part I.C and results part II.F), (Hégarat et al., 2016). 14-3-3 may then be an interesting candidate to explain the variation in SAC efficiency in *P. mammillata* embryos. If the hypothesis is correct 14-3-3 would be an activator of the SAC.

Another change that arises during embryogenesis is a reduction in cell volume, due to subsequent divisions without intervening cell growth typical of the cleavage stage. Work carried out in *C. elegans* embryos and *M. musculus* oocytes (see introduction part III.B), (Galli and Morgan, 2016; Gerhold et al., 2018; Kyogoku and Kitajima, 2017) showed that the bigger the cell, the less efficient the SAC. However, SAC efficiency is not influenced by cell volume in embryos of *M. musculus*, *D. rerio* and *X. laevis* (Clute and Masui, 1995, 1997; Vázquez-Diez et al., 2019; Zhang et al., 2015). As already explained in the introduction (part III.B.2) the effect of cell volume on SAC efficiency depends on the number of kinetochores and is thought to be a consequence of the dilution of the SAC signal generated at unattached kinetochores in the cytoplasm (Galli and Morgan, 2016; Gerhold et al., 2018). SAC efficiency is therefore thought to vary in relation with kinetochore to cytoplasmic ratio. This ratio changes continuously in the embryo as cell division occurs without cell growth during early development resulting in a reduction in cell volume and therefore an increase in kinetochore to cytoplasmic ratio. It is therefore possible that SAC acquisition occurs when this ratio reaches a threshold. In *P. mammillata*, 2-cell stage embryos treated with nocodazole undergo several subsequent cell cycles without intervening cytokinesis, increasing kinetochore to cell volume ratio, assuming that kinetochores are formed properly at each cycle (Chenevert et al., 2019). A kinetochore to cytoplasmic ratio of $4*10^{-4}$ Kt/μm^3, equivalent to that of epidermal cells in 128-cell (8^{th} cell cycle) control embryos, is reached after five cycles. However, those endo-replicating 2-cell embryos do not acquire an efficient SAC (mitotic duration 1.3 of DMSO in nocodazole, data not show) in contrast with the corresponding control 128-cell, indicating that an increase in kinetochores to cell volume ratio does not allow SAC acquisition in *P. mammillata* early embryos.

Similarly, in *P. mammillata* at the 9^{th} cell cycle (256-cell embryo), the difference in SAC efficiency within an embryo does not correlate with changes in cell volume. However, it does in VC-deficient embryos suggesting that in wild type embryos the effect of cell volume is dampened by the effect of other parameters. In VC-deficient embryos, all cells have acquired the same identity, a parameter that was shown to impact SAC efficiency in *C. elegans* (Gerhold et al., 2018). In *P. mammillata*, I could show that acquisition of an anterior identity by FoxA-a overexpression leads to the acquisition of a more efficient SAC. However, the anterior identity is not sufficient to increase SAC efficiency in VC-deficient embryos. This difference may be due to dilution of the SAC signal in the larger cell volume observed in VC-deficient cells. Alternatively, as VC-deficient embryos also lack vegetal cells that are required to induce correct epidermal patterning along the anteroposterior axis (Takatori et al., 2007; Wada et al., 1999), a signal produced by vegetal cells may be required for boosting SAC efficiency in the anterior ventral ectoderm. To distinguish between these two hypotheses, it would be interesting to test SAC efficiency in animal explants where wild type animal blastomeres are isolated form vegetal cells.

C/Developmental events that would require the lack of SAC efficiency

The lack of SAC efficiency in early embryos is surprising and poses the question of why animals would not use a mechanism that safeguards their genome while forming a new organism. Some non-mutually exclusive hypotheses can be proposed.

In early embryos of *P. mammillata,* the absence of an active SAC may be related to its invariant cleavage pattern (Conklin EG, 1905). Indeed, the invariant cleavage pattern offers no flexibility for the formation of cell lineages required to make the embryo. Therefore, if SAC activation were to arrest a cell in mitosis no other cell could take over the lineage that the arrested cell should have made.

Even a short delay in mitotic progression could impair embryogenesis. It has been shown that in *P. mammillata* the pattern of division is required for proper morphogenesis and cell differentiation (see introduction part IV), (Dumollard et al., 2017; Ogura and Sasakura, 2016; Ogura et al., 2011). This pattern requires that cell cycles of different blastomeres in the embryo are coordinated, albeit asynchronous. As spindle orientation and orientation of cytokinesis are dictated by cell shape which in

turn depends on the interaction with neighboring cells, cell cycle coordination within the embryo guarantees proper orientation of cell division necessary for embryonic patterning and proper development (Dumollard et al., 2017). If the SAC was efficient in early embryos, mitotic duration would vary depending on how fast chromosomes are attached, resulting in loss of cell cycle coordination. The cells would then divide when their neighboring cells have a different shape than in control embryos resulting in a change in the place where cytokinesis occurs in the cell. Consequently, the daughter cells would not be placed correctly within the embryo leading to developmental defects. In addition, the surface contact of the daughter cells with the other cells of the embryo would be changed resulting in the alterations in the pattern of intercellular signals.

In the later stages, SAC activity is acquired even if mitotic duration still needs to be coordinated between cells of the embryo. Along the anteroposterior axis, the mitotic wave which appears as a consequence of interphase lengthening is required for proper neurulation at the 11th cell cycle (Ogura and Sasakura, 2016; Ogura et al., 2011). However, interphase is longer in late stages compared to early stages (Ogura and Sasakura, 2016; Ogura et al., 2011). Small changes in mitotic duration would therefore be less significant relative to the full cell cycle length and would barely modify cell cycle coordination between cells. This could allow SAC acquisition but with a low efficiency in the 8th cell cycle. Then, SAC becomes more and more efficient at each cell cycle as interphase lengthens. Especially, SAC is more efficient in anterior cells where interphase is longer than in posterior ventral ectoderm.

Even if SAC activation may not disturb the correct development it may delay it resulting in depletion of all energetic resources before the embryo reaches the stage at which it can feed. Indeed, *P. mammillata* embryos, as most early embryos, are not feeding and have a finite amount of available resources. The inactivation of checkpoints during embryonic development may prevent embryos from running out of energy. Among chordates, mammals are the only animals to have an efficient SAC in early embryos, but their development occurs in utero with a continuous external nutritional income (Gilbert, 2000b). A caveat is that *P. mammillata* embryos acquire the SAC before acquisition of feeding capacity but at these stages the risk associated with the lack of SAC activity might become more important than the cost of SAC activation.

D/ Survival despite an inefficient SAC in early embryos

In somatic cells, the SAC is required to ensure proper chromosome segregation and avoid the appearance of aneuploid cells. Based on this canonical role of the SAC to prevent chromosome mis-segregation, one would expect that in embryos lacking an efficient SAC, there would be a higher incidence of aneuploidy. This is indeed the case for human embryos that have an active but inefficient SAC and which show 20 to 70% aneuploidy in preimplantation embryos (Nagaoka et al., 2012) raising the question of how embryos manage to survive, and more generally how a species is maintained, without an efficient SAC.

Aneuploidy is a change in chromosome copy number. In human it was shown that the cell can deal with supernumerary chromosomes, by losing the extra copies and re-establishing normal ploidy (Mantikou et al., 2012). Alternatively, aneuploid cells were shown to become senescent or undergo apoptosis, as it occurs in somatic cells, preventing their propagation hence their harmful accumulation in the embryo (Mantikou et al., 2012). In addition, in human, aneuploid blastomeres can be segregated toward extra-embryonic tissues, like the placenta, which are required for embryogenesis but are not maintained in the adult (Mantikou et al., 2012). In *P. mammillata,* that has an invariant cleavage pattern, a similar mechanism is difficult to envisage as removal or displacement of a cell is not possible due to the invariant cell lineage discussed above (Conklin EG, 1905). However, the tadpole undergoes metamorphosis resulting in the elimination of many cells by apoptosis, mainly in the tail region (Sasakura and Hozumi, 2018). Tail regression is accompanied to the death of notochord and posterior ectodermal cells, while cells of the anterior ectoderm are conserved in adults (Sasakura and Hozumi,

2018). Therefore, aneuploidy would be most harmful in anterior cells, which survive metamorphosis and become part of the adult. Interestingly cells of the anterior ventral ectoderm, which are maintained in the juvenile, have a more efficient SAC than posterior ventral ectodermal cells and notochord cells that are eliminated during metamorphosis.

Along this line, we would expect germline cells and their precursors to have the most efficient SAC, as their aneuploidy would affect viability of the offspring impacting long-term species survival. Indeed, in *C. elegans* the SAC was shown to be strongest in the germline lineage (Gerhold et al., 2018). In *P. mammillata*, technical limitations did not allow to study germline precursors which are embedded in the embryo. The expression of a germ cell specific marker would be required to identify and follow these cells. Due to this technical constraint, I focused on differences existing in the most external layer of cells, the ventral ectoderm, along the anteroposterior axis, but other differences in SAC efficiency depending on cell types and embryonic domains might be present in *P. mammillata* embryos.

Checkpoints are surveillance mechanisms that ensure proper cell cycle progression (see introduction part I.A), (Barnum and O'Connell, 2014), but are not directly required for cell cycle progression. During mitosis, the SAC assesses if chromosomes are properly attached to spindle microtubules, but kinetochore-microtubule attachments and chromosome segregation can take place in the absence of an efficient SAC. In *D. melanogaster*, for example, Mad2 is not an essential gene and Mad2 mutants, although SAC deficient, still give rise to fertile adults and at the third instar larva, only a small rate of aneuploidy can be detected (Buffin et al., 2007). In mouse embryos, instead, SAC impairment by Mad2 depletion induces high levels of aneuploidy and results in embryonic death (Dobles et al., 2000; Michel et al., 2001). This difference in Mad2 requirement between species suggests that factors other than the SAC can increase the probability of correct chromosomes segregation.

One factor that has been suggested to modulate the success of chromosomes segregation is chromosome number. When the SAC is inactive, prometaphase duration is dictated by the time required for the degradation of Cyclin B1 and Securin. The probability that all chromosomes are correctly attached in a given amount of time is higher if the chromosome number is low, like for *D. melanogaster* that has only 4 chromosome pairs (Buffin et al., 2007). SAC efficiency, however, does not correlate with chromosome numbers across species. Both *P. mammillata* that has only 16 chromosomes per cell (Colombera, 1971), and *D. rerio* that has 50 chromosomes per cell are SAC deficient during early development, while the cnidarian *C. hemisphaerica* which has 30 chromosomes per cell is SAC efficient (Chenevert et al., 2019). Hence, other parameters may increase the probability of the formation of correct microtubule-chromosome attachments.

The capacity of microtubules to correctly attach to chromosomes may also be modulated by kinetochore size and structure. In cells of the deer *Muntiacus muntjak,* some chromosomes have unusually large kinetochores. These chromosomes congress more frequently than other chromosomes when the microtubule motor CENP-E is inhibited, but are more prone to merotelic attachments, when one kinetochore is attached by microtubules from both poles leading to an increase in chromosomes lagging in anaphase. These merotelic attachments are mostly resolved in anaphase resulting in proper chromosome segregation (Drpic et al., 2018). Interestingly, merotelic attachments are not detected by the SAC (Musacchio and Salmon, 2007). Altogether, these suggest that in the case of large kinetochores, SAC is not as useful as in the case of small kinetochores. Kinetochore size is a parameter that affects the efficiency at which chromosomes are attached by microtubules, but other parameters may also influence it. To see if the absence of the SAC is compensated by optimized, for example in size, kinetochores in *P. mammillata*, it would be interesting to see their ability to form proper attachments with microtubules.

Finally, aneuploidy rates could be high in embryos and result in a high incidence of embryonic death. However, each *P. mammillata* generates millions of gametes increasing the probability to generate a suficient number of healthy adults to maintain the species.

Conclusions

During my thesis, I could describe for the first time SAC efficiency during embryogenesis of *Phallusia mammillata*. I could show that SAC efficiency varies both temporally and spatially. Temporally, the SAC is acquired at the 8th cell cycle and then becomes more efficient in the following cell cycles. Spatially, the SAC is more efficient in anterior than in posterior cells of the ventral ectoderm. I started to analyze mechanisms that could influence SAC efficiency during *P. mammillata* embryogenesis, but the understanding of this regulation will need further work (Fig. 33).

This work shows that *P. mammillata* embryos are an interesting resource to decipher molecular mechanisms that control SAC efficiency as well as cellular parameters that modulate it. These mechanisms and parameters may be conserved in embryos of other species and in somatic cells and underlay the pathological lack of SAC efficiency observed in many cancer cells (Bharadwaj and Yu, 2004).

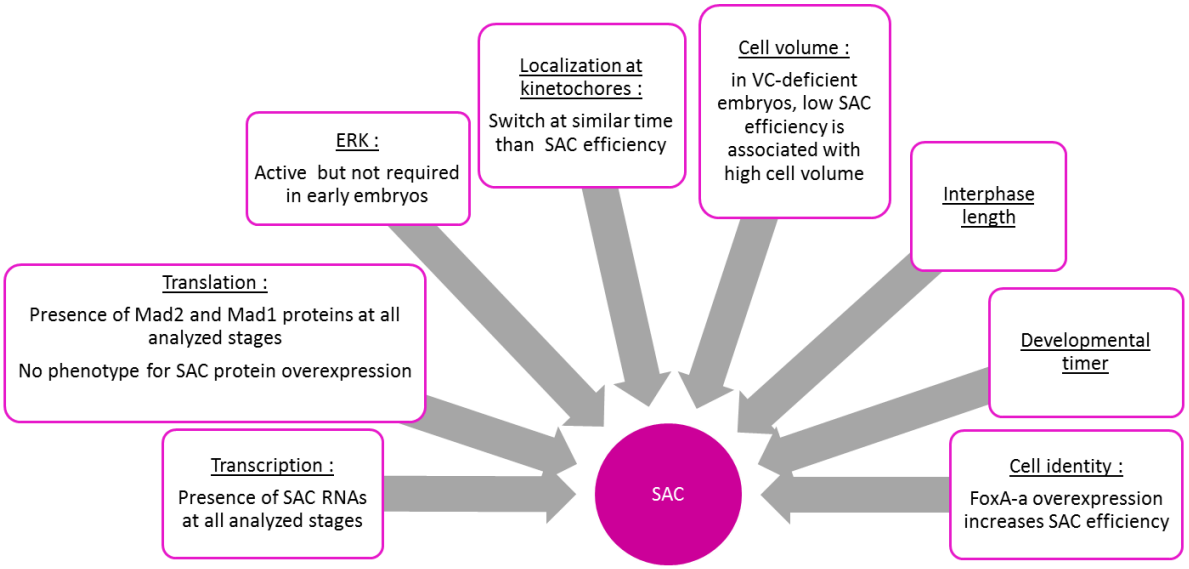

Figure 33 : Parameters influencing SAC efficiency in *P. mammillata* embryos.

SAC activity during embryogenesis can be modulated by several parameters (underlined) indicated in the boxes. Each box indicates the evidence related to each parameter obtained in my work.

Material and methods

A/Plasmids and RNAs

Table 1: Plasmids used in the work reported in this thesis: primers, vectors and methods used are indicated.

Plasmid	Primers (F= forward, R=reverse)	Receiver Vector	Method
Mps1-Tomato	F: CACCATGTTCAAAGAAAACGAATGTGTC R: TGAATGTTTGATAAGTTGTTCA	pSPE3 RFA-Tomato	gateway LR clonase II
Bub3-Venus	F: CACCATGTCAAATGAGTTCAAGCT R: TGATGATGACTTTGGCTTAG	pSPE3 RFA-Venus	gateway LR clonase II
Venus-Bub3	F : cgcAGATCTAAAATGTCAAATGAGTTCAAGCT R: cgcGCGGCCGCTTATGATGATGACTTTGGCTT	pRN3 venus	enzymatic digestion: BglII and Not1
Mad1-2Cherry	F: CGCGGATCCATGGAGGATTATTCCGAAACA R: GCGCTCGAGTGCCAGGGTTTGTTGACTG	pRN3 2Chery	enzymatic digestion : BglII and XhoI
Mad1-6His	F: CGCGGATCCATGACATCTCACACAACACAA R: GCGCTCGAGTGCCAGGGTTTGTTGACTG	pET11a	enzymatic digestion: BamHI and XhoI
Mad2-Tomato	F : CACCATGGCTGCGGCTAAGCA R : CATTGAAAACTTGTATGACAC	pSPE3 RFA-Tomato	gateway LR clonase II
Mad2-Venus	F : CACCATGGCTGCGGCTAAGCA R : CATTGAAAACTTGTATGACAC	pSPE3 RFA-Venus	gateway LR clonase II
Venus-Mad2	F : CACCATGGCTGCGGCTAAGCA R : CATTGAAAACTTGTATGACAC	pSPE3 Venus-RFA	gateway LR clonase II
Mad2-tag	F CGCGAGATCTAAAATGGAGGATTATTCCGAAACA R : cgcGCGGCCGCTTACATTGAAAACTTGTATGACAC	pRN3	enzymatic digestion: BglII and Not1
Mad2	F: cgcAGATCTAAAATGGCTGCGGCTAAGCA R:cgcGCGGCCGCTTACATTGAAAACTTGTATGACAC	pRN3	enzymatic digestion: BglII and Not1
Mad2-6His	F : CGCGGATCCATGGCTGCGGCTAAGCAAT R : CGCGAGCTCCATTGAAAACTTGTATGACACT	pET11a	enzymatic digestion: BamHI and SacI
Mad2-Sgo	Amplification of Mad2 F1:cgcAGATCTAAAATGGCTGCGGCTAAGCA R1:GAAGATCCAACACTTTCCATCATTGAAAACTTGTATGACAC Amplification of Sgo F2:GTGTCATACAAGTTTTCAATGATGGAAAGTGTTGGATCTTC R2:cgcGCGGCCGCTTATTTCATGGCCTTGTACAA	pRN3	enzymatic digestion: BglII and Not1
pFog>Venus-FoxA-a	F: cgcTGTACAAGATGATGTTGTCGTCTCCC R:cgcTGTACATTAGTTGGCCGGTACGCA	pSP72BSSPE-pFOG::-Venus-RFA	enzymatic digestion: BsrGI

The following genes were identified by blast using the public database Aniseed (Brozovic et al., 2018) and the internal database of the LBDV Octopus (http://octopus.obs-vlfr.fr/index.php):

- *Mad1* identified as Phmamm.g00005985 was amplified from the clone AHC0AAA113YL05RM1
- *Mad2* identified as Phmamm.g00002288 was amplified from cDNA template
- *Mps1* identified as Phmamm.g00008523 was amplified from the clone AHC0AAA225YB11RM1
- *Bub1* identified as Phmamm.g00012351 was amplified from the clone AHC0AAA42YG09RM1

- *Bub3* identified as Phmamm.g00001423 was amplified from the clone AHC0AAA13YG15RM1
- *sFRP1/5* identified as Phmamm.g0000599 was amplified from the clone AHC0AAA17YL13RM1
- *Cdc20* identified as Phmamm.g00009298 was amplified from the clone AHC0AAA215YE24RM1
- *FoxA-a* identified as Phmamm.g00001891 was amplified from cDNA template

C. intestinalis Sgo sequence (KH.C12.362) was retrieved from Dumollard et al., 2013

The gateway strategies rely on the excision system of the bacteriophage lambda that is based on the recombination between attL and attR sequences (Bushman et al., 1985). Cloning was performed using the gateway cloning system (Invitrogen) and plasmids made by Agnes Roure (Roure et al., 2007), see table 1. Briefly, protein coding sequences were amplified using the primer pairs reported in table 1. The forward primer starts always with CACC allowing the integration of the amplified fragment in the TOPO vector between attLs sequences (Invitrogen). After amplification in bacteria and purification, TOPO vector bearing the sequence of interest (100 ng) was mixed with receiver plasmid (450 ng) (see table) containing the RFA gene sequence flanked by attR sequences. After addition of 0.5 µl of LR clonase II, the mix was incubated at 25°C overnight to allow the recombination between attR and attL leading to the integration of the sequence of interest in place of the RFA.

To obtain the construct Mad2-Sgo, Mad2 sequence was amplified using the primers F1 and R1 and Sgo sequence was amplified using the primers F2 and R2 (see table 1). Primers R1 and F2 allow the addition of identical sequences at the 3' of Mad2 and the 5' of Sgo allowing the hybridization of the two amplicons. Consequently, a PCR using these two amplicons and the primer F1 and R2 results in the addition of Sgo sequence at the C-terminal of Mad2. The resulting amplicon Mad2-Sgo was cloned by enzymatic digestion into the plasmid pRN3.

All constructs were verified by enzymatic digestion and sequencing.

The plasmid coding for NLS-tomato was provided by Alex McDougall (McDougall et al., 2015)

RNAs were synthetized using T3 RNA polymerase (mMessage-mMachine kit, Invitrogen) following plasmid linearization with either Acc65i or Sfi1. RNAs coding for H2B-RFP, H2B-GFP, EB3-3GFP, NLS-3Venus, PH-tomato and PH-GFP were provided by Alex McDougall (McDougall et al., 2015). If not otherwise stated, RNAs were injected at the concentration of 4 g/L. PH-tomato and PH-GFP were injected at a concentration of 1 g/l.

The cDNA encoding Mad2-DN, a phosphomimic form of the human Mad2, was provided by Katja Wassmann (Wassmann et al., 2003b) and was cloned into the plasmid pCS2 to allow RNA synthesis using SP6 RNA polymerase (mMessage-mMachine kit, Invitrogen). Differently from other plasmids used for RNA production in this study, pCS2 does not encode a polyA-tail. Following RNA production, a poly(A) tail was added using a polyA-tailing kit (Invitrogen). The Mad2-DN RNA was injected at 8 g/l.

The FoxA-a coding sequence was used to replace RFA in pSP72BSSPE-pFOG::-Venus-RFA provided by Patrick Lemaire (Roure et al., 2007) by enzymatic digestion using BsrGI. The resulting plasmid pFog>Venus-FoxAa was injected at a concentration of 35 ng/µl.

B/*Phallusia mammillata* gamete collection

Phallusia mammillata adults were collected either in Sete or in Roscoff, France and were kept in aquaria at the Laboratoire de Biologie du Developpement de Villefranche sur mer (LBDV) by the centre de ressources biologiques (CRB) until dissection. Dissection of adult animals allowed collection of both sperm and eggs. Dry sperm was kept at 4°C for a maximum of 3 weeks. Eggs were collected in microfiltered sea water (MFSW) containing 5 mM TAPS (McDougall et al., 2015). The chorion was removed by treatment with 1 ml of 1% trypsine in 10 ml MFSW containing TAPS for 1.5-2h at room temperature (Sardet et al., 1989). Dechorionated eggs were washed in MFSW and kept at 16/18°C in MFSW with TAPS. Experiments were performed within 36 hours from collection, at 18/20°C. As

dechorionated eggs stick to plastic and glass, all glass and plastic ware used in the experiments, were coated with 0.1% gelatin and 0.1% formaldehyde (GF) (McDougall et al., 2015).

C/Fertilization

To achieve efficient and synchronized fertilization, sperm was activated using sea water at basic pH. Two protocols were used to activate sperm. 9 µl of sperm from 2 or 3 different animals were mixed and incubated in 1 ml of MFSW pH 9.2±0.2 for 30 minutes, the sperm was then active for the following 6 hours. Otherwise, 4 µl of sperm were added to 500 µl MFSW and 0.5 µl of 3 M NaOH were add in the lid of the tube and then quickly mixed. With this protocol the sperm was activated immediately but remained active only for a short time.

Once activated the sperm was added on the top of the eggs with approximatively 10 µl of sperm for 5/20 eggs or 100 µl for 10 ml MFSW for large cultures. For injected eggs, sperm was washed out at the first sign of ooplasmic segregation to avoid polyspermy, by transfer into a fresh dish with clean MFSW. For cultures, sperm was left 5-10 minutes and then washed out by several consecutive dilutions in MFSW and removal of excess water.

D/Injection

Microinjection of unfertilized eggs was carried out as previously described (Yasuo and McDougall, 2018) with few changes.

I used glass capillaries without filament (GC100 T10, Harvard Apparatus) that were stretched to form needles with a Narishige horizontal puller (PN-30). Capillaries were also used to store RNA/DNA to be injected. Capillaries were filled with 2 µl of mineral oil, then 0.5-1.5 µl RNA/DNA and again 1 µl of mineral oil and were then kept at 4°C for several weeks. Prior to loading, RNA/DNA mix was centrifuged at 13000 rpm at 10°C for 10 min to pellet impurities that could block the needle.

To prevent egg movement during injection, I used a chamber containing an edge. The edge was made by sticking a piece of coverslip on a GF coated coverslip, using VALAB (Vaseline/Lanolin/Beeswax 1:1:1), leaving a gap of ~1mm from the border (Fig. 34A). Using Dow Corning High Vacuum Grease, the coverslip with the edge was fixed to the bottom of an indentation in a plexyglass slide (made by the mechanical workshop of the IMEV) while a second coverslip was fixed at the top to form a chamber (Fig. 34B). The chamber was then filled with ~400 µl MFSW and eggs were loaded in the chamber against the edge, using a binocular microscope. The RNA/DNA capillary was fixed next to the chamber with Dow Corning High Vacuum Grease (Fig 34B).

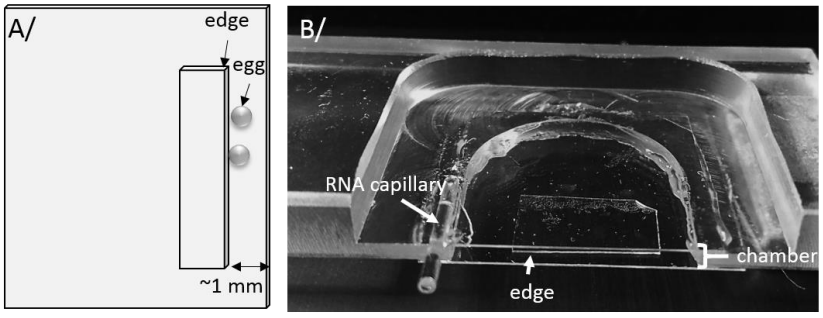

Figure 34 : Injection system

A/ A small piece of coverslip is stuck on a GF coated coverslip forming an edge against which eggs are pushed to avoid their movement while injected. **B/** A chamber is formed between two coverslips with the bottom one carrying the edge. RNA/DNA capillary is placed next to the chamber. This system allows the injection of *P. mammillata* eggs using an inverted microscope.

Injections were performed using a Leica DM IL LED inverted microscope (10x objective) in transmitted light. The needle was manipulated using a three-axis hydraulic micromanipulator (Narishige MMO-203) associated with a stage-mounting equipment (NarishigeNO-SIX-2) and a Needle holder (Narishige HI-7). First, the needle was opened by breaking its end against the DNA/RNA capillary

and then filled with RNA/DNA. Using the edge to prevent eggs movement, eggs were injected to around 5-20% of their volumes. Eggs were then retrieved and left overnight at 18°C to allow protein expression.

E/Ablation of the 1st contraction pole

Vegetal cytoplasm (VC) deficient embryos were obtained as follow. Injection needles were broken to obtain a blunt edge, roughly the size of the 1st contraction pole. The needle was then connected to a mouth pipette. Eggs were fertilized in a dish and transferred immediately into an injection chamber. Using the same set up used for microinjection, the 1st contraction pole (vegetal) was aspirated into the needle. A quick movement of the needle perpendicularly to the animal-vegetal axis of the egg, sealed the membrane and removed the 1st contraction pole (Fig. 26B). Eggs were then transferred to a new dish and left to develop.

Images showing the manipulation required to ablate the first contraction pole were obtained using a 10x objective with a Leica MC170 HD camera.

F/Drug treatments

Nocodazole (Sigma) was resuspended in DMSO to obtain a 33 mM stock solution and was then used at a final concentration of 10 µM (3 mg/l). Reversine (Axon Medchem,) was resuspended in DMSO at 5 mM and used at a final concentration of 0.5 µM. U0126 (Invivogen, Ref TLRL-U0126) was resuspended in DMSO and used at a final concentration of 5 µM. Ionomycine (Invivogen, Ref NH-ION) was resuspended in DMSO and used at a final concentration of 2 µM. All drugs were stored at -20°C.

Drugs were added to MFSW at the stage analyzed and embryos were maintained in the presence of the drug for the entire duration of the experiment, unless otherwise stated.

G/Immunofluorescence

For immunofluorescence, embryos were fixed overnight in 90% methanol containing 50 mM EGTA at -20°C. After fixation, embryos were washed 3 times in PBS containing 0.1% tween 20 (PBSTw), then blocked in PBS containing 3% BSA for 1 hour at room temperature (RT) and then incubated overnight at 4°C in PBS containing 3% BSA with the antibody raised against *P. mammillata* Mad1 (made by Covalab in mice from recombinant proteins, 1/100). After 3 washes in PBSTw, embryos were incubated with PBS containing goat serum and an anti-mouse fluorescently-labelled secondary antibodies (Jackson ImmunoResearch, 1/200) at RT for 1-2 hours. Following 2 further washes in PBSTw, embryos were incubated for 10 minutes in PBSTw containing Hoechst (5 µg/ml), washed twice and then mounted in citifluor AF1 (Science Services) for imaging with a Leica sp8 inverted confocal microscope and a 40x objective.

H/*In situ* hybridization

In situ hybridization experiments were performed as previously described with few changes (Paix et al., 2009). *In situ* hybridization probes covering the coding sequence, were generated by PCR (see paragraph plasmids and RNAs) and purified using the Qiagen MinElute PCR purification kit, (Qiagen). These amplicons were used to synthetized Digoxygenin-labeled antisense RNA probes (DIG RNA Labeling Mix, Roche).

Eggs and embryos were fixed overnight at 4°C (ISH fix: 4% formaldehyde, 100 mM MOPS, 0.5 M NaCl, pH 7.6), washed 3 times in PBS, progressively dehydrated in ethanol (25%, 50%, 75%, 100%, 100%) and stored at −20°C until analysis. Eggs and embryos were re-hydrated by addition 1:1 of PBS/0.1% Tween (PBSTw), washed once and incubated with 2 µg/ml proteinase K in PBSTw (25 min) at

room temperature (RT). After 3 washes, embryos were fixed again in PBS containing 4% formaldehyde (1 h, RT) and washed again to remove formaldehyde. Embryos were then incubated in hybridization buffer (50% formamide, 6× saline sodium citrate (SSC), 5× Denhardt's solution, 1 mg/ml yeast RNA, 0.1% Tween, pH = 6.5/7.5) for 1 h at 65 °C. Probes were added to fresh hybridizations solution at a final concentration of 0.5 ng/µl and hybridization was performed overnight at 65 °C. After hybridization, embryos were washed at 65 °C twice in 50% formamide, 5× SSC, 1% SDS (30 min), twice in 50% formamide, 2× SSC, 1% SDS (15 min), once in 2× SSC, 0.1% Tween (15 min) and twice in 0.2× SSC, 0.1% Tween (15 min). All solutions were at pH 6.5/7.5. Embryos were incubated in blocking buffer (0.15 M NaCl, 0.5% BBR, 0.1M Tris pH8) for 1h at RT. Anti-DIG AP antibody (Roche, 1:4000) was add in fresh blocking solution and incubated at 4 °C overnight. After incubation, embryos were washed 5 time in PBSTw (3*10 min, 30 min, 1 h) and then in TBSTw at 4°C overnight. Embryos were washed once with reaction buffer (0.1 M Tris pH 9.5, 50 mM $MgCl_2$, 0.1M NaCl, 0.1% Tween) and then the detection reaction was carried out in a buffer containing 3.5 µl/ml of NBT and BCIP (Roche). The reaction was stopped with 0.05 M EDTA in PBS and embryos were washed in PBSTw. Embryos were fixed in 4% formaldehyde in PBS, washed and mounted in 80% Glycerol. *In situ* hybridization experiments were imaged using an optical microscope (Zeiss Axiovert 2) with a 20x objective.

I/Image acquisition

For live imaging, embryos were mounted between GF coated slide and coverslip, using Dow Corning vacuum grease as spacer. For brightfield a z-stack covering the entire embryo with a z step of 2 µm was acquired using a Zeiss Axiovert inverted microscope with bright field optics, 40x objective lenses, and Metamorph acquisition software. Images were acquired every minute, with the exception of U0126 treatment and the corresponding controls when images were acquired every 2 minutes. Control and treated embryos were always mounted on the same slide. For NLS expressing embryos, confocal images were acquired every 2 minutes using a Leica sp8 inverted microscope, 40x water objective lenses and Leica application suite acquisition software.

Image acquisitions were performed on the plateforme d'imagerie microscopique de villefranche (PIM).

J/Image analysis

Images were analyzed using the following softwares: Metamorph, imageJ-Fiji, Icy and Imaris. Presence or absence of nuclei as well as beginning of cytokinesis were determined manually by following each cell overtime through the entire Z stack. At the 512-cell stage, some cells did not perform NER before the end of the movie, those cells were taken into account only if movie continued for at least one hour after NEB, to avoid an underestimation of SAC efficiency. The number of nuclei was assessed with Imaris using the Spot tool. Cell volume was determined using the surface tool in Imaris. The cell contour was drawn in each frame based on the signal from the PH domain. The resulting shape was confirmed using the 3D visualization of the embryo and the cell volume retrieved.

K/Western blot

To evaluate the phosphorylation state of PP1A during meiosis, eggs were first treated for 15 minutes with DMSO or nocodazole and then activated with ionomycine. Eggs (20 per sample) were then collected every minutes for 12/15 minutes. This experiment was performed three times.

To evaluate the phosphorylation status of ERK during mitosis, 40 to 50 embryos were collected every 5 minutes between 44 and 98 minutes post fertilization. The experiment was repeated three times.

To assess Mad2 levels, I used 5 injected embryos or 12µl of compacted eggs/embryos corresponding to around 1300 eggs/embryos (2-cell, 32-cell and gastrula).

To asess Mad1 levels, 30 eggs/embryos were collected for each samples from egg to 256-cell.

Embryos were collected in MFSW and mixed with the same volume of 2x Laemmli (50 mM Tris-HCl (pH 6.8), 2% SDS, 0.1 % bromophenol blue, 10 % glycerol, 100 mM dithiothreitol). Samples were heated for 5 minutes at 95°C and then kept at -20°C. Samples were warmed up again for 2 minutes before loading on a 10% SDS-polyacrylamide gel. Following complete protein separation, samples were transferred to a nitrocellulose membrane. For detection of specific proteins, membranes were blocked for 1h in TBS containing 3% BSA, 0.1% tween and then incubated in blocking solution containing either anti-PP1A (AbCam ab62334, rabbit, 1:1000) or anti-dpERK (cell signaling #4370, rabbit, 1:500) antibody for 2h at RT or overnight at 4°C. Antibodies made by Covalab in mice by injection of *P. mammillata* recombinant proteins against Mad2 (1:1000) or Mad1 (1:500) was used overnight at 4°C. NN18 antibody (Sigma Monoclonal Anti-Neurofilament 160 antibody produced in mouse NN18 Ref N5264, 1:4000) targeting ATP synthase in ascidian embryos, was used as loading marker (Chenevert et al., 2013). Following antibody incubation, membranes were washed 3 times with TBSTw and incubated with an appropriate secondary horseradish peroxidase-conjugated antibody (1:10000) in TBSTw (Jackson ImmunoResearch) for 1 hour at RT. After 3 washes with TBSTw, signal detection was carried out using the SuperSignal West Pico chemiluminescent substrate (Thermo Scientific) as described by the manufacturer.

Band intensity was determined with Fiji/image J using the protocols of the University of Queensland available on the following webpage: https://di.uq.edu.au/community-and-alumni/sparq-ed/sparq-ed-services/using-imagej-quantify-blots.

L/Affinity purification of Mad2 interacting protein

Recombinant proteins used for this analysis were produced using the following protocol. Bacteria carrying the plasmid coding for Mad2-His were grown overnight at 37°C in LB containing ampicillin (100 mg/l). Protein expression was induced by treatment with isopropyl β-D-1-thiogalactopyranoside (IPTG, 1 mM) for 5h at 37°C. Bacteria were pelleted by centrifugation (6000 rpm, 10 minutes at 14°C) and frozen at -20°C. Pellets were resuspended in 30 ml LEW buffer (50 mM NaH_2PO_4, 300 mM NaCl, pH=8) containing lysozyme (1 g/l) and cells were incubated for 30 minutes on ice. Two to three rounds of sonication (60 pulse) were performed on ice, each followed by freezing in liquid nitrogen. Following centrifugation (25000 rpm, 25minutes, 4°C), pellets were resuspended in LEW buffer. The presence of proteins in the supernatant was checked by SDS gel electrophoresis. A small amount (around 1 g) of Ni-resin (Machery-nagel) was added to the supernatant and loaded on a column. The column was washed once with LEW buffer, once with 1M NaCl, and then once again with LEW buffer and purity was checked by SDS gel electrophoresis. To improve the purification, Mad2-6His was eluted using EB (50 mM NaH_2PO_4, 300 mM NaCl, 250 mM imidazole pH=8). The imidazole was then removed by dialysis (20 kDa) against LEW buffer. Mad2-6His was reloaded onto the column and the resulting Mad2 column was kept in 150 mM NaCl. The same protocol was carried out using total protein extract from uninduced bacteria to generate the control Mad2-6His free column, called hereafter bacterial column.

Total protein extracts from unfertilized eggs treated with nocodazole were prepared as follow. Eggs were collected in 15 ml tubes, washed twice with MFSW, pelleted and transferred to 1.5ml tubes. Eggs were then lysed in LEW buffer containing 1% NP40 and protease inhibitors (free of TRIS and EDTA) for 30 minutes on ice with regular vortexing. Following centrifugation (13000 rpm, 30 min, 4°C) the supernatant, which contains all soluble proteins, was retrieved and kept at -80°C.

Prior to loading, protein extracts were diluted 1:1 in 50mM NaH_2PO_4. They were first loaded on the bacterial column and left overnight at 4°C to remove protein binding to the Ni-resin. The protein extract was then recovered and a fraction kept to be run on gel as control. The remaining protein extract was loaded on Mad2-6His containing column and washed with a solution containing 150 mM NaCl and 50 mM NaH_2PO_4. Elution was performed using increasing concentrations of NaCl from 300mM to 2M. The remaining resin was heated up in Laemmli buffer (50 mM Tris-HCl (pH 6.8), 2% SDS, 0.1 % bromophenol blue, 10 % glycerol, 100 mM dithiothreitol). The different fractions were precipitated with Trichloroacetic acid (TCA, 4 volume protein extract for 1 volume TCA) for 15 minutes

on ice. Following centrifugation (13000 rpm, 10 minutes, 4°C), pellets were washed twice with cold acetone (100%) and resuspended in 2x Laemmli buffer.

Protein were separated using a 10% SDS-polyacrylamide gel and visualized using Sypro Ruby protein gel stain. Bands of interest were cut out of the gel and kept in 5% acetic acid at 4°C. They were then sent for analysis to the plateforme d'analyse protéomique de Paris Sud Ouest. There, samples were washed with 10 % formic acid, 40 % ethanol and then twice with 50% CAN, 50 mM NH_4HCO_3 for 15 minutes. Disulphide bridges were reduced using 10mM dithiothreitol (DTT) at 56°C for 30 minutes. Samples were then incubated at RT for 1 hours with 50mM iodoacetamide. Bands were washed with 50% ACN, 50 mM NH_4HCO_3 then 100% ACN and dried. Proteins were digested with 100 ng trypsine overnight at 37°C. The digestion was stopped by addition of 0.1% TFA and peptides extracted with 40% acetonitrile, 0.1% TFA then 100% ACN. Extracts were dried by speed-vacuuming and dissolved in 20µl chromatographic loading buffer (2% ACN, 0.1%FA). Samples were then analyzed by mass spectrometry using the method LC-MS/MS.

F/Graphs and data analysis

To analyze my results, I used the median which is the value that split in half the series of value obtain for the variable studied while the mean is the ratio of the sum of the values by the number of values (Gaddis and Gaddis, 1990).

Graphic were realized using the R software (R Core Team, 2016) and the library pretty R (Grosjean and Lemon, 2015) was used to retrieve median, mean and standard deviation. Graphics in annex 1 were made using the package ggplot2 (Hadley Wickham, 2016).

Statistical tests were performed using the R software. Similar results were obtained with both t-test and Wilcoxon–Mann–Whitney test for all experiments. The only exceptions were for tests performed when comparing cell volume in VC-deficient embryos against control embryos and when assessing the impact of U0126 on interphase duration. In both cases, t-test results are indicated in the relevant figures.

References

- Alberts, B., Johnson, A., Lewis, J., Raff, M., Roberts, K., and Walter, P. (2002). Meiosis. Mol. Biol. Cell 4th Ed.
- Arellano, M., and Moreno, S. (1997). Regulation of CDK/cyclin complexes during the cell cycle. Int. J. Biochem. Cell Biol. *29*, 559–573.
- Barnum, K.J., and O'Connell, M.J. (2014). Cell Cycle Regulation by Checkpoints. Methods Mol. Biol. Clifton NJ *1170*, 29–40.
- Bates, D., and Eastman, A. (2017). Microtubule destabilising agents: far more than just antimitotic anticancer drugs. Br. J. Clin. Pharmacol. *83*, 255–268.
- Bharadwaj, R., and Yu, H. (2004). The spindle checkpoint, aneuploidy, and cancer. Oncogene *23*, 2016–2027.
- Borysova, M.K., Cui, Y., Snyder, M., and Guadagno, T.M. (2008). Knockdown of B-Raf impairs spindle formation and the mitotic checkpoint in human somatic cells. Cell Cycle Georget. Tex *7*, 2894–2901.
- Brito, D.A., and Rieder, C.L. (2006). Mitotic Checkpoint Slippage in Humans Occurs via Cyclin B Destruction in the Presence of an Active Checkpoint. Curr. Biol. *16*, 1194–1200.
- Brozovic, M., Dantec, C., Dardaillon, J., Dauga, D., Faure, E., Gineste, M., Louis, A., Naville, M., Nitta, K.R., Piette, J., et al. (2018). ANISEED 2017: extending the integrated ascidian database to the exploration and evolutionary comparison of genome-scale datasets. Nucleic Acids Res. *46*, D718–D725.

- Buffin, E., Emre, D., and Karess, R.E. (2007). Flies without a spindle checkpoint. Nat. Cell Biol. *9*, 565–572.
- Bushman, W., Thompson, J.F., Vargas, L., and Landy, A. (1985). Control of Directionality in Lambda Site Specific Recombination. Science *230*, 906–911.
- Cheeseman, I.M., and Desai, A. (2008). Molecular architecture of the kinetochore–microtubule interface. Nat. Rev. Mol. Cell Biol. *9*, 33–46.
- Chen, R.-H., Waters, J.C., Salmon, E.D., and Murray, A.W. (1996). Association of Spindle Assembly Checkpoint Component XMAD2 with Unattached Kinetochores. Science *274*, 242–246.
- Chen, R.-H., Shevchenko, A., Mann, M., and Murray, A.W. (1998). Spindle Checkpoint Protein Xmad1 Recruits Xmad2 to Unattached Kinetochores. J. Cell Biol. *143*, 283–295.
- Chenevert, J., Pruliere, G., Ishii, H., Sardet, C., and Nishikata, T. (2013). Purification of mitochondrial proteins HSP60 and ATP synthase from ascidian eggs: implications for antibody specificity. PloS One *8*, e52996.
- Chenevert, J., Roca, M., Besnardeau, L., Ruggiero, A., Nabi, D., McDougall, A., Copley, R.R., Christians, E., and Castagnetti, S. (2019). The spindle assembly checkpoint functions during early development in non-chordate embryos. BioRxiv 582759.
- Chunduri, N.K., and Storchová, Z. (2019). The diverse consequences of aneuploidy. Nat. Cell Biol. *21*, 54–62.
- Cleveland, D.W., Mao, Y., and Sullivan, K.F. (2003). Centromeres and Kinetochores: From Epigenetics to Mitotic Checkpoint Signaling. Cell *112*, 407–421.
- Clijsters, L., Ogink, J., and Wolthuis, R. (2013). The spindle checkpoint, APC/C(Cdc20), and APC/C(Cdh1) play distinct roles in connecting mitosis to S phase. J. Cell Biol. *201*, 1013–1026.
- Clute, P., and Masui, Y. (1992). Development of Microtubule-Dependence of the Chromosome Cycle at the Midblastula Transition in Xenopus laevis Embryos. Dev. Growth Differ. *34*, 27–36.
- Clute, P., and Masui, Y. (1995). Regulation of the appearance of division asynchrony and microtubule-dependent chromosome cycles in Xenopus laevis embryos. Dev. Biol. *171*, 273–285.
- Clute, P., and Masui, Y. (1997). Microtubule dependence of chromosome cycles in Xenopus laevis blastomeres under the influence of a DNA synthesis inhibitor, aphidicolin. Dev. Biol. *185*, 1–13.
- Colombera, D. (1971). The Chromosomes of Phallusia Mammillata Cuvier (Ascidiacea). Caryologia *24*, 65–70.
- Conduit, P.T., Wainman, A., and Raff, J.W. (2015). Centrosome function and assembly in animal cells. Nat. Rev. Mol. Cell Biol. *16*, 611–624.
- Conklin EG, C.E. (1905). The Organization and Cell-Lineage of the Ascidian Egg. J. Acad., Nat. Sci. Phila.
- Cooper, G.M. (2000). The Eukaryotic Cell Cycle. Cell Mol. Approach 2nd Ed.
- Costache, V., McDougall, A., and Dumollard, R. (2014). Cell cycle arrest and activation of development in marine invertebrate deuterostomes. Biochem. Biophys. Res. Commun. *450*, 1175–1181.
- De Antoni, A., Pearson, C.G., Cimini, D., Canman, J.C., Sala, V., Nezi, L., Mapelli, M., Sironi, L., Faretta, M., Salmon, E.D., et al. (2005). The Mad1/Mad2 Complex as a Template for Mad2 Activation in the Spindle Assembly Checkpoint. Curr. Biol. *15*, 214–225.
- De Rop, V., Padeganeh, A., and Maddox, P.S. (2012). CENP-A: the key player behind centromere identity, propagation, and kinetochore assembly. Chromosoma *121*, 527–538.
- Delsuc, F., Philippe, H., Tsagkogeorga, G., Simion, P., Tilak, M.-K., Turon, X., López-Legentil, S., Piette, J., Lemaire, P., and Douzery, E.J.P. (2018). A phylogenomic framework and timescale for comparative studies of tunicates. BMC Biol. *16*, 39.
- Dobles, M., Liberal, V., Scott, M.L., Benezra, R., and Sorger, P.K. (2000). Chromosome Missegregation and Apoptosis in Mice Lacking the Mitotic Checkpoint Protein Mad2. Cell *101*, 635–645.
- Drpic, D., Almeida, A.C., Aguiar, P., Renda, F., Damas, J., Lewin, H.A., Larkin, D.M., Khodjakov, A., and Maiato, H. (2018). Chromosome Segregation Is Biased by Kinetochore Size. Curr. Biol. *28*, 1344-1356.e5.

- Dumollard, R., Levasseur, M., Hebras, C., Huitorel, P., Carroll, M., Chambon, J.-P., and McDougall, A. (2011). Mos limits the number of meiotic divisions in urochordate eggs. Development *138*, 885–895.
- Dumollard, R., Hebras, C., Besnardeau, L., and McDougall, A. (2013). Beta-catenin patterns the cell cycle during maternal-to-zygotic transition in urochordate embryos. Dev. Biol. *384*, 331–342.
- Dumollard, R., Minc, N., Salez, G., Aicha, S.B., Bekkouche, F., Hebras, C., Besnardeau, L., and McDougall, A. (2017). The invariant cleavage pattern displayed by ascidian embryos depends on spindle positioning along the cell's longest axis in the apical plane and relies on asynchronous cell divisions. ELife *6*, e19290.
- Dupré, A., Haccard, O., and Jessus, C. (2011). Mos in the Oocyte: How to Use MAPK Independently of Growth Factors and Transcription to Control Meiotic Divisions. J. Signal Transduct. *2011: 350412.*
- Encalada, S.E., Willis, J., Lyczak, R., and Bowerman, B. (2005). A Spindle Checkpoint Functions during Mitosis in the Early Caenorhabditis elegans Embryo. Mol. Biol. Cell *16*, 1056–1070.
- Evans, T., Rosenthal, E.T., Youngblom, J., Distel, D., and Hunt, T. (1983). Cyclin: A protein specified by maternal mRNA in sea urchin eggs that is destroyed at each cleavage division. Cell *33*, 389–396.
- Extavour, C. (2009). Oogenesis: Making the Mos of Meiosis. Curr. Biol. *19*, R489–R491.
- Fang, G., Yu, H., and Kirschner, M.W. (1998). The checkpoint protein MAD2 and the mitotic regulator CDC20 form a ternary complex with the anaphase-promoting complex to control anaphase initiation. Genes Dev. *12*, 1871–1883.
- Feinberg, S., Roure, A., Piron, J., and Darras, S. (2019). Antero-posterior ectoderm patterning by canonical Wnt signaling during ascidian development. PLOS Genet. *15*, e1008054.
- Flemming, W. (1965). Contributions to the knowledge of the cell and its vital processes. J. Cell Biol. *25*, 3–69.
- Fraschini, R., Beretta, A., Sironi, L., Musacchio, A., Lucchini, G., and Piatti, S. (2001). Bub3 interaction with Mad2, Mad3 and Cdc20 is mediated by WD40 repeats and does not require intact kinetochores. EMBO J. *20*, 6648–6659.
- Fung, T.K., and Poon, R.Y.C. (2005). A roller coaster ride with the mitotic cyclins. Semin. Cell Dev. Biol. *16*, 335–342.
- Gaddis, G.M., and Gaddis, M.L. (1990). Introduction to biostatistics: Part 2, Descriptive statistics. Ann. Emerg. Med. *19*, 309–315.
- Galli, M., and Morgan, D.O. (2016). Cell size determines the strength of the spindle assembly checkpoint during embryonic development. Dev. Cell *36*, 344–352.
- Gao, Y.-F., Li, T., Chang, Y., Wang, Y.-B., Zhang, W.-N., Li, W.-H., He, K., Mu, R., Zhen, C., Man, J.-H., et al. (2011). Cdk1-phosphorylated CUEDC2 promotes spindle checkpoint inactivation and chromosomal instability. Nat. Cell Biol. *13*, 924–933.
- Gavet, O., and Pines, J. (2010). Progressive activation of CyclinB1-Cdk1 coordinates entry to mitosis. Dev. Cell *18*, 533–543.
- Gerhart, J., Wu, M., and Kirschner, M. (1984). Cell cycle dynamics of an M-phase-specific cytoplasmic factor in Xenopus laevis oocytes and eggs. J. Cell Biol. *98*, 1247–1255.
- Gerhold, A.R., Poupart, V., Labbé, J.-C., and Maddox, P.S. (2018). Spindle assembly checkpoint strength is linked to cell fate in the Caenorhabditis elegans embryo. Mol. Biol. Cell *29*, 1435–1448.
- Gheghiani, L., Loew, D., Lombard, B., Mansfeld, J., and Gavet, O. (2017). PLK1 Activation in Late G2 Sets Up Commitment to Mitosis. Cell Rep. *19*, 2060–2073.
- Gilbert, S.F. (2000a). Oogenesis. Dev. Biol. 6th Ed.
- Gilbert, S.F. (2000b). Early Mammalian Development. Dev. Biol. 6th Ed.
- Goto, T., Kanda, K., and Nishikata, T. (2019). Non-centrosomal microtubule structures regulated by egg activation signaling contribute to cytoplasmic and cortical reorganization in the ascidian egg. Dev. Biol. *448*, 161–172.
- Grosjean, P., and Lemon (2015). prettyR: Pretty Descriptive Stats.
- Hadley Wickham, H.W. (2016). ggplot2: Elegant Graphics for Data Analysis.

- Hardy, K., Handyside, A.H., and Winston, R.M. (1989). The human blastocyst: cell number, death and allocation during late preimplantation development in vitro. Dev. Camb. Engl. *107*, 597–604.
- He, X., Patterson, T.E., and Sazer, S. (1997). The Schizosaccharomyces pombe spindle checkpoint protein mad2p blocks anaphase and genetically interacts with the anaphase-promoting complex. Proc. Natl. Acad. Sci. *94*, 7965–7970.
- Hégarat, N., Rata, S., and Hochegger, H. (2016). Bistability of mitotic entry and exit switches during open mitosis in mammalian cells. BioEssays News Rev. Mol. Cell. Dev. Biol. *38*, 627–643.
- Hein, J.B., and Nilsson, J. (2016). Interphase APC/C–Cdc20 inhibition by cyclin A2–Cdk2 ensures efficient mitotic entry. Nat. Commun. *7*, 10975.
- Hiruma, Y., Sacristan, C., Pachis, S.T., Adamopoulos, A., Kuijt, T., Ubbink, M., Castelmur, E. von, Perrakis, A., and Kops, G.J.P.L. (2015). Competition between MPS1 and microtubules at kinetochores regulates spindle checkpoint signaling. Science *348*, 1264–1267.
- Holland, L.Z. (2016). Tunicates. Curr. Biol. *26*, R146–R152.
- Homer, H.A., McDougall, A., Levasseur, M., Yallop, K., Murdoch, A.P., and Herbert, M. (2005). Mad2 prevents aneuploidy and premature proteolysis of cyclin B and securin during meiosis I in mouse oocytes. Genes Dev. *19*, 202–207.
- van Hooff, J.J., Tromer, E., van Wijk, L.M., Snel, B., and Kops, G.J. (2017). Evolutionary dynamics of the kinetochore network in eukaryotes as revealed by comparative genomics. EMBO Rep. *18*, 1559–1571.
- Hotta, K., Mitsuhara, K., Takahashi, H., Inaba, K., Oka, K., Gojobori, T., and Ikeo, K. (2007). A web-based interactive developmental table for the ascidian Ciona intestinalis, including 3D real-image embryo reconstructions: I. From fertilized egg to hatching larva. Dev. Dyn. *236*, 1790–1805.
- Howell, B.J., McEwen, B.F., Canman, J.C., Hoffman, D.B., Farrar, E.M., Rieder, C.L., and Salmon, E.D. (2001). Cytoplasmic dynein/dynactin drives kinetochore protein transport to the spindle poles and has a role in mitotic spindle checkpoint inactivation. J. Cell Biol. *155*, 1159–1172.
- Hoyt, M.A., Totis, L., and Roberts, B.T. (1991). S. cerevisiae genes required for cell cycle arrest in response to loss of microtubule function. Cell *66*, 507–517.
- Hunt, T., Luca, F.C., and Ruderman, J.V. (1992). The requirements for protein synthesis and degradation, and the control of destruction of cyclins A and B in the meiotic and mitotic cell cycles of the clam embryo. J. Cell Biol. *116*, 707–724.
- Hwang, L.H., Lau, L.F., Smith, D.L., Mistrot, C.A., Hardwick, K.G., Hwang, E.S., Amon, A., and Murray, A.W. (1998). Budding yeast Cdc20: a target of the spindle checkpoint. Science *279*, 1041–1044.
- Iimori, M., Watanabe, S., Kiyonari, S., Matsuoka, K., Sakasai, R., Saeki, H., Oki, E., Kitao, H., and Maehara, Y. (2016). Phosphorylation of EB2 by Aurora B and CDK1 ensures mitotic progression and genome stability. Nat. Commun. *7*, 11117.
- Ikegami, R., Zhang, J., Rivera-Bennetts, A.K., and Yager, T.D. (1997). Activation of the metaphase checkpoint and an apoptosis programme in the early zebrafish embryo, by treatment with the spindle-destabilising agent nocodazole. Zygote Camb. Engl. *5*, 329–350.
- Jacobs, K., Van de Velde, H., De Paepe, C., Sermon, K., and Spits, C. (2017). Mitotic spindle disruption in human preimplantation embryos activates the spindle assembly checkpoint but not apoptosis until Day 5 of development. Mol. Hum. Reprod. *23*, 321–329.
- Jia, L., Kim, S., and Yu, H. (2013). Tracking spindle checkpoint signals from kinetochores to APC/C. Trends Biochem. Sci. *38*, 302–311.
- Kaiser, J., and Went, D.F. (1987). Early embryonic development of the dipteran insect Heteropeza pygmaea in the presence of cytoskeleton-affecting drugs. Rouxs Arch. Dev. Biol. Off. Organ EDBO *196*, 356–366.
- Karaiskou, A., Swalla, B.J., Sasakura, Y., and Chambon, J.-P. (2015). Metamorphosis in solitary ascidians. Genesis *53*, 34–47.
- Karess, R.E., Wassmann, K., and Rahmani, Z. (2013). New insights into the role of BubR1 in mitosis and beyond. Int. Rev. Cell Mol. Biol. *306*, 223–273.
- Kawano, Y., and Kypta, R. (2003). Secreted antagonists of the Wnt signalling pathway. J. Cell Sci. *116*, 2627–2634.

- Kocot, K.M., Tassia, M.G., Halanych, K.M., and Swalla, B.J. (2018). Phylogenomics offers resolution of major tunicate relationships. Mol. Phylogenet. Evol. *121*, 166–173.
- Kolano, A., Brunet, S., Silk, A.D., Cleveland, D.W., and Verlhac, M.-H. (2012). Error-prone mammalian female meiosis from silencing the spindle assembly checkpoint without normal interkinetochore tension. Proc. Natl. Acad. Sci. *109*, E1858–E1867.
- Kouznetsova, A., Lister, L., Nordenskjöld, M., Herbert, M., and Höög, C. (2007). Bi-orientation of achiasmatic chromosomes in meiosis I oocytes contributes to aneuploidy in mice. Nat. Genet. *39*, 966–968.
- Kramer, E.R., Scheuringer, N., Podtelejnikov, A.V., Mann, M., and Peters, J.-M. (2000). Mitotic Regulation of the APC Activator Proteins CDC20 and CDH1. Mol. Biol. Cell *11*, 1555–1569.
- Kronja, I., and Orr-Weaver, T.L. (2011). Translational regulation of the cell cycle: when, where, how and why? Philos. Trans. R. Soc. B Biol. Sci. *366*, 3638–3652.
- Kyogoku, H., and Kitajima, T.S. (2017). Large Cytoplasm Is Linked to the Error-Prone Nature of Oocytes. Dev. Cell *41*, 287-298.e4.
- Lamy, C., Rothbächer, U., Caillol, D., and Lemaire, P. (2006). Ci-FoxA-a is the earliest zygotic determinant of the ascidian anterior ectoderm and directly activates Ci-sFRP1/5. Development *133*, 2835–2844.
- Lane, S.I.R., and Jones, K.T. (2017). Chromosome biorientation and APC activity remain uncoupled in oocytes with reduced volume. J. Cell Biol. *216*, 3949–3957.
- Lau, D.T.C., and Murray, A.W. (2012). Mad2 and Mad3 Cooperate to Arrest Budding Yeast in Mitosis. Curr. Biol. *22*, 180–190.
- Lemaire, P. (2011). Evolutionary crossroads in developmental biology: the tunicates. Dev. Camb. Engl. *138*, 2143–2152.
- LeMaire-Adkins, R., Radke, K., and Hunt, P.A. (1997). Lack of Checkpoint Control at the Metaphase/Anaphase Transition: A Mechanism of Meiotic Nondisjunction in Mammalian Females. J. Cell Biol. *139*, 1611.
- Levasseur, M., Dumollard, R., Chambon, J.-P., Hebras, C., Sinclair, M., Whitaker, M., and McDougall, A. (2013). Release from meiotic arrest in ascidian eggs requires the activity of two phosphatases but not CaMKII. Dev. Camb. Engl. *140*, 4583–4593.
- Lewis, C.W., Taylor, R.G., Kubara, P.M., Marshall, K., Meijer, L., and Golsteyn, R.M. (2013). A western blot assay to measure cyclin dependent kinase activity in cells or in vitro without the use of radioisotopes. FEBS Lett. *587*, 3089–3095.
- Li, R., and Murray, A.W. (1991). Feedback control of mitosis in budding yeast. Cell *66*, 519–531.
- Liu, D., Davydenko, O., and Lampson, M.A. (2012). Polo-like kinase-1 regulates kinetochore–microtubule dynamics and spindle checkpoint silencing. J. Cell Biol. *198*, 491–499.
- Lou, Y., Yao, J., Zereshki, A., Dou, Z., Ahmed, K., Wang, H., Hu, J., Wang, Y., and Yao, X. (2004). NEK2A Interacts with MAD1 and Possibly Functions as a Novel Integrator of the Spindle Checkpoint Signaling. J. Biol. Chem. *279*, 20049–20057.
- Ma, H.T., and Poon, R.Y.C. (2016). TRIP13 Regulates Both the Activation and Inactivation of the Spindle-Assembly Checkpoint. Cell Rep. *14*, 1086–1099.
- MacLennan, M., Crichton, J.H., Playfoot, C.J., and Adams, I.R. (2015). Oocyte development, meiosis and aneuploidy. Semin. Cell Dev. Biol. *45*, 68–76.
- Madgwick, A., Magri, M.S., Dantec, C., Gailly, D., Fiuza, U.-M., Guignard, L., Hettinger, S., Gomez-Skarmeta, J.L., and Lemaire, P. (2019). Evolution of embryonic cis-regulatory landscapes between divergent Phallusia and Ciona ascidians. Dev. Biol. *448*, 71–87.
- Maller, J.L., Schwab, M.S., Gross, S.D., Taieb, F.E., Roberts, B.T., and Tunquist, B.J. (2002). The mechanism of CSF arrest in vertebrate oocytes. Mol. Cell. Endocrinol. *187*, 173–178.
- Malmanche, N., Maia, A., and Sunkel, C.E. (2006). The spindle assembly checkpoint: Preventing chromosome mis-segregation during mitosis and meiosis. FEBS Lett. *580*, 2888–2895.
- Manic, G., Corradi, F., Sistigu, A., Siteni, S., and Vitale, I. (2017). Molecular Regulation of the Spindle Assembly Checkpoint by Kinases and Phosphatases. Int. Rev. Cell Mol. Biol. *328*, 105–161.
- Mantikou, E., Wong, K.M., Repping, S., and Mastenbroek, S. (2012). Molecular origin of mitotic aneuploidies in preimplantation embryos. Biochim. Biophys. Acta *1822*, 1921–1930.

- Matsuoka, T., Ikeda, T., Fujimaki, K., and Satou, Y. (2013). Transcriptome dynamics in early embryos of the ascidian, Ciona intestinalis. Dev. Biol. *384*, 375–385.
- McConnell, J., and Lee, M. (1989). Presence of cdc2(+)-like proteins in the preimplantation mouse embryo. Dev. Camb. Engl. *107*, 481–487.
- McDougall, A., Chenevert, J., Lee, K.W., Hebras, C., and Dumollard, R. (2011). Cell cycle in ascidian eggs and embryos. Results Probl. Cell Differ. *53*, 153–169.
- McDougall, A., Chenevert, J., Pruliere, G., Costache, V., Hebras, C., Salez, G., and Dumollard, R. (2015). Chapter 17 - Centrosomes and spindles in ascidian embryos and eggs. In Methods Cell Biol., R. Basto, and K. Oegema, eds. (Academic Press), pp. 317–339.
- McGuinness, B.E., Anger, M., Kouznetsova, A., Gil-Bernabé, A.M., Helmhart, W., Kudo, N.R., Wuensche, A., Taylor, S., Hoog, C., Novak, B., et al. (2009). Regulation of APC/C Activity in Oocytes by a Bub1-Dependent Spindle Assembly Checkpoint. Curr. Biol. *19*, 369–380.
- Mena, A.L., Lam, E.W.-F., and Chatterjee, S. (2010). Sustained Spindle-Assembly Checkpoint Response Requires De Novo Transcription and Translation of Cyclin B1. PLOS ONE *5*, e13037.
- Meraldi, P., Draviam, V.M., and Sorger, P.K. (2004). Timing and checkpoints in the regulation of mitotic progression. Dev. Cell *7*, 45–60.
- Meunier, S., and Vernos, I. (2012). Microtubule assembly during mitosis – from distinct origins to distinct functions? J. Cell Sci. *125*, 2805–2814.
- Michel, L.S., Liberal, V., Chatterjee, A., Kirchwegger, R., Pasche, B., Gerald, W., Dobles, M., Sorger, P.K., Murty, V.V.V.S., and Benezra, R. (2001). MAD2 haplo-insufficiency causes premature anaphase and chromosome instability in mammalian cells. Nature *409*, 355–359.
- Minshull, J., Sun, H., Tonks, N.K., and Murray, A.W. (1994). A MAP kinase-dependent spindle assembly checkpoint in Xenopus egg extracts. Cell *79*, 475–486.
- Mondal, G., Sengupta, S., Panda, C.K., Gollin, S.M., Saunders, W.S., and Roychoudhury, S. (2007). Overexpression of Cdc20 leads to impairment of the spindle assembly checkpoint and aneuploidization in oral cancer. Carcinogenesis *28*, 81–92.
- Moura, M., Osswald, M., Leça, N., Barbosa, J., Pereira, A.J., Maiato, H., Sunkel, C.E., and Conde, C. (2017). Protein Phosphatase 1 inactivates Mps1 to ensure efficient Spindle Assembly Checkpoint silencing. ELife *6*.
- Musacchio, A., and Salmon, E.D. (2007). The spindle-assembly checkpoint in space and time. Nat. Rev. Mol. Cell Biol. *8*, 379–393.
- Nagaoka, S.I., Hodges, C.A., Albertini, D.F., and Hunt, P.A. (2011). Oocyte-Specific Differences in Cell-Cycle Control Create an Innate Susceptibility to Meiotic Errors. Curr. Biol. *21*, 651–657.
- Nagaoka, S.I., Hassold, T.J., and Hunt, P.A. (2012). Human aneuploidy: mechanisms and new insights into an age-old problem. Nat. Rev. Genet. *13*, 493–504.
- Nasmyth, K., and Haering, C.H. (2009). Cohesin: its roles and mechanisms. Annu. Rev. Genet. *43*, 525–558.
- Nishida, H. (1994). Localization of determinants for formation of the anterior-posterior axis in eggs of the ascidian Halocynthia roretzi. Development *120*, 3093–3104.
- Nishida, H. (1996). Vegetal egg cytoplasm promotes gastrulation and is responsible for specification of vegetal blastomeres in embryos of the ascidian Halocynthia roretzi. Development *122*, 1271–1279.
- Nishikata, T., Hibino, T., and Nishida, H. (1999). The centrosome-attracting body, microtubule system, and posterior egg cytoplasm are involved in positioning of cleavage planes in the ascidian embryo. Dev. Biol. *209*, 72–85.
- Oda-Ishii, I., and Satou, Y. (2018). Initiation of the zygotic genetic program in the ascidian embryo. Semin. Cell Dev. Biol. *84*, 111–117.
- Oda-Ishii, I., Abe, T., and Satou, Y. (2018). Dynamics of two key maternal factors that initiate zygotic regulatory programs in ascidian embryos. Dev. Biol. *437*, 50–59.
- Ogura, Y., and Sasakura, Y. (2016). Developmental Control of Cell-Cycle Compensation Provides a Switch for Patterned Mitosis at the Onset of Chordate Neurulation. Dev. Cell *37*, 148–161.

- Ogura, Y., Sakaue-Sawano, A., Nakagawa, M., Satoh, N., Miyawaki, A., and Sasakura, Y. (2011). Coordination of mitosis and morphogenesis: role of a prolonged G2 phase during chordate neurulation. Development *138*, 577–587.
- Oliveira, R.A., Hamilton, R.S., Pauli, A., Davis, I., and Nasmyth, K. (2010). Cohesin cleavage and Cdk inhibition trigger formation of daughter nuclei. Nat. Cell Biol. *12*, 185–192.
- Paix, A., Yamada, L., Dru, P., Lecordier, H., Pruliere, G., Chenevert, J., Satoh, N., and Sardet, C. (2009). Cortical anchorages and cell type segregations of maternal postplasmic/PEM RNAs in ascidians. Dev. Biol. *336*, 96–111.
- Pérez-Mongiovi, D., Malmanche, N., Bousbaa, H., and Sunkel, C. (2005). Maternal expression of the checkpoint protein BubR1 is required for synchrony of syncytial nuclear divisions and polar body arrest in Drosophila melanogaster. Dev. Camb. Engl. *132*, 4509–4520.
- Philips, R.M.& R. » How big is a human cell?
- Qiao, X., Zhang, L., Gamper, A.M., Fujita, T., and Wan, Y. (2010). APC/C-Cdh1. Cell Cycle *9*, 3904–3912.
- R Core Team, R.C.T. (2016). R: A Language and Environment for Statistical Computing.
- Rahmani, Z., Gagou, M.E., Lefebvre, C., Emre, D., and Karess, R.E. (2009). Separating the spindle, checkpoint, and timer functions of BubR1. J. Cell Biol. *187*, 597–605.
- Rashid, M.S., Mazur, T., Ji, W., Liu, S.T., and Taylor, W.R. (2018). Analysis of the role of GSK3 in the mitotic checkpoint. Sci. Rep. *8*.
- Reddy, S.K., Rape, M., Margansky, W.A., and Kirschner, M.W. (2007). Ubiquitination by the anaphase-promoting complex drives spindle checkpoint inactivation. Nature *446*, 921–925.
- Reguieg, A., Kupfer, M., and Sittler, A.-P. (2018). DORIS, Phallusia mammillata (Cuvier, 1815).
- Rieder, C.L., and Maiato, H. (2004). Stuck in Division or Passing through: What Happens When Cells Cannot Satisfy the Spindle Assembly Checkpoint. Dev. Cell *7*, 637–651.
- Rieder, C.L., Cole, R.W., Khodjakov, A., and Sluder, G. (1995). The checkpoint delaying anaphase in response to chromosome monoorientation is mediated by an inhibitory signal produced by unattached kinetochores. J. Cell Biol. *130*, 941–948.
- Rodriguez-Bravo, V., Maciejowski, J., Corona, J., Buch, H.K., Collin, P., Kanemaki, M.T., Shah, J.V., and Jallepalli, P.V. (2014). Nuclear pores protect genome integrity by assembling a premitotic and Mad1-dependent anaphase inhibitor. Cell *156*, 1017–1031.
- Roure, A., Rothbächer, U., Robin, F., Kalmar, E., Ferone, G., Lamy, C., Missero, C., Mueller, F., and Lemaire, P. (2007). A Multicassette Gateway Vector Set for High Throughput and Comparative Analyses in Ciona and Vertebrate Embryos. PLoS ONE *2*.
- Santaguida, S., Tighe, A., D'Alise, A.M., Taylor, S.S., and Musacchio, A. (2010). Dissecting the role of MPS1 in chromosome biorientation and the spindle checkpoint through the small molecule inhibitor reversine. J. Cell Biol. *190*, 73–87.
- Sardet, C., Speksnijder, J., Inoue, S., and Jaffe, L. (1989). Fertilization and ooplasmic movements in the ascidian egg. Dev. Camb. Engl. *105*, 237–249.
- Sasakura, Y., and Hozumi, A. (2018). Formation of adult organs through metamorphosis in ascidians. Wiley Interdiscip. Rev. Dev. Biol. *7*, e304.
- Sebestova, J., Danylevska, A., Novakova, L., Kubelka, M., and Anger, M. (2012). Lack of response to unaligned chromosomes in mammalian female gametes. Cell Cycle *11*, 3011–3018.
- Shao, H., Li, R., Ma, C., Chen, E., and Liu, X.J. (2013). Xenopus oocyte meiosis lacks spindle assembly checkpoint control. J. Cell Biol. *201*, 191–200.
- Siefert, J.C., Clowdus, E.A., and Sansam, C.L. (2015). Cell Cycle Control in the Early Embryonic Development of Aquatic Animal Species. Comp. Biochem. Physiol. Toxicol. Pharmacol. CBP *178*, 8–15.
- Sievers, F., Wilm, A., Dineen, D., Gibson, T.J., Karplus, K., Li, W., Lopez, R., McWilliam, H., Remmert, M., Söding, J., et al. (2011). Fast, scalable generation of high-quality protein multiple sequence alignments using Clustal Omega. Mol. Syst. Biol. *7*, 539–539.
- Silió, V., McAinsh, A.D., and Millar, J.B. (2015). KNL1-Bubs and RZZ Provide Two Separable Pathways for Checkpoint Activation at Human Kinetochores. Dev. Cell *35*, 600–613.

- Silva, P.M.A., Reis, R.M., Bolanos-Garcia, V.M., Florindo, C., Tavares, Á.A., and Bousbaa, H. (2014). Dynein-dependent transport of spindle assembly checkpoint proteins off kinetochores toward spindle poles. FEBS Lett. *588*, 3265–3273.
- Sironi, L., Melixetian, M., Faretta, M., Prosperini, E., Helin, K., and Musacchio, A. (2001). Mad2 binding to Mad1 and Cdc20, rather than oligomerization, is required for the spindle checkpoint. EMBO J. *20*, 6371–6382.
- Sironi, L., Mapelli, M., Knapp, S., Antoni, A.D., Jeang, K.-T., and Musacchio, A. (2002). Crystal structure of the tetrameric Mad1–Mad2 core complex: implications of a 'safety belt' binding mechanism for the spindle checkpoint. EMBO J. *21*, 2496–2506.
- Sluder, G. (1979). Role of spindle microtubules in the control of cell cycle timing. J. Cell Biol. *80*, 674–691.
- States, D.J., and Gish, W. (1994). Combined use of sequence similarity and codon bias for coding region identification. J. Comput. Biol. J. Comput. Mol. Cell Biol. *1*, 39–50.
- Stauffer, T.P., Ahn, S., and Meyer, T. (1998). Receptor-induced transient reduction in plasma membrane PtdIns(4,5)P2 concentration monitored in living cells. Curr. Biol. CB *8*, 343–346.
- Straight, A.F., and Field, C.M. (2000). Microtubules, membranes and cytokinesis. Curr. Biol. *10*, R760–R770.
- Subramanian, R., and Kapoor, T.M. (2013). Slipping past the spindle assembly checkpoint. Nat. Cell Biol. *15*, 1261–1263.
- Sudakin, V., Chan, G.K.T., and Yen, T.J. (2001). Checkpoint inhibition of the APC/C in HeLa cells is mediated by a complex of BUBR1, BUB3, CDC20, and MAD2. J. Cell Biol. *154*, 925–936.
- Suijkerbuijk, S.J.E., van Dam, T.J.P., Karagöz, G.E., von Castelmur, E., Hubner, N.C., Duarte, A.M.S., Vleugel, M., Perrakis, A., Rüdiger, S.G.D., Snel, B., et al. (2012). The vertebrate mitotic checkpoint protein BUBR1 is an unusual pseudokinase. Dev. Cell *22*, 1321–1329.
- Takata, H., Matsunaga, S., Morimoto, A., Ma, N., Kurihara, D., Ono-Maniwa, R., Nakagawa, M., Azuma, T., Uchiyama, S., and Fukui, K. (2007). PHB2 Protects Sister-Chromatid Cohesion in Mitosis. Curr. Biol. *17*, 1356–1361.
- Takatori, N., Wada, S., and Saiga, H. (2007). Regionalization of the tail-tip epidermis requires inductive influence from vegetal cells and FGF signaling in the development of an ascidian, Halocynthia roretzi. Zoolog. Sci. *24*, 441–448.
- Takenaka, K., Gotoh, Y., and Nishida, E. (1997). MAP Kinase Is Required for the Spindle Assembly Checkpoint but Is Dispensable for the Normal M Phase Entry and Exit in Xenopus Egg Cell Cycle Extracts. J. Cell Biol. *136*, 1091–1097.
- Toda, K., Naito, K., Mase, S., Ueno, M., Uritani, M., Yamamoto, A., and Ushimaru, T. (2012). APC/C-Cdh1-dependent anaphase and telophase progression during mitotic slippage. Cell Div. *7*, 4.
- Tortelote, G.G., Reis, R.R., de Almeida Mendes, F., and Abreu, J.G. (2017). Complexity of the Wnt/β‐catenin pathway: Searching for an activation model. Cell. Signal. *40*, 30–43.
- Vasquez, R.J., Howell, B., Yvon, A.M., Wadsworth, P., and Cassimeris, L. (1997). Nanomolar concentrations of nocodazole alter microtubule dynamic instability in vivo and in vitro. Mol. Biol. Cell *8*, 973–985.
- Vázquez-Diez, C., Paim, L.M.G., and FitzHarris, G. (2019). Cell-Size-Independent Spindle Checkpoint Failure Underlies Chromosome Segregation Error in Mouse Embryos. Curr. Biol. *29*, 865-873.e3.
- Vera-Rodriguez, M., Chavez, S.L., Rubio, C., Pera, R.A.R., and Simon, C. (2015). Prediction model for aneuploidy in early human embryo development revealed by single-cell analysis. Nat. Commun. *6*, 7601.
- Vleugel, M., Hoogendoorn, E., Snel, B., and Kops, G.J.P.L. (2012). Evolution and Function of the Mitotic Checkpoint. Dev. Cell *23*, 239–250.
- Wada, S., Katsuyama, Y., and Saiga, H. (1999). Anteroposterior patterning of the epidermis by inductive influences from the vegetal hemisphere cells in the ascidian embryo. Dev. Camb. Engl. *126*, 4955–4963.

- Wang, K., Sturt-Gillespie, B., Hittle, J.C., Macdonald, D., Chan, G.K., Yen, T.J., and Liu, S.-T. (2014). Thyroid hormone receptor interacting protein 13 (TRIP13) AAA-ATPase is a novel mitotic checkpoint-silencing protein. J. Biol. Chem. *289*, 23928–23937.
- Wasserman, W.J., and Smith, L.D. (1978). The cyclic behavior of a cytoplasmic factor controlling nuclear membrane breakdown. J. Cell Biol. *78*, R15-22.
- Wassmann, K., Niault, T., and Maro, B. (2003a). Metaphase I arrest upon activation of the Mad2-dependent spindle checkpoint in mouse oocytes. Curr. Biol. CB *13*, 1596–1608.
- Wassmann, K., Liberal, V., and Benezra, R. (2003b). Mad2 phosphorylation regulates its association with Mad1 and the APC/C. EMBO J. *22*, 797–806.
- Watson, E.R., Brown, N.G., Peters, J.-M., Stark, H., and Schulman, B.A. (2019). Posing the APC/C E3 Ubiquitin Ligase to Orchestrate Cell Division. Trends Cell Biol. *29*, 117–134.
- Wei, Y., Multi, S., Yang, C.-R., Ma, J., Zhang, Q.-H., Wang, Z.-B., Li, M., Wei, L., Ge, Z.-J., Zhang, C.-H., et al. (2011). Spindle Assembly Checkpoint Regulates Mitotic Cell Cycle Progression during Preimplantation Embryo Development. PLOS ONE *6*, e21557.
- Weiss, E., and Winey, M. (1996). The Saccharomyces cerevisiae spindle pole body duplication gene MPS1 is part of a mitotic checkpoint. J. Cell Biol. *132*, 111–123.
- Westhorpe, F.G., Tighe, A., Lara-Gonzalez, P., and Taylor, S.S. (2011). p31comet-mediated extraction of Mad2 from the MCC promotes efficient mitotic exit. J. Cell Sci. *124*, 3905–3916.
- Wieser, S., and Pines, J. (2015). The Biochemistry of Mitosis. Cold Spring Harb. Perspect. Biol. *7*, a015776.
- Winey, M., Goetsch, L., Baum, P., and Byers, B. (1991). MPS1 and MPS2: novel yeast genes defining distinct steps of spindle pole body duplication. J. Cell Biol. *114*, 745–754.
- Wu, J.Q., Guo, J.Y., Tang, W., Yang, C.-S., Freel, C.D., Chen, C., Nairn, A.C., and Kornbluth, S. (2009). PP1-mediated dephosphorylation of phosphoproteins at mitotic exit is controlled by inhibitor-1 and PP1 phosphorylation. Nat. Cell Biol. *11*, 644–651.
- Yajima, M., and Wessel, G.M. (2011). The DEAD-box RNA helicase Vasa functions in embryonic mitotic progression in the sea urchin. Dev. Camb. Engl. *138*, 2217–2222.
- Yam, C.H., Fung, T.K., and Poon, R.Y.C. (2002). Cyclin A in cell cycle control and cancer. Cell. Mol. Life Sci. CMLS *59*, 1317–1326.
- Yamagishi, Y., Yang, C.-H., Tanno, Y., and Watanabe, Y. (2012). MPS1/Mph1 phosphorylates the kinetochore protein KNL1/Spc7 to recruit SAC components. Nat. Cell Biol. *14*, 746–752.
- Yang, W., Wightman, R., and Meyerowitz, E.M. (2017). Cell Cycle Control by Nuclear Sequestration of CDC20 and CDH1 mRNA in Plant Stem Cells. Mol. Cell *68*, 1108-1119.e3.
- Yasuo, H., and McDougall, A. (2018). Practical Guide for Ascidian Microinjection: Phallusia mammillata. Adv. Exp. Med. Biol. *1029*, 15–24.
- Yeh, P.-C., Yeh, C.-C., Chen, Y.-C., and Juang, Y.-L. (2012). RED, a Spindle Pole-associated Protein, Is Required for Kinetochore Localization of MAD1, Mitotic Progression, and Activation of the Spindle Assembly Checkpoint. J. Biol. Chem. *287*, 11704–11716.
- Yoshida, S., Marikawa, Y., and Satoh, N. (1996). Posterior end mark, a novel maternal gene encoding a localized factor in the ascidian embryo. Development *122*, 2005–2012.
- Zhang, G., Kruse, T., Guasch Boldú, C., Garvanska, D.H., Coscia, F., Mann, M., Barisic, M., and Nilsson, J. (2019). Efficient mitotic checkpoint signaling depends on integrated activities of Bub1 and the RZZ complex. EMBO J. *38*.
- Zhang, M., Kothari, P., and Lampson, M.A. (2015). Spindle assembly checkpoint acquisition at the mid-blastula transition. PloS One *10*, e0119285.
- Zhang, W.L., Huitorel, P., Glass, R., Fernandez-Serra, M., Arnone, M.I., Chiri, S., Picard, A., and Ciapa, B. (2005). A MAPK pathway is involved in the control of mitosis after fertilization of the sea urchin egg. Dev. Biol. *282*, 192–206.
- Zhao, Y., and Chen, R.-H. (2006). Mps1 phosphorylation by MAP kinase is required for kinetochore localization of spindle-checkpoint proteins. Curr. Biol. CB *16*, 1764–1769.
- Zhu, J., Tsai, H.-J., Gordon, M.R., and Li, R. (2018). Cellular Stress Associated with Aneuploidy. Dev. Cell *44*, 420–431.

Annexes

Annex 1: The same differences in SAC efficiency between cell identity is found in every embryo for each experiment

Quantification of mitotic duration in cell treated with nocodazole. Each boxplot corresponds to one embryo in 128-cell, 256-cell and 512-cell stage. Mitosis was measured as time from NEB to NER. Each dot represents one cell. Boxes represent 25-75th percentiles and the median is shown. **A/** control (anterior, posterior and dorsal). **B/** Embryos overexpressing FoxA-a. **C/** VC-deficient embryos.

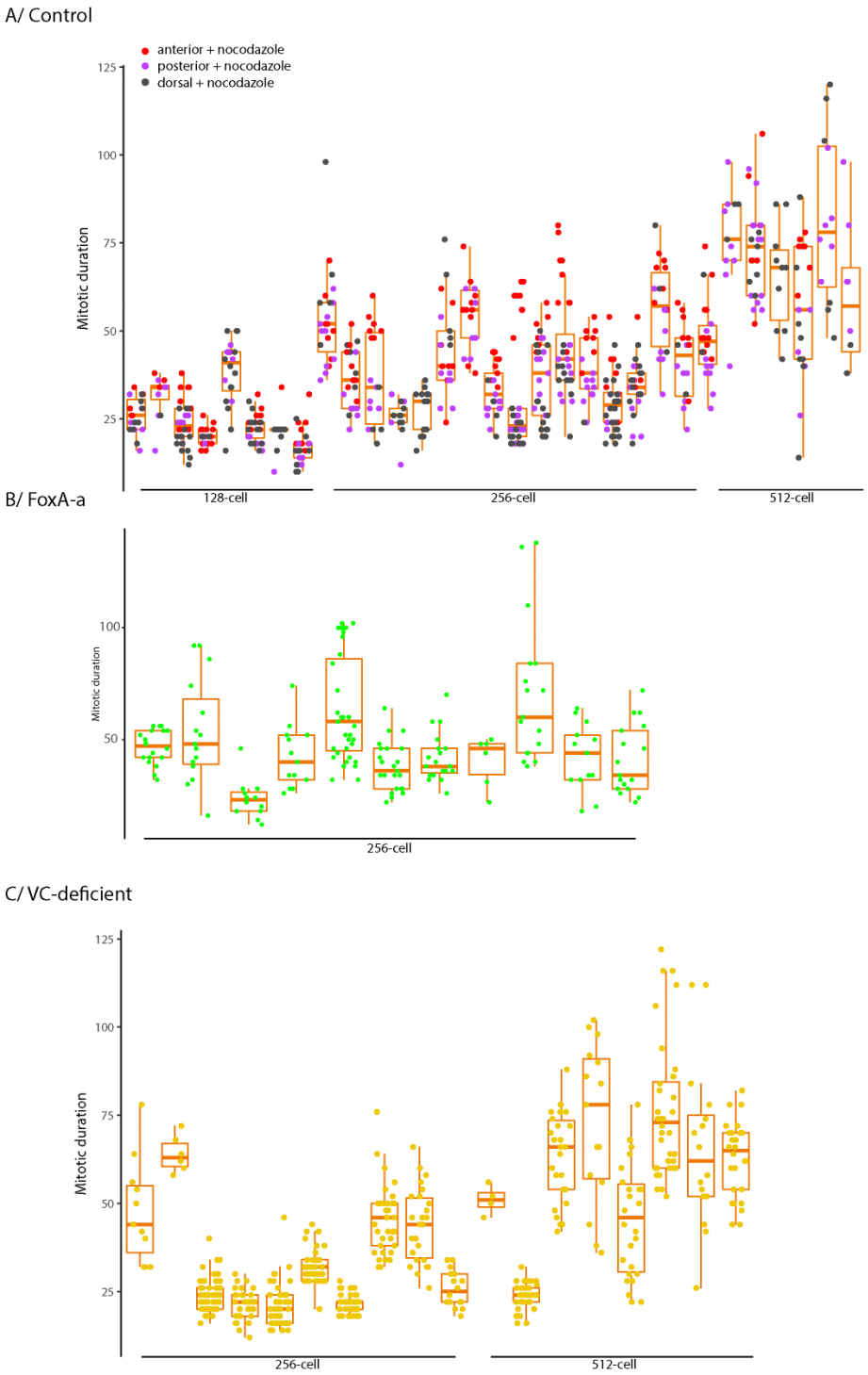

Annex 2: SAC protein sequences are conserved, especially in their functional domains

Protein alignment and percent identity matrix for all core SAC components, obtained using Clustal omega. In the alignment, domain or amino acid known to be important in *H. sapiens* are highlighted in the human sequence. When two *P. mammillata* sequences were retrieved for the same protein from the database Aniseed and from the database octopus, the latter was called *P. mammillata2*.

A/Mps1

Percent Identity Matrix - created by Clustal2.1

S.cerevisiae	100.00	29.93	25.92	28.37	26.84	25.32	25.38	26.55
S.pombe	29.93	100.00	28.27	29.32	29.98	32.77	30.84	31.38
D.melanogaster	25.92	28.27	100.00	32.30	32.60	31.54	31.53	31.46
C.robusta	28.37	29.32	32.30	100.00	44.57	36.15	33.01	32.90
P.mammillata	26.84	29.98	32.60	44.57	100.00	32.74	32.83	32.20
P.lividus	25.32	32.77	31.54	36.15	32.74	100.00	37.08	38.34
H.sapiens	25.38	30.84	31.53	33.01	32.83	37.08	100.00	75.78
M.musculus	26.55	31.38	31.46	32.90	32.20	38.34	75.78	100.00

CLUSTAL O(1.2.4) multiple sequence alignment

Site of post translational modification, kinase domain, amino acid required for kinase activity

```
S.cerevisiae        MST------NSFHDYVDLKSRTNTRQFSDDEE-------------------------FT      28
S.pombe             ------------------------------------------------------------      0
D.melanogaster      ------------------------------------------------------------      0
C.robusta           ---------------------------------------------MASQFTTEGLGD      12
P.mammillata        ------------------------MFKENECVAESDKENTN-TQNVTGKVTSNLKEVGD      34
P.lividus           ------------------KMSGNTRDNTTGNLTSNLTSLASFHSMTDHTQWMSELARHGN      42
H.sapiens           MESEDLSGRELTIDSIMNKVRDIKNKFKNEDLTDELSLNKISADTTDNSGTVNQIMMMAN      60
M.musculus          MEAEELIGSSVTIDSIMSKMRDIKNKI-NEDCTDELSLSKICADH---TETVNQIMRVGN      56
                                                  33  37

S.cerevisiae        TPPKLSNFGSALLSHTEKTSA---SEILS-----------------SHNNDKIANRLEE-      67
S.pombe             ------------------------------------------------------------      0
D.melanogaster      ------------------------------------------------------------      0
C.robusta           NPDKWFSMLQSCLNLQNGEEK---NNLLKQIFVTANRSLTAEKHKTSEIYAKILAEEAAF      69
P.mammillata        DPEKWNQILQDCLKLDNTLHK---KRMLKQFFLQAKKNIDPAVHRRSETYARILAQEALF      91
P.lividus           KPCDWLAYLSLVESHTLHAEETSRFRFLTVAYNRATKHIPIDKYCEDPSYARIIIKLAHL      102
H.sapiens           NPEDWLSLLLKLEKNSVPLSD-ALLNKLIGRYSQAIEALPPDKYGQNESFARIQVRFAEL      119
M.musculus          TPENWLNFLLKLEKNSSPLND-DLLNKLIGRYSQAIEVLPPDKYGQNESFARIQVRLAEL      115
                                       80

S.cerevisiae        --------------MDRSSSRSHPP----PSMGNLTSGHTSTSSHSTLFGRYLRNNHQT-      108
S.pombe             ------------------------------------------------MSKRNPPVT      9
D.melanogaster      ------------------------------------------------MTTPVPRRT      9
C.robusta           VGSTNVNKGRNMFKHAVYVCRTIPIIHLTYAQFEVRNGHFDKALHILEFGKMVTGCKLLF      129
P.mammillata        ISLSSRQDAGVAFRFATDTCRPVPFIHVAFAQYEVDSGRLEKAKKILELGKMVLPDSKEI      151
P.lividus           KATQDVDDGRMIFKFARANVRKQAIVHLEAAKFEEVHGDTRKCLNILEKGLKVTSDPRLT      162
H.sapiens           KAIQEPDDARDYFQMARANCKKFAFVHISFAQFELSQGNVKKSKQLLQKAVERGAVPLEM      179
M.musculus          KAIQEPDDARDYFQMARENCKKFAFVHVSFAQFELSQGNLKKSEQLLHKAVETGAVPLQM      175


S.cerevisiae        ----SMTTMNT--------SDI-------------------------EINVGNSLDKSF      130
S.pombe             NIADLVSD-------SSLDEDS---LSFLEELQDPELYFKNDTFSSKSSHSDGTVTGDTL      59
D.melanogaster      ----------KDMMALGLDSDSEDDF--------NTPYRPRQA----AAGERKQQPVASF      47
C.robusta           --EQAISKLENGYVKF--------NSTLSMDLNQATPLK--NI----TNTEC---NEKVT      170
P.mammillata        --SDAIKRLKSNETNLGLKNDPMFNSSVLRDNTNSMSTP--KV----AKYDFGDSIMKIF      203
P.lividus           ---EALHRVKN---------------GLPILLESQEPM----------DSHDGPQATS--      192
H.sapiens           -LEIALRNLNLQKKQLLSEEEK-KNLSASTVLTAQESF----------SGSLGHLQNRNN      227
M.musculus          -LETAMRNLHLQKKQLLPEEDK-KSVSASTVLSAQEPF----------SSSLGNVQNRSI      223


S.cerevisiae        ERIRNLRQNMKEDITAKYAER-----------------RSKRFLISNRTTKLGPAKRA-      171
S.pombe             RRQSSGATAL----ERLVSHPRTK-----------------NFDLQGNGGQNSALKEVN      97
D.melanogaster      QVQTRGKENEPHPLPINMLPRRVSELT-------MMDSDSDEEDIKS-NHNLNCAILND-      98
C.robusta           ECQKRSYTDT-----ALKTPP---------------------S---------------YR      189
```

```
P.mammillata        PTSKHSLTDT-----CIKSPIRPAHIXRELEALDFPESPRPPTFVQTPSGKMMTPIQKNR      258
P.lividus           ------VAAQASVHPSYRIPPQPK--------------------FESSDHESDTMPINTA-      226
H.sapiens           SCDSRGQTTKARFLYGENMPPQDAEIGYRN------------SLRQTNKTKQSCPFGRV-      274
M.musculus          SCESRGQAGAARVLYGENLPPQDAEVRHQN------------PFKQTHAAKRSCPFGRV-      270

S.cerevisiae        ---MT-LTNIFDEDVPNSPN---Q------PINARETVELPLE--DSHQTNFKERRE---      213
S.pombe             TPAYQSMHHFEHLITPLPST------NA--------------SHSEVSLSAGVNDLN--S      135
D.melanogaster      --------SF--VLSPSQ-------------------------ELTNS-NSNITTRRT---      120
C.robusta           FRALD--TKYYDIKTPSPPMLKMSPTN---TFPNRFTFNMPTSISKSSVTNFTPTPA---      241
P.mammillata        SSVTK--PSFFGITTPSPPRLSFSVTK---SLANRHALQTKQEHL----TTSVQKPM---      306
P.lividus           -------PKHSGLQTPDVPN-KFSVFGSSRRKRSGINIGMPMRVTRTSLPQLKKES--KG      276
H.sapiens           -------PVN-LLNSPDCDV----------------------KTDDSVVPCFMKRQTSRS      304
M.musculus          -------PVN-LLNSPDFYV----------------------KTDSSAVTQLTTRKG-SG      299
                             *
                          281
S.cerevisiae        -----------NTDYDSIDFGDLNPIQY-------IKKHN----------LPTSDLPLIS      245
S.pombe             NSEHDLLPKSVNKTPGSLSISRRRRI------------GRIGLGPPKRAEYTLTDPSKTS      183
D.melanogaster      -------PSAAPLKQSDSNLSFLGRF------------NDMGIN---C---SSQGSPVAN      155
C.robusta           -------SATKTTGLTKGPQRVLRSLKSSLENADNDKEHDIGTH---QTPYSLKHHPLVS      291
P.mammillata        -------MTSKTNGQRSGPVNKPRRIPCALQPENDQK-H--------KSEYPMV-FPLAS      349
P.lividus           DDDD------DDDDDDDDDIRPLKSSPQ-----------------------EVKPESLAP      307
H.sapiens           ECRDLVVPGSKPSGNDSCELRNLKSVQN-----------------------SHFKEPLVS      341
M.musculus          PDRDAILPGSRPRGSDSYELRGLKPIQT-----------------------IYLKDSLVS      336
                              .
                        317  321
S.cerevisiae        Q-----------IYFDKQREENRQAALRKHSSRELLYKSRSSSSSLSSNNLLANKDNSIT      294
S.pombe             DTKNS-------------------------------TE---------------ADEDIEMK      198
D.melanogaster      SEK----------QVAKKTAPTLQAAPSATERRPLQETE-----------TPLRNELPST      194
C.robusta           ---------------------------------NVEPQ-----------IPDSPKPPV-      305
P.mammillata        EV----------------------GATPTD--N--RIEKV----------FPTQPVSQV-      372
P.lividus           -----------ITEKTNESDSGIQTTPRD-----LT-------------QIDRNPFTMK      337
H.sapiens           DEKSSELIITDSITLKNKTESSLLAKLEE--TKEYQEPE----------VPESNQKQWQ      388
M.musculus          NEKSSELM-SDLIALKSKTDSSLT-KLEE------TKPE----------IAERRPMQWQ      377


S.cerevisiae        SNNGSQPRRKVSTGSSSSKSSIEIRRAL-------KENIDTSNNSNFNSPIHKIY----K      343
S.pombe             SRE-------------VSPASNSVAAT------TLKPLQ------LHNTPLQTSQEHPKP      233
D.melanogaster      S------KTKPD-ADFITPQVRTIGSTLAGKSRSAVSNDFRAQKVLFQTPMT-V-SRAAP      245
C.robusta           ---------------IIDPSPI----NP---PTPIIPL----KKEIFPYPSK-QTPQPKL      338
P.mammillata        ---------------SASP--T----R-----------------PTFPPPI--RQPQPNL      392
P.lividus           ARNM---EMAAE-ATVPGPSASSLQR-----PDPALPVQQHQL--------Q-QQQQQAT      379
H.sapiens           S------KRKSE-CINQNPAASSNHWQI---PELARKVNTEQKHTTFEQPVF-SVSKQSP      437
M.musculus          S------TRKPE-CVFQNPAAFAPLRHV---PDVTPK-----------------ADKESP      410
                           393                                              436

S.cerevisiae        GISRNKDSDSEKREVLRNISINANHADNLLQQENKRLKRSLDDAIT--NENINSK-----      396
S.pombe             SFHPSQFESSFS------PRVQFDHD------VERRASELHSRPVTVFQEPQRS------      275
D.melanogaster      VAS---DSISFS------LCDTITES------PD------IP------EP--PKKAEPPK      276
C.robusta           TPNPPKNLGTLN------PEIRQNPS------K-S-----TPM--KTDTSNLNHNSMPPP      378
P.mammillata        AAHA----ISMS------PAVRPSSV------PTP-----TPARVPHTEPPAIANLMPPP      431
P.lividus           PMSMPYL-----------------------------------------QPPHMQPVQPPH      398
H.sapiens           PISTSKWFDPKS------ICKTPSSN--------T-----LDDYMSCFRTPVVKNDFPPA      478
M.musculus          PISVPKWLDPKS------ACETPSSS--------S-----LDDYMKCFKTPVVKNDFPPA      451
                                     455

S.cerevisiae        --------NLEVFYHRPAPK---PPVTKKVE----IVEPA----KSASLSNNRNIITVND      437
S.pombe             ---------ASQPYESHALSPKVAPLFDN-S--Q----------ATPIPKRQQDVVTVAN      313
D.melanogaster      SQHPSKKS-LDHVFRESDKD-NVPDKVDNVEPKELVSIPAVAVPPEQPSHKTSNILKIKN      334
C.robusta           KKFPP----QRVPCSK-------PAEPQN-G----L----------HTWFNPNSAICVNN      412
P.mammillata        ASLPV--------------------ARETD-E----I----------ASWMNNVQVLRIHH      457
P.lividus           M-QPVQPQLFQQPYRH-------PAVQPN----HQFSVPHMVA-PVPQQPKSKNTLQVNG      445
H.sapiens           C-Q------LSTPYGQ-------PACFQQ-QQHQILATPLQNL-QVLASSSANECISVKG      522
M.musculus          C-P------SSTPYSQ-------LARLQQ-QQQQGLSTPLQSL-QISGSSSINECISVNG      495
                                       .                      . : :

S.cerevisiae        SQYEKIELLGRGGSSRVYKVKGSG-NRVYALKRVSFDAFDDSSIDGFKGEIELLEKLKD-      495
S.pombe             LQFIKLGVVGKGGSSMVYRIFSPDNSRLYALKEVNFINADQTTIQGYKNEIALLRKLSG-      372
D.melanogaster      HEYTIDKKLGCGGSSSVFLARRSDSGNEFALKVVDLQ-ADPQVVQGYLNETKLLAKLQG-      392
C.robusta           KHYLVIRELGEGGSSKVLQVFCAETKAILALKKVSLKDCDESTKNEFTNEIEFLLKLRN-      471
P.mammillata        KSYIVLKMIGEGGSSKVFEVFDVAAKQIKAVKHVSLKNCDAAVKKGFLDEVKFLEQLRN-      516
P.lividus           KGYTIIRLIGKGGSSKVFQVLTEDSKKLLALKYVKLDFADEMAMQSYMNEITLLERLKS-      504
H.sapiens           RIYSILKQIGSGGGSSKVFQVLNEK-KQIYAIKYVNLEEADNQTLDSYRNEIAYLNKLQQH      581
M.musculus          RIYSILKQIGSGGGSSKVFQVLNEK-KQINAIKYVNLEDADSQTIESYRNEIAFLNKLQQH      554
                      :     :* **** *           *:* *.:   *    . : .*   * :*

S.cerevisiae        QKRVIQLLDYEMGD--GLLYLIMECGDHDLSQILN--QRSGMPLDFNFVRFYTKEMLLCI      551
S.pombe             NDRIIKLYAAEVNDTLGQLNMVMECGETDLANLLMKN--MKKPINLNFIRMYWEQMLEAV      430
```

```
D.melanogaster      NVCVVALYDYQLVREESKLYMVMEKGDCDLNKIL---QSYTTNLPLYSLMNILYQMLQAV      449
C.robusta           NPHIVHLYDFELTP--DFIHLVMECGSTDLAKLLHSHKTQNSRLEVYEIIYFWKKMLLAV      529
P.mammillata        NPNIVHLYTYELTG--DDLYLVMECGSTDLSKSL---KRNNGRLEPYEVWYFWKKMLAAL      571
P.lividus           FKRIIHLYDYEITE--DYIYLVMECGSIDLSTFL---KKNKDNLSPHHMWCYWQEMLEAV      559
H.sapiens           SDKIIRLYDYEITD--QYIYMVMECGNIDLNSWL---KKKK-SIDPWERKSYWKNMLEAV      635
M.musculus          SDKIIRLYDYEITE--QYIYMVMECGNIDLNSWL---KKKK-SINPWERKSYWKNMLEAV      608
                       :: *   ::      : ::** *. **   *         :          :** .:

S.cerevisiae        KVVHDAGIVHSDLKPANFVLVKGILKIIDFGIANAVPEHTVNIYRETQIGTPNYMAPEAL      611
S.pombe             QVVHDQNIVHSDLKPANFLLVEGNLKLIDFGIAKAIGNDTTNIHRDSHIGTINYMAPEAL      490
D.melanogaster      NYIHQHGVIHSDLKPANFLMVSGRLKLIDFGIASNIAVDSTSIIKFSQAGTFNYISPEAL      509
C.robusta           QTIHKHGVIHRDLKPANFLLVKGNLKLIDFGISNAINADATSVIKETQCGTLNYMAPEAI      589
P.mammillata        NTVHQHGIIHLDLKPANFLIVKGTLKLIDFGIANSIQSDVTSVFKDTMVGTLNYMAPEAI      631
P.lividus           DVIHKEGIVHSDLKPANFIFVEASLKLIDFGIANAIQSDQTSLVKESQVGTLNYMSPEAI      619
H.sapiens           HTIHQHGIVHSDLKPANFLIVDGMLKLIDFGIANQMQPDTTSVVKDSQVGTVNYMPPEAI      695
M.musculus          HIIHQHGIVHSDLKPANFVIVDGMLKLIDFGIANQMQPDTTSIVKDSQVGTVNYMAPEAI      668
                    . :*. .::* *******::*.. **:*****:. :  . ..: : :  ** **: ***:
                                                664                 686
S.cerevisiae        VAMNYTQNS-ENQHEGNKWKVGRPSDMWSCGCIIYQMIYGKPPYGSFQGQ-NRLLAIMNP      669
S.pombe             TDMNAHTNS-----GVKLVKLGRPSDVWSLGCILYQMVYGRAPFAHLKM-IQAIAAIPNE      544
D.melanogaster      TDTSTGNSPM-RRADQPKIKISTKSDVWSLGCILYLLLYQKTPFGHIRNVYAKMSAITTP      568
C.robusta           LDMSGGYNP-----DSPKFKISPMADVWSLGCILYSMLYGCTPFQHIKHQLLKLNAITND      644
P.mammillata        VDMSSGGDG-----NDLKFKISPRADVWSLGCILYLMMYGRTPFQHINHQIRKLSAITNP      686
P.lividus           QDTSPVTEVNEYGHKKPRLKINCKSDVWSLGCILYSMVYGRTPFQHIVHRLLKMQAICNP      679
H.sapiens           KDMSSSREN-----GKSKSKISPKSDVWSLGCILYYMTYGKTPFQQIINQISKLHAIIDP      750
M.musculus          RDMSSSREN-----SKIRTKVSPRSDVWSLGCILYYMTYGRTPFQHIINQVSKLHAIINP      723
                       .   .           *:.  :*:** ***:* : *   *:  :      : **

S.cerevisiae        DVKIPFPEHTSNN------------EKIPKSAIELMKACLYRNPDKRWTVDKVLSSTFLQ      717
S.pombe             QYHIHFPEVALPANAVQEKEGSLPGVTVGPDLMDVMKRCLERDQRKRLTIPELLVHPFLN      604
D.melanogaster      GTSIEYPAIPP---------------YYPIMLVHMAKNCLQLNPKKRPSCTELLQYPFHM      613
C.robusta           QHRIEFPPFK------------------DENFVKIVQKCLKRNPKHRPTVDQLLQFS---      683
P.mammillata        NTRIEFPQYG------------------DKRLVQIVQSCLMRDAKRRPTVEQLIKHS---      725
P.lividus           DHVIDFPPIE------------------NELLLDVMKKCLTRDVKRRPSIQELLNHPYVK      721
H.sapiens           NHEIEFPDIP------------------EKDLQDVLKCCLKRDPKQRISIPELLAHPYVQ      792
M.musculus          AHEIEFPEIS------------------EKDLRDVLKCCLVRNPKERISIPELLTHPYVQ      765
                       * :*                        .: : **  :  .* :  :::

S.cerevisiae        PFMISGSIMEDLIRNAVRYGSEKP-------HISQDDLNDVVDTVLRK------------      758
S.pombe             PLPSYLTPLAKKP-LPVSGHTNNAHPLRLSTEISASQLSMIIERSVELSKHK---RLNKE      660
D.melanogaster      IIPLQNLQI---P-SR-TANSN-------------------------------------      630
C.robusta           ------------------------------------------------------------      683
P.mammillata        ------------------------------------------------------------      725
P.lividus           RSFTTAAEK---P-AA-SLTTEH--------------ISALVAQLSQLNSPRSIARLTKG      762
H.sapiens           IQTHPVN-----Q-MA-KGTTEE--------------MKYVLGQLVGLNSPNSILKAAKT      831
M.musculus          IQPHPGS-----Q-MA-RGATDE--------------MKYVLGQLVGLNSPNSILKTAKT      804
                                                                  821

S.cerevisiae        -FADYKI-------------------------------------------------------      764
S.pombe             LIDSM------------AYDCVS-----NLRKMPE--------------------------      678
D.melanogaster      ------------------------------------------------------------      630
C.robusta           ------------------------------------------------------------      683
P.mammillata        ------------------------------------------------------------      725
P.lividus           VVDQISKGQQIDISSAVGADAHHQVLGHDSQQMPQASQPYQHHPQHQPSQHHHPHHQQGQ      822
H.sapiens           LYEHYSGGESHNSSSSKTFEKKRGKK-----------------------------------      857
M.musculus          LYERYNCGEGQDSSSSKTFDKKRERK-----------------------------------      830


S.cerevisiae        ------------------------------------------------------------ 764
S.pombe             ------------------------------------------------------------ 678
D.melanogaster      ------------------------------------------------------------ 630
C.robusta           ------------------------------------------------------------ 683
P.mammillata        ------------------------------------------------------------ 725
P.lividus           QCPVSGHEGGSYRSQRAPLRVINSSDVMASHHSLLKPLSASKYSISNSQENEQINS 878
H.sapiens           ------------------------------------------------------------ 857
M.musculus          ------------------------------------------------------------ 830
```

B/Bub1

Percent Identity Matrix - created by Clustal2.1

S.cerevisiae	100.00	29.16	22.52	21.44	24.12	26.16	25.76	23.51	23.79
S.pombe	29.16	100.00	21.37	19.05	19.75	20.18	23.80	23.68	23.70
D.melanogaster	22.52	21.37	100.00	23.73	24.49	25.77	26.29	26.63	26.22
C.robusta	21.44	19.05	23.73	100.00	37.13	37.38	28.24	25.42	25.06
P.mammillata2	24.12	19.75	24.49	37.13	100.00	96.11	25.87	23.74	23.36
P.mammillata	26.16	20.18	25.77	37.38	96.11	100.00	24.46	24.24	23.75
P.lividus	25.76	23.80	26.29	28.24	25.87	24.46	100.00	31.04	33.36
M.musculus	23.51	23.68	26.63	25.42	23.74	24.24	31.04	100.00	73.82
H.sapiens	23.79	23.70	26.22	25.06	23.36	23.75	33.36	73.82	100.00

CLUSTAL O(1.2.4) multiple sequence alignment

Site of post translational modification, kinase domain, kinetochore localization, Bub3 interaction, loading of Mad1/Mad2 at kinetochores.

```
S.cerevisiae        ----------------------------MNLDLGSTVRGYESD-KDTFPQSKGVSS----      27
S.pombe             -----------------------------------MSDWRLT-ENVLDQNIPETK----      19
D.melanogaster      --------------------------MAMH-----------------SYMRQGSGSGGGA      17
C.robusta           ---------------------------------MS-NEITWEVCKENVQPLRHGR----NV      23
P.mammillata2       ----------------------------MEYDEQ-ADVMLEASKENVQPLRTGR----NM      27
P.mammillata        ------------------------------------------------------------      0
P.lividus           NNGIIGVIKAENCSFLPEISILNRLEMERDHDMK-SVDEWELSKENVLPLKQGR----KM      55
M.musculus          ------------------------------------------------------------      0
H.sapiens           ------------------------------------------------------------      0

S.cerevisiae        ----------SQKEQHSQLNQTKIAYEQRLLNDLEDMDDPLDLFLDYMIWISTSYIEVDS      77
S.pombe             ----------PRESKTRLEEIQRLALFQEELDIIEELDDPVDVWYRCIEWLLETRFL---      66
D.melanogaster      GAVAAGAPPLASPDEMHGFLNDKQAWEHA--ISLYQGPDPLDHWYNYICWYENHAQS---      72
C.robusta           SYLNASLQT-SDEISH-SLMKQKKMLEEEI-LTDGNLHDPIDPWDRYFKWSQQHFPE---      77
P.mammillata2       NCLKAALKP-SEEDLQ-VLRKERQRFEEDI-LAGENSTDPIDAWDNAFQMRVARASS---      81
P.mammillata        ------------------------------------------------------------      0
P.lividus           TNLTAALQP-QNFDRQQQLILQRQGYETE--LRTYNGDDPLDPWIRYIQWTEQNFPQ---     109
M.musculus          ------------MD---NLENVFRMFEAH--MQSYTGNDPLGEWESFIKWVEENFPD---      40
H.sapiens           ------------MD---TPENVLQMLEAH--MQSYKGNDPLGEWERYIQWVEENFPE---      40

S.cerevisiae        ESGQE--VLRSTMERCLIYIQDMETYRNDPRFLKIWIWYIN--LFLSNNFHESENTFKYM     133
S.pombe             --GME--TVNKMLDDAIQYLERCRFALNDVRHLLIQLAKIKQSYETPDELQQAAKQFYQL     122
D.melanogaster      --DPE-LKYRETLERCLTVYEHNDYYRQDVRLVRLWLKYIAMQ-------TDPLHFYQVL     122
C.robusta           --GKE--DLKNFLQKYIVKFQNSDRYRNDPRYVNAWLTMSQIH-------DDAPTTFAYM     126
P.mammillata2       --KQ--------------------------------------------------------      83
P.mammillata        ------------------------------------------------------------      0
P.lividus           --GGKDSHLGVLMQKCLIQFKNDDLYKQDTRYVSIWLKMAQYD-------SESLEIFKFM     160
M.musculus          --NKE--YLMTLLEHLMKEFLHKKNYHNDSRFINYCLKFAEYN-------SDRHQFFEFL      89
H.sapiens           --NKE--YLITLLEHLMKEFLDKKKYHNDPRFISYCLKFAEYN-------SDLHQFFEFL      89
                                          NLS

S.cerevisiae        FNKGIGTKLSLFYEEFSKLLENAQFFLEAKVLLELGAENNCRPYNRLLRSLSNYEDRLRE     193
S.pombe             ASKGIGLELALFYEEYGSLLIRMQRWKEASEVFHAAVSREARPLVRLLRNAAEFSRAYDL     182
D.melanogaster      FQRGTGRQVAAFYIGWAAYYESREEYKDAEAVFNLAFQEK QSTSELQHAHTKFAYARSL     182
C.robusta           KSKSIGINCASFYIMWAEELEKSGNIKKAHSIYELGEEND EPTELLSKMRNAFQLRAAR     186
P.mammillata2       --------------------LEQMQNL---------------------------------      90
P.mammillata        ------------------------------------------------------------      0
P.lividus           QANQIGSQLTMFYEAWAWELEQLGNTKKADAIYKEGLVCN QPRDRLERAMIEFQSRVGR     220
M.musculus          YNQGIGTKSSYIYMSWAGHLEAQGELQHASAIFQTGIHNE EPKELLQQQYRLFQARLTG     149
H.sapiens           YNHGIGTLSSPLYI-WAGHLEAQGELQHASAVLQRGIQNQ-EPREFLQQQYRLFQTRLTE     149
                                  106             122     130

S.cerevisiae        MNIVENQNS----VPDSRERLKGRLIYRTAPFFIRKFLTSSLMTDDKENRANLNSNVGVG     249
S.pombe             HNAHPSIHD----APYSSPFPPPRIVLGSKPVSS------STLP----------------     216
D.melanogaster      FYQRQQQQQQQQQQHQQHPPQDALQQLTNYAQ----------------------------     214
C.robusta           SISTKLNENEDDKNKSELDSRRQRQALGSLDG--RGKHKVLG-----TTRIGNTTAG-VV     238
P.mammillata2       ---------DEPETMTQQRGNDQRKALGTLSG--RGTRKAVG-----TTRTGHVLAG-PT     133
P.mammillata        ------------------------------------------------------------      0
P.lividus           ATVQQMQEG--MMNPTSAPVEDQRATLGDLRA--RGKLQKVG-----TSRTGVAKLSGRG     271
M.musculus          IHLPAQA-------TTSEPLHSA------------QILNQVM-----MTNSS------PE     179
H.sapiens           THLPAQA-------RTSEPLHNV------------QVLNQMI-----TSKSN------PG     179
```

```
S.cerevisiae        --KSAPNVYQD-------SIVVADFKSET-----------------------E---RLNL      274
S.pombe             ---SKPKSFQ----------VFSDASSS-----------------------------RDSQ      235
D.melanogaster      ------------------------------------------------------------      214
C.robusta           RSQPRTSFKENRSS--TKFKIFSEDENNE-------QH--CVGNFASMPNNQINSKE-NT      286
P.mammillata2       SVKQTTQLQQPKAQKNSKLLIYNDANEET-------DQIAGGSGWAELPDKKRAAKENLI      186
P.mammillata        ------------------------------------------------------------      0
P.lividus           GLQAAPAPLQQ---RSNQISIFCDDGAAAAAAATGPAAPKAAGQWQHLPSRTEAQKE-NT      327
M.musculus          -KNSACVPRSQGSECSGVASSTCDEK-----------------------------------      204
H.sapiens           -NNMACISKNQGSELSGVISSACDKE-----------------------------------      204

S.cerevisiae        NSSKQPSNQRLKNGNK---------------KTSIYADQK---QSNN-----------P-      304
S.pombe             NASDLPQAKSLES------------------------------EANT-----------P-      253
D.melanogaster      -------------QQMPQSYNQHRPQPYQQNVYQQYHPQAQAHQAPQPHQPAPQQQLPPE      261
C.robusta           TAPSVWKGAEVQLNRNKTTTAISS----SNKPFTIC-------QDV---DVPSQEQATPL      332
P.mammillata2       NDPKMWKGEKVKQKPRSTALTVKVPPPVASTLFAIY-------QEETPENSATGENLCPP      239
P.mammillata        ------------------------------------------------------------      0
P.lividus           RSAGQWTGQRLPQRNMPRMT-FQEVSSYSRPDFAVH-------VDDNADQMTT-----PR      374
M.musculus          -------------SNMEQ-----RVIMISKSECSVS-------------------------      222
H.sapiens           -------------SNMER-----RVITISKSEYSVH-------------------------      222

S.cerevisiae        -------VYK--LINTPGRKP-------------------ERIVFNFNLIYPENDEEFNT      336
S.pombe             -------NLPLLYDKSSGKRV-------------------EYSAFNFLALYENGEERSME      287
D.melanogaster      ---------------------------------------QQVPYQTH--YQE-------      272
C.robusta           ASRKLSKSVEVILTERKWKKHEESDFHRAIREQHGDADHNVVRMYPVEKVYSAV-GEFQP      391
P.mammillata2       SARKVCPNVEKILTDRKINPFEESDFHKRIRESYGDKDSNVIRMYPVDKVYSVM-GEFSP      298
P.mammillata        ------------------------------------------------------------      0
P.lividus           --KPLEMGF-QVLSEKKQHKP--TNALQ--HIKQDNSNDNTRAMYCKHLIYGGA-REMSF      426
M.musculus          -------------------------------SSVAPKPEA-QQVMYCKEKLIRGD-SEFSF      250
H.sapiens           -------------------------------SSLASKVDVEQVVMYCKEKLIRGE-SEFSF      251

S.cerevisiae        EEILAMIKGLYKVQRRGKKHTED---YTSDKNRK--------------------------      367
S.pombe             E-CRA----------------QR---YLS------------------------------      296
D.melanogaster      ----------RPR------------------------------------------------      275
C.robusta           EEILAACWLKKQREEEEQKRLQRQ----LEEQRKQIVESE-----RREIEAQRAY-DDKV      441
P.mammillata2       EEIMAAKWRKRKREREEKEKIERE----LEEKRRQEEQTR-----REK--------EMLE      341
P.mammillata        ------------------------------------------------------------      0
P.lividus           EELRGIKDRTKRKERELQAKMDEAERMRVDMVRKQKEQDEMIAKMQEKLEQQRLQQEQYI      486
M.musculus          EELRAQKYNQRKKHEQWVSED------RNYMKRK----------------------EANAFE      284
H.sapiens           EELRAQKYNQRRKHEQWVNED------RHYMKRK----------------------EANAFE      285

S.cerevisiae        -----------KRKLDVLVER-RQDLPSSQ------P-PVVPK------------------      391
S.pombe             -------------------SI-QPNTAASF------P-KVVPK------------------      312
D.melanogaster      ------------------YEP----HPA-----TQSP------------TAIPPSQVQQQ      296
C.robusta           NQLKH-RE-QQLRNLLQLFKDKE--MQ------IEDKVEMVKE------------------      474
P.mammillata2       EKLLR-RE-DQLKQLIQLVEEKD--LM------ETDE-PIADT------------------      373
P.mammillata        ------------------------------------------------------------      0
P.lividus           ELLVKQKVEAMAPQLSQRPEPEQ------IQPQTVQPCPMVPQQPAQPAPLVPPQQPAPS      540
M.musculus          EQLLKQKMDELHKKLHQVVELSHKDLPASENRPDVSLVCVGQNT-----------------      328
H.sapiens           EQLLKQKMDELHKKLHQVVETSHEDLPASQERSEVNPARMGPSV-----------------      329
                                        307    314

S.cerevisiae        -------------------------------STRIEVF-----------------------      398
S.pombe             -------------------------------NE-ISVHHDSS-----SSNVSP--------      328
D.melanogaster      SHYAPVAESHYAPAQQSQLPPQQTTVPQLHAQQPQQQQNGNGNPPPQQS--PPVTNEVAG      354
C.robusta           ---------------------------------EQEMT---------------I---------      480
P.mammillata2       -------------------------------NTEMT---------------V---------      379
P.mammillata        ------------------------------------------------------------      0
P.lividus           AQYAPAAPIA----------------PIAPAQQCLQ-PQGSSSQAPTTSHTSPL-DSIAD      582
M.musculus          -------------------------------CSQQELR-----GPSLSSISHQTSE------      348
H.sapiens           -------------------------------GSQQELR-----APCLPVTYQQTPV------      349

S.cerevisiae        ------------------------------------------KDDDNPSQSTHH-----      410
S.pombe             ----------------------------------IYKNPVA--EQSDTPTRSLPK-----      347
D.melanogaster      LRLPRNFHAYGR-------------------NNHETWKPALTLEEPDDPSRVCHYAKQLV      395
C.robusta           -------------------------------ALHKVCSQLQ--------------------      490
P.mammillata2       -------------------------------KLNSVYSKVL--QRKNL------------      394
P.mammillata        ------------------------------------------------------------      0
P.lividus           FDVTNQRHRSNSGDMACTKQLVFDDLTGATGNFNIFCDPAQ--DPPAKPAPQYPTVTAAA      640
M.musculus          ----------------------------------SSGEKPQE--EP-SVPLMVN-AVNSTL      371
H.sapiens           ----------------------------------NMEKNPRE--APPVVPPLAN-AISAAL      373
```

```
S.cerevisiae        ------------------------------------------------------------      410
S.pombe             ------------------------------------------------------------      347
D.melanogaster      YPPGAGV-----------------------------------EYSPEEILARKFKQLMDQ      420
C.robusta           ------------------------------------------------------HMQQ      494
P.mammillata2       --------QLQNRPMPQQTKE---------------------EIELVHEEVAEEVEFMND      425
P.mammillata        ------------------------------------------------------------      0
P.lividus           KPPTVPISQRVAAPTPRN--PSTTSAFSIHQQSVSAPPSSKTSQQAEQETVTPNQSFLAN      698
M.musculus          LFPAA--NLP-ALPVPVSGQS---------LTDSRC-------VNQ-------SVHEFMPQ      406
H.sapiens           VSPAT--SQSIAPPVPLKAQTVTDSMFAVASKDAGC------VNK-------STHEFKPQ      418
                     375

S.cerevisiae        -----------------KNTQVQVQTTTSILPLKPVVDGNLAHETPVKPSLTSNASRSPT      453
S.pombe             -----------------NYAYVAKSTSPELKVFDTVMPVALSP---------KPAQKPPS      381
D.melanogaster      KAK---PSEPPEQEQQTLYDSYETEKSY----YMTAVDG------ALYGQN---------      458
C.robusta           KNNIV---EVATSS------------QA-IQG----------GKSLLEDEV--MECKPSS      526
P.mammillata2       DVKVL---PLPEAE------------EIAMRDY---------SQTSLSNSLNRSKLTQPS      461
P.mammillata        ----M---PLTNTG----------------------------AS-----------VLTD      13
P.lividus           TSSTNPNGAVPHDEKTPQYS-MMSEKTPSSASFTSSSKGH-TRMGRLSNIRTPKGLTAPS      756
M.musculus          CGPETKEV-------------CETNKVASINDFHTT------PNTSLGMVQGTPCKVQPS      447
H.sapiens           SGAEIKEG-------------CETHKVANTSSFHTT------PNTSLGMVQATPSKVQPS      459


S.cerevisiae        VTAFSKDAINEVFSMFNQHYSTPG----------------------A---------------      478
S.pombe             PTIHTKAALADILDIFNQPLRSESLEKSSKSPISAQS----SYLGT---------------      423
D.melanogaster      -TSSGQENTGEEDEDND---AEEGEEEEDGGEENE-----EDDSD---------------      494
C.robusta           PTVCTKEAMGEIFGMFQKPLNTDVNVT-------------KHEPS---------------      558
P.mammillata2       PTIFTKEAIGEINGMFQMPLTNTGASVLTDSVYGG-----DNEVSM-------MPLAE--      507
P.mammillata        SVYGGDNEVSEINGMFQMPLTNTGASVLTDSVYGG-----DNEVSM-------MPLAE--      59
P.lividus           PTINTREAMGVINAMLNCSLKSNQFDLDDGGEFQNQVTHQENDFEMEFANDDVKPVSKPA      816
M.musculus          PTVHTKEALGFIMDMFQAPTLPDISD--DKDEW-PSLDQNEDAFEAQFQKNAV-------      497
H.sapiens           PTVHTKEALGFIMNMFQAPTLPDISD--DKDEW-QSLDQNEDAFEAQFQKNVR-------      509
                     .             :

S.cerevisiae        ---------------------------LLDGDDT--T-T----------------------      487
S.pombe             ---------------------------PLKNDEN--SSNSGATSL----------T----      440
D.melanogaster      --------------------------EEEEDDEEEEEHSGPYTNGVQFSAQTTFEQ---      524
C.robusta           ---------------------MMQQSQFSIYCDAEMKD-----------------------      575
P.mammillata2       --------------------PVDKPAFEIFCDDETDEQ-----------------------      525
P.mammillata        --------------------PVDKPAFEIFCDDETDEQ-----------------------      77
P.lividus           IFEDNSAFKRIGGFGGNQGIIPRRQPLALRSDKSTEQSHQGVPP-----PSTSTFPSSSI      871
M.musculus          ---------SSGDWGVKKIM-TLSSAFPIFED--GNKENYGLPQ-----------------      529
H.sapiens           ---------SSGAWGVNKIISSLSSAFHVFED--GNKENYGLPQ-----------------      542
                                      525     *    535

S.cerevisiae        ----------------SKFNVF---------ENFTQ----------------------EF      500
S.pombe             -----------GRSQEEHLDFIP---SLTPSKNYPSKIYSPNKN-----LDFSHTASKAE      481
D.melanogaster      ------------ENRSIKIKF-RKEPSSTYSAYTIENVYQQQQQQQQEQHQIIHQPPQAV      571
C.robusta           -------------KTPVKFDIYED--ASDNSENIPTPEYKQAPKR--EGLSGILQPAVGF      618
P.mammillata2       -------------QMPLN----------------PTPGYVSPPKR--HNLSGILQPAVGF      554
P.mammillata        -------------QMPLKFNIFKDDDKSEDSENIPTPGYVSPPKR--HNLSGILQPAVGF      122
P.lividus           PIYHDIVKPEPKEAAAGKITIFEDEPMDNTKENTPPSEYKQVKEK--REMMGVLQSSKSI      929
M.musculus          ----------PKNKPLGARTFGE-RSLSKYS-SR-S----------------------NEM      555
H.sapiens           ----------PKNKPTGARTFGE-RSVSRLP-SKPK---------------------EEV      569


S.cerevisiae        TAKN-------IEDLT--EVKD--PKQETVSQQTT--------STNETNDRYERLS----      537
S.pombe             TYKN-------SNELE--NVKREQPFSELLPSTLQ--------EETATGTTSTTFA----      520
D.melanogaster      HHPS-----------------------PDPAPA-----------------------------      581
C.robusta           KLEEDDFDDDGKDEDE-RLFDDVYPL-CDDNQSLYLDDRTVARAPMEKTTKNTEFPESS-      675
P.mammillata2       ELADPDEDSQEEEDDN--I-VGVEPLLTVEPAPTFLDDVTIAAGQNLPG--ETNLPLTQL      609
P.mammillata        ELADPDEDSQEEEDDN--I-VGVEPLLTVEPAPTFLDDVTIAAGQNLPG--ETNLPLNQL      177
P.lividus           PFMSLE--DQEKEDAIETDAMEVQPS--TDPLAISQHTMNVTLPPTGAGSNNYSFD--AA      983
M.musculus          PH---------TDEFM-------------DDSTVCGIRCNKTLAPSPKS--IGDFT--SA      589
H.sapiens           PH---------AEEFL-------------DDSTVWGIRCNKTLAPSPKS--PGDFT--SA      603
                                             563         593 596

S.cerevisiae        ---------NSS------------TRPEKADYMT---------PI----------------      552
S.pombe             ---------NAK------------RRPEDSNISPTNP--KKLHTLPRSP--Q---------      547
D.melanogaster      ----------------------------------------SPIPIQRQRNGSHHHFHP      599
C.robusta           ----------FLNTLSHNPPSLQSTMHVTNEIGDDFN-NPHFSAESTTRWGGGATTA---      721
P.mammillata2       QDIPCISSNNLTNSYQANRSAMSTTNKFDDSIQINFGNRNKISAESTTYWQGSAIHDVTK      669
P.mammillata        QDIPCISSNNLTNSYQANRSAMSTTNKFDDSIQINFGNRNKISAESTTYWQGSAIHDVTK      237
P.lividus           ARMASIPFNDASTHKLSFIPPMSTIKPREVEPEPIFPSKKE-MVLPLQQRSGADLTGVNR      1042
M.musculus          AQLSSIPFHKFPADLVQIPE----------------DKE-NVVATQY-THMALD----      625
H.sapiens           AQLASIPFHKLPVESVHILE----------------DKE-NVVAKQC-TQATLD----      639
                         609                                625
```

```
S.cerevisiae        -------------------------KETTETDVVPIIQTPK--EQIRTED----------      575
S.pombe             -------------------------YSTVDSNSVLSPAMPK--GYMFVNE----------      570
D.melanogaster      YMLGQTS---TPK----SEANGYRRARTKVKRSKFQPDLC--------SNSNSASSVADV      644
C.robusta           -------------------------TTTEEGVVKLSPILEATNEYEKSMSTKYQSGL---      753
P.mammillata2       QDVIE--KTVNPPQEVTSEANCTEIGNQQQGVKKLSPILEASYEYEKSVQSRSRLTSSET      727
P.mammillata        QDVIE--KTVNPPQEVTSEANCTEIGNQQQGVKKLSPILEASYEYEKSVQSRSRLTSSET      295
P.lividus           DAVGATASRVPPP---SNESFEKTEFTVNHSGGPLSPIMETSAENARSSASSSASTTNSH      1099
M.musculus          --------------------S-CKENIVDLSKGRKLGPIQEKI----------SASLP---      652
H.sapiens           --------------------S-CEENMVVPSRDGKFSPIQEKSPKQALSSHMYSASLL---      676
                                                 655   661      668    672

S.cerevisiae        ---------------KKSGDNTE--------T----------------------------      584
S.pombe             ---------------NQSMKHES--------SVSNPVA----------------------      585
D.melanogaster      ASSSVLAGAPGTFNDNANFSFSSATALDNSNSSLALAVDR----------------------      684
C.robusta           ---VSL-----------------------------IPSMHRTNVST-----------AATE      771
P.mammillata2       DGQASVAITTTG----KSFI-------------HPPTINRKPLGE-----------LS--      757
P.mammillata        DGQASVAITTTG----KSFI-------------HPPTINRKPLGE-----------LS--      325
P.lividus           ASSSSLEGHQTS---NASHINKERDVAPNATSVQGFSIHIDNVPQHQARPFMQEESLSAC      1156
M.musculus          ----------------------------------------CPSQPA------TGGLFTQ      665
H.sapiens           ----------------------------------------RLSQPA------AGGVLTC      689

S.cerevisiae        ------------------------------------------------QTQLTSTTIQSSPFL      599
S.pombe             --------------------------------TIPHENGK-----HDFGQLSPIEHKPFF      608
D.melanogaster      -LNFRD-----TSQQQILHPV---------NKTLQIHNNNNNTSNNNNGTSTMADFSTF-      728
C.robusta           KFKFGAIGLEDDIT----IPEQSRLVDS------DVIDES------Q---AIDYDFKDLC      812
P.mammillata2       AITYDPMKTSTAPTMYDMEPEFSSFMPHQGISKLQLHNDN------D---ETTTSYSPMC      808
P.mammillata        AITYDPMKTSTAPTMYDMEPEFSSFMPHQGISKLQLHNDN------D---ETTTSYSPMC      376
P.lividus           DPMFAPKAPSTASGFHIHIDNKESFAAPQSADNVPQHQPKPVMQ--E---NSLSAFDPMF      1211
M.musculus          EAVFGL-----------------------------------------------------      671
H.sapiens           EAELGV-----------------------------------------------------      695

S.cerevisiae        TQ-PEPQA----------EKLLQTA-E---------------------------------      614
S.pombe             PK-NDDEL-----------------------------------------------------      615
D.melanogaster      ---------------QENSYFATQHDT---------------------------------      740
C.robusta           DE-----------------------------------------------------------      814
P.mammillata2       LPVLN-------------------------------------------NTSIHPIELN      823
P.mammillata        LPVLN-------------------------------------------NTSIHPIELN      391
P.lividus           APKPASTASGFHIHIDNEESFSATQMSHSKGEAVEHSMKEKSFNAHSHLDSQPSQPKTKE      1271
M.musculus          ------------------EAFKCTGIDH--------A-----------------------      682
H.sapiens           ------------------EACRLTDTDA--------A-----------------------      706

S.cerevisiae        ----HSEK--SKEHYPTI--IP-------------PFTK--IKNQPPVIIENPLSNNLRA      651
S.pombe             -------P--GPSGYLTMPYEE-------------AMAS--LSNLP--TLINPLDQSLRD      649
D.melanogaster      -------E------------AQERRLSKAVETIAR---------HMDKEAIDPFNSELCR      772
C.robusta           ---LMSTSLCKTTI----DLMPDG------------IGDLSKPSLGLNIIPDPWNDQLLQ      855
P.mammillata2       PDAIMEDELCDQMS-T-------------------KTNNLTVSGRLTIVEDPWDEELLN      862
P.mammillata        PDAIMEDELCDQMS-TSLQIAPPPDHSVFDVTTFLSETNNLTVSGRLTIVEDPWDEELLN      450
P.lividus           TNFLHKDDLPD----LEMSFIPDRTLQDA-EQVEQDITTFG-MGEEPLDYSDPFNAGLQN      1325
M.musculus          ----TVEDLSDANAGLQVECV----------------QTLGNVNAPSFTVENPWDDELIL      722
H.sapiens           ----IAEDPPDAIAGLQAEWMQ--------------MSSLGTVDAPNFIVGNPWDDKLIF      748
                                                                    :* .  *

S.cerevisiae        KFLSEISPPLFQYN--TFYNYNQELKM----SSLLKKIHRVSR------NEN----KNP-      694
S.pombe             LLFQVLRPSLLRDK--DYHEHETSFALVEHIESFVSKIKPKAGGPGRRRSSNRHSLDGPE      707
D.melanogaster      AFLAKLDFPGNHDAHASYKIVQTPLPK----------ISNT------------------R      804
C.robusta           GLIPSTL-----EG--VI--VASESKV----------FRKG------------------S      878
P.mammillata2       RLLPPQF-----AK--NLHVIHGKTPV----------ARKG------------------S      887
P.mammillata        RLLPPQF-----AK--NLHVIHGKTPV----------ARKG------------------S      475
P.lividus           LLLSSLSKPLSMYK--GIYQHDQMMPA----------IKPD------------------L      1355
M.musculus          KLLSGLSKPVTSYS--NTFEWQSKLPA----------IKTK------------------T      752
H.sapiens           KLLSGLSKPVSSYP--NTFEWQCKLPA----------IKPK------------------T      778
                     ::

S.cerevisiae        IVDFKKTGDLYCIRGELGEGGYATVYLAES----------------SQGHLRALKVEKPA      738
S.pombe             FHLFYPPNTNLSVISKLGQGAFAPVYLVKSKIETENGDVSQGGAENNESKLFALKIETPP      767
D.melanogaster      TLNVLE-GVTFSIDKEVGRGSYGSVYKATDSRT---------------GNVVALKYQKPP      848
C.robusta           DVRIGNE--TYHLVKEIGKGAFAKAYKATMVSG----------------DEVAVKVQSPA      920
P.mammillata2       TLNLGDT--TYHLADMLGRGGFAKVYKATVEGKS--------------NTIAAVKIQSPP      931
P.mammillata        TLNLGDT--TYHLADMLGRGGFAKVYKATVEGKS--------------NTIAAVKIQSPP      519
P.lividus           AVNFGDEIHVYNVMEKIGEGAFATIYLAACLDAQDMT-----DLDCCELRRVALKVQQPP      1410
M.musculus          EYQLGSLLV--YVNHLLGEGAFAQVFEAIHGDVRNAK-----S-----EQKCILKVQRPA      800
H.sapiens           EFQLGSKLV--YVHHLLGEGAFAQVYEATQGDLNDAK-----N-----KQKFVLKVQKPA      826
                       .        :   :*.*.:.  : .                        :* : *
                                                                        821 ATP
```

```
S.cerevisiae        SVWEYYIMSQVEFRLRKS----TILKSIINASALHLFLDESYLVLNYASQGTVLDLINLQ      794
S.pombe             SCFEFYLTRQAMTRLKGL----RETNSILPVHQLHMFHDTSHLLMDYRPQGSILDLVNSM      823
D.melanogaster      NTWEIYICDQVLKRIKEP----EVLPGVMDISTAIIAPNASLIATEFSPFGSLLDINNKI      904
C.robusta           YKWEIHMLQEVRRRLEAK--GHDVCKDYMTIMTAAVFQNSSCVVTQYLPSGTLLDFLNTN      978
P.mammillata2       HIWESYIVSEAKRRCNSD--S--FRSSLLQIHATSVFPEASFIVSEFLSGGTLLEFVRDC      987
P.mammillata        HIWESYIVSEAKRRCNSD--S--FRSSLLQIHATSVFPEASFIVSEFLSGGTLLEFVRDC      575
P.lividus           CPWEMYIIKELHARLSRLPSQIDVRPSLMKAECAHIYQDKSCLVTEYQSKGTLLDFINRY     1470
M.musculus          NSWEFYIGMQLMERLKP-----EVHHMFIKFYSAHLFKNGSILVGELYSYGTLLNVINLY      855
H.sapiens           NPWEFYIGTQLMERLKP-----SMQHMFMKFYSAHLFQNGSVLVGELYSYGTLLNAINLY      881
                      :* ::  :   *              :      :  : * :  :    *::*:  .

S.cerevisiae        REKAIDGNGIMDEYLCMFITVELMKVLEKIHEVGIIHGDLKPDNCMIRLEKPGE-PLGAH      853
S.pombe             HNSTFSSSG-MDEILVVFFSIEFLRIIEALHTHKIIHGDLKADNALLRLETVADSEWSPI      882
D.melanogaster      RQA---TTKVMHESLVMHFSAQICNIVDHLHRQHIIHADIKPDNFLLMRVPN--------      953
C.robusta           K-----NNTVDR----ENIALQIFHLVHSLHAIGVIHGDVKPDNILIANVSN--------     1021
P.mammillata2       AVH---SRVIDD----IDITFKVMKIVNSLHEAGIIHGDIKPDNFMVVSERDPC------     1034
P.mammillata        AVH---SRVIDD----IDITFKVMKIVNSLHEAGIIHGDIKPDNFMVVSERDPC------      622
P.lividus           KAA---HKRELHENSVLFFAIEILQVVEFMHRCKIIHGDIKPDNFLISTNNDDN------     1521
M.musculus          KNT---SEKVMPQALVLTFAIRMLYMVEQVHSCEIIHGDIKPDNFILGHRFLEQ------      906
H.sapiens           KNT---PEKVMPQGLVISFAMRMLYMIEQVHDCEIIHGDIKPDNFILGNGFLEQ------      932
                                  :: ..  ::. :*   :**.*:* ** ::
                                                  917 proton acceptor
S.cerevisiae        YMRNGEDGWENKGIYLIDFGRSFDMTLLPPG--TKFKSNWKADQQDCWEMRAGKPWSYE-      910
S.pombe             YSPEGLYGWSFKGIYLIDFGRGIDLSLFEEK--VKFIADWDTDLQDCIEMREGRPWTYQ-      939
D.melanogaster      ------VDSPLPSLRLIDFGCAIDMTLFPDGEKTKFRKVVQTDGFTCIEMQEGRSWSYE-     1006
C.robusta           -------RGPAPTLRLIDFGRAIDLSSLPPN--TAFTDNCGTSGFVCSQMKTNQPWNYH-     1071
P.mammillata2       ---KGRLGPLAPVLKLIDFGRAIDMKAFPAG--TAFKKNCGTSGFVCSQMMDQLPWNYH-     1088
P.mammillata        ---KGRLGPLAPVLKLIDFGRAIDMKAFPAG--TAFKKNCGTSGFVCSQMMDKLPWNYHI     677
P.lividus           ---MTCSQDSSNLLKLIDMGRSIDMSLFPEG--TVFTAKCKTSGFNCTEMQSNKPWTYQ-     1575
M.musculus          ---A-DE-DLATGLALIDLGQSIDMKLFPKG--TVFTGKCETSGFQCPEMLSNKPWNYQ-      958
H.sapiens           ---D-DEDDLSAGLALIDLGQSIDMKLFPKG--TIFTAKCETSGFQCVEMLSNKPWNYQ-      985
                             : ***:* .:*:. :     . *     :.   * :*     *.*.

S.cerevisiae        --------ADYYGLAGVIHSMLFGKFIETIQ-LQN--GRCKLKNPFKRYWKKEIWGVIFD      959
S.pombe             --------IDYHGLAAIIYTMLFGQYIETRIEVINGQRRQVLTQRMKRYWNQDLWHRLFD      991
D.melanogaster      --------TDLFCIAATVHVMLFGDYMQPQ----KKGSSWEIRQKLPRYLKKHVWTKFFG     1054
C.robusta           --------IDFNGVAGTLHVLLHSAYMKTML---NNKQEWVTTKKLPRWCDE-KWSSAFH     1119
P.mammillata2       --------TDFHGLAGTIHVVLYNCYMTIIK---QNSGEWSITKSFPRGNRH-LWSSFFK     1136
P.mammillata        FKLDSFQQTDFHGLAGTIHVVLYNCYMTIIK---QNSGEWSITKSFPRGNRH-LWSSFFK      733
P.lividus           --------VDYYGIAGTVHCLLFGKYMKVF----KEGGIWKMTSKVQRCCKV-DWKSFFH     1622
M.musculus          --------IDYFGVAATIYCMLFGSYMKVK----NEGGVWKPEGLFRRLPHLDMWEEFFH     1006
H.sapiens           --------IDYFGVAATVYCMLFGTYMKVK----NEGGECKPEGLFRRLPHLDMWNEFFH     1033
                             *   :*. :: :*.. ::       :          . *      *   *

S.cerevisiae        LLLNSGQ-ASNQALPM-TEKIVEIRNLIESHLEQHAEN--HLRNVILSIEEELSHFQYKG     1015
S.pombe             LLLNPTLHVSEENLPM-TEELSKIRIEMEEWLVNHSTGGSGLKGLLKSIEKRKI------     1044
D.melanogaster      DLLNMQADKLPA---LHEMRLI--FEEEAYRMDSELQKQ------IRTL--------SNI     1095
C.robusta           DLLNFPTPTNDWCPSLQDSPLPHLIQL----FDA--------------------------     1149
P.mammillata2       SLLNVSTPTDEN--PFVESPLPNLLQL----FGEAAT----------------------     1167
P.mammillata        SLLNVSTPKDEL--PFVDSPLPNLLQL----FGEAAT----------------------      764
P.lividus           TLLNVPSCDPSD-----LLRLGDLRRQLEKHVDLAKKAK--------VI-YEIDVLLSNT     1668
M.musculus          IMLNIPDCHNLP-----SLDF--LRQNMKKLLEQQYSNK------IKTLRNRLIVMLSEY     1053
H.sapiens           VMLNIPDCHHLP-----SLDL--LRQKLKKVFQQHYTNK------IRALRNRLIVLLLEC     1080
                     :**               :          .

S.cerevisiae        KPSRRF   1021
S.pombe             ------   1044
D.melanogaster      LHRR--   1099
C.robusta           ------   1149
P.mammillata2       ------   1167
P.mammillata        ------   764
P.lividus           M-----   1669
M.musculus          KRSRK-   1058
H.sapiens           KRSRK-   1085
```

C/Bub3

Percent Identity Matrix - created by Clustal2.1

S.cerevisiae	100.00	28.25	25.95	28.89	28.25	28.48	29.71	29.07	29.07
S.pombe	28.25	100.00	33.86	36.68	35.74	35.74	35.65	35.53	35.42
D.melanogaster	25.95	33.86	100.00	54.63	54.01	53.85	60.68	60.06	60.06
C.robusta	28.89	36.68	54.63	100.00	80.12	80.12	67.49	70.06	69.63
P.mammillata2	28.25	35.74	54.01	80.12	100.00	100.00	66.87	68.83	68.62
P.mammillata	28.48	35.74	53.85	80.12	100.00	100.00	64.58	68.40	68.20
P.lividus	29.71	35.65	60.68	67.49	66.87	64.58	100.00	76.92	76.92
M.musculus	29.07	35.53	60.06	70.06	68.83	68.40	76.92	100.00	99.69
H.sapiens	29.07	35.42	60.06	69.63	68.62	68.20	76.92	99.69	100.00

CLUSTAL O(1.2.4) multiple sequence alignment

Site of post translational modification, WD40 domain

```
S.cerevisiae        ----------------------MQIVQIEQAPKDYISDIKIIPSKS-LLLITSWDGSLT      36
S.pombe             ----------------------MNFSKTLLKNSKDGISSVIFSPSVKNELIAGCWDGSLL      38
D.melanogaster      ----------------------MRPPEFKLNNPPEDLISAVKFGPKSNQYMAASSWDGTLR      39
C.robusta           ----------------------MANEFKLNNCPTDGISSVKFSPSTSQFLLASSWDMSVR      38
P.mammillata2       ----------------------MSNEFKLNECPKDGISSVKFSPSTAQFLLASSWDVSVR      38
P.mammillata        ---------RFHHKTIVQTKLKMSNEFKLNECPKDGISSVKFSPSTAQFLLASSWDVSVR      51
P.lividus           GNLKDNQRGIFGYLITCDNMGESVNEFKLDQPPEDGISSVKFGPNSSQFLLVSSWDETVR      60
M.musculus          --------------------MTGSNEFKLNQPPEDGISSVKFSPNTSQFLLVSSWDTSVR      40
H.sapiens           --------------------MTGSNEFKLNQPPEDGISSVKFSPNTSQFLLVSSWDTSVR      40
                                         : :   * ** : : *.    :   .** ::

S.cerevisiae        VYKFDIQAKNVDLLQSLRYKHPLLCCNFIDNTDLQIYVGTVQGEILKVDLIGSPSFQALT      96
S.pombe             HYQISE---NPELLGKYDLSSPILSLEYTDEK--TALVGNLDGTVTTLDLNTRNH-EFLG      92
D.melanogaster      FYDVPA---NQ-LRQKFVQDAPLLDCAFMDIV--HVVSGSLDNQLRLFDVNTQAE-SIIG      92
C.robusta           LYDVTE---NS-QRFKYEHKSPVLDCCFSDSV--HSWSGGLDGSVMMYDLNTGRE-TVVG      91
P.mammillata2       LYDITE---NT-CRFRYDHKAPVLDCCFSDSV--HAWSGALDGSLLMYDFNMGRE-SLAG      91
P.mammillata        LYDITE---NT-CRFRYDHKAPVLDCCFSDSV--HAWSGALDGSLLMYDFNMGRE-SLAG     104
P.lividus           LYDVQA---NQ-LRAKYKHDRPVLDCCFCDQT--HTYSGGLDNMLKVFDINTNTE-SVLG     113
M.musculus          LYDVPA---NS-MRLKYQHTGAVLDCAFYDPT--HAWSGGLDHQLKMHDLNTDQE-NLVG      93
H.sapiens           LYDVPA---NS-MRLKYQHTGAVLDCAFYDPT--HAWSGGLDHQLKMHDLNTDQE-NLVG      93
                     *..     *            :*   : *        * ::  :   *.

S.cerevisiae        NNEANLGICRICKYGDDKLIAASWDGLIEVIDPRNYGDGVIAVKNLNSNNTKVKNKIFTM     156
S.pombe             NHGKGVSCISKLR-LENCFISGSWDKSFRVWDVRVKQPV--------EGQDI-GKKIFAS     142
D.melanogaster      AHEEPIRCVEHAE-YVNGILTGSWDNTVKLWDMREKRCV--------GTFEQNNGKVYSM     143
C.robusta           RHNNSIRCVEYCS-DTNVVVTGSWDQTIKLWDPRSHNNI--------GSYSQ-PGKVFTM     141
P.mammillata2       MHNAAIRCVEYCS-ETNVIATGGWDETVKLWDPRNKSSI--------GSYSQ-PGKVYTM     141
P.mammillata        MHNAAIRCVEYCS-ETNVIATGGWDETVKLWDPRNKSSI--------GSYSQ-PGKVYTM     154
P.lividus           THEDAVKCVEFCP-DVNVVVTGSWDQTVKLWDPRIGRST--------GSFSQ-PDKVYTM     163
M.musculus          THDAPIRCVEYCP-EVNVMVTGSWDQTVKLWDPRTPCNA--------GTFSQ-PEKVYTL     143
H.sapiens           THDAPIRCVEYCP-EVNVMVTGSWDQTVKLWDPRTPCNA--------GTFSQ-PEKVYTL     143
                     :   :          : . :..**  ..: * *                   *:::

S.cerevisiae        DTNSSRLIVGMNNSQVQWFRLPLCEDDNGTIEESGLKYQIRDVALLPKEQ----------     206
S.pombe             SSRDNILVLGCSERENLVYDIRNLK-LPFQRRPSSFKYMTRSVCCNQNF----------     190
D.melanogaster      SVIDEKIVVATSDRKVLIWDLRKMD-SYIMKRESSLKYQTRCIRLFPNK----------     191
C.robusta           SVCGDHIIVGTCGKSVVVWDLRNMG-YVEQRRESSLKYQTRCIKSFPNK----------     189
P.mammillata2       SVCGHRLIVGTSGKSVVVWDLRNMG-YVEQRRESSLKYQTRCIRSFPNK----------     189
P.mammillata        SVCGHRLIVGTSGKSVVVWDLRNMG-YVEQRRESSLKYQTRCIRSFPNKQVISQPKQSIC     213
P.lividus           AVTGDRLVVGTAGRKVLVWDLRNMG-YVQQRRESSLKYQTRCIRAFPNQ----------     211
M.musculus          SVSGDRLIVGTAGRRVLVWDLRNMG-YVQQRRESSLKYQTRCIRAFPNK----------     191
H.sapiens           SVSGDRLIVGTAGRRVLVWDLRNMG-YVQQRRESSLKYQTRCIRAFPNK----------     191
                       .  :::.        : :          . *.:**  * :    :
                                                  179
S.cerevisiae        --------EGYACSSIDGRVAVEFFDDQGDDYNSSKRFAFRCHRLNLKDTNLAYPVNSIE     258
S.pombe             --------EGFVSSSIEGRTSVEYINPSQE--AQSKNFTFKCHRQIQKDYDIVYPVNDLK     240
D.melanogaster      --------EGYVMSSIEGRVAVEYLDHDPE--VQRRKFAFKCHRNREQNIEQIYPVNALS     241
C.robusta           --------QGYVLSSIEGRVAVEYLDPSVE--VQKKKYAFKCHRIKENGIEHIYSVHAIA     239
P.mammillata2       --------QGFVLSSIEGRVAVEYLDPSAE--EQKKKYAFKCHRIKEDGIERIFSVHTIA     239
P.mammillata        ESCNKNILQGFVLSSIEGRVAVEYLDPSAE--EQKKKYAFKCHRIKEDGIERIFSVHTIA     271
P.lividus           --------QGYVLSSIEGRVAVEYLDPSPE--IQKKKYAFKCHRLKVDGVEQIYPVNAIA     261
M.musculus          --------QGYVLSSIEGRVAVEYLDPSPE--VQKKKYAFKCHRLKENNIEQIYPVNAIS     241
H.sapiens           --------QGYVLSSIEGRVAVEYLDFSPE--VQKKKYAFKCHRLKENNIEQIYPVNAIS     241
                           :*:. ***:**.:**::: . :   . :.::*:***   .. :  : *: :
                                          211    216
```

```
S.cerevisiae        FSPRHKFLYTAGSDGIISCWNLQTRKKIKNFAKFNEDSVVKIACSD--NILCLATSDDTF      316
S.pombe             FHPIHQTLATAGGDGVVAFWDIQVRKRLRVLNPSKINIS-SISFNVDGSMLAIATCAQ-E      298
D.melanogaster      FHNVYQTFATGGSDGIVNIWDGFNKKRLCQFHEYDTSIS-TLNFSSDGSALAIGCSYL-D      299
C.robusta           FHQRYSTFATGGADGYVNMWDGFNKKRLCQFHLFPAAVS-SLAFSNDGSMLAVASSPL-Y      297
P.mammillata2       FHNRYNTFATGGADGFVNMWDGFNKKRLCQFHRFPAPVS-SVAFSDDGSVLAVAASPL-Y      297
P.mammillata        FHNRYNTFATGGADGFVNMWDGFNKKRLCQFHRFPAPVS-SVAFSDDGSVLAVAASPL-Y      329
P.lividus           FHNRHNTFATGGCDGFVNIWDGFNKKRLCQFHCYPTSIS-SLAFSNDGSVLAIASSYT-Y      319
M.musculus          FHNIHNTFATGGSDGFVNIWDPFNKKRLCQFHRYPTSIA-SLAFSNDGTTLAIASSYM-Y      299
H.sapiens           FHNIHNTFATGGSDGFVNIWDPFNKKRLCQFHRYPTSIA-SLAFSNDGTTLAIASSYM-Y      299
                    *   :. : *.* ** :  *:   :*::  :         .:  .   . *.:. .

S.cerevisiae        KTNAAIDQTIELNASSIYIIFDYEN----------- 341
S.pombe             E---A--------AGNIYVHALESNFAAPKLKS--- 320
D.melanogaster      Q---LPETPATVPHPAIYIRYPTDQETKQK------ 326
C.robusta           G---AELSPSSNGEDAIYIRHVTDAETKPKTSSGLA 330
P.mammillata2       S---SDLEPNRDVEDAIFIRHVTDAETKPKSSS--- 327
P.mammillata        S---SDLEPNRDVEDAIFIRHVTDAETKPKSSS*-- 359
P.lividus           E---E--GDIEHPEDAVFIRKVSDQETKPKS----- 345
M.musculus          E---M--DDTEHPEDGIFIRQVTDAETKPKST---- 326
H.sapiens           E---M--DDTEHPEDGIFIRQVTDAETKPKSPCT-- 328
                               :::    .
```

D/Mad1

Percent Identity Matrix - created by Clustal2.1

S.cerevisiae	100.00	22.87	19.51	15.74	18.57	19.70	19.32	17.86	18.83
S.pombe	22.87	100.00	18.57	21.47	23.53	24.44	23.72	22.59	23.09
D.melanogaster	19.51	18.57	100.00	23.88	24.00	23.82	22.69	18.43	21.44
P.lividus	15.74	21.47	23.88	100.00	33.04	33.73	32.45	27.65	30.79
M.musculus	18.57	23.53	24.00	33.04	100.00	81.17	34.00	28.57	31.93
H.sapiens	19.70	24.44	23.82	33.73	81.17	100.00	33.11	29.24	32.68
C.robusta	19.32	23.72	22.69	32.45	34.00	33.11	100.00	44.68	49.33
P.mammillata	17.86	22.59	18.43	27.65	28.57	29.24	44.68	100.00	96.96
P.mammillata2	18.83	23.09	21.44	30.79	31.93	32.68	49.33	96.96	100.00

CLUSTAL O(1.2.4) multiple sequence alignment

Site of post translational modification, interacting domain with Ik, interacting domain with NEK2 interacting domain with Mad2

```
S.cerevisiae        --------------------------MDVRAALQCFFSALSGRFTGKKLGLEIYSIQYKM      34
S.pombe             MSSKLTVYQATTSMADSPR-----DPFQSRSQLPRFLAT---S-----------------      35
D.melanogaster      ------------MDDIRSS-----IDDMMDRFNDSITH---SA-PKKLLFNRLS----A      34
P.lividus           ------------MESPG---DNTEVVRMMGDFDRFIAK---D-----------------      24
M.musculus          ------------MEDLGE---NTTVLSSLRSLNNFISQ---R-----------------      24
H.sapiens           ------------MEDLGE---NTMVLSTLRSLNNFISQ---R-----------------      24
C.robusta           ------------------------------------------------------------      0
P.mammillata        ------------MEDYSETAENTTTFRIMGDFKRFLSS---H-----------------      27
P.mammillata2       ------------MEDYSETAENTTTFRIMGDFKRFLSS---H-----------------      27
                                                    16

S.cerevisiae        SNSGGSSPFLESPGGS-PD------VGSTNGQSNRQIQ----------ALQFKLNTLQNE      77
S.pombe             --VKKP--NLKKPSVN-----------SANETK-------------------NPKLASLE      61
D.melanogaster      SFDLGVSPNKRRRERESPERSLNDTASSLNMPANDSMASLQNSKLRTELIETKAIVIQLR      94
P.lividus           --IEKRKREQRTRERE----------GDLHTAH---------------------GRIAKLE      52
M.musculus          --MEGTS-GLDVSTSA---------SGSLQKQYEYHM----QLEERAEQIRSKSYLIQVE      68
H.sapiens           --VEGGS-GLDISTSA---------PGSLQMQYQQSM----QLEERAEQIRSKSHLIQVE      68
C.robusta           ------------------------------------------------------------      0
P.mammillata        --SDNPSSELTIKENT---------SKASDVMM-------------------RVKMKQIE      57
P.mammillata2       --SDNPSSELTIKENT---------SKASDVMM-------------------RVKMKQIE      57
                                                                          61

S.cerevisiae        YEIEKLQLQKQTNILEKKYKATIDELEKALNDTKYLY----ESNDKLEQELKSLKERSAN     133
S.pombe             FQLENLKNDLKRKELE---------FEREQIELQRKLAEEHEQKNSLQLRLTLVEKQL--     110
D.melanogaster      NEIEKKSREHKEAILL---------AENKSTALKDQCDITSKKNLELQDDLKALRKRELV     145
P.lividus           MEMELMKANNKKARLE---------ADDDVDKLKQKLQMKTN-------AVAELQSQL--      94
M.musculus          REKMQMELSHKRARVE---------LERAASTNARNYEREVDRNQELLARIRQLQECEAT     119
H.sapiens           REKMQMELSHKRARVE---------LERAASTSARNYEREVDRNQELLTRIRQLQEREAG     119
C.robusta           ------------------------------------------------------------      0
P.mammillata        AAHASSERAHVKANIE---------LESK-------FEQLTAQNKVLKDKADSLQGKVNS     101
P.mammillata2       AAHASSERAHVKANIE---------LESK-------FEQLTAQNKVLKDKADSLQGKVNS     101

S.cerevisiae        SMN-----------------------------------------------------DKDKC--     141
S.pombe             -EEQSTSYQKEIEEVRNEKEATQVKIHELLDAKWKEI-AEL-----------KTQIEKND     157
D.melanogaster      LKNE-------ASR------ATAE--LNQLRLKFDESTLKLQKEKYLQKEDARDVHLCIN     190
P.lividus           --EFILKHESQLKRDLEEEKSTKA----GMRKQFNDQIQDL-----------REKKLKVE     137
M.musculus          AEEK---MREQLERHRLCKQNLDA--VSQQLREQEDSLASA-----------REMISSLK     163
H.sapiens           AEEK---MQEQLERNRQCQQNLDA--ASKRLREKEDSLAQA-----------GETINALK     163
C.robusta           ------------------------------------------------------------      0
P.mammillata        LTTKLLDMQDEVKQMR---KDKEA-----EISKWENSYLHL-----------ETLKQEAD     142
P.mammillata2       LTTKLLDMQDEVKQMR---KDKEA-----EISKWENSYLHL-----------ETLKQEAD     142

S.cerevisiae        --IEELRTTLQNKD--LEME-----TLRQQYDSKLSKVTNQCDH--------FK--LEAE     182
S.pombe             QALSEKNHEVMVSNQALQMKDTNLTNLEKLFADSREQLETKCKE----------------     201
D.melanogaster      NELSEYRRIAQRAD--LELQ--STRNELERLR----QLNEELQARA-------------S     229
P.lividus           TMLQELQFSSRDTI-----S--KLSNDLTKKDGEMKLLQTDLEEATTQMRYHMKRGIGAS     190
M.musculus          GRVSELQLSAMDQK--VQVK--RLESEKQELKEQLELQQRKWQEAN--------------     205
H.sapiens           GRISELQWSVMDQE--MRVK--RLESEKQELQEQLDLQHKKCQEAN--------------     205
C.robusta           ------------------------------------------------------------      0
P.mammillata        SRLSEEMMMVTSQN-----Q--QLSEHNLMLQSQNNILNLKCEEHYTHMDQ-YKRSLEAS     194
P.mammillata2       SRLSEEMMMVTSQN-----Q--QLSEHNLMLQSQNNILNLKCEEHYTHMDQ-YKRSLEAS     194

S.cerevisiae        SSHSLLMKYEKE---IKRQSVDIKDLQHQVMEKDDELSSVKASKMINSHPNYSTEEFNEL     239
S.pombe             ---------------LAAAEQQLQELSVHNQQLEESIK-----------------QVSSS     229
D.melanogaster      GFEQLRANHEKQTQSLKVANDRIQELEFE-------IQ-----------------SYSDW     265
```

```
P.lividus           SQRRAIEDY---KAQLVNAQHKIQVLEQQ-------IE-----------------AQKDS      223
M.musculus          ---QKIQELQASQDERAEHEQKIKDLEQK-------LC-----------------LQEQD      238
H.sapiens           ---QKIQELQASQEARADHEQQIKDLEQK-------LS-----------------LQEQD      238
C.robusta           ------------------------------------------------------------      0
P.mammillata        --QTVLKDYQETKSKLARSEQQVNRLKQE-------LA-----------------TLQDT      228
P.mammillata2       --QTVLKDYQETKSKLARSEQQVNRLKQE-------LA-----------------TLQDT      228
                              214

S.cerevisiae        TEMNKMIQDQVQYTKELELANMQQANELKKLKQSQDTSTFWKLENEKLQNKLSQLHVLES      299
S.pombe             IELEKINAEQRLQISELEKLKAAQEERIEKLSSNNRNVEILKEEKNDLESKLYRFEEYRD      289
D.melanogaster      KEVVKTSRERLASVPDLLAEVEHLRSHNKHLNTLIGDKLLLEEQVYDYKTRLEREEGARA      325
P.lividus           AVVARAVQNDVQKVSKLEQDITKLKQENAYYRETCENNSLLKEKMSGLEAKLLRAEERSS      283
M.musculus          AAVVKSMKSELMRMPRMERELKRLHEENTHLREMKETNGLLTEELEGLQRKLSRQEKMQE      298
H.sapiens           AAIVKNMKSELVRLPRLERELKQLREESAHLREMRETNGLLQEELEGLQRKLGRQEKMQE      298
C.robusta           ----------MNRLRQLEIDVSHLSRENSNLKLNQENCALLKEQLIAANTKLQRLEEKCN      50
P.mammillata        KTLAKTLKEEMNRLRHIEVEFKKIHEENYLLRQNNDNFALLQEKLHSVESKLARAELQCA      288
P.mammillata2       KTLAKTLKEEMNRLRHIEVEFKKIHEENYLLRQNNDNFALLQEKLHSVESKLARAELQCA      288
                                    :         .           :   :    : :* : .

S.cerevisiae        QYENLQLENIDLKSKLTKWEIYNDSDDDDDNNVNNNDNNNNNKND------N--NND-NN      350
S.pombe             KVATLELENEKIQTELNSWKSLITNELPT----PEAVSNKLVFLQ----NTNANLGERVS      341
D.melanogaster      EAASLQVKLLHMEQELKEWVKVAQDHCLANT--LVSPMALRSRIEQLLKEDIIHVAEKTS      383
P.lividus           QLAHLQFENEDLKSRLHRWETISSDQPSR----PKSPSEMVQQISDLQ-RGQVSLLEQQG      338
M.musculus          ALVDLELEKEKLLAKLQSWENLDQTMGLN-LRTPEDLSRFVVELQ----QRELTLKEKNN      353
H.sapiens           TLVGLELENERLLAKLQSWERLDQTMGLS-IRTPEDLSRFVVELQ----QRELALKDKNS      353
C.robusta           EIPKIVAENEALKEKLNKTQNATTANVDDNVSLLQNHSSFNAKLEK----EIETLKEQLA      106
P.mammillata        NVPSLEVENNMLTQRIEQLQNMSVTKNEH-SSLQIELSSLSQKLSTAQ-EENLNLKAELS      346
P.mammillata2       NVPSLEVENNMLTQRIEQLQNMSVTKNEH-SSLQIELSSLSQKLSTAQ-EENLNLKAELS      346
                        :  :   :  .:                              .

S.cerevisiae        NDTSNNNNINNNNRTKNNIRNNPEEIIRDWKLTKKECLILTDMNDKLRLDNNNLKLLNDE      410
S.pombe             SLESQLSN-KPAN--------------QP----------------------------LGA-      358
D.melanogaster      SA-SDTKHLNTTI--------------RD----------------------------LEHK      401
P.lividus           QYMASAHSHEEAY--------------KA----------------------------TKED      357
M.musculus          SITSSARGLEKVQ--------------QQ----------------------------LQDE      372
H.sapiens           AVTSSARGLEKAR--------------QQ----------------------------LQEE      372
C.robusta           TS--KSRSLE-----------------------------------------------DRKN      118
P.mammillata        TL--RNHNIE-----------------------------------------------LNSS      358
P.mammillata2       TL--RNHNIE-----------------------------------------------LNSS      358
                          :

S.cerevisiae        MALERNQILDLNKNYENNIVNLKRLNHELEQQKSLSFEECRLLREQLDGLYSAQNNAL--      468
S.pombe             NEKDAAHITELETKL----KELHEQNRRLQRQKSLATQEIDLLRENLKS-YDDEEAILSE      413
D.melanogaster      CAIYLKNIEDLNIGL----KRHKNFKERLQRKLITVSKERDFYKQLVEN-FDKDTTLSNA      456
P.lividus           LKSANQKLLKEQERN----KQQEDLVKRLQRRLLMLTKERDGMRQILNS-YDAEVTHSGF      412
M.musculus          VRQANAQLLEERKKR----ETHEALARRLQKRNALLTKERDGMRAILGS-YDSELTQTEY      427
H.sapiens           LRQVSGQLLEERKKR----ETHEALARRLQKRVLLLTKERDGMRAILGS-YDSELTPAEY      427
C.robusta           AAEYEIKFTEQTEAI----SSLKAQLIRLKKRASLFAYERDSIRSLLQT-YDAELTMTSH      173
P.mammillata        IKAIDQKLTEKSEIC----ASLNAQLLRLRKRAGLLAKERDSIREILQS-YDAELTMTSH      413
P.mammillata2       IKAIDQKLTEKSEIC----ASLNAQLLRLRKRAGLLAKERDSIREILQS-YDAELTMTSH      413
                          :: .            .    .*.::      *    :  :   :. :

S.cerevisiae        -----LEVENSETHASNKNVNEDMNN----------LIDTYKNKTEDLTNELKKLNDQLL      513
S.pombe             KNTDMKKLER--IEGLVKLVDE------------------YKLKLESMPVSLD---VDET      450
D.melanogaster      SVADMTQ-------DMQVR--VRMEVLER-------TVTGYKDMCATLEREIQSLRQQEL      500
P.lividus           ELQANTRLKQ--AEDNVQMCHRQIEQLDGALAKRTEEAGQYRVQVKQLELELAHLKDELT      470
M.musculus          STQLTQRLWE--AEDMVQKVHAHSSEMEAQLSQALEELGVQKQRADTLEMELKMLKAQTS      485
H.sapiens           SPQLTRRMRE--AEDMVQKVHSHSAEMEAQLSQALEELGGQKQRADMLEMELKMLKSQSS      485
C.robusta           TTQLNKRLDN--MTSVNKKLHDRIVELELESQRHVEDTLRHKLQVKQMQLGGS-LSSGQK      230
P.mammillata        TTQLNKRIEN--EAASNKRLYHRIEELEDENKKLAEEAMKNRLGIKTLESQKE-LKETPD      470
P.mammillata2       TTQLNKRIEN--EAASNKRLYHRIEELEDENKKLAEEAMKNRLGIKTLESQKE-LKETPD      470
                          .                                        :    :
                    428
S.cerevisiae        SNSNDVETQRKKRKLTSDQIGLNYSQRLNE-----------LQLENVSVSRELSKAQTTI      562
S.pombe             SDEVSLQKRRRKNEH--K--DAGYVTELYRKNQHLLFQVKEKTNIEAFLREQIITLESSI      506
D.melanogaster      ------------------------------------VNEPAGEGYDSVKKELDTLRMEN      523
P.lividus           MTKESLAKA-----------------------------GSEGTTGTEEELKKRVMELEEEC      502
M.musculus          SA----ES-----------------------------SFSFCKEEVDALRLKVEELEGER      512
H.sapiens           SA----EQ-----------------------------SFLFSREEADTLRLKVEELEGER      512
C.robusta           QEEMSISS-----------------------------VLEEKSNEVLALKEKITSFETER      261
P.mammillata        S-----PM-----------------------------VSQTMNEENSVLREKVKKYEAER      496
P.mammillata2       S-----PM-----------------------------VSQTMNEENSVLREKIQKYEAER      496
                                                           :  .:   .

S.cerevisiae        QLLQEKLEK----------LTKLKEKKIRILQLRDGPFIKDQFIKKNKLLLLEKENADLL      612
S.pombe             ATLRQELAQV------------TEINSCRVLQHRSNPTLKYERIKAAQLEMLNAENSALK      554
D.melanogaster      DRLRRRKEELEMEMMHRCLRGDFNMKDFKVVHFSENPAAEAYESTKNMMEKLQAEIERLK      583
```

```
P.lividus           RKLAERNESLELHVERSALKGDYDPSKTKIISFSMNPAAMAKKQRGEELERLRAECETLR      562
M.musculus          SRLEQEKQVLEMQMEKLTLQGDYNQSRTKVLHMSLNPISMARQRQHEDHDRLQEECERLR      572
H.sapiens           SRLEEEKRMLEAQLERRALQGDYDQSRTKVLHMSLNPTSVARQRLREDHSQLQAECERLR      572
C.robusta           TNLMEKIANLEAWIEQRNLNGDYNPDKTKVLHFTMNPADLAHQQSKRDITELKEQNAKLQ      321
P.mammillata        PTLIEKIEQLEAWIEQGKIKGDYNPENTKVIHFAMNPADLAHQKSKQDVANLKEECIRLR      556
P.mammillata2       PTLIEKIEQLEAWIEQGKIKGDYNPENTKVIHFAMNPADLAHQKSKQDVANLKEECIRLR      556
                      * ..                . .  :::    .*             *. :   *
                                        531            550
S.cerevisiae        NELKKNN--PAVETVPISVYDSLNF----ELKQFEQEVFKSNKRFSRLKQVFNNKSLEFI      666
S.pombe             ALLED----KKVDCLP---IQSFKI-AERKALDLKKEVAEREKRIQRLKEIFSVKSLEFR      606
D.melanogaster      RRNKKLEDDNEQRLNETTSTGGMTL-NFKEFNQLQAELESANGKMRKMRDCFKAAREEFR      642
P.lividus           QRVRVLEESSGDRDSTEMVTNRIQEEQTRAVQDVKKELELSELRNQRLKEVFAQKIQEFR      622
M.musculus          GLVHALERGGPIPADLEA--A-SSLPSSKEVAELRKQVESAELKNQRLKEVFQTKIQEFR      629
H.sapiens           GLLRAMERGGTVPADLEA--AAASLPSSKEVAELKKQVESAELKNQRLKEVFQTKIQEFR      630
C.robusta           LKLRQLEEGHEVSMS--------EIE---FSKEAKTKLNAAELKNQRLKEVFSKKIQEFR      370
P.mammillata        QKLREAADGHEVSVA--------EVE---SLKLAQEEASRAELRNQRLKEVFTKKIQEFR      605
P.mammillata2       QKLREAADGHEVSVA--------EVE---SLKLAQEEASRAELRNQRLKEVFTKKIQEFR      605
                       .                              . :    : :  :::: *     **

S.cerevisiae        DVVNSLLGFKLEFQ-QDSRVKIFSCFK--PEKYLIADLNE---NTLKSNLDADIEGWDDL      720
S.pombe             EAVFSLFGYKLDFM-PNGSVRVTSTYSREDNTAFIFDGES---STMKLVGNPSGPEFERL      662
D.melanogaster      DVCYMLLGYRIDRIGANSNYRISSMFAEGPDDYLDISLNE--SNCLALLESPYSHTFNPP      700
P.lividus           QACYRLTGYQINNP-TSNQYKLLSMYAETPNDILHFQMTS--AGEMNLLANEFSSSLSHM      679
M.musculus          KVCYTLTGYQIDVT-TESQYRLTSRYAEHQTDCLIFKATGPSGSKMQLLETEFSRSVPEL      688
H.sapiens           KACYTLTGYQIDIT-TENQYRLTSLYAEHPGDCLIFKATSPSGSKMQLLETEFSHTVGEL      689
C.robusta           QVCYSLMGFQVVCS-SDGKFKLLSMYADSETDCLEFEVKS--SGEIELLETEYTKTLTDL      427
P.mammillata        QVDMQT--YILV------------ILKTCVLHVFL*-----------------------      626
P.mammillata2       QACYSLTGYRIDTL-NDSQFRLVSMYAECESDYLLFEMNE--RGEMKLLETEYSTTLTEL      662
                    ..      : :                       :

S.cerevisiae        MNLWVEDRGQLPCFLATITLRLWEQRQAK--      749
S.pombe             IRFWCDERKTIPGMLAALTLELLDKND----      689
D.melanogaster      IDQQLA-ASNFPAFFSALTLELFQKATVTMT      730
P.lividus           VEEFLLHGHSIPAFLSTVTLDLFSRQTVMR-      709
M.musculus          IELHLLQQDSIPAFLSALTIELFSRQTSI--      717
H.sapiens           IEVHLRRQDSIPAFLSSLTLELFSRQTVA--      718
C.robusta           ISLHLHHQNSIPMFLSALTVNLFGQQTMMAD      458
P.mammillata        -----------------------------      626
P.mammillata2       VNLHLHHQNSIPMFLSAISVNLFSQQTLA--      691
```

E/Mad2

Percent Identity Matrix - created by Clustal2.1

S.cerevisiae	100.00	48.45	35.57	44.04	42.49	44.56	40.41	42.49	42.49
S.pombe	48.45	100.00	37.13	43.07	42.08	43.56	42.08	44.78	45.27
D.melanogaster	35.57	37.13	100.00	44.78	45.27	47.26	41.38	44.83	44.83
C.robusta	44.04	43.07	44.78	100.00	79.31	82.27	55.94	58.21	57.71
P.mammillata2	42.49	42.08	45.27	79.31	100.00	97.04	53.47	55.72	55.72
P.mammillata	44.56	43.56	47.26	82.27	97.04	100.00	55.94	58.21	58.21
P.lividus	40.41	42.08	41.38	55.94	53.47	55.94	100.00	62.93	63.90
M.musculus	42.49	44.78	44.83	58.21	55.72	58.21	62.93	100.00	94.15
H.sapiens	42.49	45.27	44.83	57.71	55.72	58.21	63.90	94.15	100.00

CLUSTAL O(1.2.4) multiple sequence alignment

safety belt, phosphorylation site, site mutated in the dominant negative, interacting domain with Cdc20, site mated in human

```
S.cerevisiae        -------MSQSISLKGSTRTVTEFFEYSINSILYQRGVYPAEDFVTVKKYDLTLLKTHDD      53
S.pombe             MS--SVPIRTNFSLKGSSKLVSEFFEYAVNSILFQRGIYPAEDFKVVRKYGLNMLVSVDE      58
D.melanogaster      -MSTAQATKNCITLKGSAQIIVEYLKYGINSILFQRGIYPAEDFNNTQQYGLTILMSKDP      59
C.robusta           MA--SNKQLNKITLKGSAAIVSEFFFYGINNILYQRGVYPPEMFKQEKKYGLTILTTTDP      58
P.mammillata2       MA--AAKQLNKITLKGSAAIVSEFFFYGMNNILYQRGVYPPEMFKQEKKYGLTILVSTDE      58
P.mammillata        MA--AAKQLNKITLKGSAAIVSEFFFYGINNILYQRGVYPPEMFKQEKKYGLTILVSTDE      58
P.lividus           MAGVQQTTKNTITLKGSSEIVAEFFYYGINNLLYQRGIYPAETFTRCDMYKLPLLTTTDE      60
M.musculus          -MAQQLAREQGITLRGSAEIVAEFFSFGINSILYQRGIYPSETFTRVQKYGLTLLTTTDP      59
H.sapiens           -MALQLSREQGITLRGSAEIVAEFFSFGINSILYQRGIYPSETFTRVQKYGLTLLVTTDL      59
                              ::*:**:  : *:: :.:*.:*:***:** * *     * * :* : *
                      2    6      13
S.cerevisiae        ELKDYIR-KILLQVHRWLLGGKCNQLVLCIVDKDEGEVVERWSFNVQHISGNSNGQ----      108
S.pombe             EVKTYIR-KIVSQLHKWMFAKKIQKLILVITSKCSGEDLERWQFNVEMVDTADQFQNI--      115
D.melanogaster      KIKTFLQ-NVLSQTEEWLSKNMINKISMVITNAHTKEVLECWDFNMQAELGDGDISDPTK      118
C.robusta           NLLTYLNENVLPQLTEWIEQGVVKRLVVVIRECETNETLERWQFEIECQSDGKENSNP--      116
P.mammillata2       TLLTYLNDNVLPQLQEWLEKGAVKGLVVVMRESETNETLEGWQFEIQCESDKSENGKP--      116
P.mammillata        TLLTYLNDNVLPQLQEWLEKGAVKRLVVVIRESETNETLERWQFEIQCESDKSENGKP--      116
P.lividus           SLKAYLS-SVMEQLKEWLNQQIVQKVVVTISSEENDEVLERWQFDIECDKAITHDSKP--      117
M.musculus          ELIKYLN-NVVEQLKEWLYKCSVQKLVVVISNIESGEVLERWQFDIECDKTAKEEGVR--      116
H.sapiens           ELIKYLN-NVVEQLKDWLYKCSVQKLVVVISNIESGEVLERWQFDIECDKTAKDDSAP--      116
                     :  ::  .:: *   *:     : : : : .    * :* *.*:::      .
                                75
S.cerevisiae        -DDVVDLNTTQSQIRALIRQITSSVTFLPELTKEGGYTFTVLAYTDADAKVPLEWADSNS      167
S.pombe             -GNKEDELRVQKEIQALIRQITATVTFLPQLEEQ--CTFNVLVYADKDSEVPTDWVDSDP      172
D.melanogaster      ATTTKELSRIQNEIRDVMRQISATVSYLPLLDCI--CTFDIMIHTLQNTELPAKWDETGA      176
C.robusta           --KSKDISVINSEIRAVIRQITATVTFLPLLEVP--CSFDLLFYTNHDLVAPEHWEDSSA      172
P.mammillata2       --ATKSKETINSEIRAVIRQVTATVTFLPLLECP--CSFDLLFYTDKNLEVSEKWEDSSP      172
P.mammillata        --ATKSKETINSEIRAVIRQVTATVTFLPLLECP--CSFDLLFYTDKNLEVSEKWEDSSP      172
P.lividus           --KEKSLGEIHKGIQAVIKQITASVTFLPLLETA--CKFNLLIYTDKDLNTPEKWEESGP      173
M.musculus          --REKSQKAIQDEIRSVIRQITATVTFLPLLEVS--CSFDLLIYTDKDLVVPEKWEESGP      172
H.sapiens           --REKSQKAIQDEIRSVIRQITATVTFLPLLEVS--CSFDLLIYTDKDLVVPEKWEESGP      172
                         .    :. *: :::*::::*::** *      .* :: ::  :     .* ::.
                              130 133                  153 156         170
S.cerevisiae        KEIPDGEVVQFKTFSTNDHKVGAQVSYKY----    196
S.pombe             RILRDAEQVQLRSFSTSMHKIDCQVAYRVNP--    203
D.melanogaster      IVIQNPQAVQLRSFSTGLHKVDTVVNYKMST--    207
C.robusta           CLINNSEVVKLRSFSTSVHKVDGAVSYKFSM*-    203
P.mammillata2       CLMPNSEEVKLGSFSTSVHKVDGAVSYKFSM--    203
P.mammillata        CLIPNSEEVKLRSFSTSVHKVDGAVSYKFSM--    203
P.lividus           SLIANSEEVRLRSFTTSIHKVDAMVSYKLMDGI    206
M.musculus          QFITNCEEVRLRSFTTTIHKVNSMVAYKTPVND    205
H.sapiens           QFITNSEEVRLRSFTTTIHKVNSMVAYKIPVND    205
                      : : : *:: :*:*  **:.  * *:
                     178   185186/188/191/193195197/199
```

Annex 3: List of potential Mad2-interacting proteins

List of proteins recovered from *P. mammillata* eggs treated with nocodazole after purification on an affinity column loaded with Mad2-His. Cytoskeleton protein (blue), un-selected proteins (black), pre-selected candidates (orange), selected candidates (green) are indicated.

116 kDa U5 small nuclear ribonucleoprotein,
14-3-3 protein epsilon,
26S protease regulatory subunit 1,
26S proteasome non-ATPase regulatory subunit 1
26S proteasome non-ATPase regulatory subunit 8
26S proteasome regulatory subunit 1
26S proteasome regulatory subunit 8
28S ribosomal protein S27, mitoch
2-aminoadipate transaminase-like
2-oxoisovalerate dehydrogenase subunit alpha
39S ribosomal protein L3
40S ribosomal protein S12-like
40S ribosomal protein S13
40S ribosomal protein S16-like
40S ribosomal protein S18
40S ribosomal protein S19-like
40S ribosomal protein S2
40S ribosomal protein S23
40S ribosomal protein S24
40S ribosomal protein S4
40S ribosomal protein S8
60 kDa heat shock protein, mitoch...
60S ribosomal protein L10a-like
60S ribosomal protein L13
60S ribosomal protein L14-like
60S ribosomal protein L22
60S ribosomal protein L3
60S ribosomal protein L4
60S ribosomal protein L5
60S ribosomal protein L6
60S ribosomal protein L7a
60S ribosomal protein L7-like
60S ribosomal protein L8
60S ribosomal protein RPL31
6-phosphogluconate dehydrogenase
actin cytoplasmic
actin muscle
actin, cytoplasmic-like
alpha centractin like
alpha-1 tubulin
alpha-actinin-2 isoform X1
alpha-enolase-like
AP-2 complex subunit mu
AP-3 complex subunit beta-1
apolipoprotein B-100
Argininosuccinate synthase
atlastin-2
ATP synthase F(0) complex subunit
ATP synthase subunit beta
ATP synthase subunit gamma, mitochondrial
ATP-dependent Clp protease proteolytic subunit, m.
ATP-dependent RNA helicase DDX19B
ATP-dependent RNA helicase DDX3Y
ATP-dependent RNA helicase DDX6
beta actin
bifunctional glutamate/proline--tRNA ligase
Calreticulin
cartilage-associated protein
Cdc20
chaperonin containing T-complex polypeptide subun.
chromatin target of PRMT1 protein-like isoform X1
citrate synthase, mitochondrial-l
coatomer subunit alpha-like
cold shock domain-containing protein E1
COP9 signalosome subunit 4
cyclin-dependent kinase 9 isoform X1
cyclin-dependent-like kinase 5
cysteine desulfurase, mitochondrial
cytoplasmic dynein 1 heavy chain 1
cytoplasmic dynein 1 light intermediate chai.
death-associated protein 1-like
dehydrogenase/reductase SDR family member 4
DNA replication licensing factor
dnaJ homolog subfamily A member 1
dnaJ homolog subfamily A member 3.
dnaJ homolog subfamily B member 1
dnaJ homolog subfamily C member 9
elongation factor 1 alpha
elongation factor 1-beta
elongation factor 1-delta
elongation factor 1-gamma-A
elongation factor Tu, mitochondri..
elongation factor-1 gamma
embryonic ectoderm development protein short isof
endoplasmin-like
Enoyl-CoA hydratase domain-containing protein 3
estradiol 17-beta-dehydrogenase 8
Eukaryotic peptide chain release factor subunit 1
eukaryotic translation initiation factor 1A
Eukaryotic translation initiation factor 3
eukaryotic translation initiation factor 4E
Eukaryotic translation initiation factor 4H
eukaryotic translation initiation factor 5
eukaryotic translation initiation factor 6
glutathione S-transferase kappa 1.
glyceraldehyde-3-phosphate dehydrogenase,
glycine-rich RNA-binding protein 3, mitochon
guanine nucleotide binding protein beta polypep
heat shock 70 kDa protein cognate

Heme-binding protein 2
Heterogeneous nuclear ribonucleoprotein K
heterogeneous nuclear ribonucleoprotein R
histone acetyltransferase type B catalytic
Hydroxysteroid dehydrogenase protein 2
hypoxanthine-guanine phosphoribosyltransfera
importin-5
insulin-like growth factor 2 mRNA-binding pr
isocitrate dehydrogenase [NAD] subunit beta
isocitrate dehydrogenase [NADP] cytoplasmic
isoleucine--tRNA ligase, cytoplasmic
KH domain-containing, RNA-binding...
leucine--tRNA ligase
Lipoamide acyltransferase component of branched
long chain specific acyl coA dehydrogenase
lupus La protein homolog
lysine--tRNA ligase
Macrophage erythroblast attacher
Mad2 A
methylthioribose-1-phosphate isomerase-like
mitochondrial ATP synthase beta subunit
mitochondrial import inner membrane translocase
mitochondrial ornithine transporter 1
mitochondrial succinyl-CoA ligase [ADP-forming]
mitochondrial-processing peptidase subunit a.
Nascent polypeptide-associated complex subunit al.
optineurin-like
peroxiredoxin-6-like
peroxisomal 2,4-dienoyl-CoA reductase
peroxisomal trans-2-enoyl-CoA reductase-like
Phb2 / prohibitin 2
phosphate carrier protein
phosphate carrier protein, mitochondrial
phosphoglycerate kinase 1-like
phospholipase A2 inhibitor-like
Phosphoribosyl pyrophosphate synthase-associated
PITH domain-containing protein 1
plasminogen activator inhibitor 1
polyribonucleotide 5'-hydroxyl-kinase Clp1
Pre-mRNA-processing-splicing factor 8,
prohibitin-like
proliferating cell nuclear antigen
proline--tRNA ligase (probable)
proteasome 26S subunit-like
proteasome subunit alpha 4
proteasome subunit alpha type-3-like
proteasome subunit alpha type-5
proteasome subunit alpha type-6
proteasome subunit alpha type-7
proteasome subunit beta type-3
proteasome subunit beta type-4 isoform X1
proteasome Z subunit isoform X1
protein disulfide-isomerase A3
protein phosphatase 1 regulatory subunit 37
Prpf8 protein
RNA recognition motif 1 in
RNA-binding protein 28
RNA-binding protein 39-like isoform X5
RNA-binding protein 4.1-like
RNA-binding protein lark
ruvB-like 2
ruvB-like helicase 1
septin
septin-11-like
septin-7 isoform X2
serine/threonine-protein kinase 24-like
Signal recognition particle receptor subunit beta...
small nuclear ribonucleoprotein Sm D2
splicing factor 3B subunit 3
squamous cell carcinoma antigen recognized b.
staphylococcal nuclease domain containing 1
Staphylococcal nuclease domain-containing protein
stathmin
succinate--CoA ligase
succinate-CoA ligase, beta subunit
succinyl-CoA ligase [ADP-forming]
SWI/SNF-related matrix-associated
talin-2 isoform X5
TATA elemenTATA element modulatory factor
T-complex protein 1 subunit beta
transcription factor CP2-like
transitional endoplasmic reticulum ATPase
translation initiation factor eIF-2B
transmembrane protein 53-A-like
trifunctional enzyme subunit beta, mitochond.
tryptophan--tRNA ligase, cytopla
tubulin alpha-1A chain-lik
tubulin beta chain
tubulin beta-4B chain
U5 small nuclear ribonucleoprotei
ubiquitin-like modifier-activating enzyme 1
UPF0568 protein C14orf166 homolog
VASA DEAD-box protein
V-type proton ATPase subunit H
zinc finger RNA-binding protein-like isoforme
zygote arrest protein 1-like isof

Annex 4: The spindle assembly checkpoint functions during early development in non-chordate embryos.

In parallel with my thesis project, the team has performed a comparative study of SAC efficiency in metazoan embryos. Results of this work were used to put into perspective my experiments throughout the manuscripts. This study has been reported in a paper available in BioRxiv (Chenevert et al., 2019) and a more recent version that was submit in September 2019 to Development, is included here.

I participated in the preparation of this paper by analyzing mitotic duration in 2-cell embryos of *P. mammillata* and by performing all boxplots.

Tittle: The spindle assembly checkpoint functions during early development in non-chordate embryos.

Short title: The mitotic checkpoint in animal embryos

Janet Chenevert[1], Marianne Roca[1], Lydia Besnardeau[1], Antonella Ruggiero[1,†], Dalileh Nabi[1#], Paola Oliveri[2], Alex McDougall[1], Richard R. Copley[1], Elisabeth Christians[1] and Stefania Castagnetti[1]*

Sorbonne Universités, CNRS, Laboratoire de Biologie du Développement de Villefranchesur-mer (LBDV), 06230 Villefranche-sur-mer, France.
Research Department of Genetics, Evolution and Environment, University College London, Room 426, Darwin Building, Gower Street, London, WC1E 6BT UK.
†- current address: Centre de Recherche en Biologie Cellulaire de Montpellier (CRBM), 1919 Route de Mende, 34293, Montpellier, France.
- current address: Medical Theoretical Center, TU-Dresden, Fiedlerstrasse 42, D-01307 Dresden, Germany.
*Correspondence to: castagnetti@obs-vlfr.fr
Keywords: mitosis, spindle checkpoint, embryo, chordates

Abstract:

In eukaryotic cells, a spindle assembly checkpoint (SAC) ensures accurate chromosome segregation, by monitoring proper attachment of chromosomes to spindle microtubules and delaying mitotic progression if connections are erroneous or absent. The SAC is thought to be relaxed during early animal embryonic development. Here, we evaluate the checkpoint response to lack of kinetochore-spindle microtubule interactions in early embryos of diverse animal species from the main metazoan groups. Our analysis shows that there are two classes of embryos, either proficient or deficient for SAC activation during cleavage. Sea urchins, mussels and jellyfish embryos show a prolonged mitotic block in the absence of spindle microtubules from the first cleavage division, while ascidian and amphioxus embryos, like those of *Xenopus* and zebrafish, continue mitotic cycling without delay. SAC competence during early development shows no correlation with cell size, chromosome number or kinetochore to cell volume ratio. Our results instead indicate that SAC proficiency is the default situation of metazoan embryos.

Introduction

The mitotic checkpoint, also known as the spindle assembly checkpoint (SAC), operates during mitosis and monitors bipolar attachment of spindle microtubules to kinetochores, specialized multi-protein complexes assembled on duplicated sister chromatids. In the absence of stable bipolar kinetochore-microtubule attachments the SAC generates an inhibitory signal, the mitotic checkpoint complex (MCC), which prevents activation of the anaphase-promoting complex/cyclosome (APC/C) and so delays chromosome segregation and mitotic exit. When all chromosomes have achieved bipolar attachments to microtubules, the SAC is quickly silenced resulting in APC/C activation, which leads to the proteolytic cleavage of securin and cyclin B1. Degradation of securin activates separase, thus resulting in cohesin cleavage and physical separation of sister chromatids, while cyclin B1 degradation inactivates cyclin dependent kinase (CDK), resulting in mitotic exit (Lara-Gonzalez et al., 2012; Musacchio 2015). This mechanism increases the fidelity of mitosis by preventing premature initiation of anaphase and subsequent generation of daughter cells with unequal chromosomal complements, a condition, known as aneuploidy, which is linked to cell and organismal lethality (Ricke and Deursen, 2013).

Despite the essential role of the SAC in achieving accurate chromosome segregation, genetic fidelity and reproductive success, this checkpoint is inactive during early development of some animals. Microtubule perturbations that cause erroneous kinetochore-spindle associations do not trigger a robust spindle checkpoint response during the early rapid cell cycles (cleavage cycles) of embryonic development in fish and frog embryos. In *Xenopus laevis,* treatment with microtubule depolymerizing drugs does not delay the first 12 embryonic cycles and the associated oscillations of CDK activity, which continue with unchanged periodicity until the mid-blastula transition (MBT; Clute and Masui, 1995, Gerhart et al., 1984). Similarly, in zebrafish embryos, nocodazole treatment induces a metaphase arrest only after MBT (Ikegami et al., 1997, Zhang et al. 2015). In mouse, which like all mammals has slow (somatic-like) cleavage cycles compared to other animals, nocodazole treatment in 2-cell embryos causes a weak SACdependent mitotic delay (Kato and Tsunoda, 1992; Vázquez-Diez et al, 2019). These studies framed the hypothesis that the SAC is weak or silenced in early animal embryos especially those that undergo fast cleavage divisions. In such embryos, the SAC only becomes active later in embryogenesis, usually during early gastrulation, under the control of an as yet unidentified developmental timer (Clute and Masui, 1995; Zhang et al., 2015).

Recently an alternative hypothesis for the lack of a robust SAC response during early embryogenesis was brought to the fore by a study which showed that the ratio of kinetochore number to cell volume influences the strength of SAC response in *Caenorhabditis elegans* embryos (Galli and Morgan 2016). These findings are in keeping with earlier data from *Xenopus* egg extracts supplemented with high density sperm nuclei which displayed SAC activity at a kinetochore to volume ratio comparable to somatic cells (Minshull et al. 1994). Because a minimum signal threshold, dependent on the amount of Mad2 protein recruited on unattached kinetochores, needs to be reached to inhibit APC/C activity and elicit a SAC-mediated mitotic block (Collin et al. 2013), it was suggested that in large embryonic cells, the SAC is active but the signal generated by unattached kinetochores might be too dilute to trigger a significant checkpoint response (Galli and Morgan 2016). Thus, during early embryogenesis, the SAC would only become apparent when, following the decrease in cell size due to division without growth typical of embryonic cleavage, a sufficient kinetochore to cell volume ratio is reached. Contrary to this hypothesis, however, several earlier reports show that treatment with

microtubule depolymerizing drugs delays cyclin B degradation and extends mitosis in zygotes of the sea urchins *Arbacia punctulata* and *Lytechinus variegatus* and of the clam *Spisula solidissima* (Sluder et al., 1994; Evans et al., 1983, Hunt et al., 1992), indirectly suggesting that the SAC may be effective in those embryos as early as the first cleavage, despite their large cell volume.

Here we use a comparative approach to assess the variability in SAC response during the early cell cycles of embryonic development in species representative of the main metazoan groups and to determine whether specific cellular characteristics, like cell size and kinetochore number, are good predictors of SAC competence. To complement the extensive data already available for vertebrates, we examined the mitotic response to complete microtubule depolymerization in early embryos of a range of invertebrate species. We found that lack of SAC activity is not a general feature of embryonic cleavage cycles. While ascidian (tunicate) and amphiouxus (cephalochordate) early embryos, like previously studied fish and frog embryos (vertebrates), continue to cycle without spindles, sea urchin and starfish (echinoderm), mussel (mollusk) and jellyfish (cnidarian) embryos show a prolonged checkpoint-dependent mitotic block from the first division in response to spindle perturbations. This species-specificity in SAC competence does not correlate with cell size, chromosome number or kinetochore to cell volume ratio, ruling out the hypothesis that lack of SAC activity during early development is due to the dilution of checkpoint signal in large cells. Instead our analysis suggests that silencing of SAC signaling during cleavage arose during animal evolution as a novel feature in the chordate lineage.

Results

Multispecies survey identifies two classes of embryos with different mitotic responses to spindle defects

The SAC monitors kinetochore-microtubule interactions and in somatic cells it delays mitotic progression in response to spindle defects. To assess SAC response during embryogenesis in diverse animal species, we monitored mitotic progression in the presence of the microtubuledepolymerizing drug nocodazole in 2-cell stage embryos from representative species of the main metazoan groups. To complement the extensive data already available in the literature for vertebrates (*Xenopus laevis* and *Danio rerio*) and nematodes (*Caenorhabditis elegans*), we chose the tunicate *Phallusia mammillata*, the echinoderms *Hacelia attenuata* (subphylum Asteroidea), *Paracentrotus lividus*, *Arbacia lixula*, *Sphaerechinus granularis* and *Strongylocentrotus purpuratus* (subphylum Echinoidea), the mollusk *Mytilus galloprovincialis* and the cnidarian *Clytia hemisphaerica*. In order to analyze SAC response under comparable conditions we used a concentration of nocodazole (10µM) that completely depolymerized microtubules (Fig. S1) to generate a full set of unattached kinetochores. Treatment with 10 µM nocodazole after first cytokinesis (2-cell stage) blocked further cytokinesis in embryos of all selected species. As histone H3 is specifically phosphorylated during mitosis (Hendzel et al, 1997), mitotic progression was assessed by following the phosphorylation status of histone H3 (Phospho Histone H3, PH3) over the equivalent of at least one cell cycle time in both control (+DMSO) and nocodazole treated (+ noco) embryos (Fig. 1A). As shown in Fig. 1B, we observed two qualitatively different responses to nocodazole treatment (red lines). In line with previous data from frog and fish, *P. mammillata* embryos continued to cycle in the presence of nocodazole, as evidenced by PH3 oscillation (Fig. 1B*i*) occurring concomitantly with rounds of chromosome condensation and decondensation, suggesting lack of efficient SAC activation in these embryos. However, the response to microtubule depolymerization of embryos from all other analyzed species was strikingly different. Within 10-30 minutes of nocodazole treatment (depending on species), embryos showed condensed chromosomes and accumulated the mitotic marker PH3, indicating mitotic commitment. Both of these mitotic markers were maintained for the length of time equivalent to at

least one cell cycle in the presence of nocodazole (Fig. 1B*ii-viii*), and for some species, like the sea urchin *P. lividus* (Fig. 1B*iii*), the mollusk *M. galloprovincialis* (Fig. 1B*vii*) and the cnidarian *C. hemisphaerica* (Fig. 1B*viii*), the mitotic arrest was extended up to two-to-three times their cell cycle duration. Thus, contrary to the generally accepted dogma that early metazoan embryos lack spindle checkpoint activity, early embryos of echinoderm, mollusk and cnidarian species significantly delay mitotic progression in the presence of spindle defects.

The mitotic delay observed in jellyfish, sea urchin and mussel embryos depends on the SAC kinase Mps1

To confirm that the mitotic delay observed in the presence of nocodazole is due to SAC activation, we further analyzed mitotic progression under conditions which compromised SAC activity. In the presence of spindle defects, the SAC kinase Mps1 binds to unattached kinetochores where it regulates recruitment of other checkpoint components Bub1, BubR1, Bub3, Mad1 and Mad2 (Abrieu et al., 2001; Sacristan and Kops, 2015). In somatic cells, inhibition of Mps1 activity leads to displacement of SAC components from kinetochores, checkpoint inactivation and cell cycle resumption (Santaguida et al 2010; Abrieu et al. 2001). If the delay in mitosis observed in the presence of nocodazole is due to the activation of the SAC, then treatment with Mps1 inhibitors, like reversine (Santaguida et al., 2010), should restore mitotic timing in nocodazole treated embryos, resulting in mitotic exit and cell cycle resumption. For this analysis, we focused on a representative species from each animal group: *P. lividus* (echinoderm, Fig. 2B-D), *C. hemisphaerica* (cnidarian, Fig. 2E-G) and *M. galloprovincialis* (mollusk, Fig. 2H-K). When embryos completed first cytokinesis, we treated them with 10 µM nocodazole alone or in combination with 0.5 µM reversine and assayed mitotic progression using several markers (Fig. 2A). As already shown, in all three species, nocodazole alone caused an increase in mitotic index within 30 minutes of treatment, as evidenced by accumulation of cells with condensed chromosomes labeled with the mitotic marker PH3 (Fig. 1B) or of cells which lack nuclear membranes labelled with the nuclear pore component Nup-153 (for *M. galloprovincialis,* Fig. 2H). In nocodazole these mitotic indicators were all maintained for at least the equivalent of two cell cycle times in all three species. Reversine treatment shortened the nocodazole-induced mitotic arrest, resulting in chromosome decondensation (Fig. 2I, Hoechst) and loss of chromatin associated PH3 staining (Fig. 2B,E,J,K). In mussel embryos, mitotic exit in reversine treated embryos was further confirmed by nuclear envelope reformation, as shown by Nup-153 staining (Fig. 2H,I). Interestingly in all three species, PH3-labelled chromosomes started to accumulate again at later time points, indicating that cells that exited mitosis upon Mps1 inhibition then resumed the cell cycle and entered a new mitosis. Similar results were also obtained using another Mps1 inhibitor, AZ3146 (Hewitt et al., 2010), further validating that the release of the mitotic arrest observed in those embryos is due to specific inactivation of Mps1 activity (Fig. S2).

For *C. hemisphaerica* and *P. lividus*, whose embryos are transparent, we could also measure the duration of mitosis in living embryos, as the time between nuclear envelope breakdown (NEB), which corresponds to prometaphase, and nuclear envelope reformation (NER), using DIC microscopy. In the presence of nocodazole, embryos of both species entered mitosis, as shown by the disappearance of discrete nuclei (NEB). NER, which marks exit from mitosis, was significantly delayed compared to control DMSO-treated embryos. In *P. lividus*, the duration of mitosis increased 5 fold, from 21 ±3 to 98 ±10 minutes, (Fig. 2C and movie 2), whereas in *C. hemisphaerica,* the interval between NEB and NER increased 3.5 fold, from 12 ±1 minutes in DMSO to 44 ±11 minutes in nocodazole (Fig. 2F). Consistent with the results obtained with fixed embryos, inhibition of Mps1 activity, by reversine treatment, resulted in a significant reduction of the mitotic arrest observed in nocodazole-treated embryos. Mitotic duration was shortened to 24 ± 5 minutes for *P. lividus* (Fig. 2C and movie 3) and to 22 ± 6 minutes for *C. hemisphaerica* (Fig. 2F). Following mitotic exit reversine-treated embryos resumed cycling and re-entered mitosis as shown by subsequent rounds of NEB and NER. To confirm mitotic exit in reversine treated *C. hemisphaerica* embryos we evaluated the phosphorylation status of PP1, a mitotic target of CDK-

cyclin B1 (Wu et al., 2009, Lewis et al., 2013). Indeed, in nocodazole PP1 phosphorylation was maintained at a constant level for at least 60 minutes, whereas SAC impairment by reversine treatment resulted in rapid loss of PP1 phosphorylation in nocodazole treated embryos (Fig. S3). In *P. lividus* embryos, cell cycle resumption was further confirmed by visualization of DNA replication, using 5-ethynyl-2'-deoxyuridine incorporation (EdU). DNA replication, which was undetectable in nocodazole treated embryos over two cell cycle times (120 minutes post treatment), resumed following reversine treatment leading to nuclear staining within 80 minutes (Fig. 2D). EdU incorporation was inefficient in *C. hemisphaerica* and *M. galloprovincialis* embryos and therefore this assay could not be carried out for these species. Taken together these results show that in sea urchin, cnidarian and mollusk embryos, the mitotic block caused by spindle perturbations is SAC-dependent.

SAC competence does not correlate with cell size across species

In our multispecies survey the tunicate *P. mammillata* was the only species whose embryos did not arrest in mitosis in the presence of nocodazole. We confirmed the lack of mitotic delay using live microscopy to follow nuclear behavior in DMSO and nocodazole treated embryos. Indeed both control and nocodazole treated embryos underwent multiple consecutive rounds of NEB and NER and chromosome condensation and decondensation (Fig. 3A, nocodazole). Measurements of the duration of mitosis, as the time from NEB to NER, showed only a slight difference between DMSO and nocodazole treated embryos (<0.5 fold). As nocodazole-treated *P. mammillata* embryos underwent subsequent cell cycles, the duration of interphase (I), measured as time from NER to NEB, increased at each cycle (Fig. 3B), consistent with previous observations in *C. elegans* (Galli and Morgan, 2016) and vertebrate tissue culture cells (Rieder and Cole, 2000). The duration of mitosis however remained unchanged, despite the increase in chromosome number and kinetochore to cell volume ratio, due to continuous cycling without intervening cytokinesis (Fig. 3C). Thus, differently from echinoderm, cnidarian, nematode and mollusk early embryos, *P. mammillata* embryos lack SAC activity during embryonic cleavage.

As it was previously shown that the strength of SAC response can be modulated by cell size, we asked whether the difference in mitotic response to spindle defects observed across species could be explained by the difference in cell size in early embryos, whose diameters range from tens of microns to millimeters depending on the animal species. We therefore compared cell size, kinetochore number and kinetochore to cell volume ratio at the 2-cell stage in all species used in our survey (Table 1). We used chromosome number as a proxy for kinetochore number and assumed that all kinetochores are equivalent across species.

Cell volume at the 2 cell stage was calculated as half the volume of the spherical egg, except for *Mytilus galloprovincialis* whose first cleavage is unequal. Cell volume was also measured empirically, by segmentation and 3D reconstruction of live 2-cell embryos stained with the membrane label CellMask Orange (Fig. S4), obtaining values in the same range as those calculated mathematically. Egg diameter and cell volume were both highly variable for *C. hemisphaerica*, but quite standardized for all other species (Table S1). We also included in our analysis published data for *C. elegans* (Galli and Morgan, 2016), *X. laevis,* (Gerhart and Kirschner, 1984) and the fruit fly *Drosophila melanogaster* (Perez-Mongiovi et al., 2005). Comparison of the extent of mitotic delay to egg size, chromosome number, cell volume, or kinetochore to cell volume ratio at the 2-cell stage (Fig. 3D,E,F and Table S1) showed that the difference in SAC response across species does not correlate with any of these parameters; in fact large cells with low kinetochore to cell volume ratio, like those of 2-cell *C. hemisphaerica* embryos, delay mitosis more efficiently than the cells of smaller embryos, like *C. elegans* or *P. mammillata*. In addition, by the 4th mitotic cycle, *P. mammillata* nocodazole treated embryos reach the same kinetochore to cell volume ratio as SAC proficient *P. lividus* 2-cell embryos, but do not significantly delay mitotic progression (Fig. 3B). Finally, the first 2 cells of the *Mytilus galloprovincialis* embryo have significantly different sizes, but behave synchronously in our SAC response assays.

Table 1: Morphometric data for embryos of all analyzed species

	Species	Oocyte diameter (µm)	Chromosome number (2n)	Kin/V_{2cell} x10^{-4} (kin/µm^3)	$V_{nucleus}$ (µm^3)	Spindle length (µm)	SAC competence
Chordates	*Xenopus laevis*	1000	36	0,0014	3053[a]	53,5[b]	– Gerhart et al. 1984
	Danio rerio	800	50	0,0037			– Ikegami et al. 1997
	Ciona intestinalis	140	28	0,39			– this study
	Phallusia mammillata	130	16	0,29	1345	20-30	– this study
	Branchiostoma lanceolatum	130	38[c]	0,66			– this study
Echinoderms	*Hacelia attenuata*	155	44[d]	0,45			+ this study
	Paracentrotus lividus	90	36[e]	1,9	1562	18[f]	+ this study
	Arbacia lixula	80	44[d]	3,3			+ this study
	Strongylocentrotus purpuratus	80	42[g]	3,1			+ this study
	Sphaerechinus granularis	110	42[d]	1,2			+ this study
Mollusks	*Mytilus galloprovincialis*	65	28[h]	Small=6,6 Large=2,5	2393		+ this study
	Spisula solidissima	60	28	6,7			+ Evans et al. 1983
Arthropods	*Drosophila melanogaster*	500	8	0,018			+ Perez-Mongiovi et al. 2005
Nematodes	*Caenorhabditis elegans*	50	12	AB= 22[k] P1= 17[k]	523[i]	13[j]	+ Encalada et al. 2005
Cnidarians	*Clytia hemisphaerica*	210	30	0,12		30-35	+ this study

a) Levy DL and Heald R. 2010. Nuclear size is regulated by importin a and Ntf2 in Xenopus. Cell 143:288-298
b) Wühr M, Chen Y, Dumont S, Groen AC, Needleman DJ, Salic A and Mitchison TJ. 2008. Evidence for an upper limit to mitotic spindle length. Curr Biol 18:1256-61 253
c)Colomber D. 1974. Male chromosomes in two populations of Branchiostoma lanceolatum.

d)Duffy L, Sewell MA and Murray BG. 2007. Chromosome number and chromosome variation in embryos of Evechinus chloroticus (Echinoidea: Echinometridae): is there conservation of chromosome number in the phylum Echinodermata? New findings and a brief review. Int. Rep and Dev. 50:219-231
e)Lipani C, Vitturi R, Sconzo G and Barbata G. 1996. Karyotype analysis of the sea urchin Paracentrotus lividus (Echinodermata): evidence for a heteromorphic chromosome sex mechanism. Marine Biol. 127:67-72
f)Lacroix B, Letort G, Pitayu L, …. and Dumont J. 2018. Microtubule dynamics scale with cell size to set spindle 260 length and assembly timing. Dev Cell 45:496-511
g)Eno CC, Boettger SA and Walker CW. 2009. Methods for karyotyping and for localization of developmentally relevant genes on the chromosomes of the purple sea urchin Strongylocentrotus purpuratus. Biol Bull 217:000-000
h)Dixon DR and Flavell N. 1986. A comparative study of the chromosomes of Mytilus edulis and Mytilus galloprovincialis.J mar boil Ass UK 66:219-228
i)Ladouceur AM, Dorn JF and Maddox PS. 2015. Mitotic chromosome length scales in response to both cell and nuclear size. J Cell Biol 209:645-51
j)Greenan G, Brangwynne CP, Jaesch S, Gharakhani J, Jülicher F and Hyman AA. 2010. Centrosome size sets mitotic spindle length in Caenorhabditis elegans embryos. Curr Biol 20:353-358
k)Galli M and Morgan DO. 2016. Cell size determines the strength of the spindle assembly checkpoint during embryonic development. Dev Cell 36:344-352

Since nuclear and spindle size also vary during development and among different cell types (Crowder et al., 2015) we also checked whether SAC competence could be related to changes in either of these features. A comparison of measurement from several species showed that there is no correlation with either of these two parameters. For example, SAC-competent P. lividus and SAC-deficient P. mammillata blastomeres have comparable sized nuclei (diameter: 14.4 ± 1µm and 13,7 ± 2µm, respectively) which both are smaller than the nuclei of M. galloprovincialis, 16,5 ± 2µm (Table 1). Similarly, SAC deficient P. mammillata blastomeres have spindles of 279 intermediate size between SAC proficient P. lividus and C. hemisphaerica (Table 1). Thus, our data show that cell, nuclear and spindle size, chromosome number and kinetochore to cell volume ratio are not good predictors of SAC activity during early embryonic development.

Chordate embryos do not arrest in mitosis in the presence of spindle perturbations

In the multispecies analysis shown above only the tunicate (*P. mammillata)* and vertebrate (*X. laevis* and *D. rerio*) embryos failed to trigger a mitotic delay in response to spindle defects during cleavage. Because tunicates and vertebrates, together with cephalochordates, form the chordate clade (Fig. 4A), we asked whether lack of SAC activity during cleavage is a common feature of chordate embryos (excluding mammals, which have highly atypical early development featuring slow, somatic-type cell cycles). To address this question, we analyzed the mitotic response to microtubule depolymerization in *Ciona intestinalis,* another tunicate species, and in *Branchiostoma lanceolatum* a species representative of the cephalochordate group.

As shown in Fig. 4, the response of both species to nocodazole treatment was very similar to vertebrates and *P. mammillata.* Although nocodazole treatment blocked cytokinesis, nuclei of both *B. lanceolatum* and *C. intestinalis* embryos continued to cycle and underwent several subsequent mitosis, as evidenced by rounds of chromosome condensation and decondensation (Fig. 4D,G), and of nuclear envelope breakdown and reformation (Fig. 4B,C for *B. lanceolatum* and Fig. 4E,F for *C. intestinalis*). As neither of these embryos is transparent, nuclear dynamics could not be followed in vivo. However, time-lapse microscopy revealed that these nocodazoletreated embryos underwent cyclic shape changes, whereas the SAC arrested *P. lividus* embryo did not. As most animal cells acquire a round shape upon mitotic entry (Lancaster et al., 2013), we

used shape change as a marker of progression through the cell cycle. Shape change was quantified on timelapse videos by measuring two parameters (Fig. 4H): contact region between the two blastomeres (midline, in orange) and total width of the embryo (long axis, in blue). In *P. mammillata, C. intestinalis* and *B. lanceolatum* nocodazole-treated embryos, midline length and embryo width oscillated cyclically and in a reciprocal fashion. This resembles the periodic rounding and flattening documented for *X. laevis* eggs induced to cycle in the absence of cell division (Hara et al., 1980). For *P. mammillata*, whose nuclei are easily visible, NEB was observed when the midline was at its shortest and the embryo width at its longest, and NER took place once cells regained full adhesion (longest midline, shortest width). In contrast for SAC proficient *P. lividus* embryos, midline length and embryo width remained essentially constant throughout the nocodazole-induced mitotic arrest (Fig. 4H, Pl +noco). When SAC signaling was inhibited by reversine treatment, cyclic cell shape changes resumed with mitosis (NEB-NER) corresponding to periods of minimal blastomere contact (Fig. 4H, Pl +noco+rev). Taken together these results show that embryos of *C. intestinalis* and *B. lanceolatum*, like those of *P. mammillata*, fish and frog, continue to cycle in the presence of spindle perturbations and are therefore not SAC competent during early embryonic development. Thus, silencing of the SAC during cleavage may be associated with the emergence of the chordate lineage during animal evolution.

Discussion

SAC activity in early embryos defines two classes of animals

The spindle assembly checkpoint operates during mitosis to delay the onset of anaphase under conditions that could otherwise compromise accurate chromosome segregation (Musacchio and Salmon 2007), and is thus important for cell and organismal viability. Despite this essential function, it has long been thought that the SAC is inefficient in early development of animal embryos with large eggs, undergoing fast cycles. Here, we have undertaken a rigorous survey of the SAC response to spindle defects in embryos of diverse animal species, combining both new experimental data and previous findings from the literature. Because different microtubule poisons can provoke variable levels of SAC activity (Collin et al., 2013), we included in our analysis only studies performed using the microtubule depolymerizing drug nocodazole at a concentration that completely depolymerizes spindle microtubules, generating a full complement of unattached kinetochores and maximum SAC signal. Our analysis shows that in the presence of unattached kinetochores, mitotic progression is unperturbed in fish, frog, amphioxus and ascidian embryos, whereas sea urchin, mussel, jellyfish, nematode and insect embryos significantly delay mitotic exit. We conclude that there is no inherent incompatibility between the fast division typical of cleavage-stage embryonic development and spindle checkpoint activation.

SAC activity in relation to kinetochore number and cytoplasmic volume

Variations in the duration of mitotic delay induced by SAC activation have been reported previously in several cellular contexts and were partially attributed to differences in cell size and kinetochore to cell volume ratio (Mishull et al., 1994; Galli and Morgan, 2016, Kyogoku and Kitjima, 2017). However, our analysis shows that SAC competence during embryo cleavage cycles does not correlate with reduced cell size across different species, with large jellyfish (diameter 210 µm) and starfish (240 µm) embryos mounting a prolonged block from first division and the smaller ascidian (130-140 µm) and amphioxus embryos (130 µm) not delaying mitosis for several divisions (Table 1). Likewise, pairwise comparisons also suggest that chromosome number (*P. lividus* and *X. laevis:* 36 chromosomes*; M. galloprovincialis* and *C. intestinalis:* 28 chromosomes) and kinetochore to cell volume ratio (*P. lividus* and *B. lanceolatum*) are not strong indicators

of SAC competence at the egg-to-embryo transition across metazoans (Table 1). Consistent with this conclusion, it was previously reported that in *D. melanogaster*, whose eggs are 500 µm long and have only 4 chromosome pairs, treatment of stage 3-6 syncytial embryos with colchicine arrests the nuclear cycle at a prometaphase-like stage, suggesting that the SAC is active from early cleavage stage in these large insect cells (Perez-Mongiovi et al. 2005, Sullivan et al. 1993). However, in early *Drosophila* embryos cyclin B degradation and CDK inactivation occur only locally (Su et al. 1998) in the area of the spindle rather than at the level of the whole embryo. This observation raises the possibility that the SAC may be regulated locally in the vicinity of the chromosomes. Indeed, previous work carried out in PtK_1 cells containing two separate spindles showed that once all kinetochores are attached to spindle microtubules within one spindle, anaphase will start irrespective of the presence of unattached kinetochores on the second spindle, suggesting that SAC signal is not diffusible (Rieder et al 1997). An alternative possibility is that the viscosity of the cytoplasm is discontinues in the cell, interfering with long-range diffusion of the SAC signal away from the spindle region. In both hypotheses, if SAC action is limited to the spindle region then the strength of the SAC response may be a function of the volume of a subcellular region local to the spindle area, rather than total cell volume. Spindle size itself, defined as pole to pole distance in metaphase, however, was shown to scale linearly with cell size across embryos of many different species (Crowder et al. 2015) and we confirmed this trend for our species. Thus for 2-cell embryos, difference in spindle size is unlikely to explain the difference in SAC activity observed across same-sized embryos. Similarly we show that SAC strength does not correlate with changes in nuclear volume. We can conclude that there is no straightforward link between any of the cellular parameters that we analyzed, which include kinetochore number, spindle length, volume of cytoplasm or nucleus, and the categorization of embryos into SAC proficient and SAC deficient.

Recent work carried out in *C. elegans* embryos showed that SAC strength is influenced by cell fate (Gerhold et al 2018). This finding suggests that the variability in SAC activity may instead be related to differences in developmental strategies and to the establishment of cell lineages during cleavage. Based on our current knowledge of cell fate specification in different species, however, this does not appear to be the case, as SAC competent species include animals with clear segregation of developmental potential at the 2-cell stage, such as *C. elegans* and *M. galloprovincialis*, as well as animals whose first two blastomeres are identical with respect to cell fate, such as *P. lividus* and *C. hemisphaerica*. We therefore favor the hypothesis that SAC is silenced during early development in some metazoan embryos, in a manner independent of specific cellular attributes like cell size, kinetochore number and cell fate, whereas those factors probably do influence SAC strength once the SAC becomes active in a given species.

SAC deficient embryos as an evolutionary novelty in the chordate linage

While we could not uncover any physical explanation for variation in SAC efficiency, it was immediately apparent when looking at their phylogenetic grouping that all species with SAC-deficient embryos are chordates, while species in all non-chordate clades possess SACcompetent embryos (Fig. 4A). Thus loss of the SAC in cleaving embryos may be associated with the emergence of the chordate lineage. Sampling a wider number of species and metazoan groups under these same experimental conditions will be required to test this hypothesis further. Some supporting examples of non-chordate species being SAC positive can already be inferred from the literature, although the use of different drugs and assays to assess mitotic progression complicates comparisons. As already mentioned, colchicine treatment blocks cyclin B degradation in clam embryos during first mitosis (Hunt et al, 1992), and addition of nocodazole blocks nuclear division in embryos of another mollusk, the gastropod *Ilyanassa obsoleta* (Cather et al. 1986). Similarly, treatment with colchicine delays nuclear division at least for the duration of one cell cycle in

embryos of the fruitfly *D. melanogaster* (Perez-Mongiovi et al, 2005) and in binucleated embryos of the gall midges *Wachtliella periscariae* (Wolf 1978) and *Heteropeza pygmaea* (Kaiser and Went 1987).

Combining all available data, we can propose that SAC proficiency during sexual reproduction is an ancestral feature of metazoan embryos, and that SAC signaling became silenced during early development in chordate embryos. At the mechanistic level, lack of SAC activity in chordates could simply reflect absence in the egg of one or more of the basic SAC components. Although further studies will be required, we do not favor this possibility since in our analysis of available transcriptomic data, we have determined that Mad1, Mad2, Bub1, Bub3 and Mps1 (Table S2) are expressed at the mRNA level both before and after fertilization in species which have no SAC activity during cleavage, like *P. mammillata*, *C. intestinalis* (Aniseed, Brozovic et al., 2018) and *B. lanceolatum* (Oulion et al., 2012; Marletaz et al., 2018, and H. Escriva personal communication). Moreover checkpoint proteins, like XMad1 and XMad2, are present in the cytoplasm of SAC-deficient *X. laevis* early embryos (Chen et al. 1998). A number of scenarios can be envisaged to explain the lack of SAC activity in the presence of SAC components. Kinetochores may be modified to hinder their recognition by the checkpoint machinery or to interfere with the efficiency of MCC generation. Alternatively, as already suggested for mouse embryos, changes in the relative concentrations of SAC components and APC/C may result in an imbalance between inhibitor and target, effectively silencing checkpoint function (Vázquez-Diaz et al., 2019). Finally an as yet unidentified SAC inhibitor may be present in chordate eggs and embryos and function to silence spindle checkpoint signaling during early development.

Given our current understanding of SAC function in maintaining ploidy, it is hard to understand what selective advantage could be associated with loss of SAC signaling in chordate embryos. At this point we can only speculate that SAC silencing is a by-product of some other change in reproductive regulation or oogenesis that could impact the levels of mitotic molecular regulators or the availability of kinetochores. The one exception to chordate SAC deficiency concerns mammalian embryos, which have undergone an extreme shift in reproductive strategy to viviparity, allowing the cleaving embryo to reduce its dependence on oocyte nutrient reserves and to lengthen its cell cycle and the duration of mitosis. In both mouse and human embryos, however, the SAC is highly inefficient leading to the formation of mosaic-aneuploid embryos (Bolton et al., 2016; Vanneste et al., 2009). Notably, in mouse pre-implantation embryos the presence of several unattached kinetochores fails to prevent mitotic progression, but extending the duration of mitosis improves SAC efficiency and reduces chromosome segregation errors (Vázquez-Diez et al., 2019), supporting a possible relationship between lengthening of mitosis and acquisition of SAC activity in mammalian embryos. Further analyses will be required to understand the underlying molecular mechanism controlling spindle checkpoint control during early development and the possible links between these changes in mitotic control and evolutionary transitions.

Materials and methods

Gamete collection and fertilization

P. lividus, *A. lixula*, *S. granularis* and *H. attenuata* adults were collected from the bay of Villefranche-sur-mer (France), *P. mammillata* and *M. galloprovincialis* at Sète (France), *C. intestinalis* at Roscoff (France) and *B. lanceolatum* at Argelès-sur-Mer (France). All these species were maintained in aquaria by CRBM at the Laboratoire de Biologie du Developpement de Villefranche-sur-mer (LBDV). *S. purpuratus* adults were obtained from Patrick Leahy (Kerchoff Marine Laboratory, California Institute of Technology, Pasadena, CA, USA) and kept in aquaria at University College London (UCL, London UK).

S. purpuratus adults were induced to spawn by injection of 0.55 M KCl and all manipulations were carried out at 15°C. For the other three sea urchin species, gametes were obtained by dissection and all

manipulations were carried out at 18-20°C; eggs were collected in microfiltered sea water (MFSW) and used within the day, whereas sperm was collected dry and maintained at 4°C for up to a week. Prior to fertilization eggs were filtered to remove ovarian tissue and debris (100 µm filter pore size for *P. lividus* and *S. granularis*, 70µm for *A. lixula*). When removal of the fertilization membrane was required (for immunofluorescence) eggs were treated with 1X FC (10 µM 3-amino-1,2,4-triazole, 5 µM EDTA, 200 µM Tris-HCl pH8.2) for 2-3 minutes prior to fertilization to prevent hardening of the membrane. The fertilization membrane was removed by filtration (70µm for *P. lividus* and *S. granularis* and 54 µm for *A. lixula*) and excess sperm was removed by rinsing twice in MFSW.

For *H. attenuata,* gametes were obtained by aspiration through a small hole in the starfish arm using a syringe with 18G needle. Oocytes were immediately matured with 10µM 1-methyladenine (1-MA, Sigma-Alderich) and after 13 minutes they were fertilized in glass dishes and cultured at 21^{o}C.

For *P. mammillata* and *C. intestinalis* gametes were obtained by dissection. Dry sperm was maintained at 4°C, and eggs were dechorionated in 0.1% trypsin for *P. mammillata* or in pronase/thioglycolate for *C. intestinalis* as described (Sardet et al., 2011). All manipulations were performed at 18°C in dishes coated with gelatin or agarose to prevent adhesion and lysis (Sardet et al., 2011). Prior to fertilization sperm was activated by resuspension in basic seawater (pH 9.2) for 20 minutes.

B. lanceolatum mature adults were maintained at 16-17°C and induced to spawn by thermal shock at 23ºC for 36 hours, as previously described (Theodosiou et al., 2011). Oocytes were collected in petri dishes and fertilized with a dilution of fresh sperm, and developing zygotes were incubated in MFSW at 19°C (Thedosiou et al., 2011).

C. hemisphaerica eggs and sperm were obtained by light induced spawning from animals raised in the laboratory and maintained at 19°C in artificial sea water (Houliston et al., 2010).

M. galloprovincialis adults were maintained in sea water at 15^{o}C. To induce spawning animals were transferred into individual containers with sea water at 24^{o}C, after rigorous cleaning and brushing of animal shells. Oocytes were fertilized in petri dishes and embryos developed at 18^{o}C.

Drug treatments

All drugs were maintained as stock solutions in DMSO at -20°C and diluted as appropriate in MFSW prior to usage. Nocodazole (Sigma, 33 mM stock solution in DMSO) was used at a final concentration of 10 µM, reversine (Axon Medchem, 5mM stock solution in DMSO) was used at a final concentration of 0.5 µM and AZ3146 (Santa Cruz Biotechnology, stock solution 22 mM in DMSO) was used at a final concentration of 2 µM.

In all experiments drugs were added when 90-95% of the embryos reached 2-cell stage to avoid regression of the cleavage furrow, and drug treatment was then maintained for the entire duration of the experiment. Each experiment was repeated between 3-5 times.

Immunofluorescence

For immunofluorescence, embryos were fixed overnight in -20°C 90% methanol containing 50 mM EGTA. After fixation embryos were washed 3 times in PBS containing 0.1% Tween 20, preblocked in PBS containing 3% BSA for 1 hour at room temperature and then incubated overnight at 4°C in PBS containing 3% BSA and

the appropriate dilution of primary antibody. The mouse anti-PH3 (phospho S10, Abcam) antibody was diluted 1:1000, the mouse antiNup153 (Covance) 1:500, the mouse anti-tubulin DM1A (Sigma-Aldrich) 1:500. Following 3 washes in PBS-0.1% Tween20, embryos were incubated with specific fluorescently-labelled secondary antibodies at room temperature for 1-2 hours. Following 2 further washes in PBS0.1% Tween20, embryos were incubated for 10 minutes in PBS-0.1% Tween20 containing Hoechst (5µg/ml), washed twice and then mounted in citifluor AF1 (Science Services) for imaging and quantification. Each experiment was repeated 3-5 times and 25-200 embryos (depending on the species) were counted for each sample.

Western Blot

To prepare protein extracts of *C. hemisphaerica,* 5 embryos were lysed in Laemmli sample buffer (50 mM Tris-HCl (pH 6.8), 2% SDS, 0.1 % bromophenol blue, 10 % glycerol, 100 mM dithiothreitol) at 5 minute intervals starting from the 2-cell stage. Protein samples were separated on 10% SDS-polyacrylamide gels and transferred to nitrocellulose membranes. After blocking in 3% BSA, to preserve phospho-antigens, membranes were incubated over-night at 4°C with mouse anti-phosho-PP1 antibody (Wu et al., 2009) (pospho-T320 Abcam, 1:1000). After washing, membranes were incubated with anti rabbit horseradish peroxidase-conjugated secondary antibody (Jackson ImmunoResearch 1:10000) and detection was carried out with SuperSignal West Pico chemiluminescent substrate (Thermo Scientific) as described by the manufacturer.

EdU staining

EdU staining was performed using the Click-iT EdU Imaging kit (Invitrogen), following the protocol provided by the manufacturer. Briefly, 10µM EdU was added to MFSW once 95% of *P. lividus* embryos had completed first cytokinesis (90 minutes post fertilization, 2-cell stage), at the same time as DMSO or drugs. Embryos were maintained in EdU for 1 to 3 generation times (50-to-60 minutes each) and then fixed in 3.7% paraformaldehyde/PBS for 15 minutes at room temperature. Following 2 washes in PBS containing 0.1% TritonX100, embryos were permeabilized in PBS-0.5% TritonX100 for 20 minutes at room temperature and washed again twice in PBS containing 3% BSA. Following a 30 minute click-IT labelling reaction, embryos were washed extensively in PBS-0.1% TritonX100 and mounted in citifluor AF1 for imaging.

Chromosome spreads

P. mammillata embryos were treated with DMSO or 10 µM nocodazole for 120 minutes, then washed in hypotonic solution (75 mM KCl), then in 37.5 mM KCl and finally washed four times in cold methanol:acetic acid (3:1), before fixation at -20°C overnight in methanol:acetic acid (3:1). After washing in 60% acetic acid, a few droplets of acetic acid containing the embryos were dripped onto cold methanol-washed slides from about 20 cm height, air dried, and mounted in 50% glycerol containing DAPI for imaging with a Leica SP5 confocal microscope.

Time-lapse microscopyand microinjection

Two cell stage embryos of *P. mammillata, C. intestinalis, B. lanceolatum, P. lividus* or *C. hemisphaerica* were placed in sea water containing appropriate drugs in glass bottom dishes (MatTek corporation) or mounted between gelatin-coated slide and coverslip using Dow Corning vacuum grease as spacer as described (Sardet et al., 2011). Images were acquiredevery 1-2 minutes with 20X or 40X objective lenses (depending on the size of the embryo), on a Zeiss Axiovert 200 inverted microscope equipped with Metamorph acquisition software or a Zeiss Axioimager A2 upright microscope equipped with DIC optics and Zen acquisition software, . Multiple embryos from two conditions were always filmed in parallel, acquiring a z-stack for

each position (2-3 µm steps). To observe chromatin dynamics, *P. mammillata* eggs were injected before fertilization with synthetic mRNA encoding histone H2B fused to GFP (see McDougall et al., 2015 for construct and methods).

CellMask staining

For 3D reconstruction of 2-cell stage volumes following first cytokinesis, live embryos were incubated in MFSW containing 1,5 µg/ml of the plasma membrane stain CellMask Orange (Invitrogen) for 3-5 minutes. Embryos were then transferred to fresh MFSW in glass bottom dishes (Mat-Tek) and imaged using a Leica SP8 confocal microscope, acquiring stacks of 50-80 z-steps (2-3µm intervals). To measure blastomere volume the CellMask signals were manually traced and 3D rendered using Imaris software.

Acknowledgments

We are grateful to E. Houliston for discussion and critical reading of the manuscript, to R. Dumollard, C. Hebras, G. Pruliere, V. Costache, S. Chevalier, T. Momose, L. Leclère, H. Yasuo, G. Williaume, F. Lahaye, M. Schubert, E. Zieger, and H. Escriva for assistance, discussion and sharing of animals and unpublished data. We also thank the members of the Service

Aquariologie (L. Gilletta, A. Jan and R. Lasbleiz) for maintaining animals, and the Institut de la Mer de Villefranche (IMEV) that is supported by EMBRC-France, whose French state funds are managed by the ANR within the Investments for the Future program under reference ANR-10INBS-02. This work was supported by funding from the CNRS and from PACA region (project Mepanep, 2014_03738). The authors declare no competing financial interests.

References

- Abrieu A, Magnaghi-Jaulin L, Kahana JA, Peter M, Castro A, Vigneron S, Lorca T, Cleveland DW and Labbe JC. Mps1 is a kinetochore-associated kinase essential for the vertebrate mitotic checkpoint. Cell. 2001;106: 83-93.
- Basto R, Gomes R, Karess ER. Rough deal and Zw10 are required for the metaphase checkpoint in *Drosophila*. Nat Cell Biol. 2000;2: 939-943.
- Basu J, Bousbaa H, Logarinho E, Li Z, Williams BC, Lopes C, Sunkel CE, Goldberg ML. Mutations in the essential spindle checkpoint gene bub1 cause chromosome misssegregation and fail to block apoptosis in *Drosophila*. J Cell Biol. 1999;146: 13-28.
- Bolton H, Graham SJL, Van der Aa N, Kumar P, heunis K, Fernandez Gallardo E, Voet T and Zernicka-Goetz M. Mouse model of chromosome mosaicism reveals lineage-specific depletion of aneuploidy cells and normal developmental potential. Nat Commun. 2016;7: 11165.
- Brozovic M, Dantec C, Dardaillon J, Dauga D, Faure E, Gineste M, Louis A, Naville M, Nitta KR, Piette J, Reeves W, Scornavacca C, Simion P, Vincentelli R, Bellec M, Aicha SB, Fagotto M, Gueroult-Bellone M, Haeussler M, Jacox E, Lowe EK, Mendez M, Roberge A, Stolfi A, Yokomori R, Brown CT, Cambillau C, Christiaen L, Delsuc F, Douzery E, Dumollard R, Kusakabe T, Nakai K, Nishida H, Satou Y, Swalla B, Veeman M, Volff JN and Lemaire P. ANISEED 2017: extending the integrated ascidian database to the exploration and evolutionary comparison of genome-scale datasets. Nucleic Acids Res. 2018;46(D1): D718-D725.
- Buffin E, Lefebvre C, Huang J, Gagou ME, Karess ER. Recruitment of Mad2 to the kinetochore requires the Rod/Zw10 complex. Curr Biol. 2005;15: 856-861.
- Cather JN, Render JA, Freeman G.The relation of time to direction and equality of cleavage in *Ilyanassa* embryos. Int J Inv Repr and Biol.1986;9: 179-194.
- Chen RH, Shevchenko A, Mann M and Murray AW. Spindle checkpoint protein Xmad1 recruits Xmad2 to unattached kinetochores. J Cell Biol. 1998;143: 283-295.

- Clute P, Masui Y. Regulation of the appearance of division asynchrony and microtubuledependent chromosome cycles in *Xenopus laevis* embryos. Dev Biol. 1995;171: 273-285.
- Collin P, Nashchekina O, Walker R, Pines J. The spindle assembly checkpoint works like a rheostat rather than a toggle switch. Nat Cell Biol. 2013;15: 1378–1385.
- Costache V, McDougall A, Dumollard R. Cell cycle arrest and activation of development in marine invertebrate deuterostomes. Biochem Biophys Res Commun. 2014;450: 1175-1181.
- Crowder ME, Strelecka M, Wilbur JD, Good MC, von Dassow G and Heald R. Comparative analysis of spindle morphometrics across metazoans. Curr Biol. 2015;25: 1542-1550.
- Dumollard R, Minc N, Salez G, Aicha SB, Bekkouche F, Hebras C, Besnardeau L and McDougall A. The invariant cleavage pattern displayed by ascidian embryos depends on spindle positioning along the cell's longest axis in the apical plane and relies on asynchronous cell divisions. Elife. 2017;6 pii: e19290. doi: 10.7554/eLife.19290.
- Encalada SE, Willis J, Lyczak R, Bowerman B. A spindle checkpoint functions during mitosis in the early *Caenorhabditis elegans* embryo. Mol Biol Cell. 2005;16: 1056–1070.
- Evans T, Rosenthal ET, Youngblom J, Distel D, Hunt T. Cyclin: a protein specified by maternal mRNA in sea urchin eggs that is destroyed at each cleavage division. Cell. 1983;33: 289-296.
- Foe VE, von Dassow G. Stable and dynamic microtubules coordinately shape the myosin activation zone during cytokinetic furrow formation. J Cell Biol. 2008;183: 457-470.
- Galli M, Morgan DO. Cell size determines the strength of the spindle assembly checkpoint during embryonic development. Dev Cell. 2016;36: 344-352.
- Gerhart J, Wu M, Kirschner M. Cell cycle dynamics of an M-phase-specific cytoplasmic factor in *Xenopus laevis* oocytes and eggs. J Cell Biol. 1984;98: 1247-1255.
- Gerhold AR, Poupart V, Labbé JC and Maddox PS. Spindle assembly checkpoint strength is linked to cell fate in the *C. elegans* embryo. Mol Biol Cell. 2018;29: 1435-1443.
- Giet R and Glover DM. *Drosophila* Aurora B kinase is required for histone H3 phosphorylation and condensing recruitment during chromosome condensation and to organize the central spindle during cytokinesis. J Cell Biol. 2001;152: 669-82.
- Grimison B, Liu J, Lewellyn AL, Maller JL. Metaphase arrest by cyclin E-Cdk2 requires the spindle-checkpoint kinase Mps1. Curr Biol. 2006;16: 1968-1973.
- Hara K, Tydeman P and Kirschner M. A cytoplasmic clock with the same period as the division cycle in *Xenopus* eggs. Proc. Natl. Acad. Sci. USA. 1980;77: 462-466.
- Hartwell LH, Weinart TA. Checkpoint: controls that ensure the order of cell cycle events. Science. 1989;246: 629-634.
- Hendzel MJ, Wei Y, Mancini MA, Van Hooser A, Ranalli T, Brinkley BR, Bazett-Jones DP and Allis CD. Mitosis-specific phosphorylation of histone H3 initiates primarily within pericentromeric heterochromatin during G2 and spreads in an ordered fashion coincident with mitotic chromosome condensation. Chromosoma. 1997;106: 348-360.
- Hewitt L, Tighe A, Santaguida S, White AM, Jones CD, Musacchio A, Green S, Taylor SS. Sustained Mps1 activity is required in mitosis to recruit O-Mad2 to the Mad1-C-Mad2 core complex. J Cell Biol. 2010;190: 25-34.
- Houliston, E., Momose, T., and Manuel, M. *Clytia hemisphaerica*: a jellyfish cousin joins the laboratory. Trends Genet. 2010;26: 159-167.
- Hunt T, Luca FC, Ruderman JV. The requirements for protein synthesis and degradation, and the control of destruction of cyclins A and B in the meiotic and mitotic cell cycles of the clam embryo. J Cell Biol. 1992;116: 707-724.
- Ikegami R, Zhang J, Rivera-Bennetts AK, Yager, TD. Activation of the metaphase checkpoint and an apoptosis programme in the early zebrafish embryo, by treatment with the spindledestabilizing agent nocodazole. Zygote. 1997;5: 329-350.
- Kaiser J and Went DF. Early embryonic development of the dipteran insect Heteropeza pygmea in the presence of cytoskeleton-affecting drugs. Roux's Arch Biol. 1987;196: 356-366.
- Kato Y, Tsunoda Y. Synchronous division of mouse two-cell embryos with nocodazole in vitro. J Reprod Fert. 1992;95: 39-43.
- Kyogoku H and Kitajima TS. Large cytoplasm is linked to the error-prone nature of oocytes. Dev Cell. 2017;41: 287-298.

- Lancaster OM, Le Berre M, Dimitracopoulus A, Bonazzi D, Zlotek-Zlotekiewicz E, Picone R, Duke T, Piel M and Baum B. Mitotic rounding alters cell geometry to ensure efficient bipolar spindle formation. Dev Cell. 2013;25: 270-283.
- Lara-Gonzalez P, Westhorpe FG, Taylor SS. The spindle assembly checkpoint. Curr Biol. 2012;22: R966-980.
- Lewis CW, Taylor RG, Kubara PM, Marshall K, Meijer L, Golsteyn RM. A western blot assay to measure cyclin dependent kinase activity in cells or in vitro without the use of radioisotopes. FEBS Lett. 2013;587: 3089-95.
- Madgwick S, Jones KT. How eggs arrest at metaphase II: MPF stabilization plus APC/C inhibition equals cytostatic factor. Cell Div. 2007;2: 4.
- Marlétaz F, Firbas PN,…..Irimia M. Amphioxus functional genomics and the origins of vertebrate gene regulation. Nature. 2018;564: 64-70.
- McDougall A, Chenevert J, Pruliere G, Costache V, Hebras C, Salez G, Dumollard R. Centrosomes and spindles in ascidian embryos and eggs. Methods Cell Biol. 2015;129: 317-339.
- Minshull J, Sun H, Tonks NK and Murray AW. A MAP kinase-dependent spindle assembly checkpoint in *Xenopus* egg extracts. Cell. 1994;79: 475-86.
- Musacchio A. The molecular biology of spindle assembly checkpoint signaling dynamics. Curr Biol. 2015;25: R1002-R1018.
- Oulion S, Bertrand S, Belgacem MR, Le Petillion Y and Escriva H. Sequencing and analysis of the Mediterranean amphioxus (*Branchiostoma lanceolatum*) transcriptome. PLoS ONE. 2012;7: e36554.
- Perez-Mongiovi D, Malmanche N, Bousbaa H and Sunkel C. Maternal expression of the checkpoint protein BubR1 is required for synchrony of syncytial nuclear division and polar body arrest in *Drosophila melanogaster*. Development. 2005;132: 4509-4520.
- Ricke RM, van Deursen JM. Aneuploidy in health, disease and aging. J Cell Biol. 2013;201: 1121 (2013).
- Rieder CL and Cole R. Microtubule disassembly delays the G2-M transition in vertebrates. Curr Biol. 2000;10: 1067-70.
- Rieder CL, Khodjakov A, Paliulis LV, Fortier TM, Cole RW and Sluder G. Mitosis in vertebrate cells with two spindles: implications for the metaphase/anaphase transition checkpoint and cleavage. Proc Natl Acad Sci USA. 1997;94: 5107-12.
- Reider CL, Schultz A, Cole R and Sluder G. Anaphase onset in vertebrate cells is controlled by a checkpoint that monitors sister kinetochore attachment to the spindle. J Cell Biol. 1994;127: 1301-10.
- Sacristan C, Kops GJ. Joined at the hip: kinetochores, microtubules and spindle assembly checkpoint signaling. Trends Cell Biol. 2015;25: 21-28.
- Santaguida S, Tighe A, D'Alise AM, Taylor SS, Musacchio A. Dissecting the role of Mps1 in chromosome biorientation and the spindle checkpoint through the small molecule inhibitor reversine. J Cell Biol. 2010;190: 73-87.
- Sardet C, McDougall A, Yasuo H, Chenevert J, Pruliere G, Dumollard R, Hudson C, Hebras C, Le Nguyen N, Paix A. Embryological methods in ascidians: the Villefranche-sur-mer protocals. Methods Mol Biol. 2011;770: 365-400.
- Schatten G, Simerly C, Palmer DK, Margolis RL, Maul G, Andrews BS, Schatten H. Kinetochore appearance during meiosis, fertilization and mitosis in mouse oocytes and zygotes. Chromosoma. 1988;96: 341-352.
- Shuster CB, Burgess DR. Transitions regulating the timing of cytokinesis in embryonic cells. Curr Biol. 2002;12: 854-858.
- Sluder G, Miller FJ, Thompson EA, Wolf DE. Feedback control of the metaphase-anaphase transition in sea urchin zygotes: role of maloriented chromosomes. J Cell Biol. 1994;126: 189198.
- Stricker SA. Comparative biology of calcium signaling during fertilization and egg activation in animals. Dev Biol. 1999;211: 157-176.
- Theodosiou M, Colin A, Schulz J, Laudet V, Peyrieras N, Nicolas J-F, Schubert M, Hirsinger E. 2011. Amphioxus spawning behavior in an artificial seawater facility. J. Exp. Zoolog. B Mol Dev Evol. 2011;316: 263-275.
- Tunquist BJ, Schwab MS, Chen LG, Maller JL. The spindle checkpoint kinase bub1 and cyclin E/cdk2 both contribute to the establishment of meiotic metaphase arrest by cytostatic factor. Curr Biol. 2002;12: 1027-1033.
- Tunquist BJ, Eyers PA, Chen LG, Lewellyn AL, Maller JL. Spindle checkpoint proteins Mad1 and Mad2 are required for cytostatic factor-mediated metaphase arrest. J Cell Biol. 2003;163: 1231-1242.

- Vanneste E, Voet T, Le Caignec C, Ampe M, Konings P, Melotte C, Debrock S, Amyre M, Vikkula M, Schuit F et al. Chromosome instability is common in human cleavage-stage embryos. Nat Med. 2009;15: 577-583.
- Vázquez-Diaz C, Gomes Paim LM and FitzHarris G. Cell-size-independent spindle checkpoint failure underlies chromosome segregation error in mouse embryos. Curr Biol. 2019;29: 1-9.
- Von Stetina JR, Orr-Weaver TL. Developmental control of oocyte maturation and egg activation in metazoan models. Cold Spring Harb Perspect Biol. 2011;3(10):a005553 doi: 10.1101/cshperspect.a005553.
- Wolf R. The cytaster, a colchicine-sensitive migration organelle of cleavage nuclei in an insect egg. Bev Biol. 1978;62: 464-472.
- Wu JQ, Guo JY, Tang W, Yang CS, Freel CD, Chen C, Nairn AC, Kornblut S. PP1-mediated dephosphorylation of phosphoproteins at mitotic exit is controlled by inhibitor-1 and PP1 phosphorylation. Nat Cell Biol. 2009;11: 644-651.
- Zhang M, Kothari P, Lampson MA. Spindle assembly checkpoint acquisition at the mid-blastula transition. PLoS One. 2-15;10:e0119285. doi: 10.1371/journal.pone.0119285.

Figure legends

Figure 1: Nocodazole-induced spindle depolymerization defines two classes of embryos with qualitatively different mitotic responses.

A) Schematic representation of assay used to test mitotic progression. Two-cell stage embryos of selected species were treated either with DMSO (0,1%) or 10 µM nocodazole and then fixed every 10 minutes for immunostaining with antibody against the mitotic marker PH3. B)

Percentage of embryos accumulating PH3 in the presence of DMSO (blue) or 10 µM nocodazole (red) over the time of 2-3 cleavages (2 to 16 cell stage), representative of at least three independent experiments. 50-200 embryos were counted for each time point in each experiment. Drugs were added when at least 90% of embryos were at 2-cells (t0). For *M. galloprovincialis* control could not be quantified past 8 cells as divisions become asynchronous within each embryo.

Figure 2: Microtubule depolymerization causes an Mps1-mediated mitotic block in cleavage stage embryos of *P. lividus*, *C. hemisphaerica* and *M. galloprovincialis*.

A) Schematic representation of the effect of the Mps1 inhibitor reversine on cell cycle progression during SAC activation (+ nocodazole). B) Quantification of duration of mitosis in *P. lividus* embryos treated with 0.1% DMSO, 10 µM nocodazole or 10µM nocodazole and 0.5 µM reversine. Mitosis was measured as time from NEB to NER. Each dot represents one embryo. Boxes represent 25-75th percentiles and the median is shown; whiskers mark 5th and 95th percentiles. Asterisks indicate statistical significance as determined by Student's t-test, $p<0.001$. The numerical values associated with this graph are reported in Table S3. C) Quantification of embryos accumulating PH3 in the presence of DMSO (blue), 10 µM nocodazole (red) or 10 µM nocodazole and 0.5 µM reversine (green) over time equivalent of two cell cycles. D) Labeling of newly replicated DNA by EdU incorporation in control (+DMSO, left), nocodazole (middle) and nocodazole/reversine (right) treated embryos. EdU was added together with drugs (90 minutes post fertilization) when embryos reached 2-cell stage. All embryos were fixed when control reached 8-cell stage (210 minutes). 50 embryos were analyzed for each condition in 3 independent repeats. E) Quantification of duration of mitosis in *C. hemisphaerica* embryos treated with DMSO, nocodazole or nocodazole and reversine. Each dot represents one embryo. Box plot parameters are as in C). F) Representative DIC images of embryos treated with 10µM nocodazole (left) or 10 µM nocodazole and 0.5 µM reversine (right). Arrows point at nuclei after NER. G) Quantification of PH3 positive *C. hemisphaerica* embryos in the presence of DMSO (blue), 10 µM nocodazole (red) or 10 µM nocodazole and 0.5 µM reversine (green). Representative

of 4 independent experiments, n=20-30 for each time point. H) Quantification of Nup153-labelled and I) PH3-labelled *M. galloprovincialis* embryos after treatment with 0.1% DMSO (blue), 10 µM nocodazole (red), or 10 µM nocodazole and 0.5 µM reversine (green). J) Representative images of embryos stained for Nup153 (top), DNA (Hoechst, bottom) and K) PH3. PB= polar body. Scale bar 30 µm.

Figure 3: SAC response across species does not correlate with cell volume

A) Selected frames from a time-lapse movie of a *P. mammillata* embryo expressing the fluorescent DNA reporter, H2B-gfp, treated with 10 µM nocodazole after first cleavage. Numbers indicate time (minutes) from treatment. Arrows indicate nuclei visible in bright field optics. See also Movie 1. B) Duration of mitosis (M, NEB to NER) and interphase (I, NER to NEB) in control (+DMSO), and nocodazole treated *P. mammillata* embryos. Kin/V indicates kinetochore to cell volume ratio following subsequent rounds of DNA replication. Box plots are as in Fig. 2C. The numerical values associated with this graph are reported in Table S4. C) Dapi stained chromosome spreads from control (DMSO) and nocodazole-treated (180 minutes) *P. mammillata* embryo. D,E) Ratio of average time spent in mitosis for nocodazole and DMSO treated embryos plotted against D) cell volume or E) kinetochore/ cell volume ratio in 2-cell stage embryos of different species. Ce= *C. elegans*, Pl= *P. lividus*, Pm= *P. mammillata*, Ch= *C. hemisphaerica* and Xl=*X. laevis*. For *Ce* as first division is asymmetric, volumes for both cells are presented (AB and P1). For *Ce* and *Xl* data were obtained from the literature. F) Egg diameter, chromosome number and kinetochore/cytoplasmic ratio at 2-cell stage for all species analyzed. For all species used in this study egg diameter was measured and is reported as average of 30-50 eggs. Red are species that do not delay mitosis, green are species that delay mitosis in the presence of nocodazole. Scale bar 30 µm.

Figure 4: Nocodazole treatment does not delay mitotic progression during cleavage in chordate embryos.

A) Phylogenetic tree indicating phyla, analyzed species and their SAC response. Species analyzed in this study are in black, species for which information has been obtained from the literature are in grey. B) Quantification of Nup153-negative *C. intestinalis* embryos (without nuclei=in mitosis) in the presence of DMSO (blue) or 10 µM nocodazole (red) over the time of 3 divisions (2-16 cells). Representative of 3 independent experiments. n=20-30 embryos per time point for each repeat. C) Representative Nup-153-stained embryos and D) Hoechst stained nuclei for *C. intestinalis*. E) Percentage of *B. lanceolatum* embryos without nuclei, as determined by Nup-153 staining, in the presence of DMSO (blue) or 10 µM nocodazole (red) over the time of two divisions (2-8 cells). Representative of 3 independent experiments. n=50-100 embryos per time point. F) Representative Nup-153 and G) Hoechst stained nuclei for *B. lanceolatum*. Duration of treatment is indicated on each image (in minutes). H) Measurement of long axis of embryo (width, blue) and cell-cell contact region (midline, orange) during 2-3 cell cycles in a representative embryo of *B. lanceolatum* (Bl), *P. mammillata* (Pm, see movie 1), *C. intestinalis* (Ci) and *P. lividus* (Pl) in the presence of 10 µM nocodazole (+noco; movie 2) or for Pl 10 µM nocodazole and 0.5 µM reversine (Pl +noco+rev; movie 3). Measurements are reported as percentage of maximum length throughout the recording. Crosses (✕) correspond to NEB, and circle (●) to NER. Scale bar 30 µm.

List of supporting information:

Figure S1.pdf Nocodazole treatment depolymerizes spindle microtubules
Figure S2.pdf The Mps1 inhibitor AZ3146 releases the nocodazole-induced mitotic block observed in *P. lividus* and *C. hemisphaerica*
Figure S3.pdf PP1-phosphorylation in *C. hemisphaerica* requires an active SAC
Figure S4.pdf Rendering of 2-cell stage embryos
Table S1.xlsx Morphometric data for analysed embryos
Table S2.pdf Sequences of analyzed SAC components
Table S3.pdf Value associated with Figure 2
Table S4.pdf Values associated with Figure 3

Movie 1: *P. mammillata* 2-cell embryos expressing H3B-Venus, in the presence of 10µM nocodazole.
Movie 2: *P. lividus* 2-cell embryos in the presence of 10 µM nocodazole.
Movie 3: *P. lividus* 2-cell embryos in the presence of 10 µM nocodazole and 0.5 µM reversine.

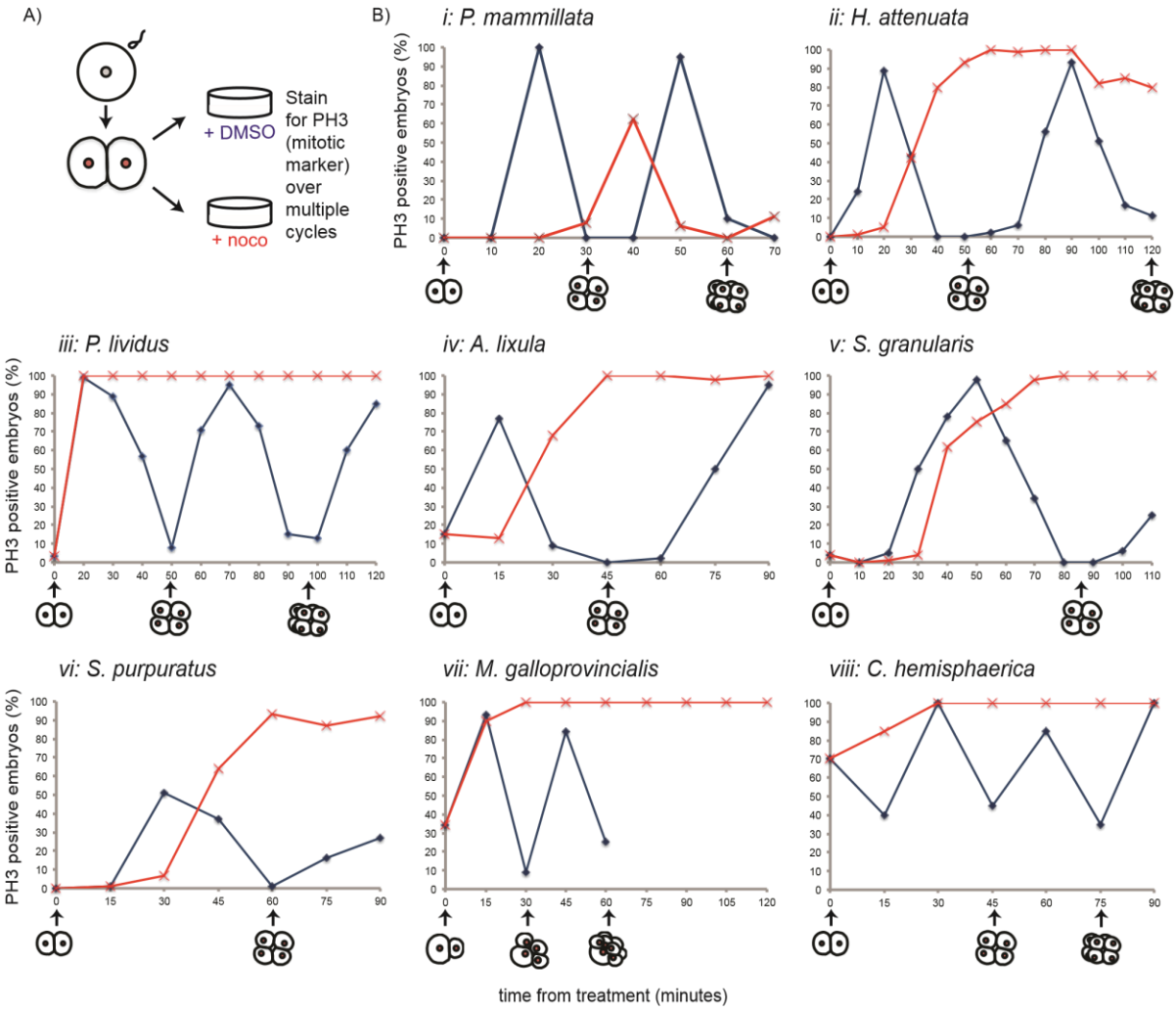

Figure 1

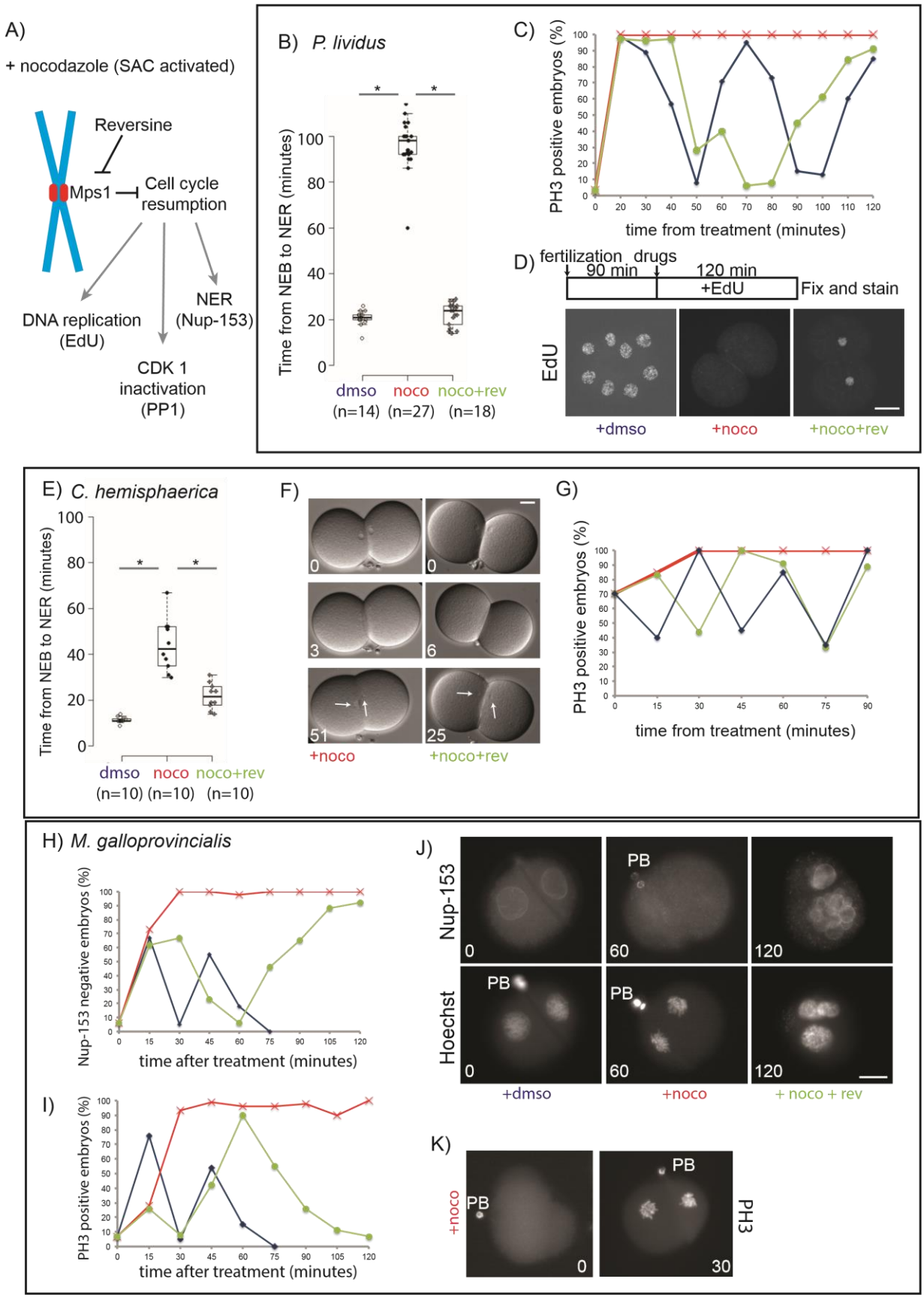
A)
+ nocodazole (SAC activated)
Reversine
Mps1
Cell cycle resumption
DNA replication (EdU)
CDK 1 inactivation (PP1)
NER (Nup-153)
B) P. lividus
Time from NEB to NER (minutes)
dmso noco noco+rev
(n=14) (n=27) (n=18)
C)
PH3 positive embryos (%)
time from treatment (minutes)
D) fertilization drugs
90 min
120 min
+EdU
Fix and stain
EdU
+dmso
+noco
+noco+rev
E) C. hemisphaerica
Time from NEB to NER (minutes)
dmso noco noco+rev
(n=10) (n=10) (n=10)
F)
+noco
+noco+rev
G)
PH3 positive embryos (%)
time from treatment (minutes)
H) M. galloprovincialis
Nup-153 negative embryos (%)
time after treatment (minutes)
I)
PH3 positive embryos (%)
time after treatment (minutes)
J)
Nup-153
Hoechst
PB
+dmso
+noco
+ noco + rev
K)
+noco
PB
PH3

Figure 2

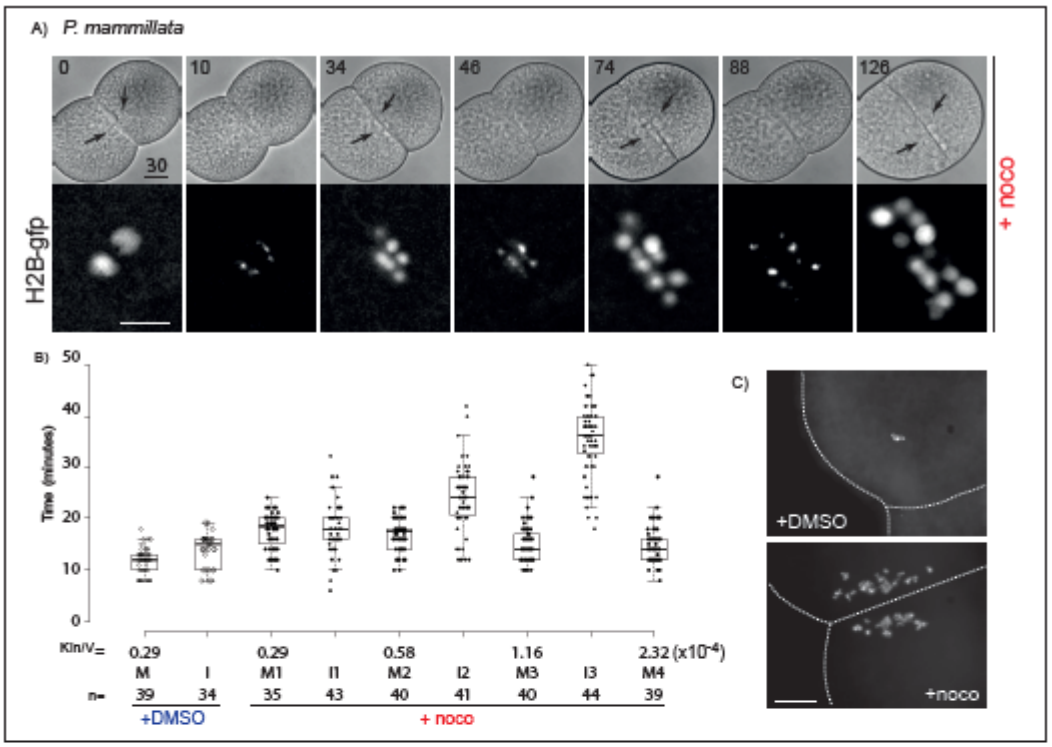
A) P. mammillata
0
10
34
46
74
88
126
30
H2B-gfp
+ noco
B)
Time (minutes)
Kin/V=
0.29
0.29
0.58
1.16
2.32 (x10-4)
M
I
M1
I1
M2
I2
M3
I3
M4
n=
39
34
35
43
40
41
40
44
39
+DMSO
+ noco
C)
+DMSO
+noco

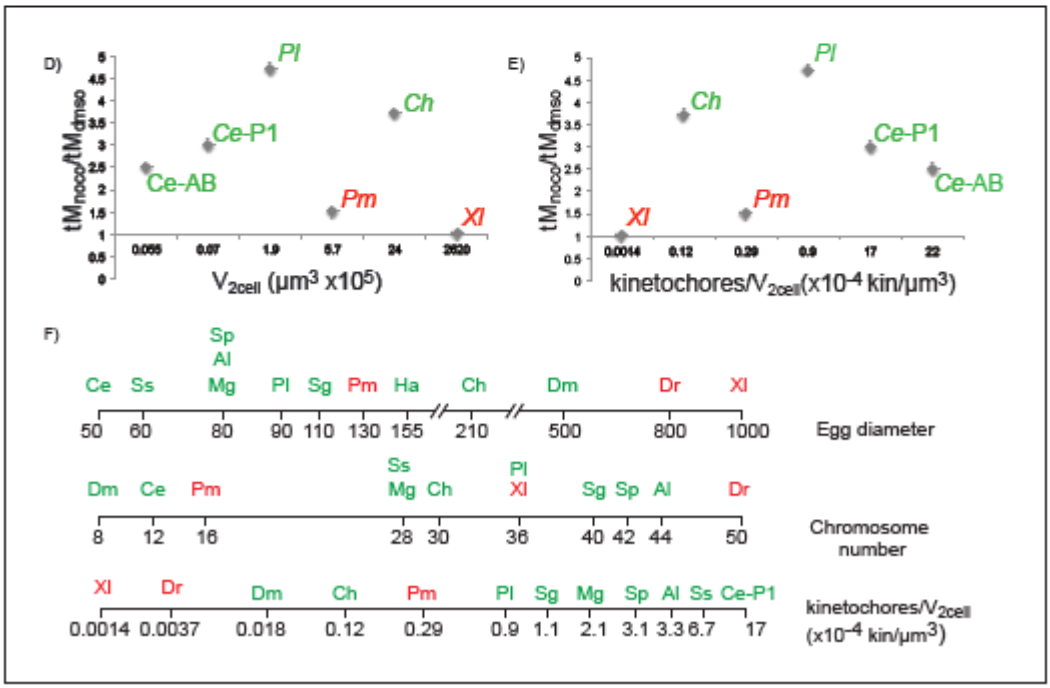
D)
tMnoco/tMdmso
Pl
Ch
Ce-P1
Ce-AB
Pm
Xl
V2cell (µm3 x105)
E)
kinetochores/V2cell(x10-4 kin/µm3)
F)
Egg diameter
Chromosome number
kinetochores/V2cell (x10-4 kin/µm3)

Figure 3

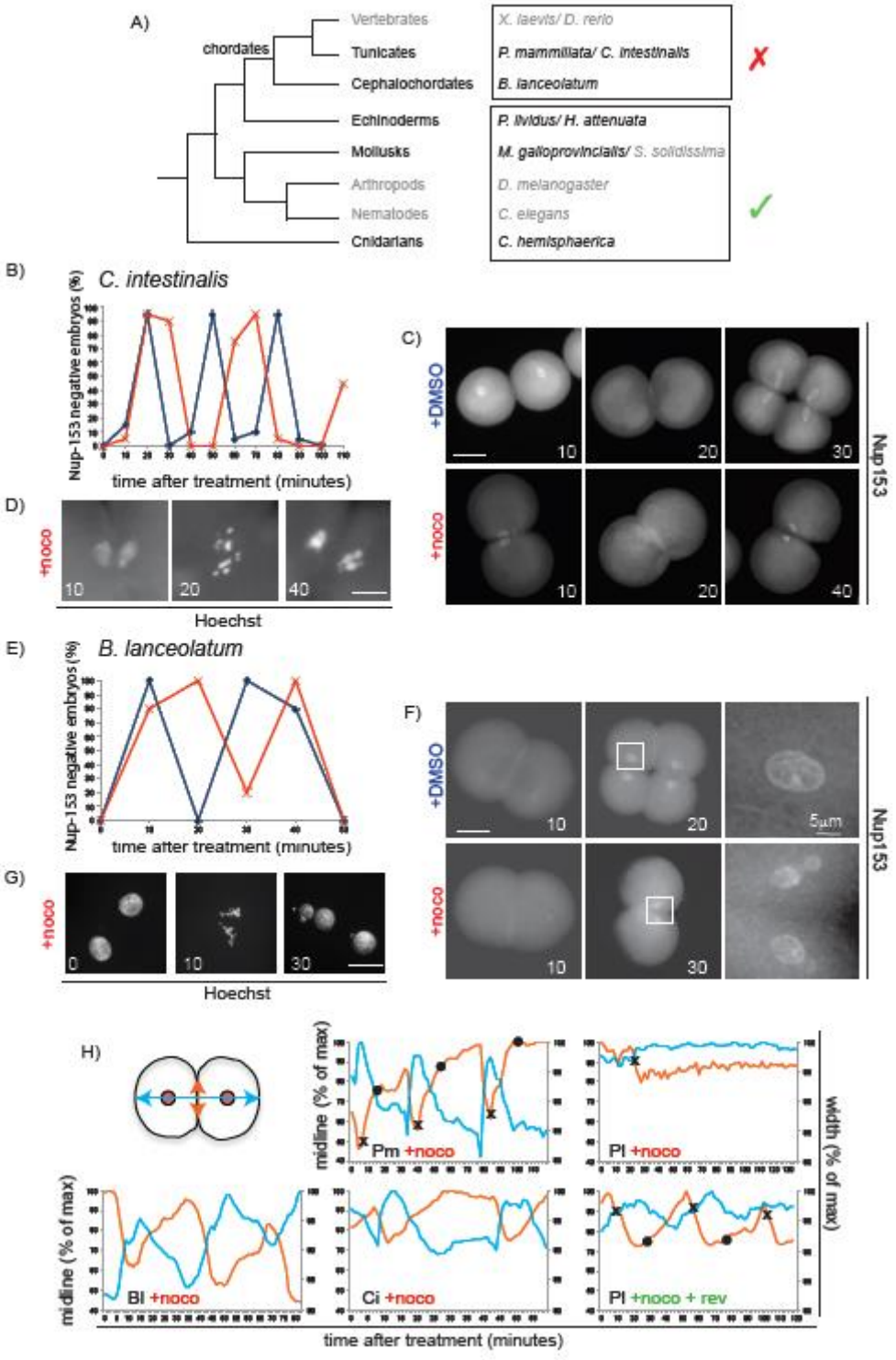
A)
chordates
Vertebrates
Tunicates
Cephalochordates
Echinoderms
Mollusks
Arthropods
Nematodes
Cnidarians
X. laevis/ D. rerio
P. mammillata/ C. intestinalis
B. lanceolatum
P. lividus/ H. attenuata
M. galloprovincialis/ S. solidissima
D. melanogaster
C. elegans
C. hemisphaerica
B)
C. intestinalis
Nup-153 negative embryos (%)
time after treatment (minutes)
C)
+DMSO
+noco
Nup153
D)
+noco
Hoechst
E)
B. lanceolatum
F)
5µm
G)
H)
midline (% of max)
width (% of max)
Pm +noco
Pl +noco
Bl +noco
Ci +noco
Pl +noco + rev
time after treatment (minutes)

Figure 4

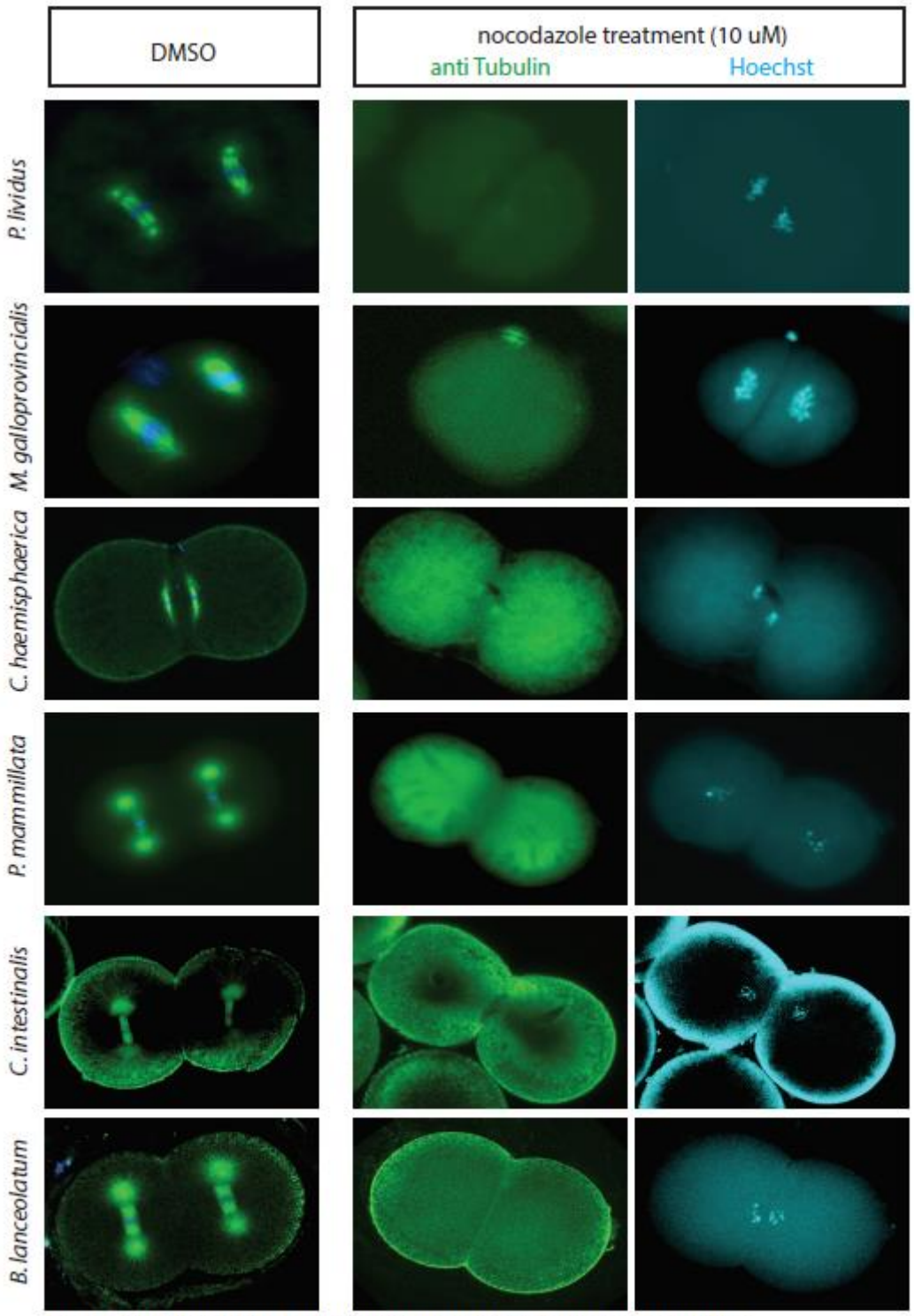

Figure S1: Nocodazole treatment depolymerizes spindle microtubules.
2-cell stage embryos fixed and stained for icrotubules (antitubuline, green) and for DNA (hoechst, blue), after 15 minutes incubation in DMSO (control, left) or in 10 µM nocodazole (right). Representative embryos in metaphase stage are shown for each species.

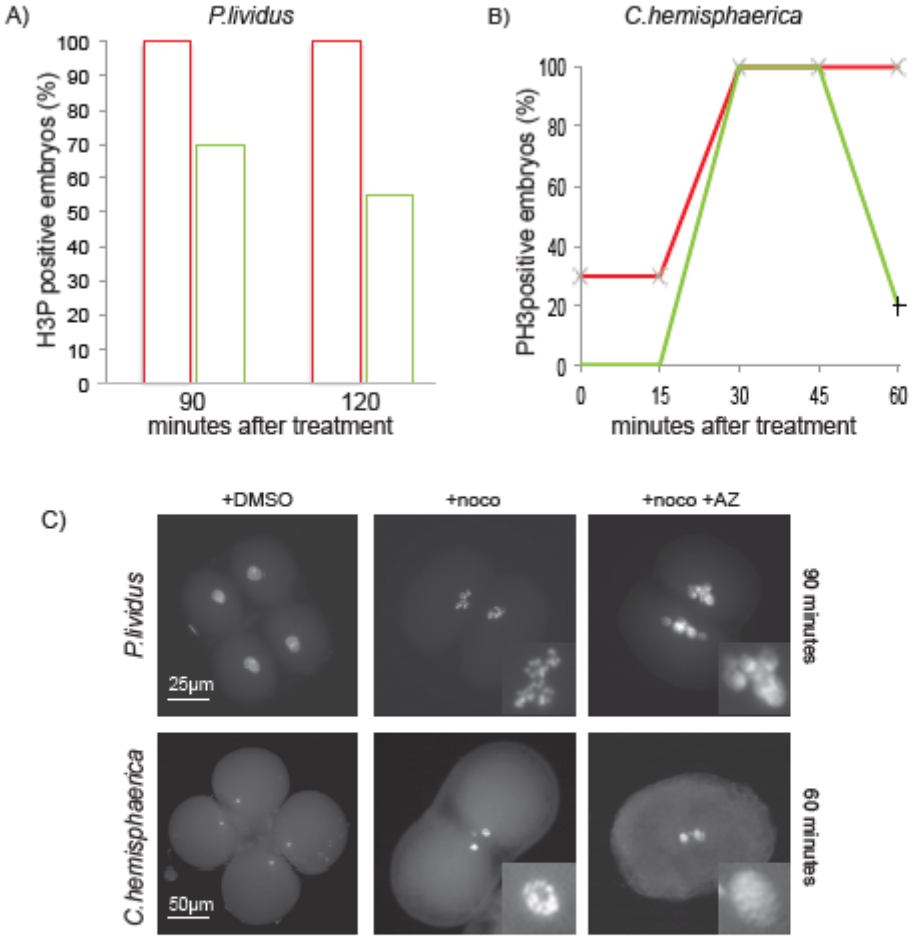

Figure S2: The Mps1 inhibitor AZ3146 releases the nocodazole-induced mitotic block observed in *P. lividus* and *C. hemisphaerica*.
Quantification of percentage of A) *P. lividus* and B) *C. hemisphaerica* embryos accumulating PH3 in the presence of 10µM nocodazole (red) or 10µM nocodazole and 0.5 µM AZ3146 (green). Representative of 3 independent experiments. C) Representative images of control (+DMSO), nocodazole (+noco) and nocodazole/AZ3146 (+noco+AZ) treated *P. lividus* (top) and *C. hemisphaerica* (bottom) embryos stained for PH3.

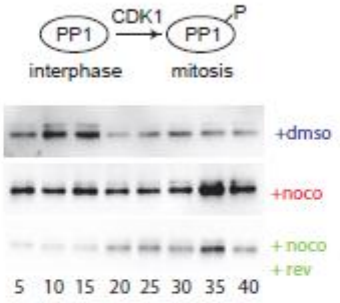

Figure S3: PP1 phosphorylation requires an active SAC in C. hemisphaerica embryos.
Western blot analysis of phospho-PP1in DMSO (top), nocodazole (middle) and nocodazole/reversine (bottom) treated embryos. At 30 minutes, control embryos were at 4-cell.

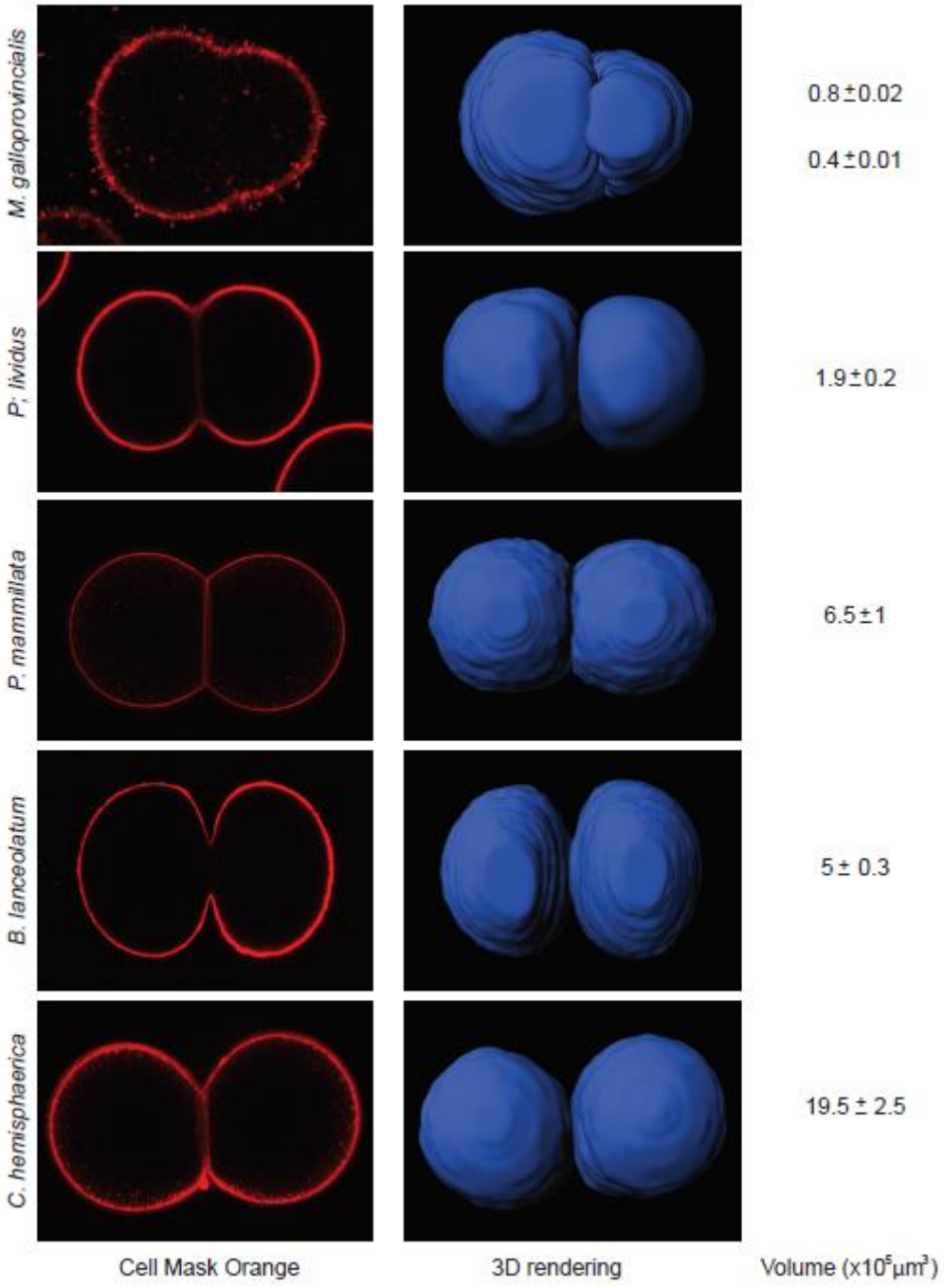

Figure S4: Cell Mask Orange staining and 3D rendering of 2 live cell stage embryos of different species.